CHARACTERIZATION OF UNCERTAINTIES IN THE MODELING OF ABLATION HEAT TRANSFER IN ROCKET NOZZLES

A Dissertation

Presented in Partial Fulfillment of the Requirements for the

Degree of Doctor of Philosophy

with a

Major in Mechanical Engineering

in the

College of Graduate Studies

University of Idaho

by

Bradley Heath

Approved by:

Major Professor: David J. Arcilesi, Ph.D.

Committee Members: Richard Christensen, Ph.D.; Michael McKellar, Ph.D.; Mark Ewing, Ph.D.

Department Administrator: Gabriel Potirniche, Ph.D.

December 2022

ABSTRACT

Ablation of carbon cloth phenolic insulators used in solid rocket motor (SRM) nozzles involves highly complex phenomena that is difficult to accurately predict. Historical and even more modern ablation predictions rely heavily on anchoring to SRM testing data to improve predictability and SRM reliability. Accelerated schedules, reductions in static SRM testing prior to flight, and a highly competitive global market are placing substantial onus on computational capability. Strong shifts from real-world testing to advanced modeling capabilities are placing emphasis on ablation modeling uncertainty. Without funding or schedule for multiple test firings it is essential to cover the proper amount of uncertainty in nozzle designs. The importance is further exacerbated by modern views of low realized risk in SRM designs. This study aims to ease these challenges by quantifying uncertainty in ablation predictions of carbon cloth phenolic insulators exposed to SRM nozzle environments. A particular historical test motor is used as a demonstration case. System response quantities of interest are erosion depth and char depth. Model and input uncertainty are quantified and characterized using a comprehensive approach. Sensitivity analysis on inputs relevant to ablation system response quantities of interest is performed to identify influential parameters. Due to the inherent extent of numerical simulations required, surrogate modeling techniques are assessed and applied based on computational efficiency and accuracy. Uncertainty in numerical models and inputs are propagated through a two-dimensional uncertainty quantification using a Latin Hyper Cube sampling methodology. Results of this study show that the primary sources of uncertainty in SRM thermal modeling are incident radiation heat flux, heat transfer coefficient, char material thermal conductivity, virgin material density, char material density, char material specific heat, and pyrolysis gas enthalpy. Uncertainty in the predictions of nozzle insulation erosion and char for the test case are provided relative to nozzle location at the 99th percentile and 95th confidence interval. Following the uncertainty quantification, approaches to reducing uncertainty and recommended future work are provided.

ACKNOWLEDGMENTS

I would like to thank Dr. Richard Christensen who always remained genuinely optimistic and patient through this doubly long process. I’m grateful for the inspiration he and Dr. Michael McKellar instilled in me through the exchange of personal life experiences and their application to conquering challenges within and without. As Dr. Christensen moves on to other passions, I appreciate Dr. David Arcilesi willingness to assist me along my journey. I am especially grateful for the countless hours given by Dr. Mark Ewing, whose mentorship, leadership, and teaching where instrumental in my understanding of ablation heat transfer, uncertainty quantification, and frankly who made possible the achievement of this dissertation. He has truly exemplified the definition of *friend.* I would also like to acknowledge Dr. Brian Liechty who helped me navigate through uncertainty quantification software and methods, and those damned constricting and slithery Python scripts. I would like to thank Northrop Grumman for providing access to thermochemical, ablation, and uncertainty quantification software packages that were used to support this effort.

DEDICATION

I am eternally grateful for my dear wife, Andrea, whose has walked, ran, and mostly crawled with me down what has been and will be a journey of life-long learning and progression. I'm grateful for my six children who have motivated me to be the best version of myself and have submitted to the idea that "Dad stares at his computer and phone all day and then limits our screentime". I'm grateful for my Father who passed away only a year ago. His educational opportunities were not as fortunate as mine, yet his intelligence and skill still baffle me today. He is truly my greatest hero. I am saddened I will not see him amongst the crowd at the culmination of my educational efforts (for which he was always proud), but I know he is here. I am content my Mother will be here. She has always been my greatest and loudest cheer leader. Much admiration for eldest my brother, Jeff, who has been an absolute trail blazer and has shown me what is possible. I'm grateful to my brother, Steven, who has lulled me away from an office chair so that I might enjoy the fruits of my labor and the beauty of nature. I dedicate this dissertation to my parents who came before, my wife and children who came after, and my siblings who helped raise me up.

I dedicate this dissertation to Family.

Lastly, in a realm where uncertainty saturates everything, I am grateful for that Being who is the same yesterday, today, and forever. I acknowledge His hands in all things.

TABLE OF CONTENTS

LIST OF TABLES

LIST OF FIGURES

NOMENCLATURE

ACRONYMS

2D-UQ	two-dimensional uncertainty quantification
ARGEIBL	Aerothermal Real Gas Energy Integral Boundary Layer Program
CCP	carbon cloth phenolic
CDF	cumulative distribution function
CM	char motor
CV	coefficient of variation
GCP	graphite cloth phenolic
ISM	ITRAC surrogate model
ITAR	International Traffic in Arms Regulations
ITRAC	Insulation Thermal Response and Ablation Code
LSM	least squares linear fit surrogate model
LSMNE	least squares linear fit surrogate model without surrogate model error
NASA	National Aerospace and Space Administration
PGS	propellant gas stream
PHSM	poly harmonic spline surrogate model
PDF	probability density function
SF	safety factor
SM	surrogate model
SRM	solid rocket motor
SRQ	system response quantity
TACOT	theoretical ablative composite for open testing
TG	thermogravimetric

TGA	thermogravimetric analysis
UQ	uncertainty quantification

ROMAN SYMBOLS

$\boldsymbol{A}$	formula matrix
A	Preexponential Factor (s^{-1}), constant in thermal conductivity dispersion equation, area (ft^2)
B	constant in thermal conductivity dispersion equation
B'	B-prime Number
B^*	blowing factor
$\boldsymbol{b}$	element abundance matrix
C	Constant, char (ft) or (in) or (mils)
C_H	Stanton Number for heat transfer
C_M	Stanton Number for mass transfer
C_p	specific heat (Btu/lbm-°R)
D	dimensional, diameter (in)
D^*	throat diameter (in)
dx	distance (ft)
E	activation energy (ft-lbf/lbm-mol), Erosion (ft) or (in) or (mils)
F	view factor
G	Gibbs function
g	enthalpy conductance (lbm/ft^2-s), function of α
$\bar{g}$	nondimensionalized Gibbs function
H	total enthalpy (Btu), heat transfer parameter

h	enthalpy (Btu/lbm), heat transfer coefficient (Btu/ft^2-s-°R)
$\bar{h}$	effective enthalpy (Btu/lbm)
h^0	heat of formation (Btu/lbm)
h^{Tw}	enthalpy evaluated at the wall (Btu/lbm)
k	thermal conductivity (Btu/ft-s-°R), element k in elemental composition
Le	Lewis Number
m	reaction order, slope from sensitivity derivative (ft)
$\dot{m}''$	mass flux (lbm/s)
$\dot{m}'''$	mass generation (lbm/s-ft^3)
$\mathcal{M}W$	molecular weight (lbm/lbmol)
N	particle number density (particles/ft^3), Number of
n	nth
$\boldsymbol{n}$	species abundance vector
P	pressure (lbf/in^2) or (lbf/ft^2) in ITRAC, volume fraction of reinforcement
Pr	Prandtl Number
Q_p	heat of pyrolysis (Btu/lbm)
q''	heat flux (Btu/ft^2-s)
q'''	volumetric heat generation (Btu/ft^3-s)
R	char yield of composite
R	Universal Gas Constant (ft-lbf/lbmol-°R)
r	resin, char yield of resin
$\dot{s}$	recession rate (ft/s)
T	temperature (°R)
t	time (s)
U	uncertainty

u	velocity (ft/s)
V	volume (ft^3)
v	Darcy velocity (ft/s)
u	velocity (ft/s)
v	Darcy velocity (ft/s)
x	mass fraction decomposed in a reaction, distance (ft), value of an input
Z^*	elemental potential of a species

GREEK LETTERS

α	extent-of-reaction
δ	thickness (in)
Γ	permeability (ft^2)
ε	emissivity
θ	ply angle (°)
μ	average, micron, dynamic viscosity (lbm/ft-s)
ξ	concentration (100 g/g-mole)
ρ	density (lbm/ft^3)
$\hat{\rho}$	pyrolysis gas density (lbm/ft^3)
$\overline{\rho c}$	effective capacitance (Btu/ft^3 - °R)
σ	standard deviation, Stephan-Boltzmann Constant (Btu/ft^2-s-$°R^4$)
τ	optical thickness
ϕ	porosity

SUBSCRIPTS

43	mass-weighted average
A	aleatory
adv, net	net advection
am	arithmetic mean
c	char
c_i	initial char, ith char elemental fraction
D	Darcy Velocity, diameter
D	diameter
E	epistemic
e	propellant gas stream, effective
F	fraction
F_{Al}	fraction aluminum
F_V	fraction volatiles
F_r	fraction resin
f	final, fiber reinforcement
f, v_{CCP}	formation, virgin CCP
f, v_r	formation, virgin resin
f, c	formation, char
f, v	formation, virgin
$f.e.g$	frozen edge gas
g	gas
gen	generation
h	heavy gas
i	ith value

$i - b$	ith perturbation minus baseline
ie	ith value in the gas stream
ij	ith row, jth column
iw	ith value at the wall
j	jth
l	local
M	Mth row
$major$	thermal conductivity parallel to ply
$minor$	thermal conductivity across ply
N	number, N_{th} row
O	overall
o	Initial, chamber condition
or	initial resin
p	particle, pyrolysis, penetration depth
p_i	ith pyrolyzed elements
r	resin, residue, recovery
rad, inc	incident radiation
rad, net	net radiation
$rerad$	reradiation
rp	resin pyrolyzed
rv	resin virgin
s	solid, surface, sublimations
s_f	solid fiber
s_i	solid initial
s_r	solid resin

SF	Safety faction
sim	simulations
so	screen-out
sto	storage
t	throat, total
tch	thermochemical
tot	total
v	virgin
v_i	initial virgin, ith virgin elemental fraction
w	wall

CHAPTER 1: INTRODUCTION

The allowable time frames and budgets for design, production, and testing of solid rocket motors (SRM's) and related space technology is being condensed. This is leading to accelerated schedules, capitalization on latest technologies, reductions in "big ticket" items, and reliance on predictive capability. A major area of reduction is on the number of SRM preflight tests that traditionally were a backbone for rocket motor production campaigns prior to flight. This reduction of time-to-flight is reflected in record space flight numbers[1] in the past year.

As a result of SRM test reduction, reliance in and scrutiny on experimental test data is shifting to computational predictive codes. A conundrum exists between the lack of preflight test data (that leaves predictive methodologies with a shallow anchor) and the questions regarding uncertainty in model predictions. Government agencies such as NASA have for some time taken notice of predictive uncertainty[2]. NASA recently issued a challenge to address uncertainty quantification[3] and optimize design in the presence of uncertainty[4]. NASA is also implementing predictive uncertainty it into their strategic plans[5]. However, common and practical methods for characterizing uncertainty have until recently been lacking in the propulsion industry. This has resulted in risks in SRM nozzle designs that cannot tolerate excessive insulation weight, but necessarily have high demands for reliability. The main purpose of this work is to quantify the uncertainty in ablation heat transfer predictions in a SRM nozzle by implementing a general two-dimensional uncertainty methodology (2D-UQ). The approach follows a methodology gaining acceptance within the propulsion industry[6]. With the exception of a brief assessment in the previous reference, 2D-UQ specific to ablation in rocket nozzles is absent in the literature.

Uncertainty has been considered for thermal protection materials (e.g. phenolic impregnated carbon ablators) in reentry vehicles[7-11] and a probabilistic risk assessment has been completed for nozzle carbon-carbon structural materials[12]. Recognition of the need for UQ is apparent in these studies. However, some of these studies are incomplete since they do not consider characterization of the model or model inputs into aleatory and epistemic uncertainties. Others apply model input uncertainty parametrically; assume input uncertainty values generally; or provide them with fidelity, but don't provide the evidence supporting these values. All perform analysis in a 1D-UQ fashion (aleatory only) and while they provide important insights into local and global sensitivity analysis techniques[13], they lack a separate quantification of both inherent variability in the system and predictability of the quantity of interest. Propagating aleatory and epistemic uncertainties separately, in a 2D-UQ, provides designers and decision-makers with much more information that allows for a targeted level of both variability and conservatism in the prediction itself.

The benefits of this work herein are five-fold. It gives experimentalists, analysts, designers, and decision makers vision into how to conduct a proper 2D-UQ in engineering predictions. It also provides a detailed estimate of expected uncertainty in ablation heat transfer predictions. The resulting quantification, both in the UQ inputs and outputs, will provide SRM nozzle analysts with valuable rationale for uncertainty estimates. It will also show where attention can be focused to reduce the uncertainty, providing for proper allocation of limited monetary resources. It also garners greater understanding of the risk associated with design decisions. Finally, the comprehensive approach presented here provides a transferrable framework that can be readily applied to other high-risk problems across government, industry, and academia.

Prior to conductivity 2D-UQ on ablation in a rocket nozzle, some brief background material on SRM's, nozzle materials, and the environments imposed on the nozzle surface are provided. An outline of the 2D-UQ methodology follows, the details and results of which are found in the succeeding chapters.

1.1 SRM'S, NOZZLE MATERIALS, AND ENVIRONMENTS

No purpose is served in investigating the reliability of 12th Century A.D. rockets[14] nor the test methods or predictive capability of the time. Instead, focus is given to rocket technology that grew out of the early 1960's[15] and into today. An example of a modern SRM is shown in Figure 1.

The igniter at the SRM forward end has embedded thru-bulkhead initiators that receive an electrical signal when the countdown reaches 0. The initiators ignite explosive pellets that start the igniter. The igniter acts like a miniature rocket motor except its propellant is extremely fast burning. The flame front propelling out of the igniter's aft end ignites the solid propellant grain in the motor. Slots in the propellant grain increase surface area allowing accelerated burning, and tailor motor pressure characteristics. Heat and pressure rapidly accumulate in the motor chamber and a high-temperature particle-laden gas mixture is expelled through the nozzle creating thrust. Since most SRM propellants are aluminized, aluminum oxide particles are present in the combustion products. These particles are entrapped in the flow and may be combusting, solid, or in a condensed phase as they pass into and out of the nozzle. Any impact on the nozzle surface can result in augmentation of both heat transfer and surface erosion. As a result, propellant grain and nozzle contours are designed to reduce particle impingement, and it predominantly occurs in nozzle entrance regions. The energy expended through the conversion of the propellants potential energy to kinetic energy is immense (on the order of 50 million hp in a couple minutes)[18]. (For additional information on this conversion process, one is directed to[14][17][19].) As this energy is recovered through thermal and viscous boundary layers to a non-slip wall, tremendous levels of heat transfer occur.

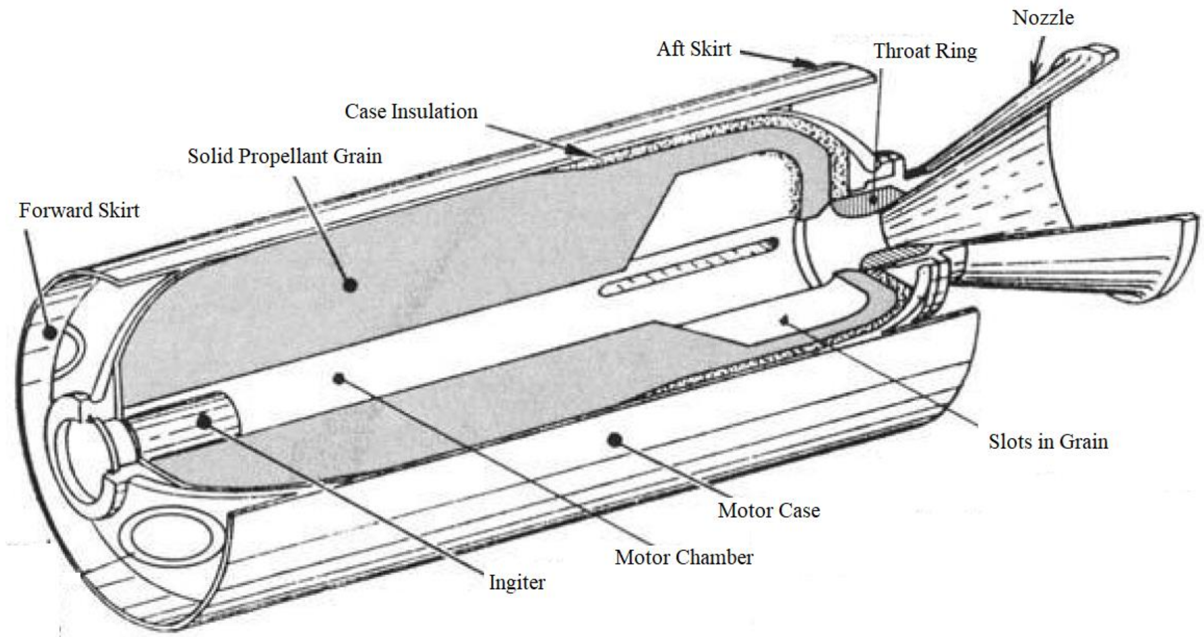

Figure 1. SRM with associated components.[16]

Figure 2 shows a cross-section of a submerged nozzle (meaning the forward end of the nozzle is submerged into the motor case) and Figure 3 shows a truncated 2D-axisymmetric section (truncated at the aft end so the entirety of the aft exit cone is not visible). The outside nozzle material is often a steel or aluminum alloy that provides for structural support against high vibrational loads, vectoring loads, drag forces, large differential pressures, and its own weight.

The insulator lining the metal alloy provides thermal protection against a flame front that is on the order of 6500°R and moving greater than Mach 5. In addition to the chemical reactions induced on the insulator surface leading to chemical erosion, particles in the flow impinge and blast the surface leading to mechanical erosion. Insulative materials vary by application. Examples for rocket nozzle insulative materials include carbon cloth phenolic (CCP), graphite cloth phenolic (GCP), carbon-carbon, silica cloth phenolic, and cork. Others are listed in refs. [20-21]. Each insulative material has its own advantages and disadvantages and often, different insulators are used in different portions of a nozzle based on needs and insulator capability. And, there are multiple variations of the same insulator material made by different manufactures under different processes. Modern large-scale SRM design predominantly use CCP for the insulation, and the 2D-UQ analysis concentrates on that CCP.

As was mentioned, these insulators are exposed to extremely high temperatures at supersonic velocities. In addition, the combustion products are chemically reactive, which subjects the insulator to chemical erosion as the carbonaceous surface reacts with oxidative species (e.g. H_2O, CO_2, OH)[22-23] in the propellant. The erosion can be augmented by thermomechanical abrasion due to alumina impact. In addition to surface erosion, the insulator loses material due to in-depth material pyrolysis (charring) as the material heats. All these effects contribute to the complex ablation process in SRM nozzles. Ablation as defined here includes all these mechanisms of material loss. Ablation heat transfer considers all the phenomena occurring at the interface (boundary layer) between the flow and the insulator surface, and associated phenomena occurring in the insulator in-depth. These phenomena are discussed more in Chapter 2 along with the mathematical formulations used to model this multi-physics problem.

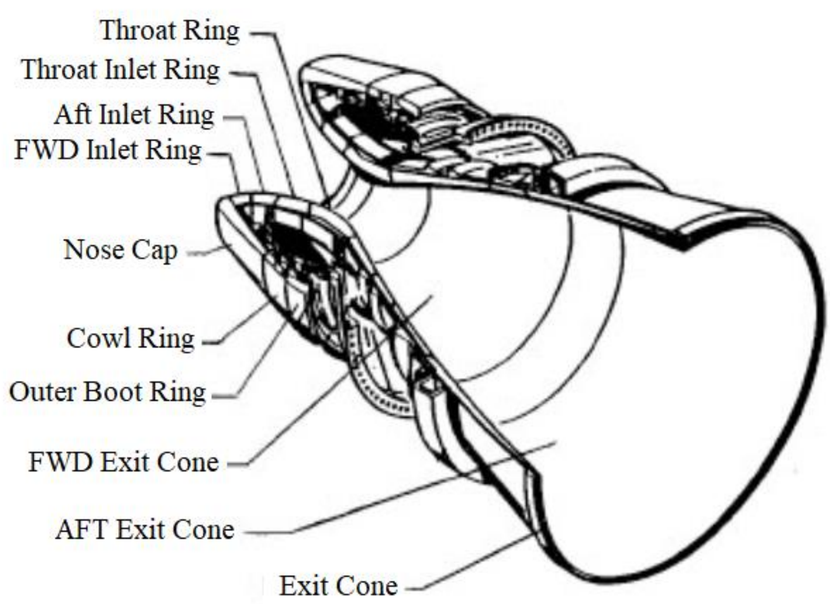

Figure 2. Submerged nozzle with associated components.[24]

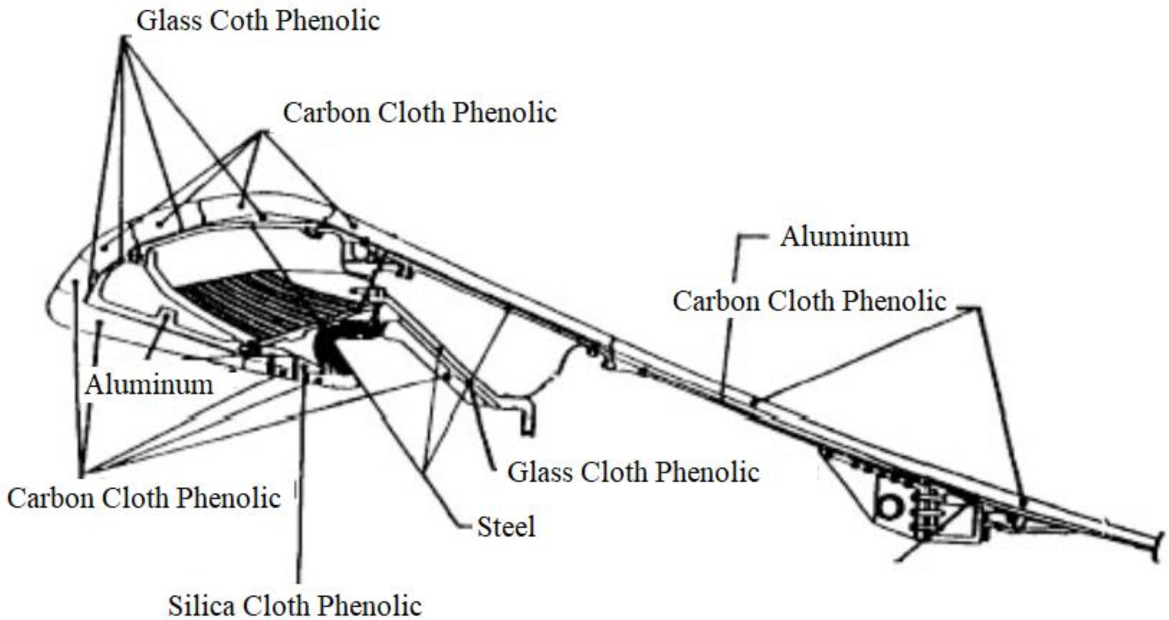

Figure 3. 2D Axisymmetric nozzle section showing various materials that provide thermal and structural protection.[24]

1.2 UNCERTAINTY QUANTIFICATION METHODOLOGY.

The 2D-UQ methodology[6] used in this work is outlined as an adaptation from Oberkampf and Roy[25]. An outline of this adaptation is below.

1. Define the system response quantity (SRQ) or quantities.
2. Define the model.
    a. Mathematical model
    b. Geometrical model
3. Identify relevant inputs.
    a. Informed through engineering judgement and sensitivity analyses
4. Classify and characterize input uncertainties.
    a. Classified into aleatory and epistemic categories
5. Propagate aleatory uncertainties in "inner loop".
    a. Aleatory Loop
6. Propagate epistemic uncertainties in "outer loop".
    a. Epistemic Loop
7. Quantify the uncertainty.
    a. System Variability
    b. Model Credibility

In this application, numerical solution error is excluded in the uncertainty quantification. Oberkampf and Roy[25] support this, saying that numerical solution error is not commonly addressed for several reasons, two of which are applicable to this work. The first reason is “because numerical solution error is assumed to be small compared to other contributors to uncertainty”. Numerical solution error is not addressed in this paper because the 1D models allow for significant discretization spatially and temporary such that numerical error is negligible. This is verified through discretization studies that confirm a negligible difference from further refinements.

Another reason noted by Oberkampf and Roy[25] is “because it is claimed adjustable parameters can be used to match the existing data and thereby make reasonable predictions”. The heat transfer boundary conditions used in this work are correlation heavy[26-27] and are calibrated to match existing data to make reasonable predictions. Predicting boundary conditions is a major challenge in ablation predictions in a rocket nozzle. The uncertainty in these boundary conditions is considered both aleatory and epistemic, but not because of numerical error. Aleatory because of natural variation and epistemic because they are not completely physics-based predictions and do not accurately hit nominal conditions without anchoring. To the author’s knowledge, current physics-based models are not physical enough to overcome this challenge (e.g., physics-based approached rely on assumed wall temperatures). The adjustable parameters used in this work are in family with model form errors and are therefore classified as epistemic.

Two SRQs are defined for step 1: the erosion depth and the char depth into the CCP insulator. Erosion and char depth in CCP nozzle insulators are illustrated in Figure 4. A pre-fired nozzle is shown in the center of the figure. Post-fire, the nozzle is sectioned for further measurements including erosion and char depths. Both are measured relative to the original (non-ablated) local surface of the nozzle. The “erosion depth” representing the distance from the original surface to the erosion front, and the “char depth” the distance to the char front. This is show in the left-most image of Figure 4

These SRQs are chosen because they are typical post-test (or post-flight) measurements taken for SRMs. SRM performance is based on chamber pressure and nozzle contour. Therefore, erosion depth impacts SRM performance. Too much erosion can have negative performance implications and too little erosion in passive nozzles restricts performance targets from being met. Char depth is chosen because it is an indirect indication of how closely the heated front approaches the nozzle structure. If the char depth is predicted accurately, insulator isotherm depths are also likely to be accurately predicted.

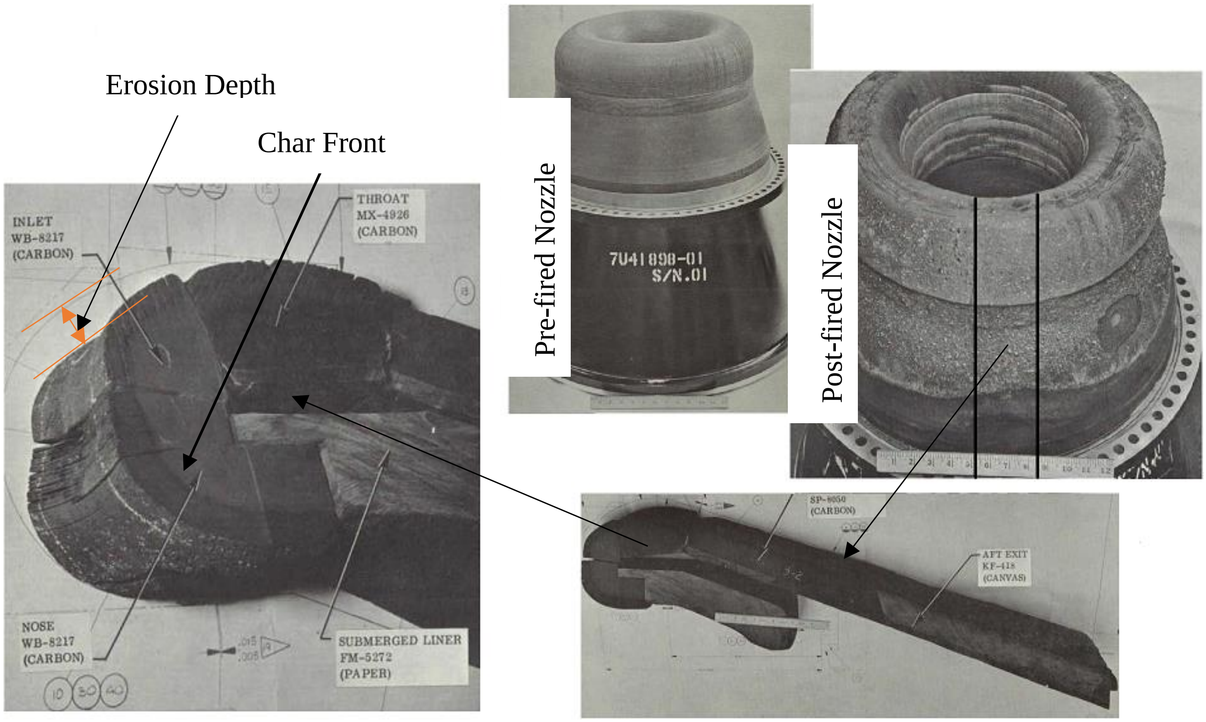

Figure 4. Pre- and Post-Fired Nozzle. Alumina slag is visible on the post-fired nozzle. The nozzle is sectioned for further measurement including erosion and char measurements.[29]

The remaining steps in the 2D-UQ process are discussed in the succeeding chapters. The model (both mathematical and geometrical) is defined in Chapter 2 and 3. Model inputs are also identified in Chapter 3 and are characterized in Chapter 4 for uncertainty and uncertainty type. Additionally, a probabilistic statement is made about each model input. To determine which model inputs are most relevant to the SRQs, sensitivity is conducted in Chapter 5. A simple ranking system is defined along with screen-out criteria to remove model inputs that have low impact on the SRQs.

The number of simulations required to perform a thorough 2D-UQ for a nozzle is on the order of 1 million. This may be beyond the computational capability available or practically inefficient. To overcome this roadblock, surrogate modeling techniques are used. Surrogate modeling is captured in Chapter 6. Various surrogate modeling techniques are explored and assessed. A surrogate model is selected based on computational efficiency and accuracy. The selected surrogate model along with input uncertainty is propagated through a 2D-UQ in Chapter 7. Uncertainty is quantified and a comparison is made with a safety factor approach. Lastly, three cases are considered to reduce uncertainty: reduction from testing, reduction from modeling improvements, and more data. Conclusions follow including areas of future research.

CHAPTER 2: MODEL THEORY

The supporting theory used here was pioneered in Charring Material Ablation[29-33] and Aerothermal Chemical Equilibrium[34] codes. Improvements in stability and formulation were made to these historic codes in the late 2010's[35]. These improvements, much of the original theory, and additional phenomena have been recast in the Insulation Thermal Response and Ablation Code (ITRAC)[35] and Chemics code[36]. ITRAC is a numerical analysis program that solves for the transient thermal, pyrolysis, and ablation response of sacrificial insulators and Chemics provides equilibrium thermochemical compositions and properties in the boundary layer edge. Put simply, Chemics provides the thermochemical boundary conditions and ITRAC provides the geometrical domain for boundary condition application along with material properties and material response. The theory relevant to ITRAC is presented first. Note: the theory provided here is condensed from refs. [35-36].

2.1 PHENOMENA

The primary phenomena captured in ITRAC for ablative insulators are illustrated in Figure 5. The insulator is heated by radiation and convection heat transfer at the front surface. The insulator temperature increases at the front surface and in depth resulting in insulative material decomposition. Decomposition drives a pyrolysis front into the insulator leaving behind a layer of porous charred material. Two regions are formed between the eroding front surface and the pyrolysis front. The first region nearest the eroded surface is referred to as the char layer, while the in-depth region is the pyrolysis zone. During material decomposition, gases are generated. These gases flow through and exchange energy with the porous char structure as they travel to the recessing surface where they interact in the boundary layer. Recession of the surface material can occur due to chemical (SRM propellant gas interaction) and mechanical (e.g., particle blasting, impingement, shear) interaction with the multi-phase boundary conditions.

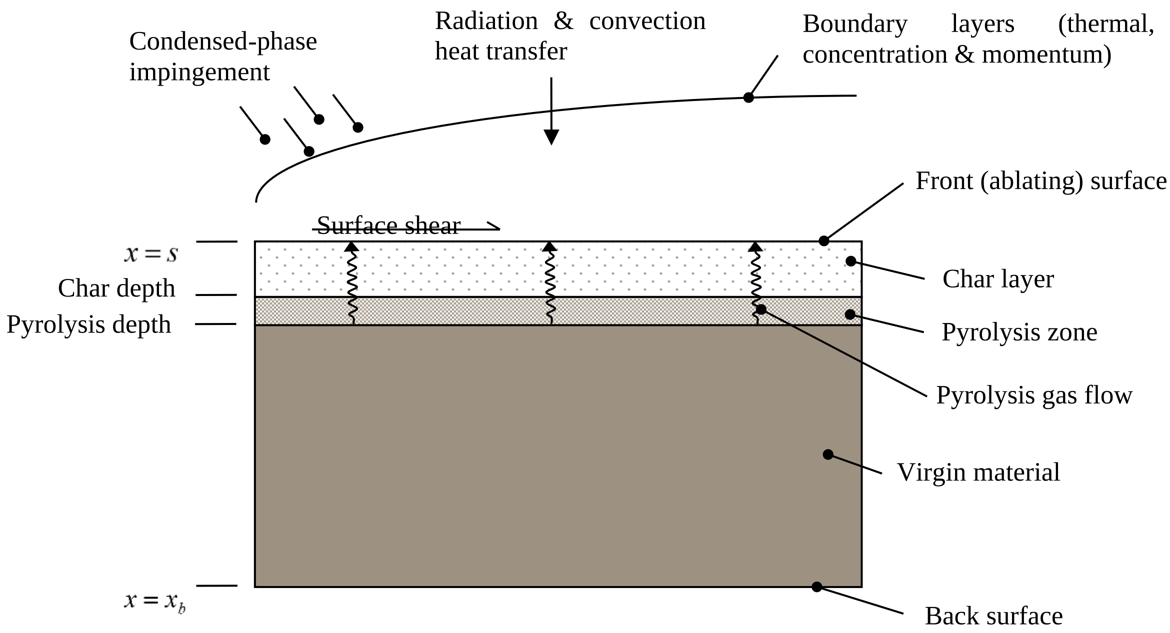

Figure 5. Phenomena associated with ablation in a solid rocket nozzle.[35]

2.2 SOLUTION VARIABLES

Primary solution variables in ITRAC include the temperature field, $T(x,t)$, extent-of-reaction field, $\alpha(x,t)$, pore pressure field, $P(x,t)$, and location of the recessed surface, $s(t)$. The temperature and extent-of-reaction fields are related through an Arrhenius expression shown in equation (2.1).

$$\frac{d\alpha_i}{dt} = A_i \exp\left(-\frac{E}{\mathrm{R}T_i}\right)(1-\alpha_i)^{m_i} \tag{2.1}$$

This expression allows for multiple decomposition reactions, each with its own extent-of-reaction (α_i), pre-exponential faction (A_i), activation energy (E_i), reaction onset temperature (T_i) and reaction order, (m_i). Each decomposition reaction results in a mass loss fraction (x_i) where the total mass loss (x_{tot}) is the summation over all reactions. The overall extent-of-reaction is derived by combining each reaction's extent-of-reaction with its mass fraction and then dividing by the total mass loss.

$$\alpha = \frac{\sum \alpha_i x_i}{x_{tot}} \tag{2.2}$$

The overall extent-of-reaction is used to derive the bulk material properties of the decomposing solid (s) such as density (ρ_s), enthalpy (h_s), specific heat (C_{p_s}), thermal conductivity (k_s), and porosity (ϕ). This is accomplished through a linear relation between properties in the fully-virgin (v) and fully-charred (c) condition. The equation for material density is shown in equation (2.3). Similar relationships follow for h, C_p, k, and ϕ.

$$\alpha = \frac{\rho_v - \rho_s}{\rho_v - \rho_c} \tag{2.3}$$

The range of values for α are between the extremes that ρ_s can take on. At a fully virgin material condition, $\rho_s = \rho_v$ and $\alpha = 0$. At a fully-charred material condition, $\rho_s = \rho_c$ and $\alpha = 1$. Equation (2.3) can be rearranged in terms of ρ_s to derive the rate of change of solid density in terms of the rate of change of α. From equation 2.3 the rearrangement and derivation is:

$$\rho_s = \rho_v(1 - \alpha) + \alpha\rho_c \tag{2.4}$$

$$\frac{\partial\rho_s}{\partial t} = -(\rho_v - \rho_c)\frac{\partial\alpha}{\partial t} \tag{2.5}$$

Assuming that the material volume is constant during the decomposition process, the bulk density of the decomposing solid is given by

$$\rho_s = \rho_v - \rho_v \sum \alpha_i x_i \tag{2.6}$$

Combining equations gives the following relation between overall rate of change for α.

$$\frac{\partial\alpha}{\partial t} = \frac{\sum \alpha_i x_i}{\sum x_i} \tag{2.7}$$

2.3 CONSERVATION EQUATIONS

Using equations (2.1-2.7) above and a control volume approach, conservation of mass, momentum, and energy can be derived. A control-volume for gaseous mass balance within the porous pyrolyzing material is shown in Figure 6. The figure shows a gaseous mass generation ($\dot{m}'''_{gen}$) associated with pyrolysis, advection of mass in the form of the mass flux ($\dot{m}''_g$), and storage of gas having density $\hat{\rho}_g$ in the solid pores.

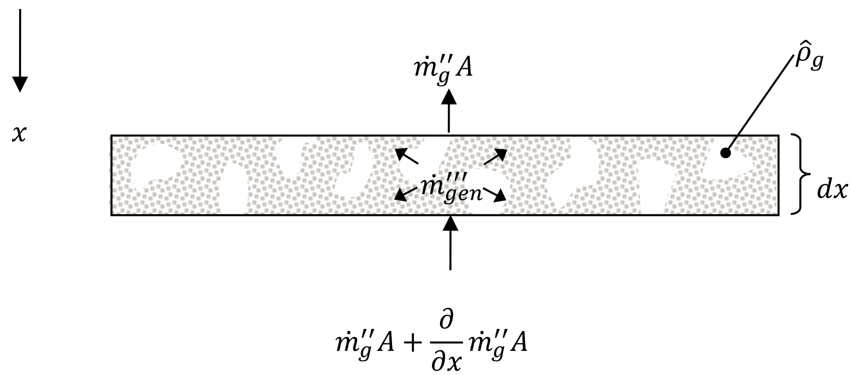

Figure 6. Control Volume for Conservation of Mass.[35]

Conservation of mass for the gaseous phase requires a balance of storage, net advection and generation as shown in equations (2.8-2.9). Ideal gas behavior is assumed for the pyrolysis gas ($\hat{\rho}_g$) as shown in (2.10).

$$\dot{m}_{sto} = \dot{m}_{adv,net} + \dot{m}_{gen} \tag{2.8}$$

$$\frac{\partial(\hat{\rho}_g \phi)}{\partial t} = \frac{1}{A}\frac{\partial(\dot{m}''_g A)}{\partial x} + (\rho_v - \rho_c)\frac{\partial \alpha}{\partial t} \tag{2.9}$$

$$\hat{\rho}_g = \frac{P}{\mathrm{R}T} \tag{2.10}$$

In terms of the Darcy velocity (v_D), also defined as positive against the x-direction, the mass flux can be written as shown in equation (2.11). Incorporating (2.10-2.11) into (2.9) gives the following for the gaseous mass conservation of mass in equation (2.12).

$$\dot{m}_g'' = \hat{\rho}_g v_D \tag{2.11}$$

$$\frac{\phi}{\mathrm{R}T}\frac{\partial P}{\partial t} = \frac{1}{A}\frac{\partial}{\partial x}\left(A\frac{Pv_D}{\mathrm{R}T}\right) + \frac{P\phi}{\mathrm{R}T^2}\frac{\partial T}{\partial t} + \left(\rho_v - \rho_c + \frac{P\phi_v}{\mathrm{R}T} - \frac{P\phi_c}{\mathrm{R}T}\right)\frac{\partial \alpha}{\partial t} \tag{2.12}$$

The Momentum Equation balances the pressure gradient with drag forces are expressed in equation (2.13)

$$v_D = \frac{\Gamma}{\mu_g}\frac{\partial P}{\partial x} \tag{2.13}$$

where Γ is the material permeability and μ_g is the pyrolysis gas viscosity. The momentum balance of equation (2.13) is combined with the conservation of mass to give the following Mass-Momentum Equation (2.14).

$$\frac{\phi}{\mathrm{R}T}\frac{\partial P}{\partial t} = \frac{1}{A}\frac{\partial}{\partial x}\left(A\frac{P}{\mathrm{R}T}\frac{\Gamma}{\mu_g}\frac{\partial P}{\partial x}\right) + \frac{P\phi}{\mathrm{R}T^2}\frac{\partial T}{\partial t} + \left(\rho_v - \rho_c + \frac{P\phi_v}{\mathrm{R}T} - \frac{P\phi_c}{\mathrm{R}T}\right)\frac{\partial \alpha}{\partial t} \tag{2.14}$$

A control-volume for energy balance within the porous pyrolyzing material is shown in Figure 7. Energy is stored in both the solid and gas phases within the control-volume. Energy enters and leaves through gaseous advection and conduction. In addition, the pyrolysis gases contribute volumetric generation as illustrated.

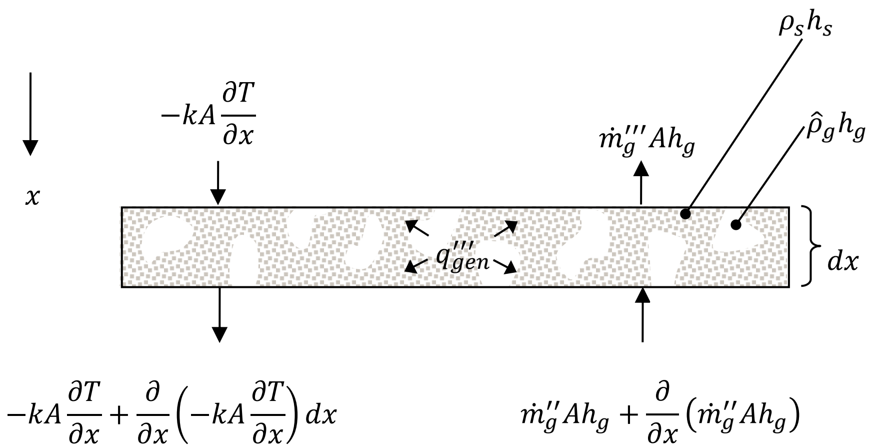

Figure 7. Control volume for conservation of energy.[35]

Effective capacitance and solid enthalpy terms are defined as

$$\overline{\rho c} = \hat{\rho}_g C_{p_g}\phi + \rho_s C_{p_v}(1-\alpha) + \rho_s C_{p_c}\alpha \tag{2.15}$$

And

$$\bar{h} = h_s + \frac{\rho_s(h_v - h_c)}{\rho_v - \rho_c} \tag{2.16}$$

A balance in the control volume results in the general Energy Equation.

$$\overline{\rho c}\frac{\partial T}{\partial t} = \frac{1}{A}\frac{\partial}{\partial x}\left(kA\frac{\partial T}{\partial x}\right) + \dot{m}_g''\frac{\partial h_g}{\partial x} - \left(Q_p - \bar{h} + h_g\right)(\rho_v - \rho_c)\frac{\partial \alpha}{\partial t} \tag{2.17}$$

2.4 BOUNDARY CONDITIONS

Solutions of the Energy and Mass/Momentum Equations require boundary conditions for the front surface. The various boundary conditions applicable to the problem being solved here are described below. A boundary condition is provided for an incident radiation heat flux ($q_{rad,abs}''$) in equation (2.18).

$$q''_{rad,abs} = \alpha_{abs} q''_{rad,inc} = \alpha_{abs} \sigma T_g^4 \tag{2.18}$$

where α_{abs} is the surface absorptivity. Along with incident radiation, reradiation follows a similar relationship where α_{abs} is replaced with surface emissivity (ε_s). A view factor (F) is also included and radiation flux from the surface is based on the wall temperature (T_w) and the Stephan-Boltzmann constant (σ).

$$q''_{rerad} = F \varepsilon_s \sigma T_w^4 \tag{2.19}$$

An enthalpy-based convection model is provided for heat transfer associated with reacting boundary flows. This type of boundary condition is referred to here as enthalpy-based convection (q''_{tch}) and incorporates thermochemical (tch) boundary layer reactions as shown in equation (2.20).

$$\dot{q}''_{tch} = \rho_e u_e C_H (H_r - h_w)_{f.e.g} + \rho_e u_e C_M \left(\sum_i Z_{ie}^* h_i^{T_w} - \sum_i Z_{iw}^* h_i^{T_w} \right) \tag{2.20}$$

where the sensible and chemical convection are captured in the two separate terms on the right-hand-side. The subscript $f.e.g$ denotes conditions for the "frozen edge gas," that is, with the composition fixed at that of the boundary layer edge. The flowing multi-phase mixture density and velocity are denoted as ρ_e and u_e. C_H and C_M are Stanton numbers for heat transfer and mass transfer, H_r and h_w are the recovery and wall enthalpies. Z_{ie}^* and Z_{iw}^* are the mass transfer driving potentials based on molar and mass fractions of each chemical species i in the multiphase stream and at the wall[29]. The enthalpy of each species evaluated at T_w is denoted as $h_i^{T_w}$. C_M can be determined based on heat and mass transfer analogy through the relationship to Le in equation (2.21).

$$\frac{C_M}{C_H} = Le^{\frac{2}{3}} \tag{2.21}$$

2.5 ENERGY BALANCE AT THE SURFACE

An energy balance is made at the ablative insulator surface as shown in Figure 8.

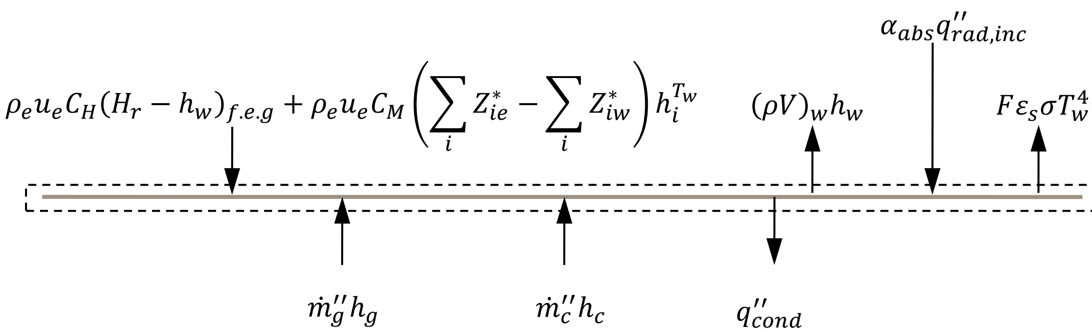

Figure 8. Energy balance at the insulator surface.[35]

Here, the expression (ρV) is the combined mass fluxes from pyrolysis gases and eroding charred material being advected away from the surface or wall. The balance becomes equation (2.22)

$$q''_{cond} = \rho_e u_e C_H (H_r - h_w)_{f.e.g} + \rho_e u_e C_M \left[\left(\sum_i Z^*_{ie} - \sum_i Z^*_{iw} \right) h_i^{T_w} + B'_c h_c + B'_g h_g + B' h_w \right] + q''_{rad,net} \tag{2.22}$$

The non-dimensional “B-prime” definitions are

$$B'_g = \frac{\dot{m}''_g}{\rho_e u_e C_M} \tag{2.23}$$

$$B'_c = \frac{\dot{m}''_c}{\rho_e u_e C_M} \tag{2.24}$$

$$B' = B'_g + B'_c \tag{2.25}$$

Erosion mass flux of the surface is then captured by $\dot{m}_c''$ and the erosion rate ($\dot{s}$) of the surface is captured by

$$\dot{s} = \frac{\dot{m}_c''}{\rho_c} = \frac{B_c' \rho_e u_e C_M}{\rho_c} \tag{2.26}$$

More information on ITRAC including numerical schemes can be found in refs. [35] [37]. In summary, solution of equation (2.17), the energy equation, provides for the predicted temperature field. It is solved simultaneously with equation (2.14), a mass/momentum equation, which governs internal porous flow in the charring ablator. Related terms in the energy equation account for thermal trasport associated with that flow. Equations (2.1) and (2.2) represent material charring, which effect both the energy and the mass/momentum equations. These are also included in the simultaneous solutions process. Finally, a surface energy balance enforces the boundary condition of equation (2.22) onto the solution of (2.17). With all of this solved, field solutions for both the temperature and extent-of-reaction fields are known. This provides for the determination of the corresponding "char depth" which represents the location of a predefined extent-of-reaction to represent the char front. In addition, the erosion depth is found from equation (2.26). These two quantities, the char depth and the erosion depth, are the quantities of interest in this study.

2.6 CHEMICS

The chemics code is used to model surface thermochemistry. It provides the various related parameters in equation (2.22). As opposed to solving simultaneously with the energy equation, surface thermochemistry is precalculated for a range of conditions and tabulated into "B-prime" tables used in ITRAC solutions. The tables cover a range of values for in-depth gas generation that evolves to the surface (represented by B_g') along with pre-defined surface consumption rates (represented by B_c'). These tables are used to provide parameters in equation (2.22).

At the heart of the Chemics approach is the assumption of chemical equilibrium at the material surface. With this assumption, chemical erosion rates are governed by species diffusion rates and surface temperatures. Chemical definitions are needed for the propellant gases (which are driven by the propellant formulation), the pyrolysis gases (based on decomposition of phenolic), and the residual char (for this study assumed to be pure carbon). The theory implemented in Chemics is described by the way a chemical system is created by the user in the code. Chemical systems can be created from a single element (e.g. hydrogen), multiple elements (e.g. carbon, oxygen, hydrogen), chemical species (e.g. carbon-dioxide) or a mixture of chemical species (e.g. say a propellant formulation). Chemics calculates the species formed from the elements along with their constitutive molar concentrations. If desired, the user can restrict which species are formed from the elements. For example, the user may only want to see gaseous species and restrict Chemics from calculating the molar concentration of condensed species.

When the system is created it is constrained by the elements in the system, the abundance of elemental molar of mass fractions, and the species those elements may form. Chemics writes this in matrix-form in equation (2.27)

$$\boldsymbol{A}\boldsymbol{n} = \boldsymbol{b} \tag{2.27}$$

where $\boldsymbol{A}$ is a formula matrix, $\boldsymbol{n}$ is a species abundance vector, and $\boldsymbol{b}$ is an element abundance vector. Each component (a_{ij}) of the formula matrix $\boldsymbol{A}$ represents the abundance of the ith element in the jth species. The matrix, $\boldsymbol{A}$ is

$$\boldsymbol{A} = \begin{bmatrix} a_{11} & a_{12} & \ldots & a_{1N} \\ a_{21} & a_{22} & \cdots & a_{2N} \\ \vdots & \vdots & \ddots & \vdots \\ a_{M1} & a_{M2} & \cdots & a_{MN} \end{bmatrix} \tag{2.28}$$

Each component of the species abundance vector n_j represents the moles of the jth species from the N equilibrium candidates. Each component (b_i) of the element abundance vector $\boldsymbol{b}$ represents the number of moles of the ith element from the M elements in the system. These vectors have the form

$$n = \begin{bmatrix} n_1 \\ n_2 \\ \vdots \\ n_N \end{bmatrix} \tag{2.29}$$

and

$$b = \begin{bmatrix} b_1 \\ b_2 \\ \vdots \\ b_M \end{bmatrix} \tag{2.30}$$

The system is such that gaseous species (n_g) and condensed species (n_c) are separated:

$$\boldsymbol{A}_g \boldsymbol{n}_g + \boldsymbol{A}_c \boldsymbol{n}_c = \boldsymbol{b} \tag{2.31}$$

The system is now constrained by the specific elements in the system, the mass of the system, and if desired, to specific species that may be formed. To solve for the species that will be formed Chemics uses a function, G for Gibbs Free Energy given in equation (2.32).

$$G = \sum_{j=1}^{N} \bar{g}_j \, n_j \tag{2.32}$$

Here, $\bar{g}_j$ is the molar Gibb's function of the jth component in the species abundance vector. The molar Gibb's function is nondimensionalized by dividing by RT where R is the gas constant in molar form and T is absolute temperature. In vector form, the total Gibb's function becomes

$$\frac{G}{\mathrm{R}T} = \hat{\boldsymbol{g}}_g^T \boldsymbol{n}_g + \hat{\boldsymbol{g}}_c^T \boldsymbol{n}_c \tag{2.33}$$

where

$$\hat{g}_j = \frac{\bar{g}_j}{\mathrm{R}T} \tag{2.34}$$

To solve for the species abundance vector, $\boldsymbol{n} = \boldsymbol{n}_g + \boldsymbol{n}_c$, Chemics determines the species abundance vector that minimizes Gibb's free energy. In essence, based on the elemental composition and elemental molar abundance, Chemics identifies the species that will form (pending any restrictions by the user and the available species in the Chemics database) at a particular set of B-prime values, temperature, and pressure. Formation of species from G is temperature and pressure dependent. Temperature and pressure are another user input and can be put in singularly, in increments, or in ranges. Figure 9 provides an example for 100% phenol (C_6H_6O) at 1 atm. Additional information on Chemics and element potential methods can be found in [36] and [38].

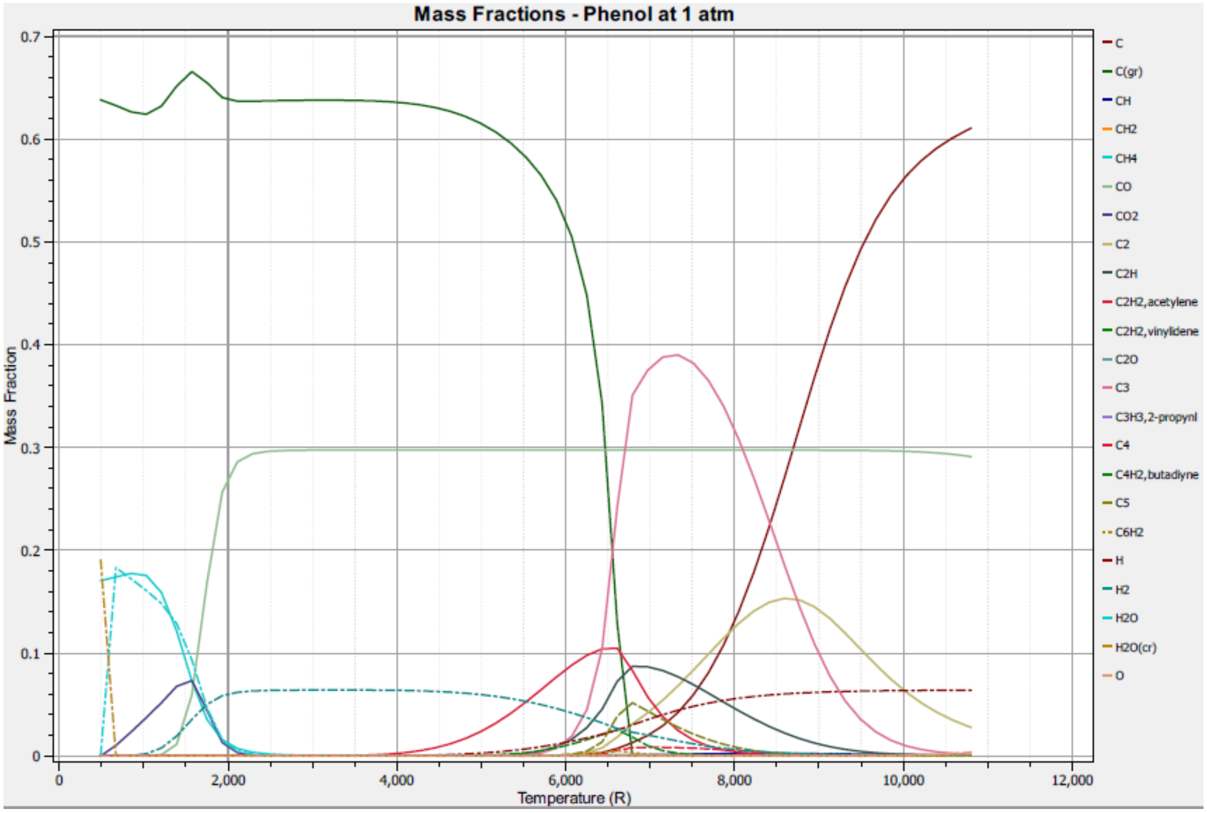

Figure 9. Equilibrium mass fractions for phenol calculated by Chemics.

For the system of interest in this study, the element abundance vector $\boldsymbol{b}$ is "known" for each table entry based on the composition of the propellant gases, the pyrolysis gases, and the charred surface, along with the corresponding B-prime values. The species abundance vector $\boldsymbol{n}$ is solved for to determine the chemical make-up of the surface reaction products at a specified temperature a pressure. With the temperature, pressure, and chemical composition, the various energy terms in the surface reaction products are known, and the terms in equation (2.22) can be populated.

CHAPTER 3: GEOMETRICAL MODEL, MATERIAL PROPERTIES, AND BOUNDARY CONDITIONS

A representative rocket motor was needed to support this study, and a historical motor used to evaluate CCP materials in nozzles was selected[39]. In this chapter definition of nozzle geometry is given along material properties and boundary conditions. In specifying the geometry there is no consideration given to manufacturing tolerances. Manufacturing tolerance is assumed to have negligible effect on erosion and char depth and would be superseded by any thermal growth effects during motor firing. The entirety of the geometrical model and nearly all material properties are in ref. [39]. Some supplementation to material properties is required for thermal conductivity[40] .

The heat transfer boundary condition was predicted by Arnold et al.[39] using both Aerothermal Real Gas Energy Integral Boundary Layer Program (ARGEIBL)[41], and for a couple locations, the Bartz correlation[24]. The radiation boundary condition correlation is in ref. [39] and will be discussed below.

3.1 GEOMETRICAL MODEL

The nozzle has a 7-in throat diameter mounted to an 84-in diameter char motor[42] (the configuration is referred herein as the CM nozzle) shown in Figure 10. The nozzle is described in detail in ref. [39]. A 2D-axisymmetric illustration of the nozzle is shown in Figure 11. This nozzle was tested in the late 1970’s with the purpose of assessing different materials for insulative capability. This is indicated by different materials in the throat ring. The different materials are identified in Figure 11.

Prior to testing, aerothermal predictions were made by Arnold et al. assuming these materials can be represented by MX4926 CCP. According to Clayton et al.[43], MX4926 uses HITCO CCA-1 rayon fabric with SC1008 resin. Use of HITCO CCA-3 is reported[44] to be used in USP FM5055B CCP (with 91 LD resin) which is a similar material to MX4926 from another manufacturer. Here, it is assumed that HITCO CCA-28 is representative of MX4926 and that FM5788 to a lesser extent (since its being tested for comparison to MX4926).

In our analysis, the nozzle is sectioned into stations as shown in Figure 12 for a total of 13 analysis stations. The throat is located at station 6. The station numbering scheme is representative of the stations measured for erosion and char in ref. [39]. Each station in the 2D geometry is analyzed separately as a 1D geometry in ITRAC.

Model geometry is input into ITRAC using station in-depth material thicknesses, ply angles relative to the surface, and radii of curvature of the surface. Material thicknesses are obtained from Figure 12 using digitization. Ply angles (see Table 1) are calculated from the local nozzle slopes and fabric orientation in the CCP. For an illustration of ply angle orientation, see Figure 13.

Table 1. Ply angles calculated from local slopes in ref. [39]

Station 1	**Station 3**	**Station 6**	**Station 8**	**Station 10**	**Station 17**	**Station 19**
98.03	86.02	90.00	83.40	75.33	27.45	27.45
Station 20	**Station 21**	**Station 22**	**Station 23**	**Station 24**	**Station 25**	
27.45	27.45	27.45	27.45	27.45	27.45	

1D-element discretization divides each material's total thickness into several 1-mil thick elements. For example, at station 6, the thickness of CCP is 2064 mils and the steel backing is 325 mils. Thus 2064 elements are defined for the CCP and 325 elements for the steel backing. The total 1D-geometry thickness is 2389 mils or elements. See Figure 14 for an illustration. Use of 1 mil thick elements provides adequate discretization to make numerical error negligible. This is shown in Figure 15 and Table 2 where element discretization size is compared to calculated depth at station 6.

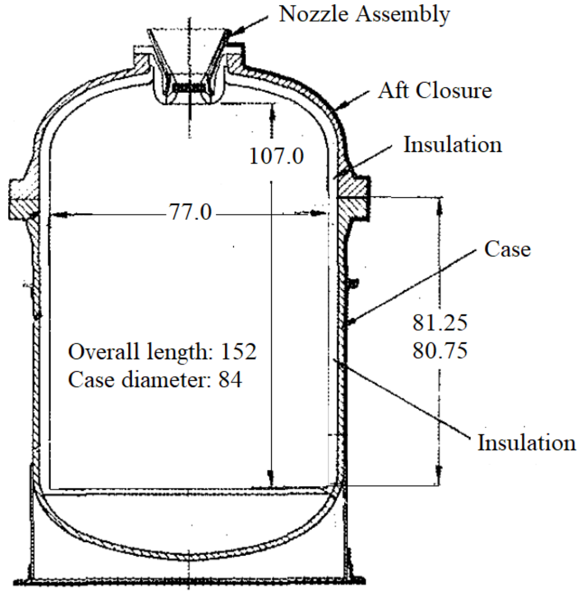

Figure 10. 84-in char motor. Modified from ref. [42].

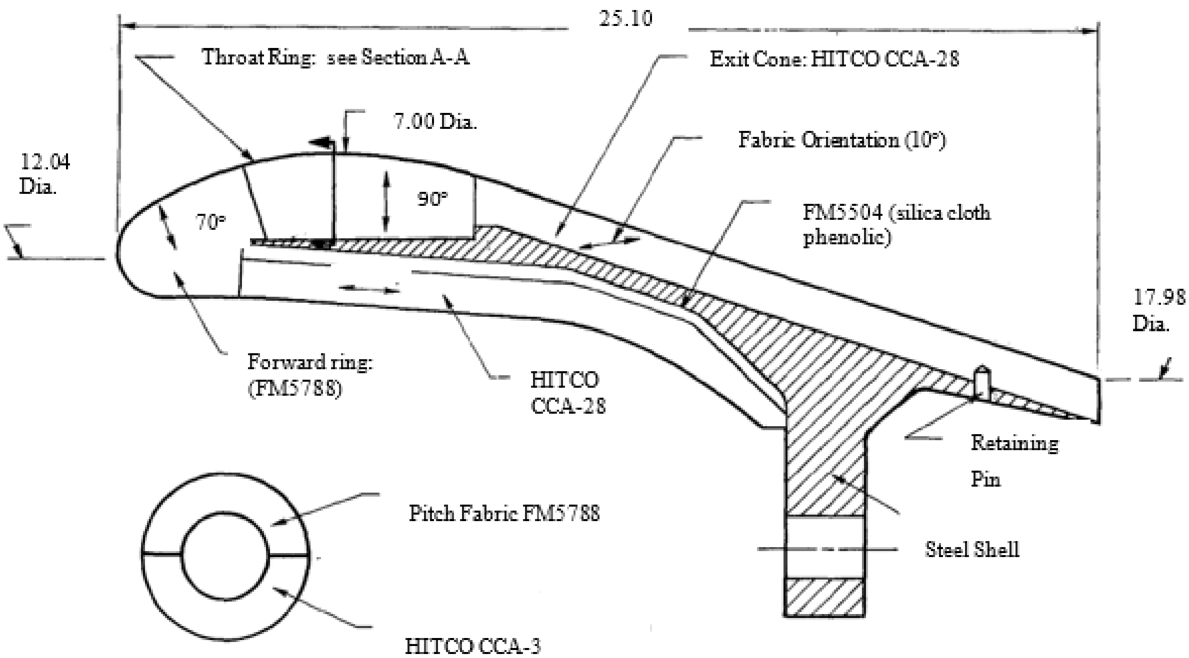

Figure 11. 2D Axisymmetric Model of the CM nozzle. Modified from ref. [39].

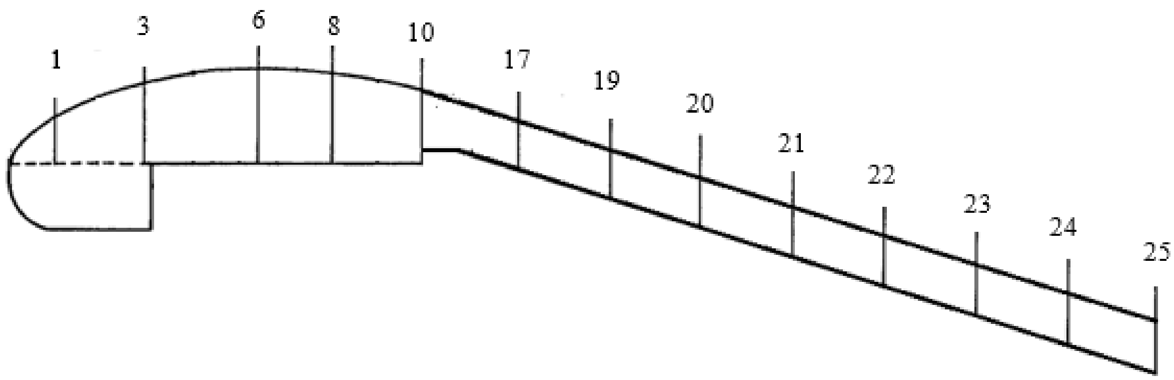

Figure 12. 2D Axisymmetric Model of the CM nozzle showing axial stations for ITRAC thermal analysis. Modified from ref. [39]

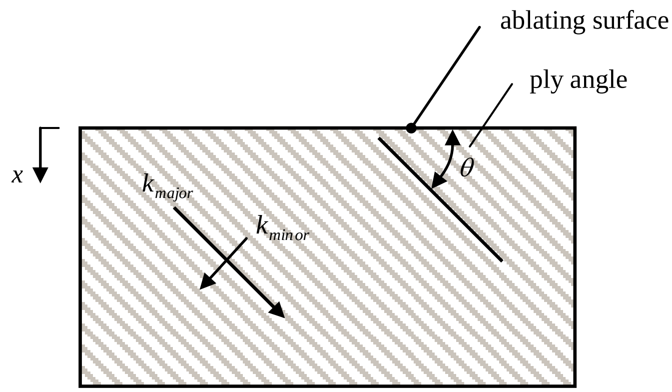

Figure 13. Ply angle orientation in ablative insulator.[35]

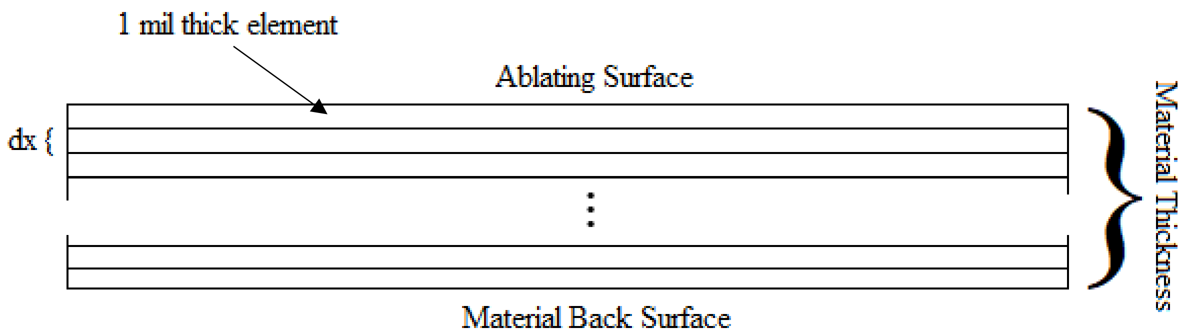

Figure 14. 1D computational model of a single station show elements of thickness, dx.

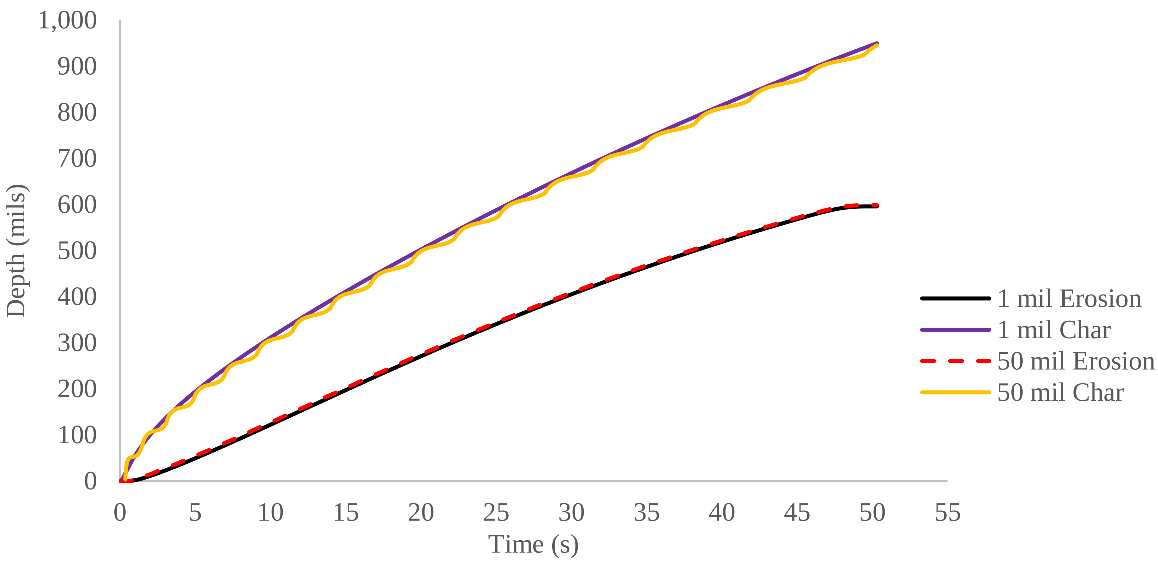

Figure 15. 1 mil element discretization vs 50 mil element discretization at station 6.

Table 2. Comparison of erosion and char depth as a function of element discretization at station 6.

Element Size (mils)	Erosion Depth (mils)	Char Depth (mils)
50	598.39	944.99
10	595.02	946.64
4	595.31	948.39
2	595.43	948.95
1	595.54	949.46
0.5	595.54	949.46

3.2 MATERIAL PROPERTIES

Material properties from ref. [39] for MX4926 are given in Table 3 and Table 4. These properties were used for over a decade and are reliable to the testing and analysis methods of that time frame.

Table 3. Density, kinetics, and heats of formation for MX4926 CCP.[39]

Property	Units	Value
ρ_v	lbm virgin/ft^3 virgin	91.30
ρ_c	Lbm char/ft^3 char	73.22
Virgin Resin Molecule	---	C_6H_6O
Char Resin Molecule	---	C
ρ_{o_1}	lbm initial a/ft^3 resin	60.75
ρ_{r_1}	lbm final a/ft^3 resin	32.40
ρ_{o_2}	lbm initial b/ft^3 resin	20.25
ρ_{r_2}	Lbm final b/ft^3 resin	0.000
ρ_{o_3}	lbm initial c/ft^3 reinforcement	97.40
ρ_{f_3}	lbm final c/ft^3 reinforcement	97.40
M_{F_r}	lbm resin/lbm virgin	0.330
V_{F_r}	ft^3 resin/ft^3 virgin	0.372
A_1	s^{-1}	9.76 x 10^8
A_2	s^{-1}	1.40 x 10^4
E_1	ft-lbf/lbmol	5.69 x 10^7
E_2	ft-lbf/lbmol	2.38 x 10^7
x_1	---	0.0825
x_2	---	0.1125
m_1	---	3.0
m_2	---	3.0
$h^0_{f,v}$	Btu/lbm virgin	-363.0
$h^0_{f,c}$	Btu/lbm char	0.0

Table 4.Specific heat, thermal conductivity, and pyrolysis gas enthalpy for MX4926 CCP.[39-40]

Temperature °R	Virgin Material			Char			Pyro Gas
	C_{p_v} $\left(\frac{\text{Btu}}{\text{lbm}\cdot°\text{R}}\right)$	$k_v \times 10^4$ $\left(\frac{\text{Btu}}{\text{ft}\cdot\text{s}\cdot°\text{R}}\right)$ 0°	$k_v \times 10^4$ $\left(\frac{\text{Btu}}{\text{ft}\cdot\text{s}\cdot°\text{R}}\right)$ 90°	C_{p_c} $\left(\frac{\text{Btu}}{\text{lbm}\cdot°\text{R}}\right)$	$k_c \times 10^4$ $\left(\frac{\text{Btu}}{\text{ft}\cdot\text{s}\cdot°\text{R}}\right)$ 0°	$k_c \times 10^4$ $\left(\frac{\text{Btu}}{\text{ft}\cdot\text{s}\cdot°\text{R}}\right)$ 90°	h_g $\left(\frac{\text{Btu}}{\text{lbm}}\right)$
500	0.21	1.39	2.36	0.21	1.83	3.11	---
800	0.36	1.58	2.69	---	---	---	---
1000	---	---	---	0.43	1.9	3.15	-1687
1160	0.36	1.83	3.11	---	---	---	-1536
1500	0.472	1.83	3.11	0.472	1.95	3.2	-1214
2000	0.484	1.83	3.11	0.484	2.35	4.15	-690
3000	0.493	1.83	3.11	0.493	5.4	8.95	833
4000	0.498	1.83	3.11	0.498	11.65	14.7	2806
5000	0.5	1.83	3.11	0.5	18.8	21.25	4175
6000	0.5	1.83	3.11	0.5	26.5	28.35	5620

3.3 BOUNDARY CONDITIONS

Two boundary conditions were imposed on the CM nozzle inside surface. The first is the heat transfer coefficient and the second is radiation heat flux. Heat transfer coefficients are discussed first.

Heat transfer coefficients in ref. [39] were predicted using the Aerotherm Real Gas Energy Integral Boundary Layer (ARGEIBL)[41] for the entire nozzle flame surface and again with Bartz's correlation[24] for two nozzle locations. ARGEIBL used the Aerothermal Chemical Equilibrium Computer Program[34] (predecessor to Chemics) to specify the boundary layer edge properties. The predicted heat transfer coefficients are shown in Figure 16. Heat transfer coefficients predicted using Bartz's correlation are indicated by black squares. ARGEIBL and Bartz's correlation appear to give similar results. The 2D-UQ study uses Bartz's correlation since ARGIEBL is not accessible. Chemics is used to generate inputs to recalculate Bartz's correlation for the entire flame surface. Bartz's correlation is shown in equation (3.1).

$$\rho_e u_e C_H = \frac{0.026}{D^{*0.2}} \left(\frac{\mu^{0.2} C_p}{Pr^{0.6}}\right)_o (\rho_e u_e)^{0.8} \left(\frac{\rho_{am}}{\rho_e}\right)^{0.8} \left(\frac{\mu_{am}}{\mu_o}\right)^{0.2} \left(\frac{D^*}{r_c}\right)^{0.1} \tag{3.1}$$

The terms in Bartz's correlation are: propellant gas stream (PGS) density (ρ_e), PGS velocity (u_e), Stanton Number for heat transfer (C_H), diameter at the throat (D^*), PGS viscosity (μ), PGS specific heat (C_p), Prandtl Number (Pr), PGS arithmetic (am) mean density and viscosity, and nozzle radius of curvature (r_c). The subscript o are for properties evaluated at chamber conditions. A comparison between AGRIEBL results from ref. [39] and Bartz's correlation recalculated with inputs from Chemics is shown in Figure 16. They are very similar except Bartz's correlation gives lower heat transfer coefficients in nozzle entrance regions. Arnold et al. say heat transfer predictions from both AGRIEBL and Bartz's correlation are reduced by 25% to be consistent with experiment results. No reference to these experimental results is given, but it is assumed they provide some level of anchoring applicable to the CM nozzle.

Chemics requires four inputs for boundary conditions and a fifth for mass transfer driving potentials in the boundary layer. The first input needed is the elemental mass or molar composition of the propellant. The mass elemental composition from ref. [39] is reproduced in

Table 6. The second and third inputs are average chamber pressure of the motor and initial propellant temperature. Figure 17 shows the measured chamber pressure during firing of the 84-in CM. Average chamber pressure calculated from this curve is 606 psi. The chamber pressure used in the original prediction in ref. [39] was 650 psi and this pressure is used in Chemics. It is uncertain what the initial propellant temperature was when the motor fired so it is assumed to be 530°R. From the first three inputs, Chemics calculates conditions in the motor chamber.

The fourth input (or inputs) needed are area ratios through the nozzle. Area ratios allow Chemics to calculate isentropic conditions through the nozzle. Area ratios are not provided by Arnold et al. except at two locations. The remaining stations are estimated by digitizing the geometry in Figure 11. Digitization returns area ratios of 1.43 and 5.59 compared to 1.44 and 5.58 from ref. [39]. This is less than 1% error from digitization.

The final input is pyrolysis gas elemental composition. This is replicated from ref. [39] in Table 7. Pyrolysis gas elemental composition is used in conjunction with propellant element composition to calculate the mass transfer driving potentials from equation (2.22) in Chapter 2.

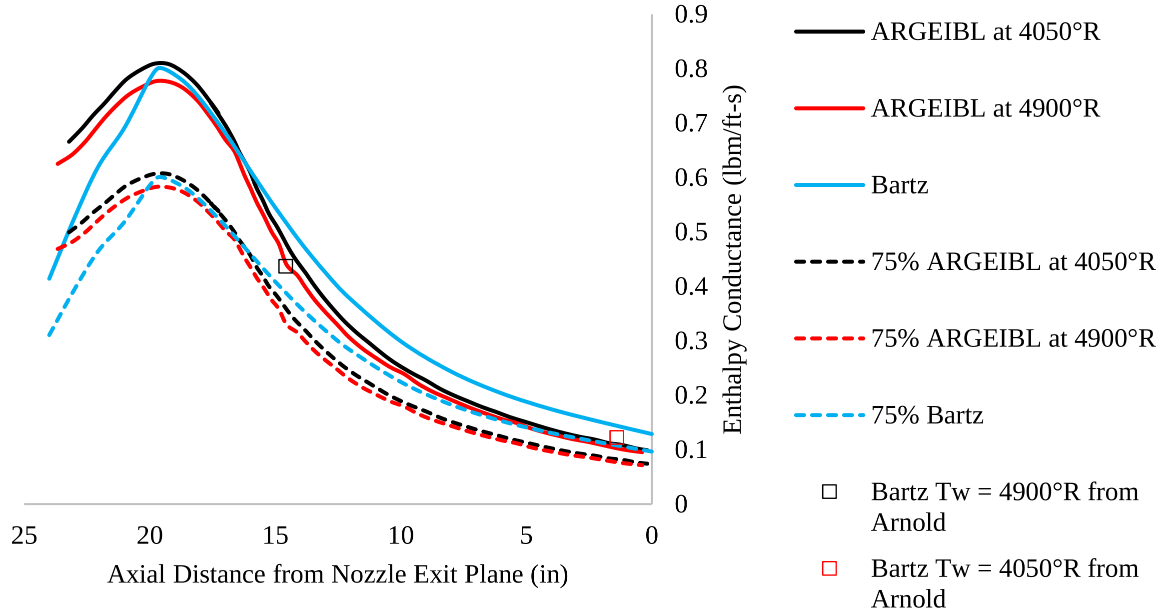

Figure 16. ARGEIBL heat transfer prediction vs Bartz Correlation. Curves reduced 25% are also shown to be consistent with predictions from ref. [39].

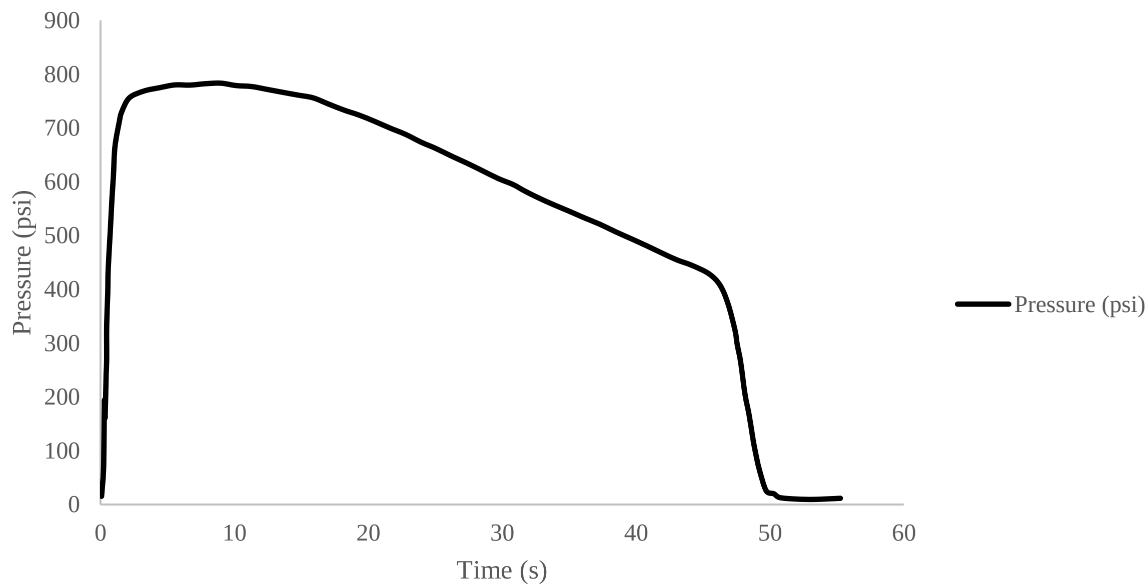

Figure 17. Measured pressure during firing of the 84-in CM.[39]

Table 5. Area Ratios for the CM nozzle.

Station 1	**Station 3**	**Station 6**	**Station 8**	**Station 10**	**Station 17**	**Station 19**
1.71	1.20	1.00	1.05	1.27	1.72	2.22
Station 20	**Station 21**	**Station 22**	**Station 23**	**Station 24**	**Station 25**	
2.75	3.38	4.06	4.80	5.59	6.43	

Table 6. Elemental composition of propellant used in the 84-in CM.[39]

Element	Symbol	$\mathcal{MW}$	M_F in Propellant
Hydrogen	H	1.008	0.03752
Carbon	C	12.001	0.11303
Nitrogen	N	14.007	0.08792
Oxygen	O	16.000	0.39023
Aluminum	Al	26.710	0.16000
Chlorine	Cl	35.457	0.21121
Iron	Fe	55.850	0.00007

Table 7. Pyrolysis gas elemental composition.[39]

Element	M_F in Pyrolysis Gas	M_F in Char Material
H	10.71%	0
C	60.96%	1
O	28.33%	0

The second boundary condition is incident radiation heat flux calculated from the correlation provided in ref. [39].

Chemics calculates this value using equation nozzle propellant gas temperatures and emissivity input by the user. Equation (3.2) is used for effective emissivity ($\boldsymbol{\varepsilon_e}$) and equation (3.3) for emissivity of the propellant gases ($\boldsymbol{\varepsilon_g}$). Inputs into (3.3) are surface emissivity ($\boldsymbol{\varepsilon_s}$), density of the particle laden stream ($\boldsymbol{\rho_h}$), local nozzle diameter ($\boldsymbol{D_l}$), and mass fraction of aluminum ($\boldsymbol{M_{F_{Al}}}$) in the propellant. Emissivity for MX4926 is 0.85[39] and is constant over the entire temperature range[40]. Propellant gas density is calculated by Chemics throughout the nozzle. Local diameter is taken from the geometrical model and $\boldsymbol{M_{F_{Al}}}$ is taken from

Table 6. The radiation heat flux can be calculated using equation (2.18) assuming blackbody radiation ($\alpha_{abs} = \varepsilon_e = 1$) calculated by Chemics. The flux is shown as a function of axial location in Figure 18 along with blackbody radiation heat flux. With the information in this chapter, ITRAC input files can be created. The ITRAC input file at the station 6 can be found in Appendix A as an example.

$$\varepsilon_e = \frac{1}{\frac{1}{\varepsilon_s} + \frac{1}{\varepsilon_g} - 1} \tag{3.2}$$

$$\varepsilon_g = 1 - \exp\left(-\frac{0.808}{16} M_{F_{Al}} \rho_H D_l\right) \tag{3.3}$$

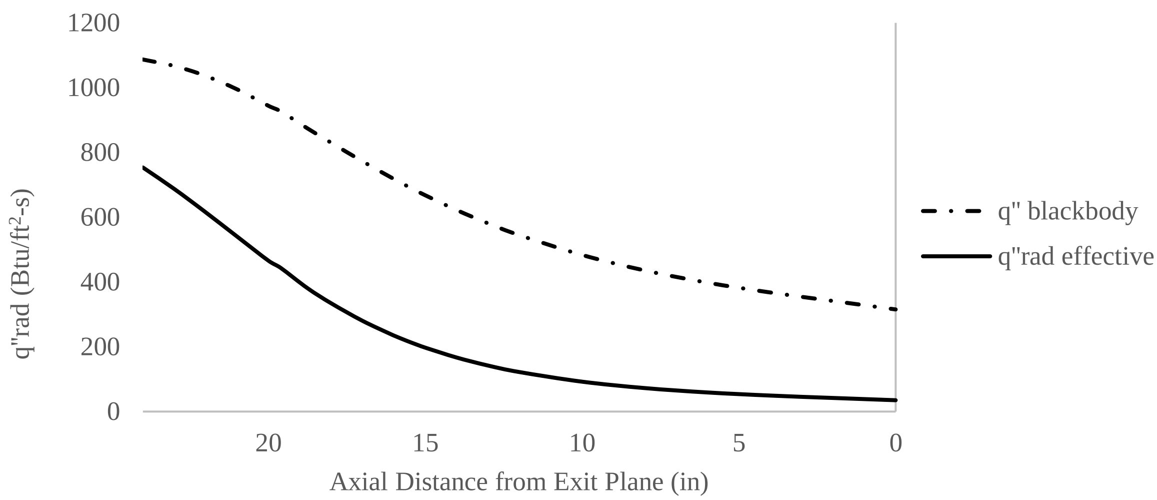

Figure 18. Incident radiation heat flux from the gas stream as it flows through the nozzle.

CHAPTER 4: INPUT UNCERTAINTIES AND DISTRIBUTIONS

In performing a UQ study, the probabilistic nature of the modeling inputs must be established. Performing sensitivity studies and uncertainty propagation requires explicit definition of a probability density function (PDF) to represent each input. The type of distribution must be defined along with the parameters of the distribution. For engineering applications, it is practically never the case that all input parameters have sufficient numbers and consistency to perfectly inform the definition of the distribution. As a result, the practitioner must often pull from multiple sources, assumptions, and engineering knowledge to build a belief about the parameter of interest. In this chapter, the information used to inform the development of input distributions is presented.

A primary difficulty in estimating uncertainty in inputs is the sparsity of data available in the open literature. The problem of data availability is also mentioned by Copeland et al.[10] in their work on-reentry vehicles. Data sparsity occurs due to the proprietary nature of the materials as they are developed and characterized. Other common limits to property data release arises from ITAR, national security classification and because only nominal values reach the literature. Property data sparsity has become so commonplace that many investigators have adapted by using theoretical ablatives such as TACOT[46], a fictitious material used for evaluation of ablation modeling tools.

As uncertainty is discussed, material properties and boundary conditions are collectively called inputs while erosion and char depth are collectively called outputs or SRQs. Each input is characterized as being aleatory or epistemic. Aleatory uncertainty is due to inherent randomness or natural variation (e.g. diameter of fruit on a tree) and epistemic uncertainty is due to lack of knowledge[6][25] (e.g. don't know the type of fruit). In general, physical quantities such as density are aleatory and follow normal distribution behavior. Although uncertainty could be reduced by better process control, it cannot be eliminated. Boundary conditions may be aleatory, epistemic, or both. Turbulence in the boundary layer has some inherent randomness, but because it is difficult to accurately predict that randomness, it carries epistemic uncertainty with it. In general, inputs with epistemic uncertainty follow a uniform distribution since the true input value is unknown, but assumed to exist over some interval.

When uncertainties are determined they are represented with coefficient of variation (CV), and a representative distribution. The CV is the ratio of the standard deviation in the data to the average in the data.

$$CV = \frac{\sigma}{\mu} \tag{4.1}$$

The average and standard deviation are not always calculated in the same way. If several data exist for a given property, then the average and standard deviation is calculated by

$$\mu = \frac{1}{N}\sum x_i \tag{4.2}$$

$$\sigma = \sum \frac{(x_i - \mu)^2}{1 - N} \tag{4.3}$$

If data are lacking or bounds are used, the average is taken as the central point between the upper and lower bound. The standard deviation is calculated by taking the upper bound in the data minus the lower bound in the data divided by 6. This assumes that the bounds represent $\mu \pm 3\sigma$. In other cases, the standard deviation may vary as a function of temperature or location. The CV may then be represented as an average of the deviations divided by the nominal value at that temperature and/or location.

After the CV is estimated for each input, a probabilistic statement is made concerning the distribution of uncertainty about an average value or whether the uncertainty is best represented as an interval. For types of distributions and their applications, one is referred to refs. [47-48]. Given the sparsity of data, the type of distribution can be subjective, and uncertainty could be prescribed to the assumed distribution. Distribution uncertainty is considered an area of future work.

Once the CV's and distributions are established, they are applied to the values in Table 3, Table 4, and the boundary conditions in Chapter 3. To be clear, the average values obtained in the literature are only used to inform the CV and the distribution. The original material properties and boundary conditions from Chapter 3 are considered to be the nominal or average values. The purpose in this is because the CM nozzle model with associated material properties and boundary condition are anchored to "experimental data" and if modified (even if believed to be incorrect) to a new nominal it would uproot the model's experimental data anchor. Since the experimental data are not available it is not possible to correct the model and then re-anchor to the data. Correcting the nominal values or models are an area of future work.

4.1 UNCERTAINTY IN VIRGIN AND CHAR MATERIAL DENSITY, ρ_v AND ρ_c

Virgin material density of MX4926 CCP has the following reported values: 91.30 lbm/ft^3[39], 89.4 lbm/ft^3[40], 94.27 lbm/ft^3[48], 90.6 and 89.9 lbm/ft^3[49], and 87.39 lbm/ft^3[43]. This results in an average value of 90.48 lbm/ft^3 with a CV of 2.53% using equations (4.2-4.3). Using the difference between the maximum and minimum density values gives a CV of 1.27%

It is also specified by Clayton el al.[48] that virgin density is 89.90 $\pm$ 1.25 lbm/ft^3 (CV = 0.46%, assuming that range represents $\mu \pm 3\sigma$ bounds). A nominal value of 90 $\pm$ 5 lbm/ft^3 for GCP is mentioned in ref. [50]. The resulting CV for GCP is 1.85%. Some of the GCP samples have resin mass fractions as large as 50% compared to the 30-38.5% allowed in cured MX4926 material[51].

A quick estimate of virgin density is made by varying the mass fractions of resin, reinforcement, and volatiles in MX4926 CCP. The resin density from Table 3 is 20.25 lbm/ft^3 + 60.75 lbm/ft3 = 81.00 lbm/ft^3 and the reinforcement density is given as 97.40 lbm/ft^3. The range in M_{F_r} is 30-38.5% and for M_{F_V} it is around 0-2.5%[51] to 0-3%[44]. Assuming the volatiles are mostly water, this results in a range on virgin density between 90.04-92.48 lbm/ft^3 (CV = 0.45%). This may be an underestimation since it doesn't capture any variation on resin and reinforcement density.

Another estimate on uncertainty in virgin density is inferred from manufacturing specifications on CCP material properties[24][44][51]. Reported specification limits on cured virgin density of MX4926 CCP from ref. [20] are 87.4 lbm/ft^3 to 94.89 lbm/ft^3. Assuming these limits represent $\mu \pm 3\sigma$ the average value is 91.14 lbm/ft^3 with a CV of 1.37%. It is assumed that 1.37% is conservative since modern manufacturing techniques would have lower process control limits to avoid risk in material wastage or worse, materials in use that are outside specification. The 1.37% value is used as the estimated CV against 91.30 lbm/ft^3 in Table 3. This input is aleatory, and its distribution is assumed to be represented by a Gamma distribution. This distribution is often used for physical quantities.[48] This distribution is used in leu of a normal distribution because process controls are assumed to make values in and beyond the specification limits less probable.

Char material density from Table 3 is 73.22 lbm/ft^3. This value is inferred by the resin mass fraction, M_{F_r}, and phenolic resin char yield (r), given by equation (4.4)

$$\rho_c = \left[1 - M_{F_r}(1 - r)\right]\rho_v \tag{4.4}$$

The value for r can be found by combining the final values for resin density divided by the combined initial values for resin density as shown in equation (4.5). This results in the resin char yield of 40%. This value for resin char yield was first reported by Ehlers[52]. The report isn't retrievable in the open literature, but it appears to be applicable to phenol formaldehyde resin.

$$r = \frac{\rho_{r_1} + \rho_{r_2}}{\rho_{o_1} + \rho_{o_2}} \tag{4.5}$$

Char density may also be inferred using thermal gravimetric analysis (TGA)[53] on virgin CCP using equation (4.6) and the char yield of the composite CCP (R), or on pure resin and r as given above. A demonstration of both methods is given below.

$$\rho_c = R\rho_v \tag{4.6}$$

Equation (4.6) above is analogous to equation (2.2) in the ITRAC theory. Where $R = 1 - x_{tot}$. The relationship between r, M_{F_r}, and R expresses the assumption that mass loss from the decomposing CCP material is entirely from the decomposition of phenolic resin. As a brief summary, TGA is the process of placing a virgin material sample into a (typically inert) gas chamber or evacuated chamber. The chamber undergoes heating at a constant heating rate (e.g. 20°C/min) and mass loss is measured simultaneously. Isothermal TGA can also be performed by placing the sample into an oven at a fixed temperature and measuring mass loss over time as the sample comes into equilibrium with the oven's environment. For additional background on TGA, one is directed to refs. [53-54].

There are some data in the open literature on R for MX4926 or char density has been measured directly from charred samples[48-50]. TGA values for R from material initially in a virgin state are given by Clayton et al.[48] as 82.5% at 1800°F and 81.2% at 1890°F. The TG analyzer used a He atmosphere and the samples were heated 9.5-10°F/min. Clayton et al.[48] also created 17 charred samples at different oven temperatures and then performed TGA after-the-fact. Total mass loss (mass loss in oven plus mass loss from TGA) from the 17 charred samples are shown in Table 8. Combining TGA mass loss from virgin samples and total mass loss from charred samples gives an average R of 82.82% with a standard deviation of 0.0109. When combined with the variation in ρ_v the CV for ρ_c is 2.68%. As a reference, the value on char density for GCP[50] is given as 76 ± 6 lbm/ft^3. This results in a CV of 2.63% for GCP.

Table 8. TGA on charred samples created in an oven.[50]

84.1%	81.7%	82.6%	82.5%	82.6%	82.4%	82.4%	80.7%
82.2%	84.5%	84.2%	83.5%	84.7%	83.7%	83.4%	---

Like what was done for ρ_v, uncertainty in ρ_c is inferred by limits from material specifications, although it is not as simple. The nominal R value[55] provided by the manufacture of MX4926 is 83.5%. This is consistent with what was measured by Clayton et al.[48] although it is higher than the 80.2% used by Arnold et al.[39] for the CM nozzle. The manufacturer value for r is 51.46%. This is also larger than the r = 40% used for the CM nozzle. A compilation of r values taken from the literature is given below in Table 9. Table 9 only includes SC1008 resin char yield since this resin is used in MX4926 CCP[48]. The SC1008 resin char yield values in Table 9 are greater than 40% reported by Ehlers[52] (included in the table for comparison). Char yield on similar resins is available in the literature[56-65] and these also have higher char yield than that reported by Ehlers.

Several of the SC1008 resin samples are performed at relatively small heating rates that would only be applicable to in-depth CCP heating compared to what is seen in a SRM nozzle at the CCP surface. The work by Stokes[66] provides TGA data that are more representative to surface conditions. Given this compiled char yield data from TGA at low and high heating rates, it is estimated that r may vary $\pm$ 10%.

Using 10% variation on r, specification limits on M_{F_r} for cured CCP (30% - 38.5%), and 1.37% CV in ρ_v, variation in ρ_c is inferred from equation (4.4). The resulting CV is 3.60% and is assumed to be conservative for a couple reasons. One reason is control processes generally have tighter control bands to avoid exceeding limits. This is observed in Figure 19 where most of the resin solids are within a tighter band (33%-36%) than the limits specify. Another reason is the test[44] to determine cured resin content includes the mass of any volatile content trapped in the cured composite material at the time the test is performed. In fact, the test has a doubling effect on the volatiles present in the CCP, so the calculated cured resin content is higher than it actually is (resin content + 2.06 $\times$ volatile content).

A CV of 3.60% is chosen against a nominal ρ_c value of 73.22 lbm/ft^3. This input is aleatory, and the distribution is assumed to be represented by a Gamma distribution. This distribution is chosen because process controls make the values at or beyond the specification limit less. In addition, the test (discussed above) to calculate resin content is an overestimation.

Table 9. Compilation of char yield data for SC1008 phenolic resin.

r	Ref.	Environment	Heating Rate (°C/min)	r	Ref.	Environment	Heating Rate (°C/min)
40.00%	[52]	---	---	51.74%			100
56.26%	[67]	Nitrogen	20	49.86%			300
56.17%	[68]	Nitrogen	20	49.99%			300
56.33%	[69]	Nitrogen	5	50.65%			300
55.76%	[70]	Argon	---	50.89%			300
55.47%	[71]	Vacuum	---	51.38%			300
58.49%	[72]	Nitrogen	10	49.24%			650
60.71%	[73]	Nitrogen	10	49.81%			650
60.90%	[73]	Helium	5	49.90%			650
62.77%	[73]	Vacuum	5	50.36%			650
50.21%	[74]	Inert	10	50.45%			650
60.00%	[75]	---	---	50.52%			650
52.17%	[76]	---	---	50.89%			650
42.58%	[77]	Inert	0.5	48.33%			1280
43.38%	[77]	Inert	1	48.78%			1280
44.98%	[77]	Inert	10	49.07%			1280
50.78%	[66]	Argon	0.25	49.86%			1280
51.11%			0.25	50.18%			1280
52.22%			0.25	50.30%			1280
50.44%			3	50.43%			1280
50.73%			3	50.61%			1280
50.93%			3	47.41%			2500
49.53%			20	47.77%			2500
50.35%			20	48.03%			2500
50.59%			20	48.20%			2500
50.70%			20	48.44%			2500
48.97%			100	49.10%			2500
49.97%			100	49.30%			2500
50.06%			100	49.39%			2500
50.75%			100	49.69%	[66]	Argon	2500

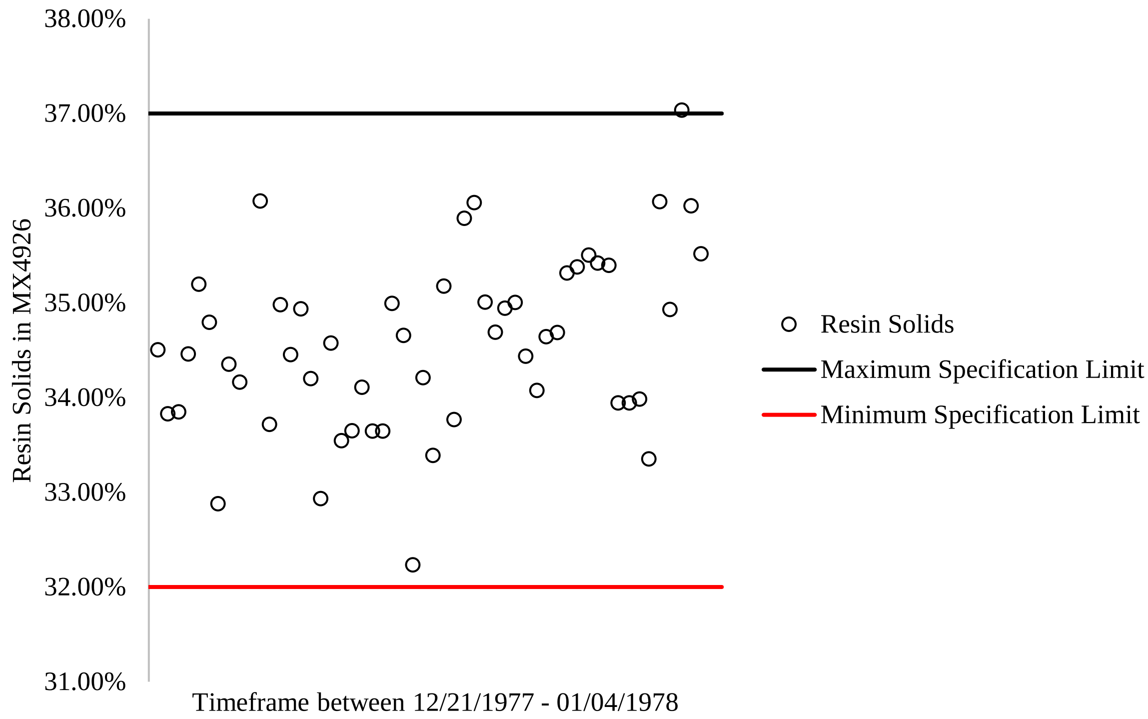

Figure 19. Percent of resin solids measured in uncured MX4926 CCP.[78]

4.2 UNCERTAINTY IN VIRGIN AND CHAR MATERIAL SPECIFIC HEAT, C_{p_v} AND C_{p_c}

Uncertainty in specific heat is based on enthalpy data. It is assumed that error in enthalpy data is equivalent to error in its derivative (i.e. specific heat). Enthalpy of MX4926 was measured by Clayton et al.[48] using vented and unvented capsules. It is qualitatively mentioned to compare well with enthalpy data from Pears et al.[79]. Unfortunately, the data from Pears et al. are not retrievable and the comparison cannot be quantified.

Only MX4926 virgin enthalpy data are provided by Clayton et al. and are reproduced in Figure 20. There are curve fit equations for virgin and char specific heat in Clayton et al. for reference. Instead of using the curve fit equations from Clayton et al. a new curve fit through the measured virgin enthalpy is made to represent average enthalpy as a function of temperature. The difference between the new curve fit and the measured data has an average absolute error of 7.31%. The accuracy of the enthalpy measurements is stated to be conservatively within $\pm$ 5% by Clayton et al. When the measured enthalpy data are allowed to shift $\pm$ 5% the average absolute error between the new curve fit and the measured data increases to 9.42%. This 9.42 % value is used as one point of reference.

Another point of reference for specific heat variation is NARMCO 4028 CCP enthalpy data reported in ref [80]. The enthalpy data on NARMCO 4028 are reproduced in Figure 21. The virgin enthalpy data are from six samples and the char data is from 2 samples. A curve fit of this enthalpy data has an absolute average error of 3.94% with the virgin data and 4.82% for char data. Adding the 5% error noted by Clayton et al. increases the absolute average error to 7.04% for virgin enthalpy and 6.55% for char enthalpy.

Finally, specific heat data in ref. [50] include 7 virgin samples and 1 char sample of GCP material. The specific heat data from these samples are said to be bound by $\pm$ 20%. This bound is nearly double the max and min of the data. Given the large range in lot-to-lot resin content and density in the GCP material, the data and the assumed bound may be an overestimate for the MX4926 material considered here.

Based on 9.42% uncertainty for MX4926 virgin CCP, 7.04% uncertainty for NARMCO virgin CCP, and 6.55% uncertainty for NARMCO char CCP, the specific heat is estimated to vary $\pm$ 10% or a CV of 3.33%. The distribution is assumed to be normal since the enthalpy data are scattered evenly across the curve fits and values away from the curve are less likely.

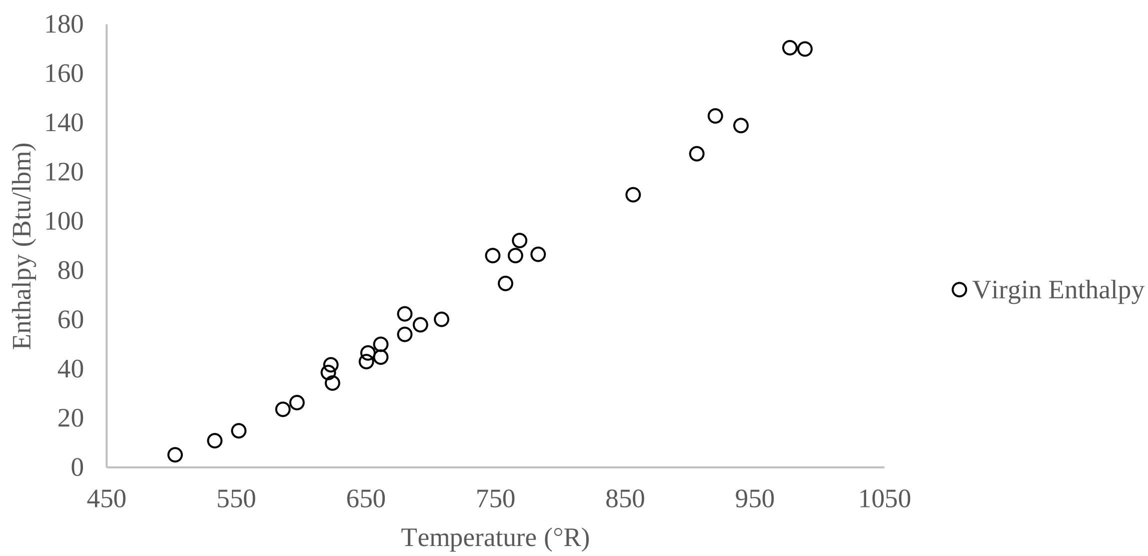

Figure 20. Enthalpy of Virgin MX4926 CCP.[48]

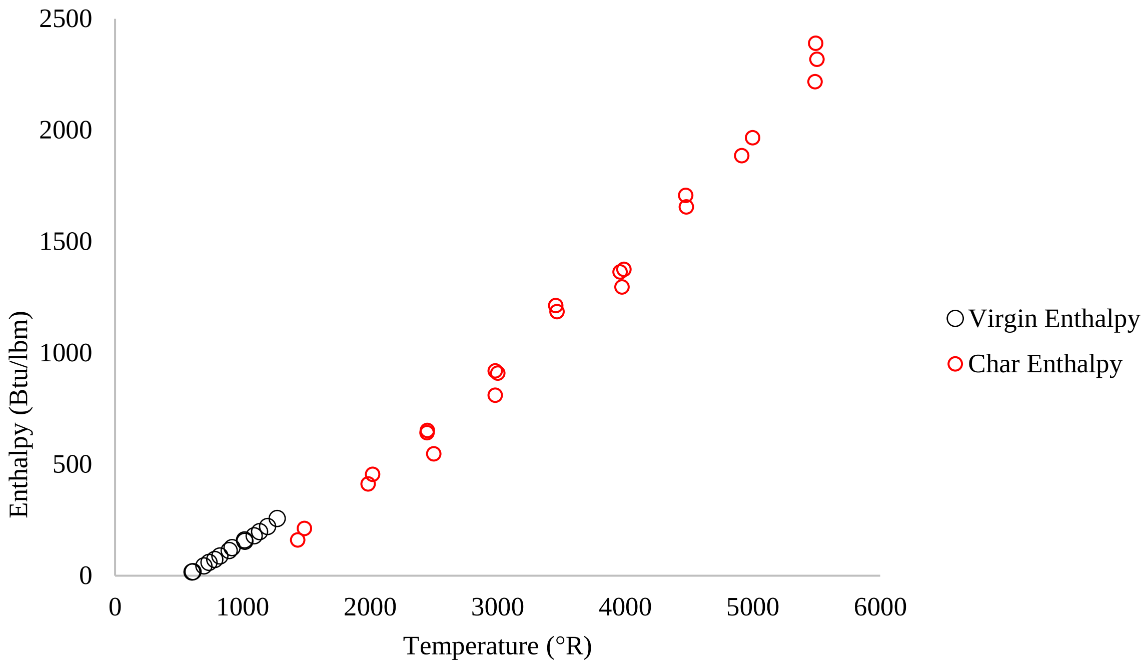

Figure 21. Enthalpy of Virgin and Char NARMCO 4028 CCP Material.[80]

4.3 UNCERTAINTY IN VIRGIN AND CHAR MATERIAL THERMAL CONDUCTIVITY, k_v AND k_c

MX4926 is a matrix of carbon cloth or carbon cloth plies laid on carbon-filled phenolic resin and the thermal conductivity through the material is anisotropic. In ITRAC, thermal conductivity is calculated using virgin and char states, extent-of-reaction, and the ply angle, θ. This is shown in equations (4.7-4.9) and ply angle is illustrated in Figure 13 above.

$$k_{s_i} = k_{v_i}(1-\alpha) + \alpha k_{c_i} \tag{4.7}$$

Here, i is either resin (r) or fiber (f) reinforcement. The overall thermal conductivity is then:

$$k_s = k_{s_r}\sin^2\theta + k_{s_f}\cos^2\theta \tag{4.8}$$

Using the relationship, $\cos^2\theta = 1 - \sin^2\theta$, equation (4.8) can be rewritten as:

$$k_s = k_{s_f}\left[1 + \left(\frac{k_{s_r}}{k_{s_f}} - 1\right)\sin^2\theta\right] \tag{4.9}$$

The uncertainty in k_s is based on dispersion relationships[44] shown in equation (4.10). Equation (4.10) is like the form in equation (4.9), but also includes the influence of carbon cloth reinforcement volume fraction (P_f). This method of creating dispersions on k_s is analogous to varying ρ_v and ρ_c using variability of M_{F_r} in the composite matrix.

$$k_s = \frac{k_f + Ak_r}{Bk_f + Ck_r}\left\{k_r + \left[\left(C - \frac{1}{P_f}\right)k_r + Bk_f\right]\frac{P_f}{2}\sin^2\theta\right\} \tag{4.10}$$

In equation (4.10), k_f is the reinforcement fiber isotropic or axial thermal conductivity; k_r is the continuous phase resin, or pyrolysis residue isotropic thermal conductivity; A, B, and C are functions of P_f.

$$A = 0.24P_f^{-2} \tag{4.11}$$

$$B = \left(1 - P_f\right)^2 \tag{4.12}$$

$$C = 2 - 25P_f^4\left(1 - P_f\right)^2 \tag{4.13}$$

The correlations and ranges of applicability for k_f and k_r are as follows:

$$k_f = 0.000503\,ln(T) - 0.0266;\ 450 < T < 1400°R \tag{4.14}$$

$$k_f = 0.0026\left(\frac{T}{1400}\right)^{-5} + 0.0146\left(\frac{T}{2000}\right)^{1.95};\ T > 1400°R \tag{4.15}$$

$$k_r = k_{rv}(1 - \alpha) + \alpha k_{rp} \quad (4.16)$$

$$k_v = 6.99 \times 10^{-4} + 17.4 \times 10^{-7}T;\ T > 450°R \quad (4.17)$$

$$k_p = 0.0008 + 1.5 \times 10^{-7}T + 10^{-4}\left(\frac{T}{3250}\right)^6;\ T > 450°R \quad (4.18)$$

Here, α is the extent of reaction discussed previously in Chapter 2, k_{rv} is the thermal conductivity of the virgin carbon-filled resin material, and k_{rp} is the thermal conductivity of the carbon-filled char residue.

Letting k_s vary as a function of θ (0 and 90°), temperature, T (536-6000°R), and P_f (0.4 – 0.5) [44] results in the dispersed thermal conductivity shown in Figure 22 along with the 7-in Char model thermal conductivity for comparison. This figure is a composite of virgin and char conductivities, meaning the virgin conductivity is blended with the char conductivity at each layup angle. Blending is between 1000°R and 3400°R. These temperature bounds are defined by Minges[49] as the upper bound on stable virgin material (upper bound of 1000°R) and the lower bound on mature char (lower bound of 3400°R).

Figure 23 shows the variation as a function of layup angle and temperature. Variation is calculated by taking the high bound minus the average and dividing the difference by the average. As noted in ref. [43] and apparent here, variation increases with temperature as decomposition occurs. Since the decomposition is in the resin, low layup angles (through-ply) have larger variation than thermal conductivity across the ply. The average variation of k_v is $\pm\frac{28.20\%}{18.68\%}$ and $\pm\frac{20.25\%}{16.52\%}$ at 0° and 90° respectively; average variation of k_c is $\pm\frac{47.34\%}{28.20\%}$ and $\pm\frac{22.82\%}{20.21\%}$ at 0° and 90° respectively. The estimated CV for k_v is 8% at 0° and 7% at 90°. The estimated CV for k_c is 13% at 0° and 7% at 90°.

The assumption on the distribution of k_v and k_c is that they are normally distributed quantities. The normal distribution is chosen because the volume fraction of fiber is tied to a specification limit that would force fiber volume fraction values away from the center of the specification limits to be less likely to occur. The distribution is not limited further using a gamma function because thermal conductivity of resin and fiber were given as deterministic values and using the entire volume fraction range given in ref. [43] compensate for that.

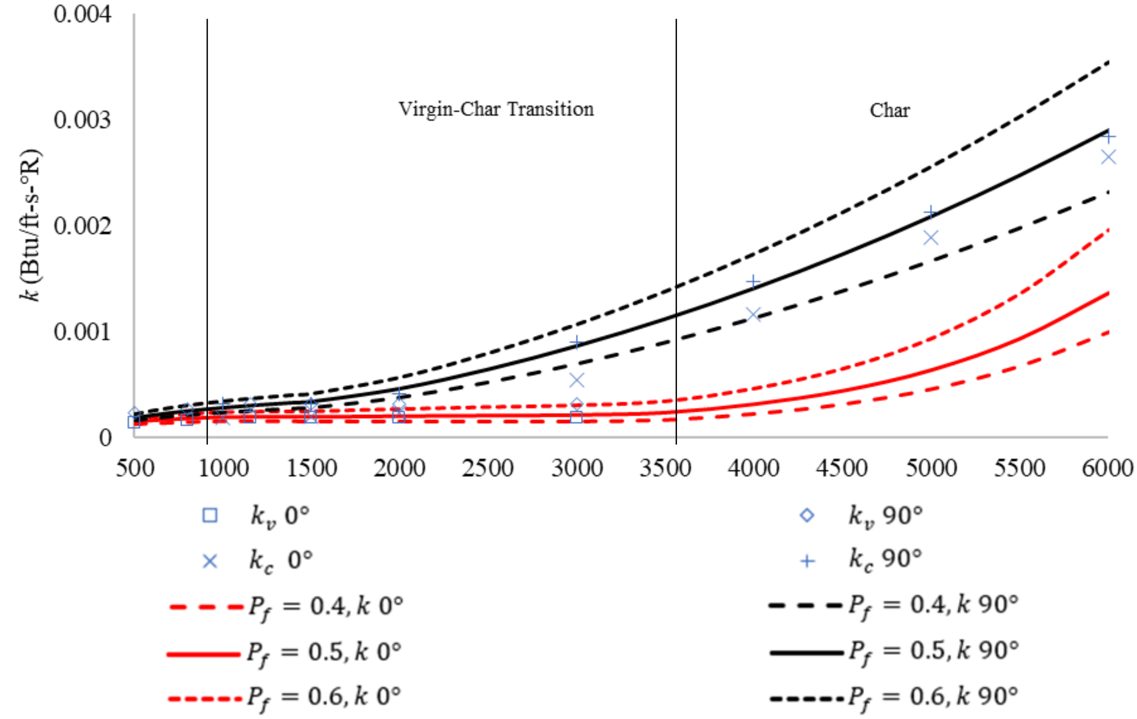

Figure 22. Composite thermal conductivity of virgin and char CCP at 0° and 90° layup angles compared to values given for MX4926 CCP from ref. [39].

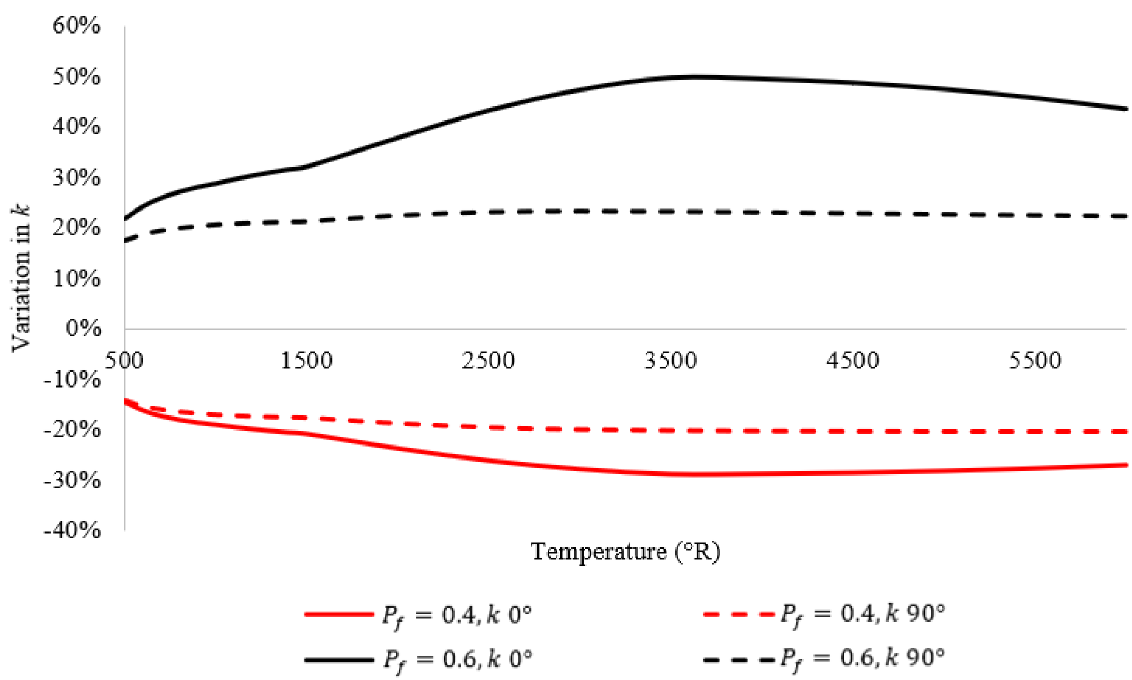

Figure 23. Uncertainty in k taken from Figure 22.

As an aside: Most of the available thermal conductivity data in the literature for MX4926 and other CCP material are on oven produced chars. Data on oven produced chars has large uncertainty for two reasons. 1. Systemic error: Clayton[43] give an accuracy of thermal conductivity measurements is $\pm$ 12% for k_v and $\pm$ 25% for k_c due to difficulty in measurements at high temperatures with ensuing kinetic effects. These systemic uncertainties are not included in the uncertainty on k because the reinforcement volume fraction range is larger than that found in MX4926 to compensate. 2. Kinetic effects: There is a large difference between measured thermal conductivity of char material produced in a laboratory oven (slow heating rate) and the measured thermal conductivity of char material produced in a rocket nozzle since the decomposition of resin is a function of both temperature and time. Figure 24 below illustrates kinetic rate effects.

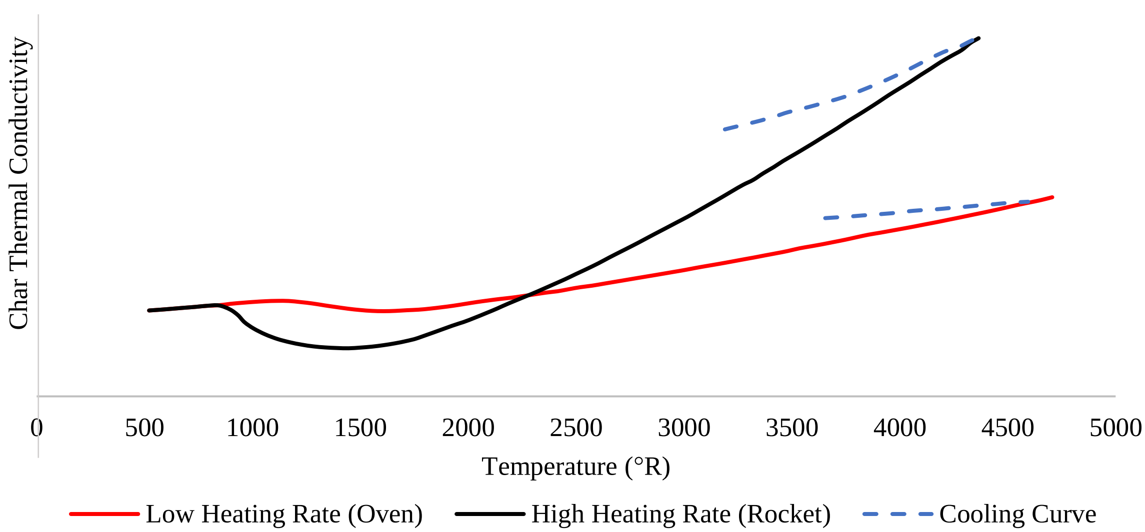

Figure 24. Effect of heating rate on char thermal conductivity.[49]

Greater accuracy on k applicable to rocket nozzle environments can be obtained using thermal response or dynamic modeling[81]. This method was first employed by Aerotherm in 1964 according to ref. [40]. An example of thermal response modeling is taking a 4-in x 4-in x 1-in thick composite sample, embedding thermal couples at various depths front-to-back through the thickness and imposing a known heat flux on the front 4-in x 4-in surface using a torch[82-83], a high energy laser[84], or an arc-image pyrolysis apparatus[85].

The boundary condition is more analogous to a rocket nozzle and is well characterized. The model's thermal conductivity is adjusted until the code prediction matches the thermocouple temperature data. An example of thermal response modeling is shown below in Figure 25.

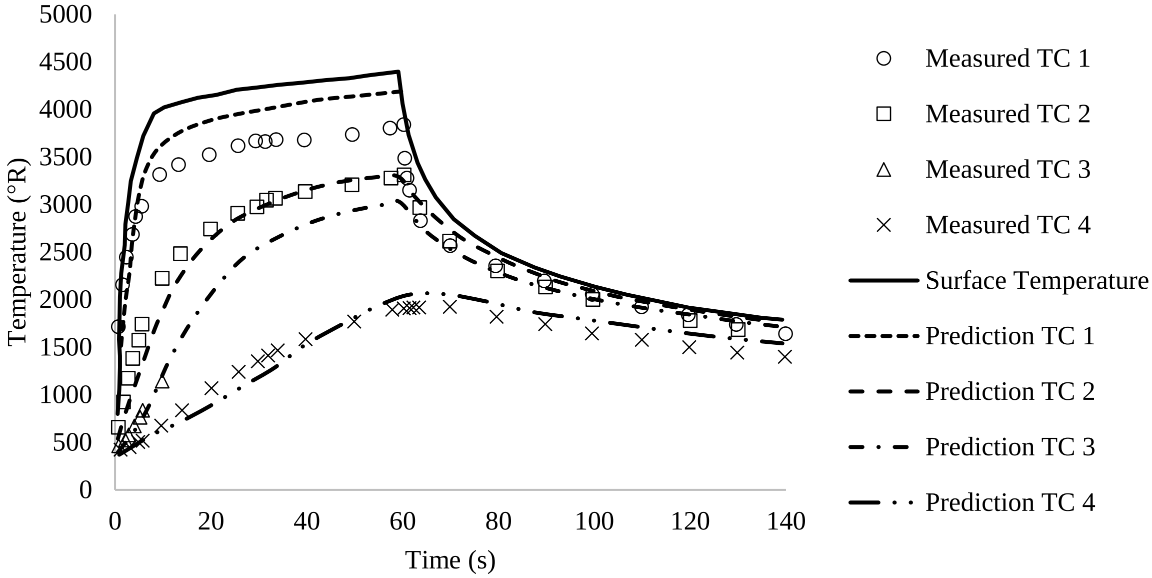

Figure 25. Thermal Response of MX4926 at 90°-degree layup angle.[40]

A compilation of these types of tests on MX4926 would be useful to establish aleatory variation in thermal conductivity. The assumed $k(T)$ model and its ability to predict several sets of thermal response modeling could be used to establish any model form error or support thermal conductivity modeling improvement.

4.4 UNCERTAINTY IN MATERIAL HEAT OF PYROLYSIS AND PYROLYSIS GAS ENTHALPY, Q_p AND h_g

Heat of pyrolysis (Q_p) is not a property given in ref. [39]. Q_p is obtained using the relationship in equation (4.19) where h_f^0 is the heat of formation of virgin (v) CCP from Table 3 and heat of formation of pyrolysis gas (g).

$$\left[Q_p = \frac{h_{f,v}^0}{1-R} + h_{f,g}^0\right]_{536°\mathrm{R}} \tag{4.19}$$

Arnold et al.[39] use a $h_g(T)$ curve that is negative at low temperatures with a $h_{f,g}^0$ of 0 Btu/lbm. In ITRAC, the $h_g(T)$ is offset (by extrapolation) to 0 Btu/lbm at a reference temperature of 536°R. The resulting offset to 536°R changes $h_{f,g}^0$ to -2126 Btu/lbm. The value for Q_p at 536°R is then 293 Btu/lbm. This offset and the values described above are given in the ITRAC input file in Appendix A. Since Q_p incorporates the heats of formation, only variation in Q_p is considered.

Q_p is varied using resin char yield, r, and heat pyrolysis data from Ladacki et al.[71]. Ladacki et al. measure Q_p at different temperatures. This data from Ladacki et al. are fit with shown in equation (4.19):

$$Q_p(T) = 1.0086 \times 10^{-4} T^2 + 9.4619 \times 10^{-2} T + 108.85 \tag{4.20}$$

In equation (4.20) Q_p is in Btu/lbm resin and T is in °R. In ITRAC, Q_p is taken as a single value at a reference temperature of 536°R and is in units of Btu/lbm pyrolysis gas. Q_p is converted to Btu/lbm pyrolysis gas using equation (4.21).

$$Q_p = \frac{Q_p(536°R)}{1 - r} \tag{4.21}$$

Using the previous assumption that r can vary $\pm$ 10% and the manufacture's average char yield of SC1008 (51.46%) [55], Q_p is estimated to range 322.40 – 488.32 Btu/lbm pyrolysis gas. The resulting CV is 14.77%. This CV is used against the Q_p value of 293 Btu/lbm that was obtained by offsetting the $h_g(T)$ to 0 Btu/lbm at 536°R. For reference, the Q_p calculated by equation (4.21) is 314 Btu/lbm. The difference is likely a result of the heat of formation of virgin resin used by Arnold et al. (-1100 Btu/lbm) and that measured by Ladacki et al. (-1050 Btu/lbm). Either value of Q_p is acceptable as long as $h_{f,g}^0$ and h_g are adjusted accordingly. The distribution on Q_p is assumed to be normal since it's variability is based on a randomly distributed quantity, resin char yield. Q_p is assumed to be aleatory.

The pyrolysis gas enthalpy in Table 4 is nearly identical to that reported by Rindal et al.[86]. Rindal et al. assumed equilibrium conditions with a restriction that carbon cannot precipitate out of the pyrolysis gas stream. These equilibrium conditions were used over the entire temperature range of interest at an average throat pressure of 40 psi. For the CM nozzle, Chemics gives an average throat pressure of 350 psi and this used in calculations of h_g. Two methods of varying h_g are considered.

The first method (equilibrium method) is identical to that used by Rindal et al. except the pressure is 350 psi instead of 40 psi. In this method, pyrolysis gas elemental composition is inputted into chemics with only gas species allowed to form. By allowing only gas species to form the carbon in the phenolic is forced into the gas phase instead of condensing out. The pyrolysis gas elemental composition is a function of resin char yield according to equation (4.22)[39]

$$k_{p_i} = \frac{k_{v_i} - rk_{c_i}}{1 - r} \tag{4.22}$$

where k_{p_i}, k_{v_i}, and k_{c_i} are the elemental mass fractions of the pyrolysis gas, virgin material, and char material. The subscript i is for each individual element (i.e. C, H, and O). Virgin resin elemental composition and char elemental composition were provided previously in Table 3. This is what was done to get the pyrolysis gas elemental composition from ref. [39] shown in Table 10, except a resin char yield of 40% was used.

Table 10. Pyrolysis gas elemental composition as a function of resin char yield.

r	C	H	O
60.00%	39.54%	16.49%	43.97%
55.00%	46.26%	14.66%	39.09%
51.46%	**51.79%**	**13.15%**	**35.06%**
50.00%	53.19%	12.77%	34.04%
45.00%	57.45%	11.61%	30.95%
40.00%	60.99%	10.64%	28.37%

In the next method (blended method) experimental data from Ladacki et al.[71] are used at lower temperatures where nonequilibrium conditions prevail. This is accomplished using $Q_p(T)$ and r for temperatures up to 1800°R. For temperatures between 1800°R and 3600°R, nonequilibrium data are blended with the equilibrium method predictions from Chemics. Above 3600°R equilibrium conditions prevail and only Chemics is used. The blending temperature range in based on experimental work from ref. [87]. The experiment description and data from ref. [87] are provided at the end of this section.

For temperatures below 1800°R, equation (4.23) is used.

$$h_g = \frac{Q_p(T)}{1 - r} + \frac{\rho_v \left(\int C_{p_v} dT + h_{f,v}^0 \right) - \rho_c \left(\int C_{p_c} dT - h_{f,c}^0 \right)}{\rho_v - \rho_c} \tag{4.23}$$

The char heat of formation, $h_{f,c}^0$, is assumed to be 0 Btu/lbm (pure carbon assumption). Inference can also be made using equation (4.4) so that equation (4.23) becomes:

$$h_g = \frac{Q_p(T)}{1 - r} + \frac{\left(\int C_{p_v} dT + h_{f,v}^0 \right) + \left(\int C_{p_c} dT \right) \left[M_{F_r}(1 - r) - 1 \right]}{M_{F_r}(1 - r)} \tag{4.24}$$

It is also noted from Table 4 that the $C_{p_v} \sim C_{p_c}$. Thus a simplification can be made:

$$h_g = \frac{Q_p(T)}{1 - r} + \frac{h_{f,v}^0}{M_{F_r}(1 - r)} + \int C_{p_c} dT \tag{4.25}$$

A final simplification is made from the relationship between $h_{f,v}^0$ of the composite and $h_{f,v}^0$ of the resin as shown in equations (4.26-4.27).

$$h_{f,v_{CCP}}^0 = M_{F_r} h_{f,v_r}^0 \tag{4.26}$$

$$h_g = \frac{Q_p(T) + h_{f,v_r}^0}{1 - r} + \int C_{p_c} dT \tag{4.27}$$

The equilibrium method and blended method curves are shown in Figure 26. For comparison, h_g from Arnold et al.[39] and Rindal et al.[86] is added to the figure. As can be seen, Chemics provides nearly the same result when resin char yield is 40%. The deviation is likely caused by the pressure differences assumed and techniques to model precipitation of carbon in the pyrolysis gas stream.

The highest variation in h_g occurs in the low temperature and blended regions. Both methods have similar error in the low and blended regions and of course the same in the equilibrium regions. Rather than apply different variations at different temperature ranges, the absolute average variation is assumed to exist for all temperatures. This is conservative since pyrolysis gas is generated at high temperatures where the variation is lower. For the equilibrium method the absolute average variation is 24% and for the blended method it is closer to 21%. A CV value of 8.00% is applied to h_g. Even though nonequilibrium is much more likely at lower temperatures, no consideration is given for variation in heat of pyrolysis measurements in the nonequilibrium method. The distribution is assumed to be normal about r and this property is assumed to be aleatory. The distribution selection is based on the distribution of the char yield of resin. Note that equation 4.27 includes C_{p_c} but not the variation of C_{p_c}. This is because the effect on h_g from the variation in r >> effect on h_g from the variation in C_{p_c}.

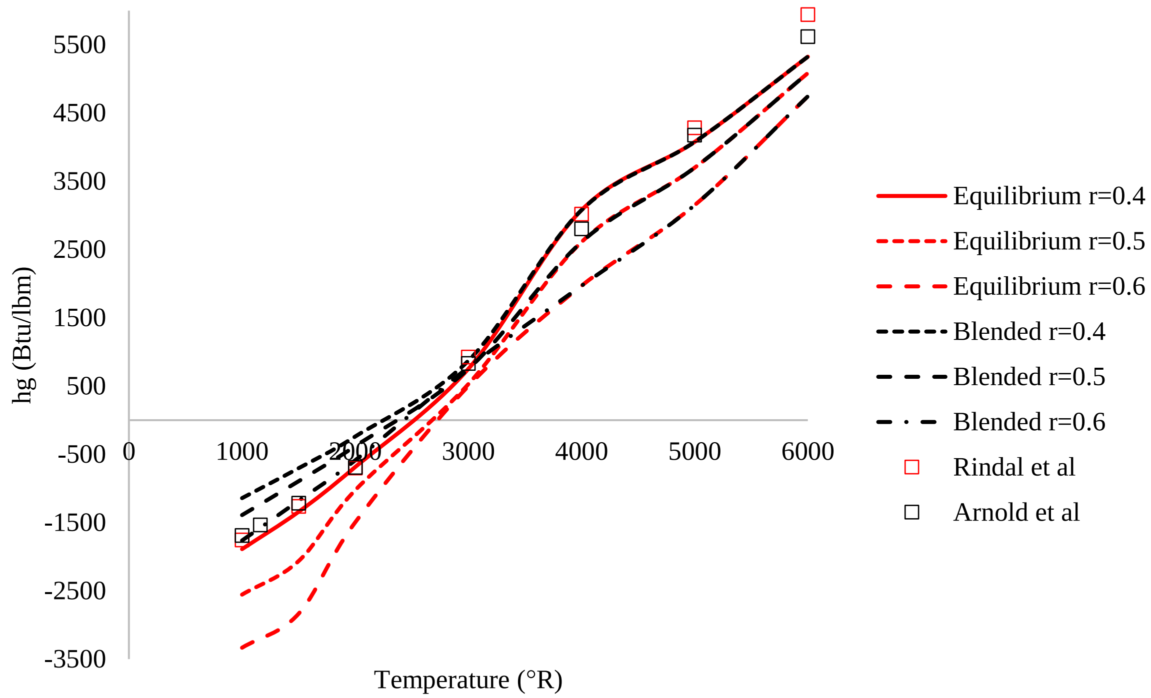

Figure 26. Variation in pyrolysis gas enthalpy as a function of resin char yield. The pyrolysis gas enthalpy from [39] and [86] is provided for comparison.

Description of equilibrium experiment from ref. [87]: Helium is passed through a heated carbon slab. The carbon slab is heated by passing an electric current through it. After the system has stabilized, the helium is replaced by a methane test gas. The power input to the carbon slab, the temperature of the slab as indicated by the optical pyrometers, and the gas flow rate are allowed to stabilize. These quantities, along with the pressure inside the test are recorded. The gas emerging from the carbon is sampled and the sample is analyzed with the use of a mass spectrometer to determine its composition.

In these equilibrium tests, the test gas is assumed to be at the same temperature as the hot carbon slab through which it passes. By performing several tests, each with a different carbon slab temperature, the composition of the gas mixture emerging from the carbon slab is determined as a function of temperature.

From equilibrium theory, it is found that above 1800°R, the mole fraction of hydrogen in a mixture of gas resulting from the decomposition of methane is an indication of the extent to which the mixture has approached the equilibrium state. If the mixture is almost all hydrogen, the equilibrium reactions are nearly complete, and the mixture is essentially in chemical equilibrium. Figure 27 provides the data from these tests.

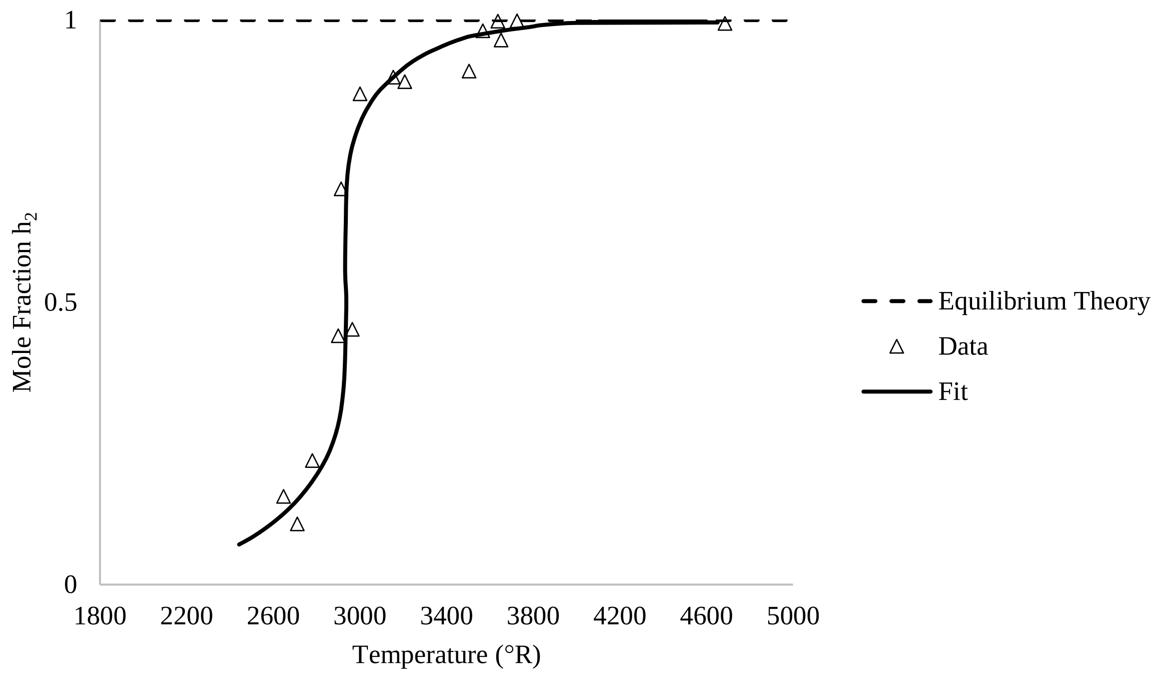

Figure 27. Change in hydrogen mole fraction flowing through a carbon slab as a function of temperature.[87]

4.5 UNCERTAINTY IN MATERIAL DECOMPOSITION KINETICS, x_i, A_i, AND E_i

The kinetics used for MX4926 in ref. [39] are based on 91LD resin[59]. The kinetic constants from 91LD resin are likely similar to SC1008 resin (used in MX4926) since they both are phenol formaldehyde-based resins. Kinetics have been derived for SC1008 by Trick et al.[77], but the model uses four reactions instead of two and uses a first order (i.e. reaction order of 1) assumption instead of third order. Three heat rates (0.5, 1, and 10 °C/min) were used by Trick et al. with the following approximate char yields: 42.58%, 43.38%, and 44.98%. E_i was calculated at each heating rate. The largest CV for E_i was 8% for the 3rd reaction. The samples were solid 1-in squares and the TGA atmosphere was nitrogen.

In the work by Kmita et al.[90], TGA is performed on a commercial phenol formaldehyde used in the casting industry. The form of TGA samples was powder and the atmosphere is described as inert. They used 4 heating rates (5, 10, 20, and 30℃/min) up to 600℃ (typically 900℃ is used for CCP) and a five-reaction decomposition with non-first order reactions. Char yield from the 4 heat rates were: 43.38%, 43.86%, 44.13%, and 43.89%. This is very close to what was found by Trick et al. When char yields are combined with Trick et al., char yield can range from 41.51% to 45.98%. If these char yields are used in combination with equation (4.4), the mass loss in the composite ranges from 16.21% to 22.52%. The mass loss for each reaction in the MX4926 kinetics from Table 3 is calculated using equation 4.28.

$$x_i = \frac{V_{F_r}\left(\rho_{o_i} - \rho_{r_i}\right)}{\rho_v} \tag{4.28}$$

The mass loss from each reaction, x_1 and x_2, is 8.25% and 11.55% for a x_{tot} of 19.8% (i.e. $1-R$). The contribution (i.e. x_i/x_{tot}) to the total mass loss from each x_i is 41.67% and 58.33% respectively. If these ratios are held constant and are applied to the mass losses of 16.21% and 22.52% above, the resulting CV on each x_i is 5.31%. The CV value is used for each x_i with a normal distribution.

The average CV for E_i from Kmita et al. was 2.06% and 2.13% depending on the method Kmita et al. used. The maximum CV was 3.8%. The smaller CV values obtained by Kmita et al. over Trick et al. was likely obtained using non-first order kinetics. In the work by Trick et al. and Kmita et al., calculation of $\log A_i$ is based on the value of E_i, so it is assumed the CV value for E_i applies to $\log A_i$. This link between E_i and $\log A_i$ is demonstrated below.

The derivation of kinetics constants is based on the method from refs. [54][88]. The heating rate over time remains constant such that

$$\frac{dT}{dt} = C \rightarrow dt = \frac{dT}{C} \tag{4.29}$$

Making the substitution from equation (4.29) and rearranging results in equation (4.30)

$$\frac{d\alpha_i}{(1 - \alpha_i)^{m_i}} = \frac{A_i}{C}\exp\left(-\frac{E_i}{\mathrm{R}T_i}\right)dT \tag{4.30}$$

Integrating both sides:

$$g(\alpha_i) = \frac{A_i E_i}{\mathrm{R}C}p(x) \tag{4.31}$$

where

$$g(\alpha_i) = \int d\,\alpha_i/(1-\alpha_i)^{n_i} \tag{4.32}$$

And $p(x)$ is the exponential integral,

$$p(x) = \int \frac{1}{x^2} e^x dx \tag{4.33}$$

Taking the log of both sides and using Doyle's approximation[93] results in equation (4.34) (expanded for clarity).

$$\log C = \log \frac{A_i E_i}{\mathrm{R}} - \log g(\alpha) - 2.315 - 0.457\left(\frac{E_i}{\mathrm{R}T}\right) \tag{4.34}$$

The equation is then differentiated with respect to $1/T$ to and solved for E_i:

$$\frac{d \log C}{d\left(\frac{1}{T}\right)} = 0.457\left(\frac{E_i}{\mathrm{R}}\right) \tag{4.35}$$

After solving for E_i, return to equation (4.34) to calculate A_i. The uncertainties based on the TGA data from Trick et al. and Kmita et al. are below. Reaction order is not considered.

Table 11. Variation (1 CV) in kinetic parameters for MX4926 CCP.

x_1	x_2	E_1	E_2	$\log A_1$	$\log A_2$	m_1	m_2
6%	6%	4%	4%	4%	4%	---	---

The uncertainties in Table 11 are used here assuming all properties are aleatory. All inputs are assumed to follow a normal distribution. This distribution is assigned because decomposition of the resin is a random process where very low and very high decomposition rates are less likely.

Aside on kinetics: Current methods[91] require a minimum of five heating rates (typically of triplicate samples at each temperature). Recently, standards[92] have been established to properly derive kinetic equations using consistent methods, atmospheres, heating rates, sample forms, drying processes, etc.

These consistent methods drive the variation in repeated testing and interlaboratory tests to be very small (e.g. 0.5%). Trick et al. and Kmita et al. both consider the use of Friedman's method[61], but their sample forms are not consistent. It is unknown if the atmospheres are same or if samples were dried by Trick et al. The materials are not the same and were not cured the same way. Trick et al. only used three heat rates. Kmita et al. used five heat rates (the fifth is used to compare the kinetics that were derived from four of the heat rates). The variation in the kinetic constants from Kmita et al. are assumed to be more representative of reality.

4.6 UNCERTAINTY IN MATERIAL SURFACE EMISSIVITY, ε_s

Variation in the emissivity of the surface is based on variation in NARMCO 4028 CCP[80] emissivity and variation in graphite and carbon surface emissivity[93-95]. Figure 28 provides a composite graph on the measured emittance of these materials. NARMCO 4028 has an average emittance of 0.75 with a standard deviation of 0.02 or a CV of 2.76%. The emissivity data from Wilson[93] have a CV of 1.83% for oxidized carbon and 2.08% for graphite. Incropera and Dewitt[96] report emissivity for graphite and carbon between 0.75 and 0.93, resulting in a CV of 3.54%.

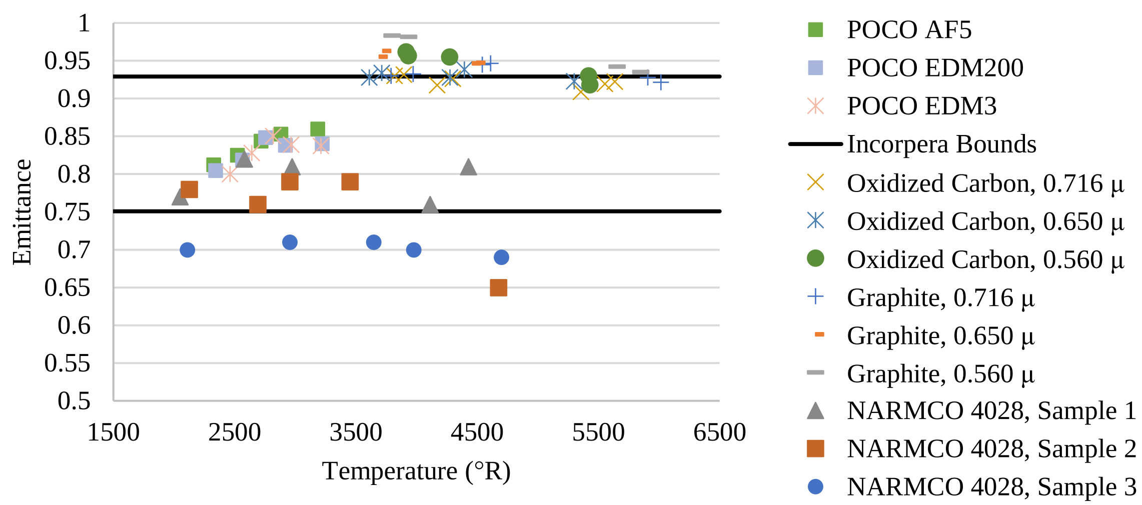

Figure 28. Compilation of emittance and emissivity for carbon and graphite materials. Compiled from refs. [80][94-95].

Data in the literature also show that surface preparation, surface roughness[94], grooves[96], and divets[98] can have an appreciable effect on emissivity. Biasetto et al.[97] reports an increase in emissivity from 0.63 (polished) to 0.84 (unpolished) in graphite attributed to surface roughness. Similar conclusions by Heath and Aydogan[98] have been correlated to eroded surfaces in graphite exposed hydrogen at high temperature. To capture these effects, the nominal emissivity of MX4926 (0.85) is allowed to vary from

0.7 to 1 (CV of 5.88%). Here, it is assumed that the distribution is uniform due to surface changes, temperature ranges, blowing, coking/sooting of the surface, and contamination of the surface by propellant gases and alumina slag. This property is assumed to be epistemic since the nominal emissivity value of nozzle surface during firing is unknown due to all the surface phenomena above.

4.7 UNCERTAINTY ENTHALPY CONDUCTANCE, g

The heat transfer coefficients calculated by Bartz's correlation are of the form $\rho_e u_e C_H = h/C_p$. This form is referred by Kays[99] as enthalpy conductance ($g = h/C_p$) and that is what it is called here. The variability in g is assumed to be both aleatory and epistemic. Aleatory because of natural variation of chemically reacting turbulent flows and epistemic because g is predicted using a correlation with inherent model form error and although g relies in part on "experimental data" it is not anchored to the CM nozzle prior to performing the 2D-UQ.

For aleatory variation it is assumed that the spread in erosion data in the CM nozzle is purely a consequence of the variability in g. This assumes all other properties are nominal with no variation. The spread in erosion data from the HIPPO nozzle[39] is used as a basis for variability in g (see Figure 29 for an illustration of the HIPPO nozzle). The erosion and char data are provided in Figure 30 for nozzles 1 (Fiberite MX4926) and 4 (ENKA MX4926). This is compared to the CM nozzle data in Figure 31. The HIPPO nozzle data are used as the basis instead of the CM nozzle because this work is demonstrating uncertainty in a prediction. It is assumed that the HIPPO nozzle data would be available prior to firing the 84-in CM and that it could be used to inform g. To identify the variation in the HIPPO nozzle, enthalpy conductance at the throat (g_t) is calibrated to the throat erosion average and then to the throat erosion extremes. Variability in g_t is the change in g_t from calibration to an erosion extreme divided by g_t calibrated to the average erosion value (i.e, $\Delta g_t/g_t$). For the HIPPO nozzle, the variability is 17% or a CV of 5.51%. It is assumed that a similar variation would exist at the throat of the CM nozzle. It is not assumed however, that the variability in g_t is applicable to all other stations, g_i. The assumption is that the Δg_t is applicable to other stations so that the variability in $g_i = \Delta g_t/g_i$. This assumes that the spread in erosion data at each nozzle location in the CM nozzle is the same. The CV for each station is given in Table 12.

It should be noted that this estimation is crude and likely mis predicts the actual aleatory variation in the nozzle since it ignores erosion caused by other inputs. Additionally, using a smaller motor with a different chamber pressure, different nozzle contour, and different ply angles is unlikely to provide representative values. This is another indication that epistemic uncertainty is needed for g. For now, the aleatory uncertainty in g is represented by a Gamma distribution. The erosion itself is a normally distributed quantity. This Gamma distribution is chosen for g because all credit in erosion variability was assumed to originate from g even though this is not case. The Gamma distribution assigns lower probability to extremes away from the average and is appropriate here.

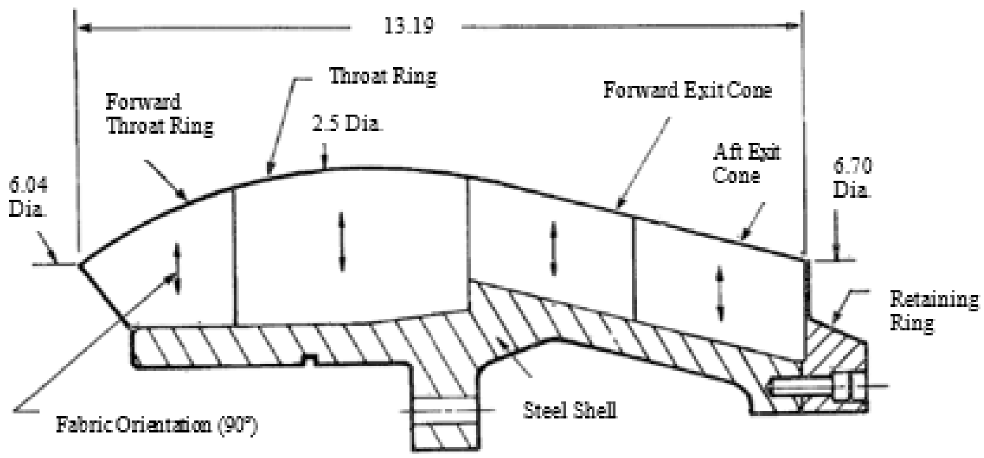

Figure 29. 2D Axisymmetric section of the HIPPO nozzle.[39]

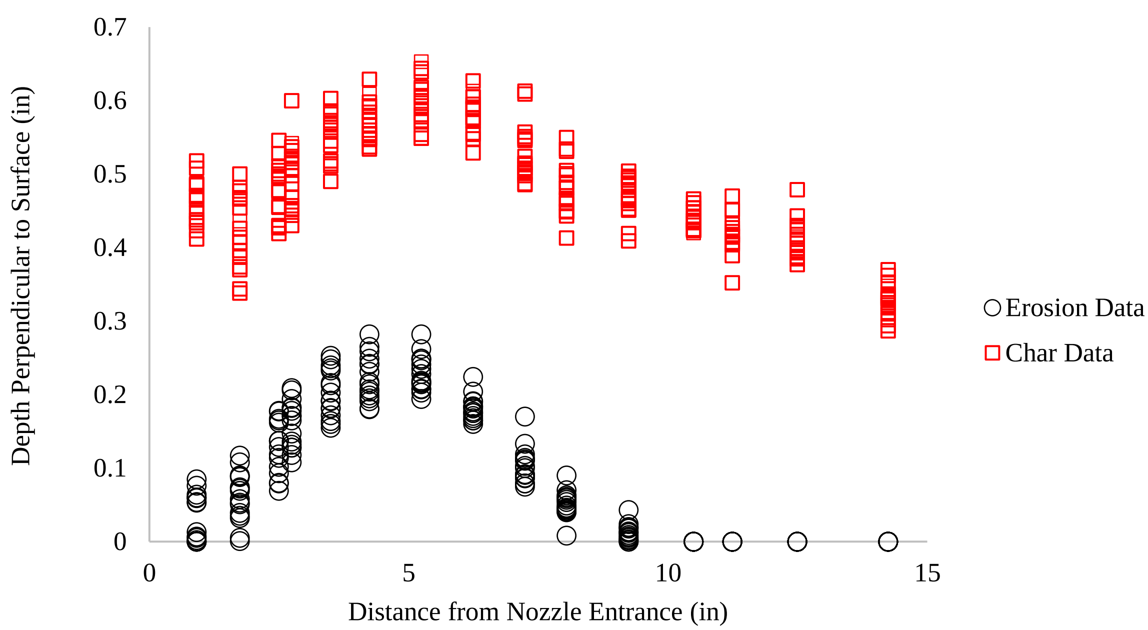

Figure 30. Erosion and char depth measurements for HIPPO nozzles 1 (MX4926 Fiberite Rayon) and 4 (MX4926 ENKA Rayon). Created from tabulated values in ref. [39].

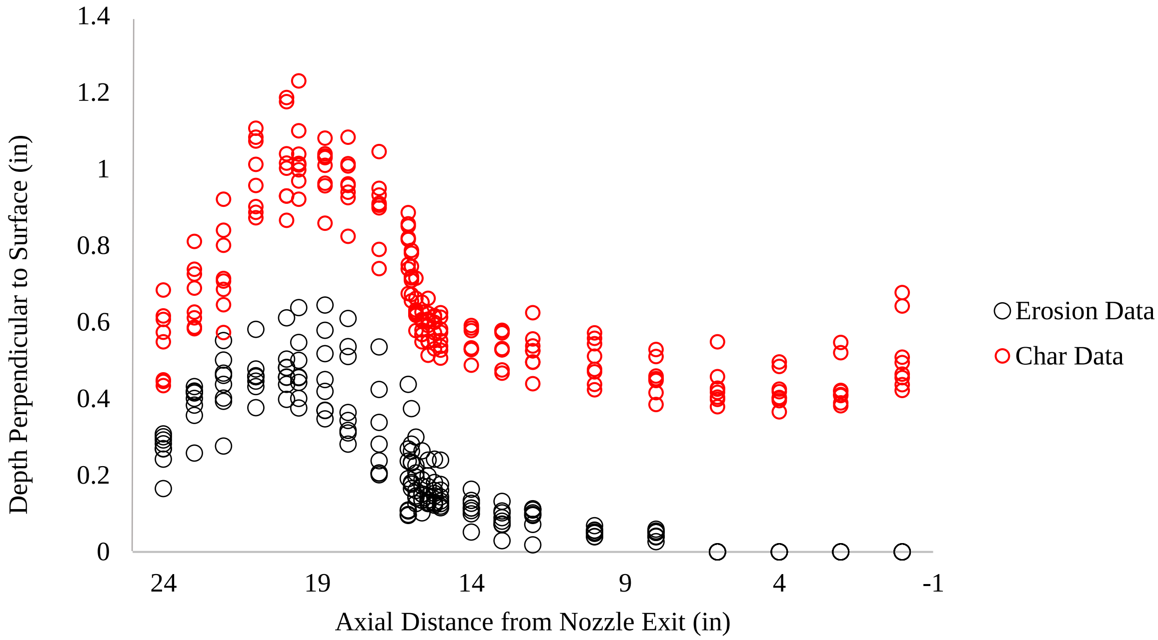

Figure 31. Erosion and char depth measurements for CM nozzle. Created from tabulated values in [39].

It has been reported by Wool and Schaefer[100] that ARGEIBL and other heat transfer predictions in turbulent boundary layers are accurate $\pm$ 25%. Bartz's correlation has already been reduced by 25% based on "experimental data". It is assumed that this experimental data anchoring reduces accuracy by at least half ($\pm$ 12.5%). An epistemic uncertainty with 1 CV of 4.16% is added for g to account for model-form error. The distribution on epistemic uncertainty is uniform since the belief is that the true value of g exits over an interval with equal probability.

Table 12. Variation (1 CV) for enthalpy conductance for the CM nozzle.

Station 1	**Station 3**	**Station 6**	**Station 8**	**Station 10**	**Station 17**	**Station 19**
10.96%	7.33%	5.67%	6.09%	7.36%	9.43%	12.06%
Station 20	**Station 21**	**Station 22**	**Station 23**	**Station 24**	**Station 25**	
15.17%	18.62%	22.27%	26.05%	30.15%	35.25%	

4.8 UNCERTAINTY IN RADIATION HEAT FLUX, q''_{rad}

Variation in q''_{rad} is inferred from variation in effective emissivity given by equation (4.36)

$$\varepsilon_e = \frac{1}{\frac{1}{\varepsilon_s} + \frac{1}{\varepsilon_g} - 1} \tag{4.36}$$

Where ε_s and ε_g are the emissivity's of the CCP surface discussed previously and the gas stream. This relationship assumes parallel plates but is the same for concentric cylinders[101] when their diameters are equal. ε_g is given as:

$$\varepsilon_g = 1 - \exp\left(-\frac{0.808}{16} M_{F_{Al}} \rho_H D_l\right) \tag{4.37}$$

where $M_{F_{Al}}$ is the aluminum mass fraction (in percent) in the propellant, ρ_H is the heavy gas density (density of particle laden stream in lbm/ft^3), and D is the local diameter in inches. This relationship was developed by Murphy and Kwong[27] for a motor with a 1.25-in diameter throat with an average pressure of 400 psia. The report with the 1.25-in motor data that validates this emissivity model cannot be retrieved from the available literature although this model form has received some criticism from Pears et al.[79] and Cross[102]

An earlier form of this equation and likely where Murphy and Kwong derived their correlation is found in ref. [103]. The coefficient, c = 0.808, is based on propellant UTP 3001. UTP 3001 propellant has a $M_{F_{Al}}$ of 16%[104]. This is the same $M_{F_{Al}}$ in the 84-in CM propellant. The variation in the coefficient was based on the ratio of alumina in the gas of another propellant compared to alumina fraction in UTP 3001 at the throat. It is noted by Stephen[103], "the absorption coefficient, $\rho_H c$, of a particle-laden gas stream is proportional to the effective beam length and the number density of the particles. The number density of the particles is, in turn, a function of the gas density. The constant, c, varies directly with the amount of alumina in the exhaust products."

$$\varepsilon_g = 1 - \exp(-0.808 \rho_H D_l) \tag{4.38}$$

There is some discrepancy between the correlations where one uses aluminum content in the propellant and the other uses alumina content in the rocket exhaust at the throat. Although the elemental formulation of the propellant used in 84-in CM is available, there is no information on its nomenclature or on variability of aluminum content in the propellant. Variation in aluminum content between 15.7% and 16.3% is assumed based on variation in another aluminized propellant[105]. This variability changes the coefficient in equation (4.38) to be between 0.7926 and 0.8234. In addition, the heavy gas density changes slightly. The effect is a change in ε_g through the nozzle between 1-3%. This is considered negligible.

Apparent phenomena not captured in equations (4.37-4.38) variability of alumina particle size that would affect optical thicknesses or attenuation of radiation[106-107]. It is assumed equation (4.37) can be modified by incorporating the optical thickness, τ:

$$\varepsilon_g = 1 - \exp(-C\tau) \tag{4.39}$$

Where τ is given by equation (4.40) and C is a constant used to match with the original expression in equation (4.37).

$$\tau = \sigma_t N D \tag{4.40}$$

σ_t is the total cross-section given by equation (4.41) and N is the particle density, given by equation (4.42).

$$\sigma_t = Q_t \pi r_p^2 \tag{4.41}$$

Q_t is the extinction efficiency factor and r_p is the particle radius of alumina in the propellant gas stream. Q_t is assumed to be equal to 2[106] given the r_p values being considered here.

$$N = \frac{M_{F_{Al}} \rho_H}{\rho_p V_p} \tag{4.42}$$

ρ_p and V_p are the alumina particle density and volume. Substituting equations (4.41-4.42) into equation (4.40) gives:

$$\tau = 2\pi r_p^2 \frac{M_{F_{Al}}\rho_H}{\rho_p V_p} D \tag{4.43}$$

Or rewritten in terms of particle radius

$$\tau = \frac{3}{2}\frac{M_{F_{Al}}\rho_H}{\rho_p r_p} D \tag{4.44}$$

Equation (4.37) then becomes:

$$\varepsilon_g = 1 - exp\left(- C\frac{M_{F_{Al}}\rho_H}{\rho_p r_p} D\right) \tag{4.45}$$

To be consistent with equation (4.37), $C/\rho_p r_p$ must be equivalent to .808/16 or $C = 0.0505\rho_p r_p$. The density of alumina can be evaluated using equation (4.46). This equation is a fit from compiled data in Figure 32 below.

$$\rho_p = -0.006796(T - T_m) + 176.93 \tag{4.46}$$

Where T is in °R, T_m is the melting point of alumina (4188.6°R), and ρ_p is in lbm/ft^3. T is calculated in Chemics at the exit plane of the CM nozzle. The resulting particle density is $\rho_p = 170$ lbm/ft^3. This assumes thermal equilibrium between particles and the gas stream. Data from Hermsen[108] on the mass-weighted average alumina particle size (D_{43}) at the nozzle exit plane indicate alumina particle size are a strong function of throat diameter (D_t) and to a lesser extent chamber residence time (t_r), chamber pressure (P_c), and alumina concertation (ξ_c). For this 84-in char motor with the 7-in nozzle, the free volume in the motor chamber is so large that the exponential term can be ignored.

$$D_{43} = 3.6304 D_t^{0.2932}[1 - exp(0.0008163 P_c \xi_c t_r)] \tag{4.47}$$

It is assumed that $D_{43}/2 \sim r_p$. This equation results in an average particle radius of 3.2 μ at the exit plane of the CM nozzle. This is like other motors with diameters between 4.04 in and 8.5 in, which gave measured particle radii between 2.62 μ and 4.49 μ. Substituting in the values for ρ_p and r_p gives a value for $C = 27.47$. The final modified version is given in equation (4.48).

$$\varepsilon_g \ = \ 1 \ - \exp\left(- 27.47 \frac{M_{F_{Al}} \rho_H}{\rho_p r_p} D \right) \tag{4.48}$$

A standard deviation of 29% is given in terms of $\log D_{43}$ by Hermsen. This standard deviation is a result of significant scatter in the data due to different laboratories, different measuring techniques, and different motors. It is assumed that one standard deviation for the 66 different measurement sets from Hermsen bounds three standard deviations for the CM nozzle. Given this assumption the particle radius at the exit ranges from 1.87 μ to 5.51μ. The nominal particle radius varies upstream of the exit plane to maintain consistency between equation (4.48) and equation (4.37).

The variation in alumina density is also considered (see Figure 32). Given the variation amongst investigators the density is of alumina is allowed to vary $\pm$ 12%. Applying the variability in r_p, ρ_p, and ε_s results in variability in $q_{rad}^{''}$ shown in Figure 33. The blackbody radiation heat flux ($\varepsilon_e \ = \ 1$) is included for comparison. The three main "branches" (solid lines) in the figure are representative of gas emissivity variation and the "forks" (dashed lines) off each "branch" are representative of surface emissivity variation. CV values from this modified model are in Table 13. Emissivity of the gas stream is dominated by r_p variations with ρ_p having a small effect and $M_{F_{Al}}$ effects being negligible.

Like g, variation in q_{rad}'' upstream of the exit has aleatory and epistemic uncertainty. Aleatory variation results from alumina particle dispersions and spatial temperature in the turbulent flow and boundary layer. Epistemic variation exists because particle dispersion between the motor chamber and the nozzle exit are unknown spatially and temporally. There is no data to validate the gas stream emissivity model, including it's modification. Additionally, no consideration is given for alumina particle agglomeration[109], thermal nonequilibrium between alumina particles and the gas stream, changes in particle emissivity from the formation of alumina caps[110], alumina boiling/vaporizing and other associated pressure effects[111] on alumina particle form. The estimation of q_{rad}'' includes the epistemic uncertainty in ε_s which followed a uniform distribution. Due to uncertainty in ε_g model form and alumina particle form, a uniform distribution is used to represent q_{rad}''. Although q_{rad}'' has some inherent aleatory variation, it is represented as an epistemic parameter in this work.

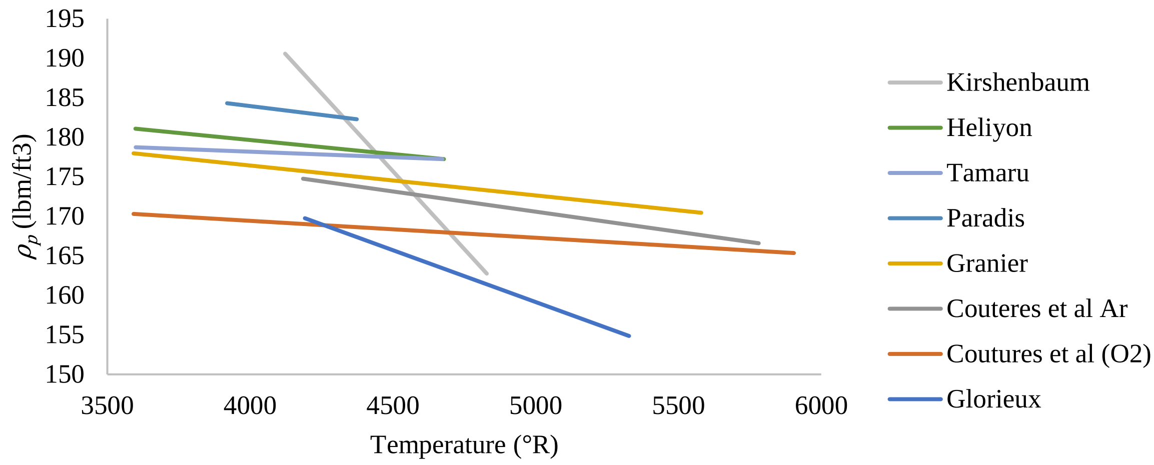

Figure 32. Composite curves for alumina density. Compiled from refs. [112-114].

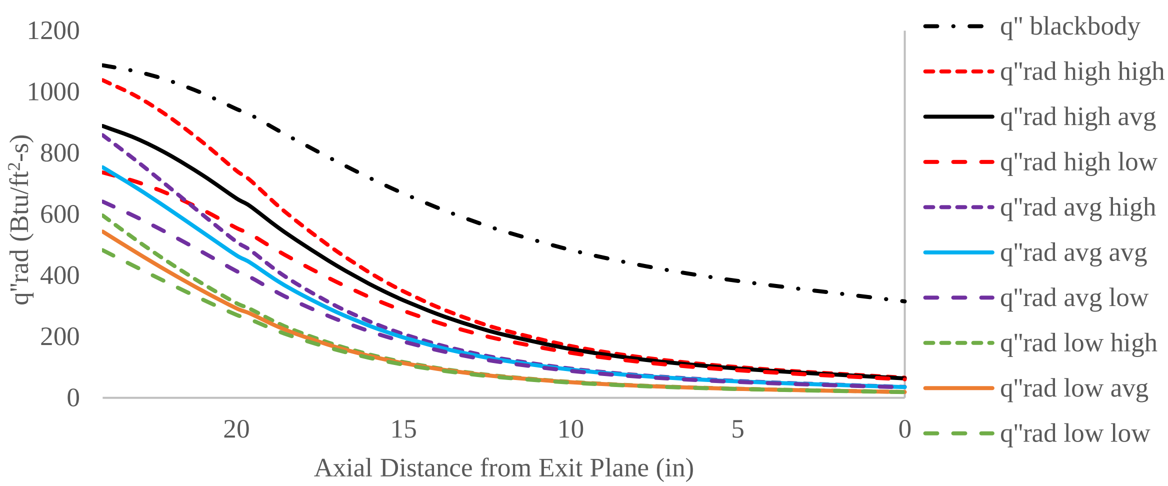

Figure 33. Variation in incident radiation heat flux. In the legend, "high high" and "low low" is interpreted as high surface emissivity high gas emissivity and low surface emissivity low gas emissivity.

Table 13. Variation (1 CV) in the incident radiation flux.

Station 1	**Station 3**	**Station 6**	**Station 8**	**Station 10**	**Station 17**	**Station 19**
12.29%	14.68%	17.15%	18.52%	19.73%	20.60%	21.20%
Station 20	**Station 21**	**Station 22**	**Station 23**	**Station 24**	**Station 25**	
21.62%	21.91%	22.10%	22.22%	22.28%	22.43%	

CHAPTER 5: SENSITIVITY STUDY

Sensitivity analysis is needed to understand the main drivers on the SRQs. Additionally, surrogate modeling techniques used in Chapter 6 benefit computationally from reducing the number of inputs to the main drivers. It is a reduction in the baggage in/baggage out.

Several sensitivity analyses have been conducted on ablation. These analyses have explored microscale effects[115], specie surface reaction effects on ablation at the surface[116], pyrolysis gas composition effects[7], various material property inputs and boundary conditions[5][8][10-11][117]. Two illustrative sensitivity studies[118-119] are discussed below.

In the first, an experimental sensitivity study used a 150 Btu/ft^2-s arc jet that produced static temperatures near 7200°R with a Mach number of 0.9 at atmospheric pressure. Flow conditions considered a gas mixture of 5%/95% O_2/N_2 and a gas mixture of 100% N_2. The study included the following inputs: k_v, k_c, C_{p_v}, Q_p, temperature of pyrolysis (T_p), and specific heat of pyrolysis gases (C_{p_g}). The SRQs of interest in this study were erosion and in-depth spatial temperature. Of all these properties, k_c (most dominant) and C_{p_g} were the most influential. Q_p and T_p had minimal effects on erosion and temperature and k_v had no effect on erosion and minor effect on temperature. The effect on erosion from k_c is shown in Figure 34.

In the second study, a carbon phenolic thermal protection system (TPS) applicable to atmospheric reentry vehicles was simulated. TPS thickness was the SRQ of interest. Required TPS thickness was based on an 810°R isotherm depth limit (temperature in the upper virgin material zone). Sensitivity of inputs was expressed as function of the required gage thickness to baseline gage thickness when an input was perturbed. An example of sensitivity results is shown in Figure 35.

Total convective heat load was 22454 Btu/ft^2 with max convective heating of 2615 Btu/hr-ft^2. Thirty-nine different inputs were considered including virgin material properties, char material properties, heat of decomposition, surface emissivity, reaction kinetics, blowing (B^*), heats of sublimation and combustion, activation temperature for sublimation (B_s), reaction constants, transpiration factors, pyrolysis gas specific heat, and convective heat transfer parameter (H_D). Sensitivity derivatives ($\partial SRQ/\partial I_i$) were calculated by Kolodziej[120] and are given in Table 14.

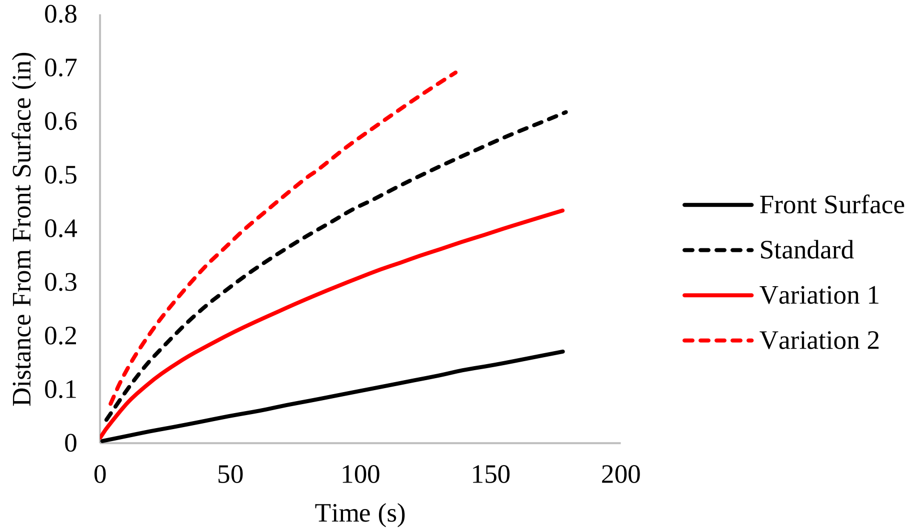

Figure 34. Effect on surface recession from variation in char thermal conductivity.[118]

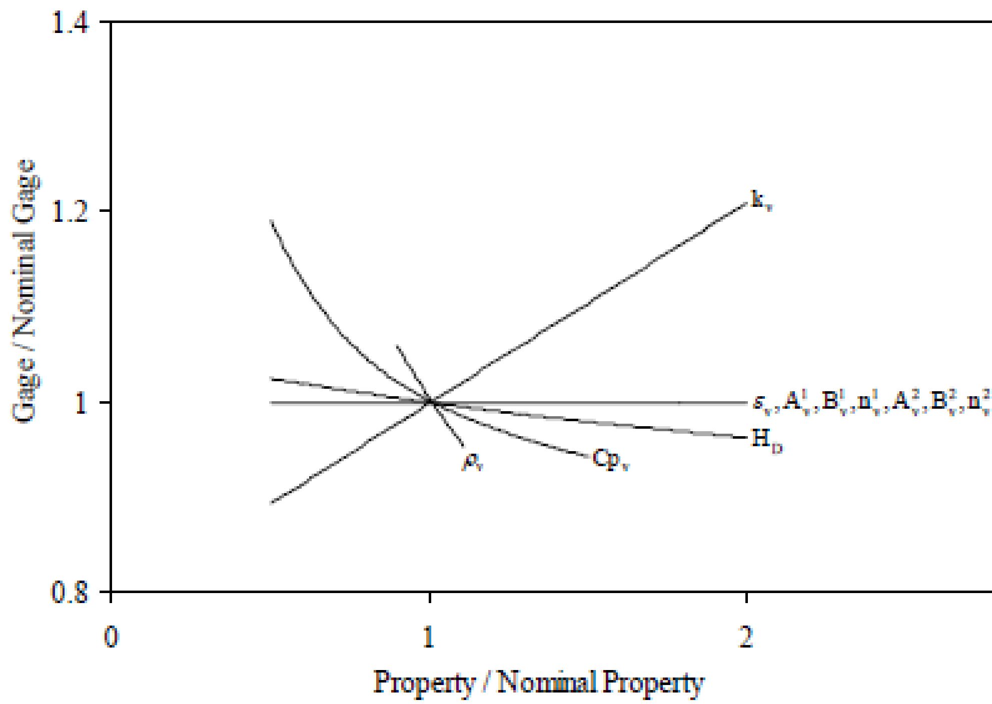

Figure 35. Sensitivity of carbon phenolic virgin properties, kinetics, and heat of decomposition to TPS thickness. The inputs that have effect are the surface emissivity and kinetics.[119-120]

Table 14. Sensitivity derivatives showing the most influential inputs for isotherm depth in a TPS.[120]

k_c	ρ_v	H_D	B_s	k_v	B^*	C_{p_v}	ρ_c	C_{p_c}
0.995	0.503	0.376	0.292	0.21	0.196	-0.172	-0.137	-0.121

The studies above give insight and expectation to what may be found in conducting sensitivity analyses on the CM nozzle. Both studies show that char thermal conductivity is the primary driver in-depth spatial temperatures. The first study shows char thermal conductivity as the primary driver to erosion with the secondary driver being pyrolysis gas specific heat. Other drivers to the temperature field include densities, specific heats, and heat transfer coefficient. The first study doesn't consider the effect of changes in boundary conditions on erosion and the second study doesn't consider effects of input variability on erosion. Neither study considers the effect of variability on the char depth which is of interest in this work. Both studies also have limited application to a rocket nozzle since the boundary conditions are not same thermochemically, in magnitude, and in duration. Additional sensitivity analyses are therefore needed. The sensitivity study conducted in section 5.1 below focuses on erosion and char depth in a rocket nozzle as the SRQs. The input uncertainties from Chapter 4 are used to conduct this study.

5.1 SENSITIVITY, INPUT CV, AND INPUT RANKING

Local sensitivity[25] is performed at each nozzle station. Following the local sensitivity, a global sensitivity is estimated using Sobol Indices[13]. The local sensitivity varies each input $\pm$ 3 CV while holding all other inputs constant. The change in SRQ value is compared to the baseline prediction. The baseline represents the nominal prediction using property values from Table 3 and Table 4, and the boundary conditions from Chapter 3. A summary of each input and associated CV is given below in Table 15. The goal of the sensitivity study is to screen-out inputs that have low impact on the SRQs. Screen-out criteria is based on a ranking system expressed in equation (5.1):

$$Rank = \Delta E_{i-b} + 2\Delta C_{i-b} \geq 1\% E_t + 2\% C_t \tag{5.1}$$

Where ΔE and ΔC are the change in erosion depth and char depth caused by perturbation of the input compared to the baseline. The "2" on char depth is to emphasize greater importance. The subscripts $i - b$ represent the ith perturbation minus the baseline and the subscript t is erosion and char at the throat. The equivalency in the equation is the established cut-off. If the effect on the SRQ due to variation in an input is not sufficient to exceed the right-hand-side of equation (5.1) then that input is screened out.

The throat is chosen because g is highest there and a high g amplifies material response. Baseline E_t and C_t values are approximately 5.95 mils and 9.49 mils respectively, resulting in a cutoff of 25 mils.

Table 15. CV table for model inputs.

Property	Aleatory/Epistemic CV	Distribution
ρ_v	1.37%	Gamma
ρ_c	3.60%	Gamma
C_{p_v}	3.33%	Normal
C_{p_c}	3.33%	Normal
$k_v 0$	8%	Normal
$k_v 90$	7%	Normal
$k_c 0$	13%	Normal
$k_c 90$	7%	Normal
Q_p	14.77%	Normal
h_g	8%	Normal
x_1	6%	Normal
x_2	6%	Normal
$E_1 \log A_1$	4%	Normal
$E_2 \log A_2$	4%	Normal
ε_s	5.88%	Uniform
g	see Table 12/4.17%	Gamma/Uniform
q''_{rad}	---/see Table 13	Uniform

5.2 RESULTS

Results of the sensitivity are summarized in Figure 36. Variables that are greater than screen-out criteria are shown above the screen-out criteria line in the legend. Other than virgin density, all other virgin material properties screen-out. This isn't surprising given that the surface is mature char and char depth has already experienced significant conversion to char. Some of the inputs screen-out in stations aft of the throat, however; these inputs are still used to generate the surrogate models. Although the SRQs and boundary conditions differ in this study, the conclusions generally agree with previous studies[118-120].

Figure 37 and Figure 38 represent the numerical sensitivity from ITRAC calculated by equation (5.2) where m is the sensitivity derivative (or slope) calculated by central difference at $\pm$ 3 CV or ($\pm 3\Delta x_i$) limits. Clearly the sensitivity the inputs for erosion are a strong function of enthalpy conductance. The y-intercept (x_{0_j}) for each SRQ can be calculated using equation (5.3). The subscript j is to denote erosion or char. The bar on x indicates the SRQ is evaluated at all inputs.

$$m_{ij} = \frac{\partial SRQ_j}{\partial x_i} \approx \frac{SRQ_j\left(x_i^0 + 3\Delta x_i\right) - SRQ_j\left(x_i^0 - 3\Delta x_i\right)}{6\Delta x_i} \tag{5.2}$$

$$x_{0_j} = SRQ_j(\bar{x}) - \sum_{i=1}^{n} \frac{\partial SRQ_j}{\partial x_i} \tag{5.3}$$

Equations (5.2-5.3) are used to estimate global sensitivity using Sobol sensitivity indices[13]. In Sobol's work, he shows that the variability in the SRQ can be attributed into the variability in the inputs through a decomposition method. Sobol does this by decomposing the variability in the SRQ into the summands of each input (first order indices), interaction of each input with each other input (second order indices), and interaction of each input with all other inputs (total indices). Sobol total sensitivity indices are shown in Figure 39 and Figure 40. Boundary conditions dominate erosion. As the propellant gas cools downstream of the throat emissivity of the gas stream drops and the contribution of q''_{rad} decreases. Surface emissivity contribution also drops off since the surface is not as hot downstream. Other main contributors to erosion are char thermal conductivity and virgin and char density. Char thermal conductivity reduces erosion by pushing heat in depth and away from the surface. Densities reduce erosion by increasing heat capacity at the surface. And lower temperatures in the exit cone, char density increases erosion due to kinetic effects.

Boundary conditions are still large contributors to char depth. About 45% of char depth in the forward end and over 80% of char depth at the exit are contributed to boundary conditions. Like the findings in refs. 118-119, char thermal conductivity is a primary contributor with secondary contribution coming from densities, pyrolysis gas enthalpy, and char specific heat. Char thermal conductivity increases char depth since it pushes heat from the surface deeper into the insulator. Anisotropic behavior is shown aft of the fifth station as the ply angle changes from ~ 90° in the forward end to ~ 27° in the exit cone.

Reduction in char depth is attributed to virgin density, char specific heat, and pyrolysis gas enthalpy. This reduction is caused by heat capacity effects. For both erosion and char, kinetic properties, virgin properties other than density, heat of pyrolysis, and surface emissivity all make negligible contributions.

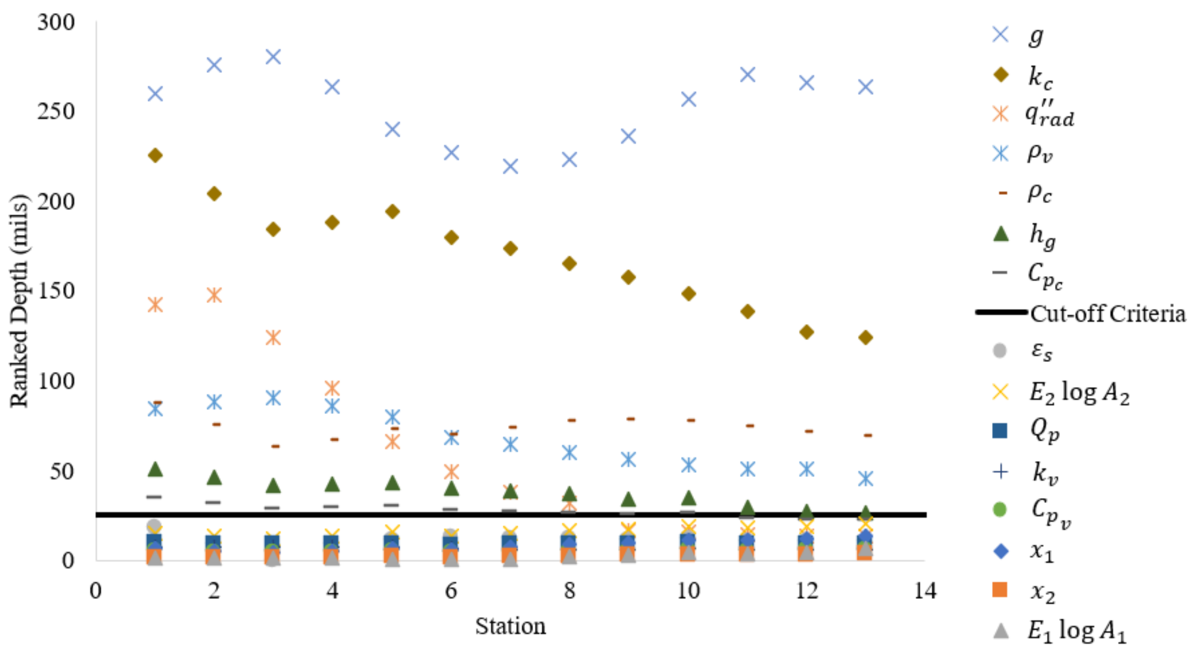

Figure 36. Sensitivity of model inputs at ± 3 CV bounds.

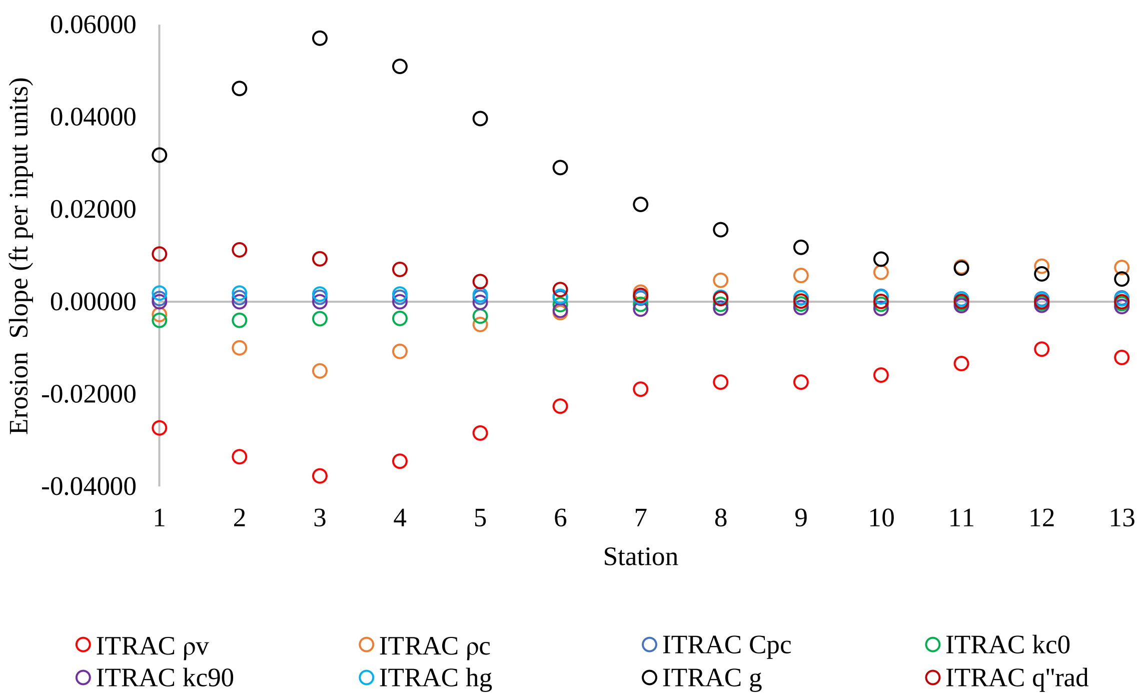

Figure 37. Calculation sensitivity in erosion depth for model inputs from equation (5.2).

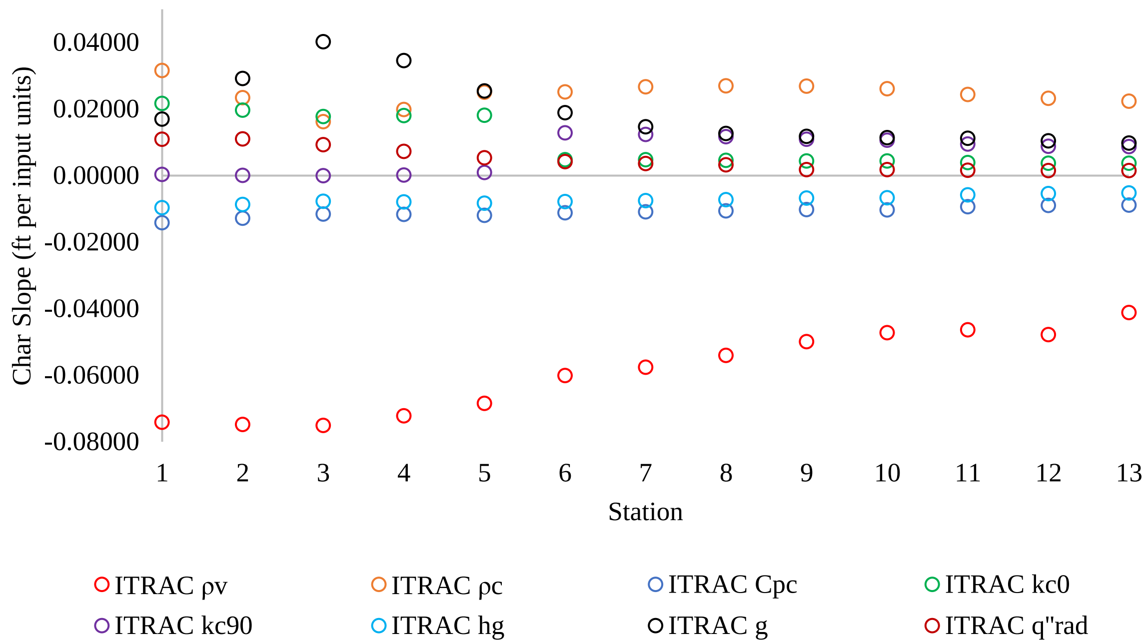

Figure 38. Calculated sensitivity in char depth for model inputs from equation (5.2).

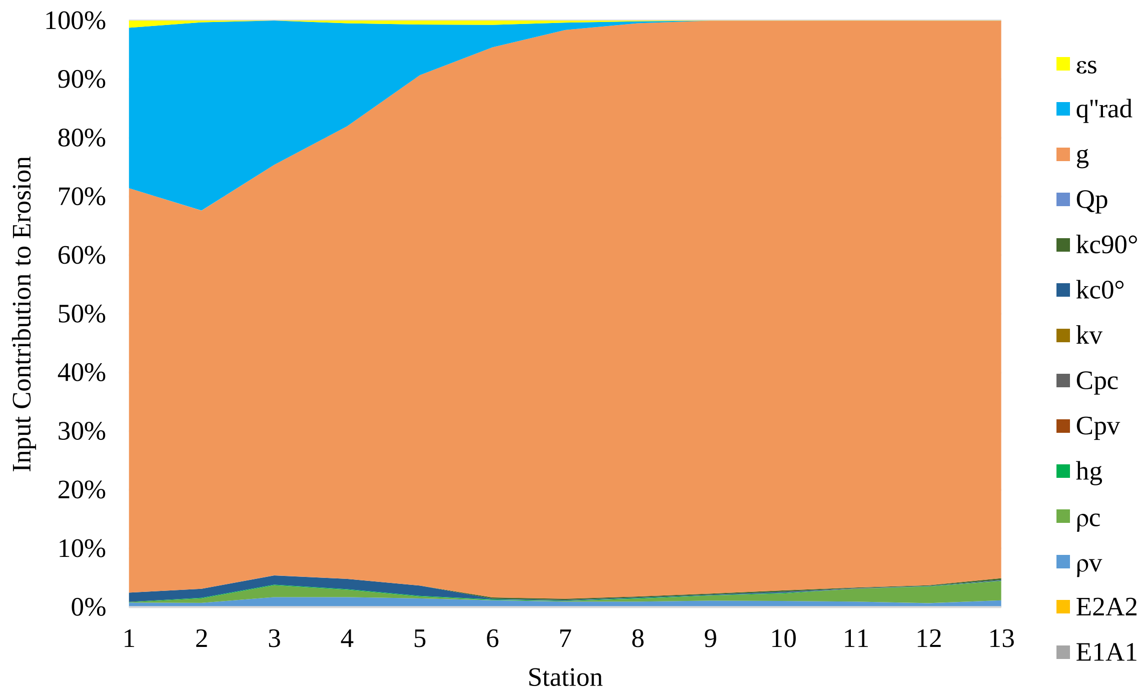

Figure 39. Sobol Indices for each input on erosion.

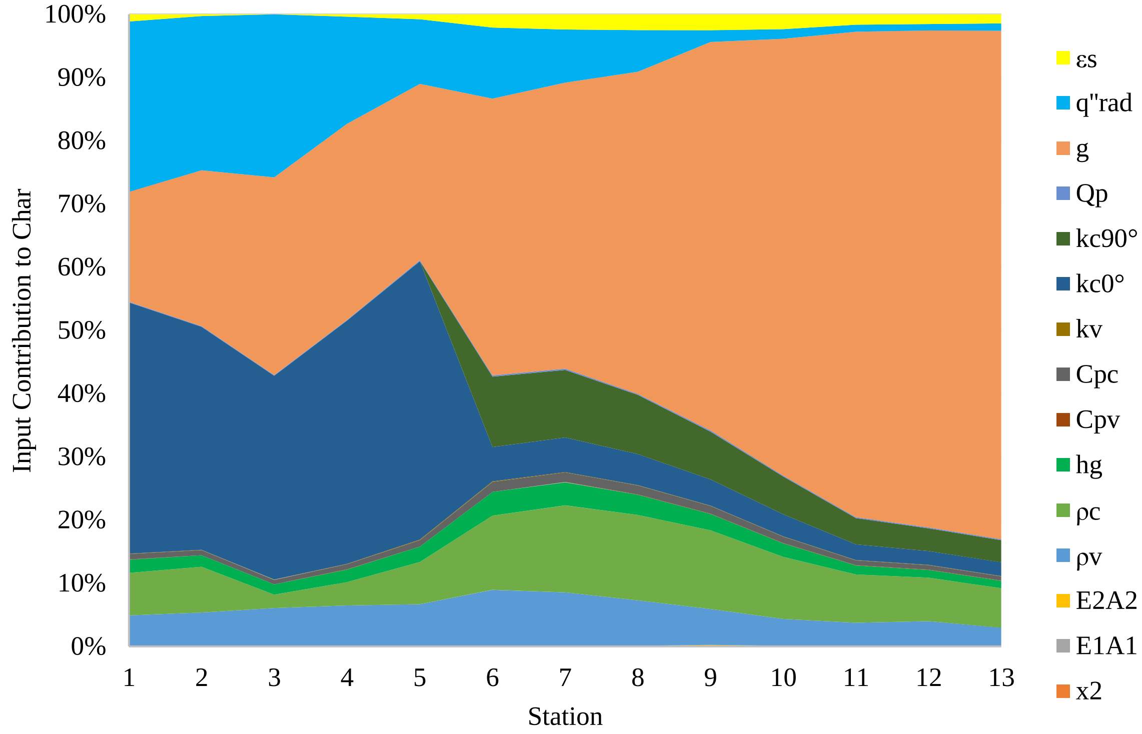

Figure 40. Sobol Indices for each input on char depth.

CHAPTER 6: SURROGATE MODELS

The 2D-UQ process requires propagation of aleatory and epistemic uncertainties in two sampling (e.g. Monte Carlo) loops. This can require over one million simulations for all CM nozzle stations. This is computational intractable, even on modern super computers. To overcome this computational roadblock, surrogate models (SMs) are needed. The SM techniques introduced and assessed in this chapter are based on work by Heath et al.[121].

A SM is a computationally faster representation of a high-fidelity complex model. These are also referred to surface response models[45] and have been in use at least since the early 1970's[122]. Unlike creating a fit or correlation that represents experimental data, a SM is a correlation, table, fit, or some other representation of output data of a higher fidelity, more complex and more expensive computational model. The functional form and coefficients of the SM give insight into the most and least important inputs driving variability in the outputs. See Figure 41 for an illustration. For more information on surrogate models and their use, one is directed to refs. [122-123].

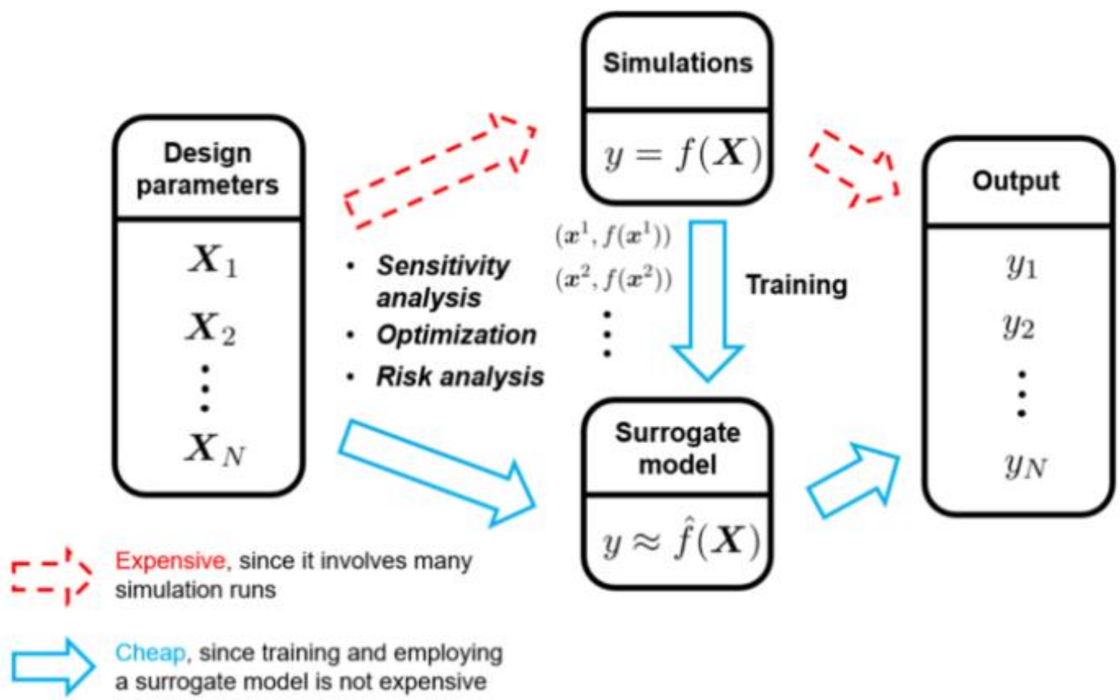

Figure 41. Illustration of surrogate model compared to computation simulations.[124]

6.1 CREATING SURROGATE MODELS

The first step in creating the SM is choosing a method to generate the model. Methods include least squares polynomial regression[125], Gaussian process regression[126] or Kriging[127], radial basis functions[128], knot-points[129], and others. Three methods are considered here. Each method is assessed at the throat and exit plane of the nozzle. These nozzle locations are where the heat transfer coefficient is the highest and lowest respectively.

The first and simplest SM method is a bit of deviation from the norm, but is shown to be a valid SM. This involves using the ITRAC numerical derivatives from Chapter 5 as a linear model with a y-intercept calculated from equation (6.1) as follows.

$$x_{0_j} = SRQ_j(\bar{x}) - \sum_{i=1}^{n_{so}} \frac{\partial SRQ_j}{\partial x_i} \tag{6.1}$$

Where subscript j is either erosion or char depth. The bar over x is to show that the SRQ is evaluated at all the baseline inputs x_1 thru $x_{n_{so}}$. The n_{so} is for inputs that passed the screen-out process. The computational efficiency is very high considered the speed of ITRAC. The number of simulations (N_{sim}) depends on the inputs varied in local sensitivity study as shown in equation (6.2). This is on a per station basis.

$$N_{sim} = 1 + 2n_i \tag{6.2}$$

where n_i is the original set of inputs that were varied in Chapter 5. This surrogate model is termed the ITRAC SM (ISM). Some obvious risks in this SM are: 1. It doesn't consider input interactions that may be observed in a global sensitivity; 2. It doesn't consider nonlinearity that may exist between 0 and 3 CV bounds; 3. It is extrapolated outside of its domain. Depending on how dominant these effects are will determine the usefulness of this SM.

The second method uses a least squares linear SM (LSM). This SM model is created by running ITRAC at 4 CV limits on the inputs where all inputs can vary at the same time in each simulation. 4 CV is used to build the domain the SM will operate in and 4 CV is deemed large enough so there is no risk of extrapolating the SM outside the domain of the ITRAC simulation data. Then one hundred Latin Hyper Cube (LHC) simulations are run to capture any nonlinearity that may exist between the nominal value and 3 CV. A linear model is fit through the LHC and 4 CV ITRAC simulation data. Although some attempt is made to capture nonlinearity, this is a linear technique and suffers similar risk as the ISM.

The number of simulations needed for the LSM is expressed in equation (6.3). This method can quickly become computationally expensive as n_f grows.

$$N_{sim} = 101 + 2n_i + \ 2^{n_{so}} \tag{6.3}$$

The third method uses poly-harmonic splines[130]. This method uses the same number of simulations as LSM; however, the poly-harmonic surrogate model (PHSM) may be given additional simulations (n_t) to increase accuracy throughout the domain. Unlike ISM and LSM, which are fits through the simulation data points, the PHSM has zero error at data points it is fit to and is an interpolator between new simulation data points. Unlike the previous methods, PHSM doesn't provide a tangible closed-form solution and is not as rapid a SM as others. Additionally, it can become more unstable beyond the domain compared to a LSM.

To assess fitting of the PHSM, an additional three hundred LHC simulations (within the 3 CV bounds) at each location. The computational efficiency of the PHSM method is expressed by equation (6.4)

$$N_{sim} = 101 + 2n_i + 2^{n_{so}} + n_t \tag{6.4}$$

6.2 SURROGATE MODEL ASSESSMENT

Accuracy of each surrogate model generation method is assessed against a new set of one hundred LHC simulations not previously used for fitting. Figure 42 and Figure 43 show comparison of ITRAC SRQ predictions against ISM and LSM SRQ predictions for throat and nozzle exit locations. Accuracy is assessed based on the difference between ITRAC SRQ predictions and SM SRQ predictions. This difference is reflected by the error bars. For throat erosion and char, the LSM is more accurate than the ISM. This is likely because the LSM captures input interactions and ISM is a local model. Interaction does appear minor and helps validate the local sensitivity study in Chapter 3. The error at the throat location for both SRQs is reasonably low. The average error for LSM erosion at the throat is 1.45 mils with an absolute max error of 9.81 mils. Average error for char is 1.90 mils and max absolute is 18.6 mils. For the ISM, average erosion error is -1.43 mils and max absolute is 18.28 mils. The ISM char average is 5.14 mils with a max absolute error of 28.01 mils. Error is being quoted in mils because if the predicted erosion is very small (e.g. 0.000001) then being 1 mil off is a catastrophe from a percentage basis.

At the exit plane, there is a markable difference between ISM and LSM on erosion depth. The ISM is more accurate at low erosion depths and has similar overall error compared to the LSM. The error appears to have increased substantially compared to ITRAC SRQ predictions at this location, but the distance in the error bars can be deceiving. In terms of percentage, the error is several orders of magnitude larger for some data points, but in terms of mils difference the error is close to error at the throat. For LSM erosion and char, average error is less than 1 mil. The max absolute error is 9.8 mils for erosion and 35.5 mils for char. The ISM has average errors of -2.19 mils on erosion and -8.24 mils on char. Max absolute error is 13.84 mils for erosion and 35.07 mils for char. The distributions of error in the LSM in given in Figure 44 and Figure 45. A normal distribution appears to be a promising empirical fit.

Figure 47 shows a comparison between the ITRAC numerical derivatives calculated from equation (5.2) and the surrogate derivatives calculated in equation (6.5). The derivatives of the LSM are its coefficients (C_i) in front of each input (x_i). The y-intercept is given as x_0.

$$SRQ_i = x_0 + \sum_{i=1}^{n} C_i x_i \tag{6.5}$$

$$\frac{\partial SRQ_i}{\partial x_i} = C_i \tag{6.6}$$

As expected, ISM and LSM are very similar besides minor discrepancies for q''_{rad}, and ρ_v and ρ_c in the nozzle exit cone. It is believed these differences can be attributed to input interaction and nonlinear behavior when the heat transfer coefficient is small.

Figure 48 assesses the accuracy of the LSM to the baseline ITRAC predictions. The agreement is excellent except for the last few stations. Even then, it is very reasonable compared to the spread in the CM nozzle data (see Figure 31). Since the y-intercept of the ISM is calculated directly from the baseline it would predict the baseline exactly.

Figure 49 and Figure 50 show the PHSM with no additional training and with the three hundred additional training cases. The PHSM achieves greater accuracy than ISM and LSM for all SRQs and at both stations. There is almost no difference from additional training. This is encouraging since it allows for less computation. The PHSM fits for all stations are located in Appendix B.

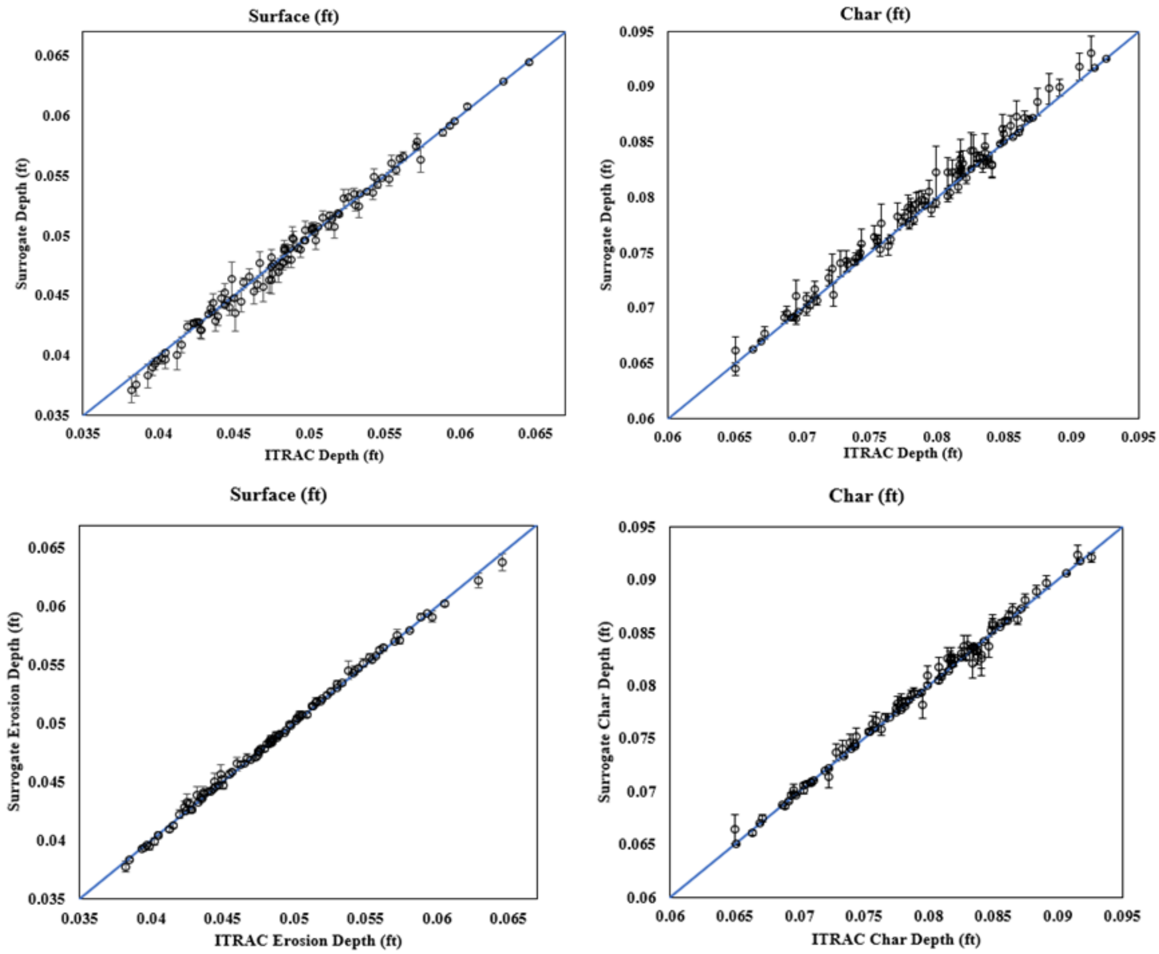

Figure 42. Error in erosion and char depths at station 6 (throat) in ISM (top two graphs) and LSM (bottom two graphs).

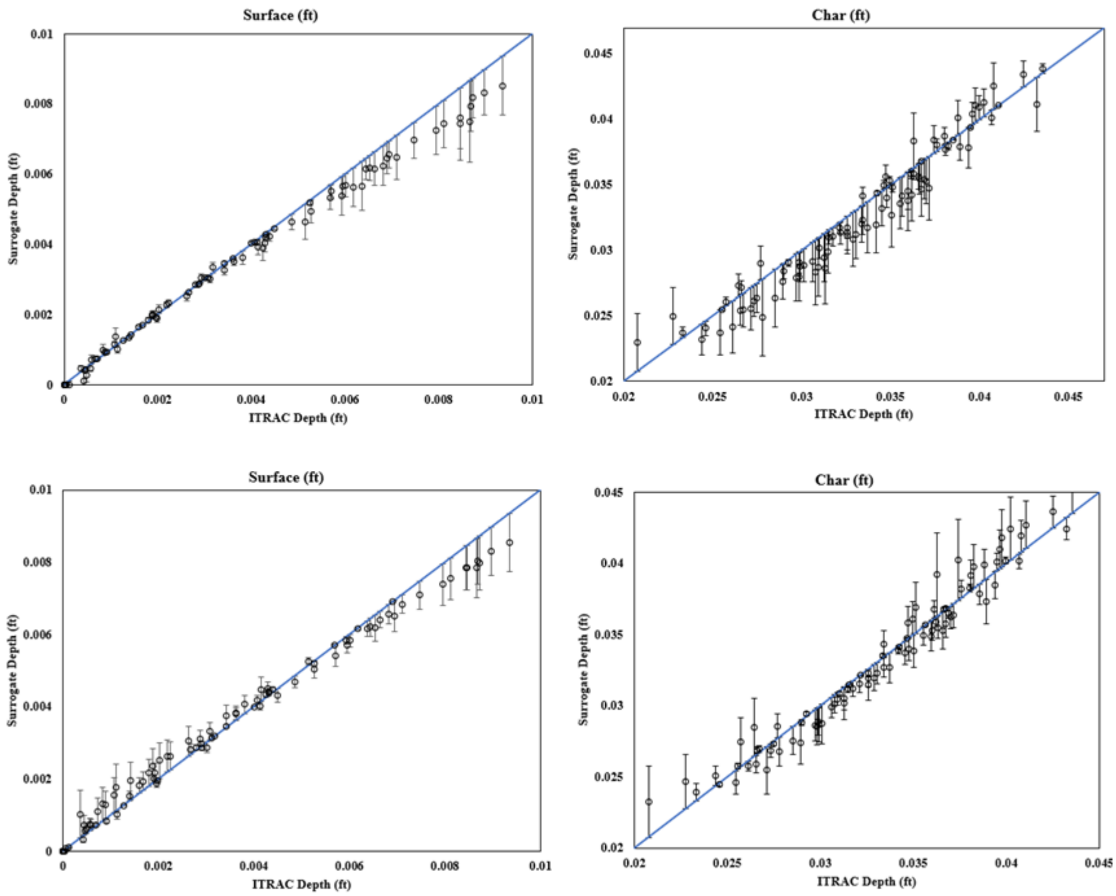

Figure 43. Error in erosion and char depths at station 25 (nozzle exit) in ISM (top two graphs) and LSM (bottom two graphs).

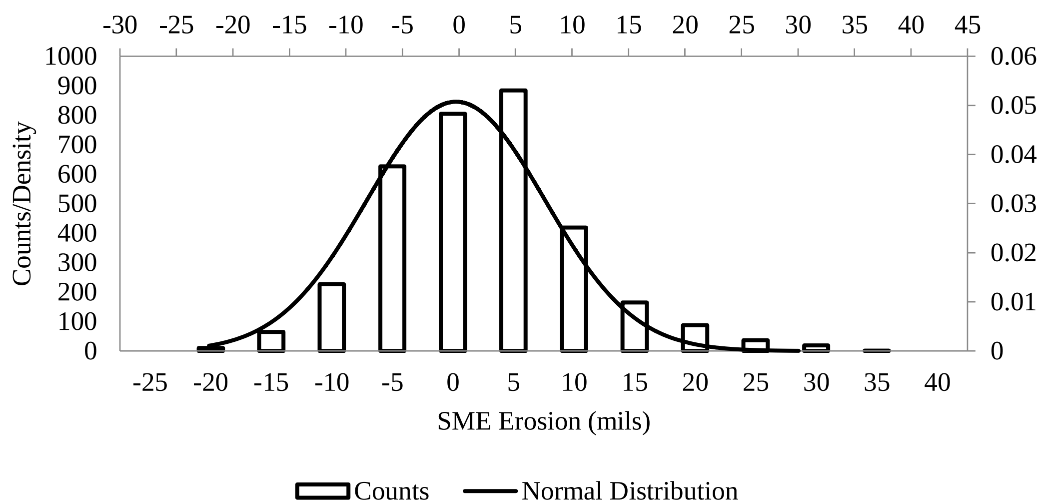

Figure 44. LSM Error in predicting erosion depth. A normal distribution is overlayed on the counts.

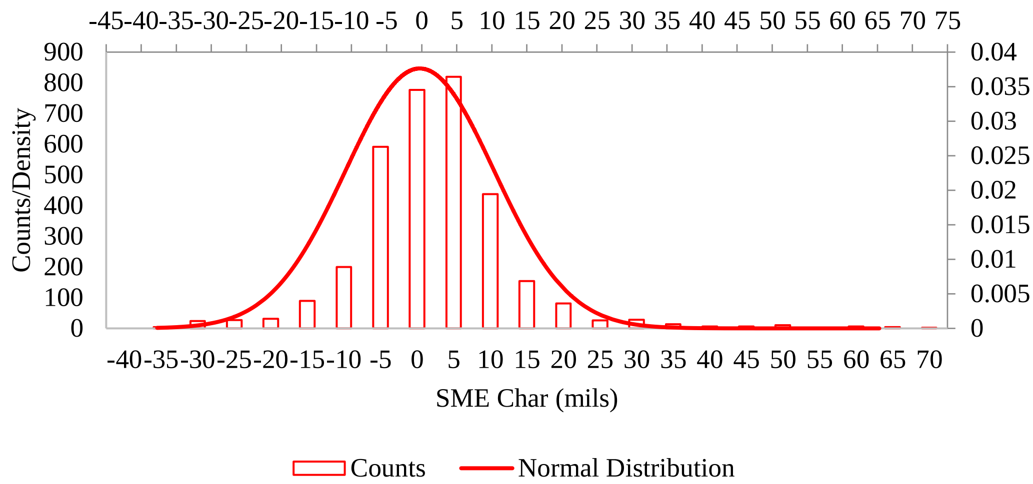

Figure 45. LSM error in predicting char depth. A normal distribution is overlayed on the counts.

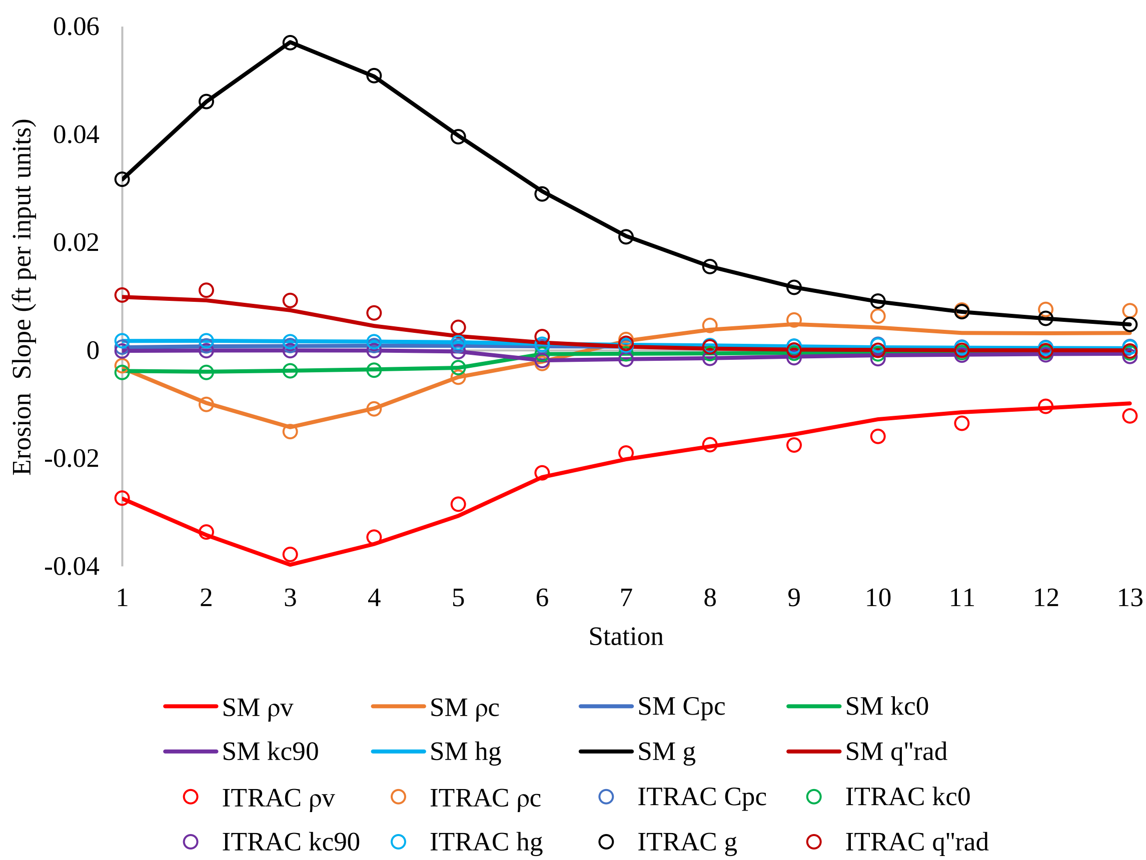

Figure 46. LSM slopes vs slope calculated from equation (6.6) for erosion.

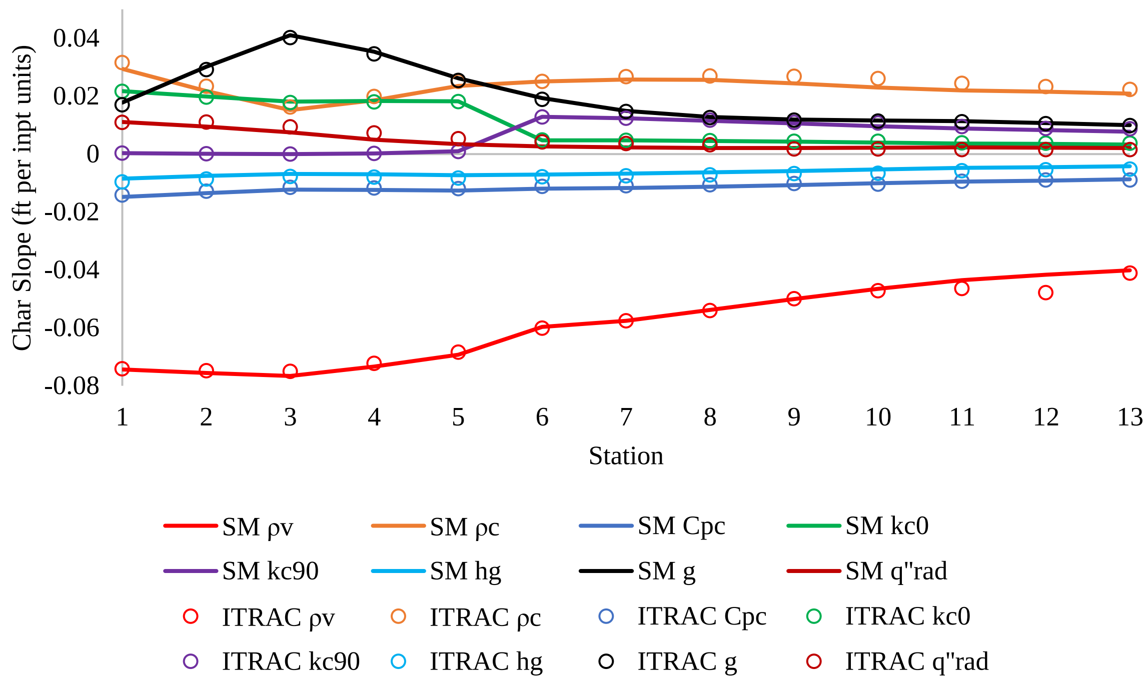

Figure 47. LSM slope vs slope calculated from equation (6.6) for char.

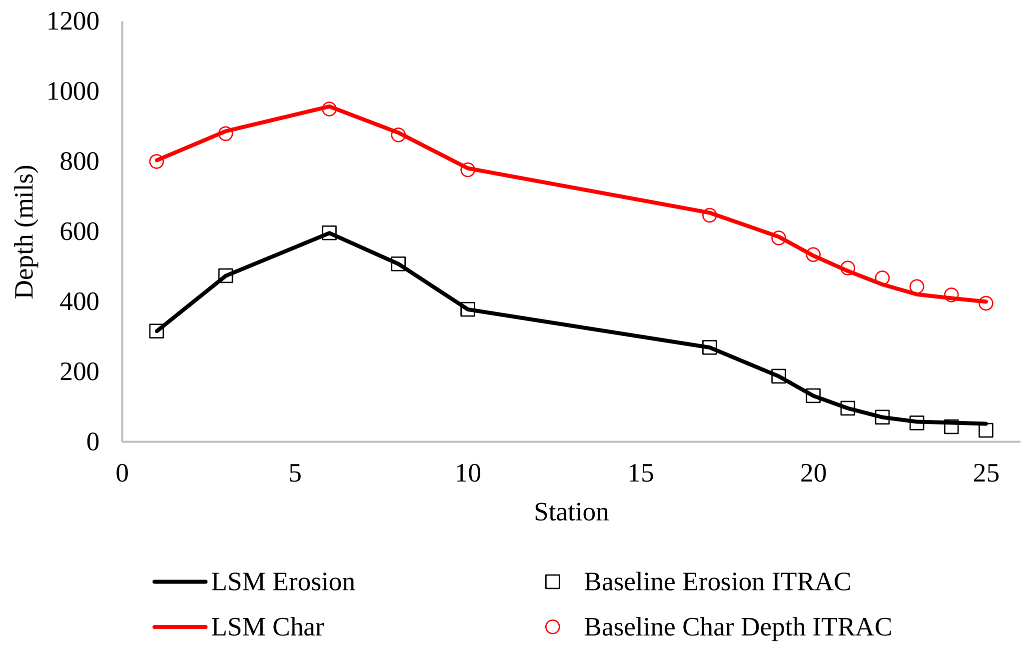

Figure 48. LSM prediction vs ITRAC baseline prediction.

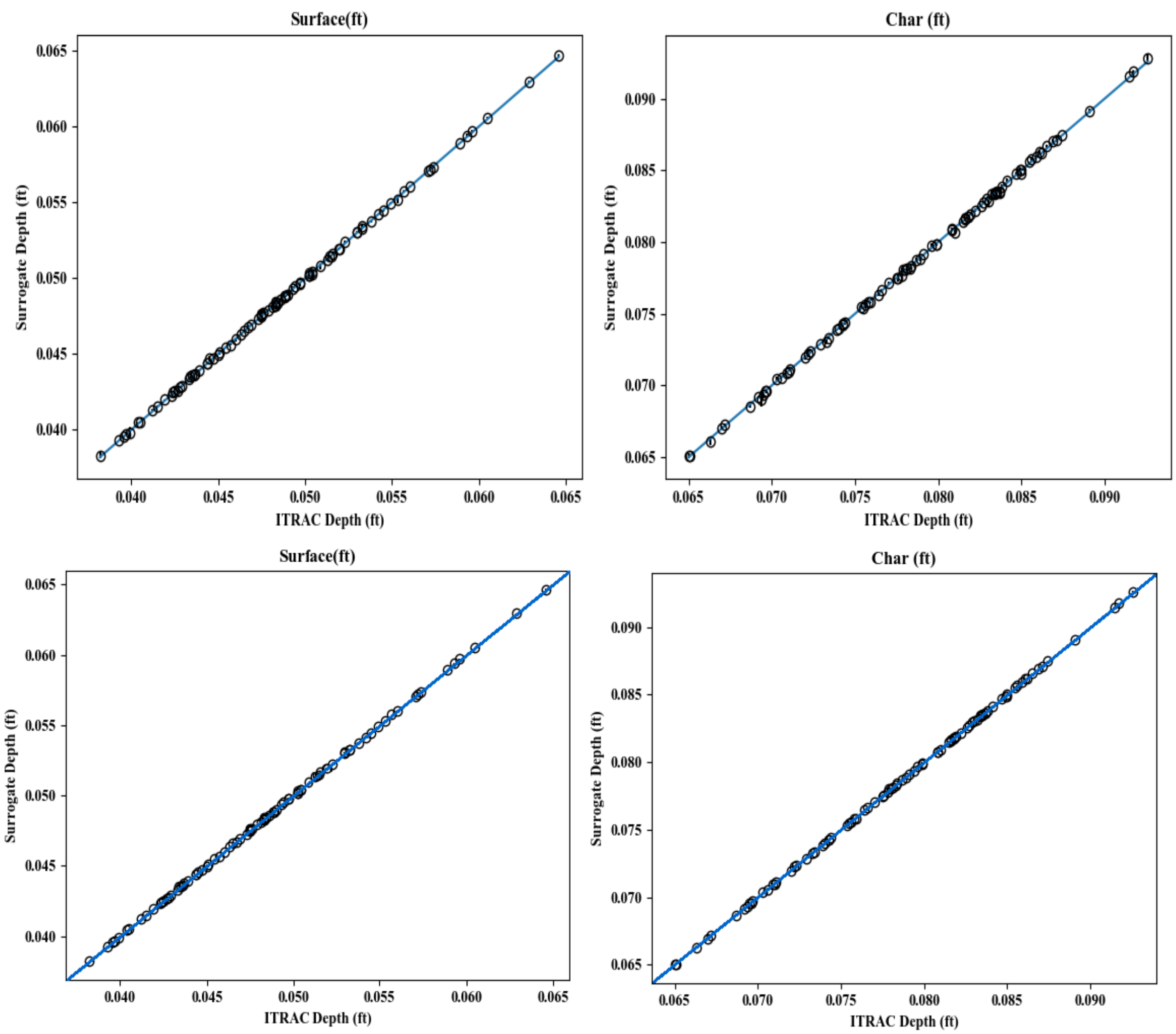

Figure 49. Comparison in PHSM to ITRAC predictions using 100 training simulations (top two graphs) vs 300 training simulations (bottom two graphs). This is at station 6 (throat).

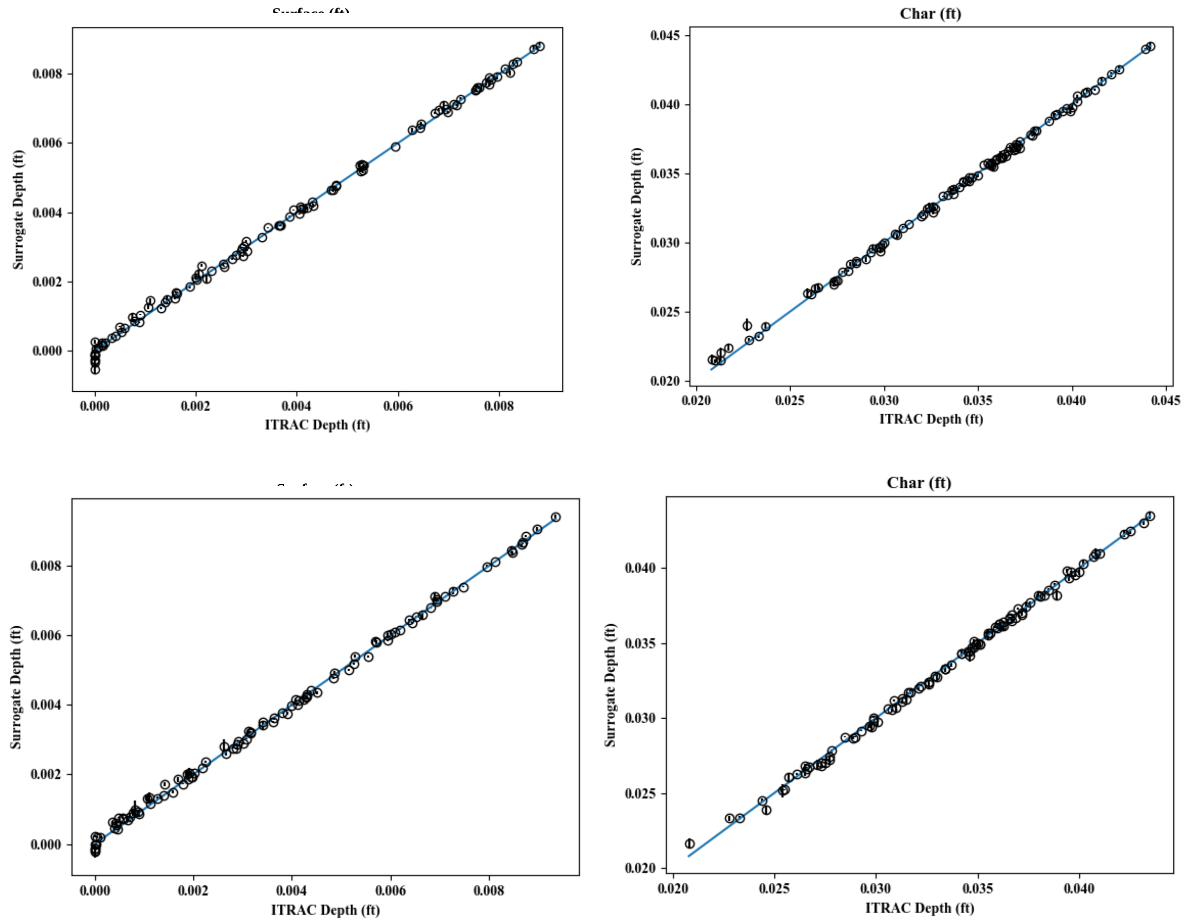

Figure 50. Comparison in PHSM to ITRAC predictions using 100 training simulations (top two graphs) vs 300 training simulations (bottom two graphs). This is at station 25 (nozzle exit).

6.3 SELECTION OF SURROGATE MODEL

The ISM is computationally more efficient than LSM and PHSM. It does predict baseline SRQs exactly, is simple, and tangible. As the ISM inputs deviate from the baseline the error is greatest in this model. It can be improved by optimizes the y-intercept to minimize error. Where error exists, it can be (and is) accounted for by adding epistemic uncertainty to the SM. Any epistemic error added to a surrogate model is assumed to be distributed normally (see Figure 44 and Figure 45).

The PHSM is nearly as accurate as the predictions from ITRAC and has lower error. It can be fitted to additional output data to reduce error, but it isn't necessary based on the assessment above. Considering the speed in which ITRAC can be run and the high accuracy over ISM, the PHSM comes across as the best choice to conduct the 2D-UQ analysis. There is an additional drawback from PHSM and other interpolating methods not apparent in its creation. That is, they do not run in a 2D-UQ loop as fast as a closed-formed solution like the ISM and LSLSM. For example, it takes the ISM and LSM about 2-3 minutes to produce 2D-UQ results on a single processor for a single station. The PHSM takes ~2 hours on 6 processors.

In Chapter 7, the PHSM is used because no significant time constraints exist, and it appears to be the most accurate. The SM error in the LSM is relatively small compared to estimates in uncertainties and the distributions assumed to represent uncertainties. The LSM could be a useful model early in a design process or during design iteration studies where quick estimates are needed.

CHAPTER 7: PROPAGATION OF INPUT UNCERTAINTY THROUGH A 2D-UQ

In Chapter 1, the SRQs of interest were defined. In Chapters 2 and 3, computational and geometrical models were defined along with uncertain inputs in computational model. In Chapter 4, input uncertainty was quantified, and probabilistic distributions were assigned to each input's uncertainty. Input uncertainty was characterized as being aleatory, epistemic, or a mixture of the two. Sensitivity analysis was completed in Chapter 5 to identify most influential inputs on the SRQs of interest. To support 2D propagation of input uncertainty, surrogate modeling was implemented in Chapter 7. As seen, establishing a 2D-UQ methodology is an extensive effort, but alas the final step or steps are here: 1D uncertainty and 2D uncertainty quantification.

7.1 2D-UQ PROPAGATION METHOD

In a traditional 1D-UQ methodology, all uncertainties, both aleatory and epistemic, are propagated through the model simultaneously. The result is a single cumulative distribution function (CDF) that represents the combined effects. This is generally not desired since it confounds aleatory and epistemic influences. In a 2D propagation, aleatory uncertainties are propagated through an initial loop followed by epistemic in a second loop. The first loop, the aleatory loop, produces a single CDF that represent variability. This can be thought of as the first dimension in a 2D-UQ. In this first loop each aleatory input is sampled at random N number of times. Each set of input samples is evaluated by the surrogate model to obtain a single realization of the SRQ. Propagating all N sample sets through the surrogate models gives the natural variability of the SRQ. See Figure 51 for an illustration. This CDF represents a single observation of the SRQ with a mean and standard deviation.

The best known and simplest sampling technique is Monte Carlo sampling[47]. Monte Carlo sampling picks random samples from the entire input distribution. This requires several samples from each input distribution to avoid error in the representation of the SRQ distribution. Error in SRQ distribution is dependent on the number of samples is given by Ang and Tang[131] as:

$$\%\ error\ in\ probability\ (P) = 200\sqrt{\frac{1-P}{NP}} \qquad (7.1)$$

Assuming 5% error is going to be allowed and the probabilities of interest are 0.003, 0.5, and 0.997, the number of samples needed (driven by the probability 0.003) from each input is 532,000.

Another common and more efficient approach is LHC sampling[132-133] and this is what is used here. LHC sampling divides the sampled input distribution into N intervals through stratification. The number of divisions in the input distribution depends on the number (N) of samples specified. For example, if 100 samples are specified, the input distribution is divided into 100 intervals. Each interval will contain equal probability $1/N$. That is, the area in each interval is the same. LHC sampling then draws a single sample randomly from within the interval based on prorating the density of the variable within that interval. The density of all samples will have the same pattern as the distribution because the width and height of each interval are a function of the distribution and N. For smaller sample sizes (e.g. 100 samples), LHC sampling provides greater reliability that the entire input distribution will be sampled compared to Monte Carlo.

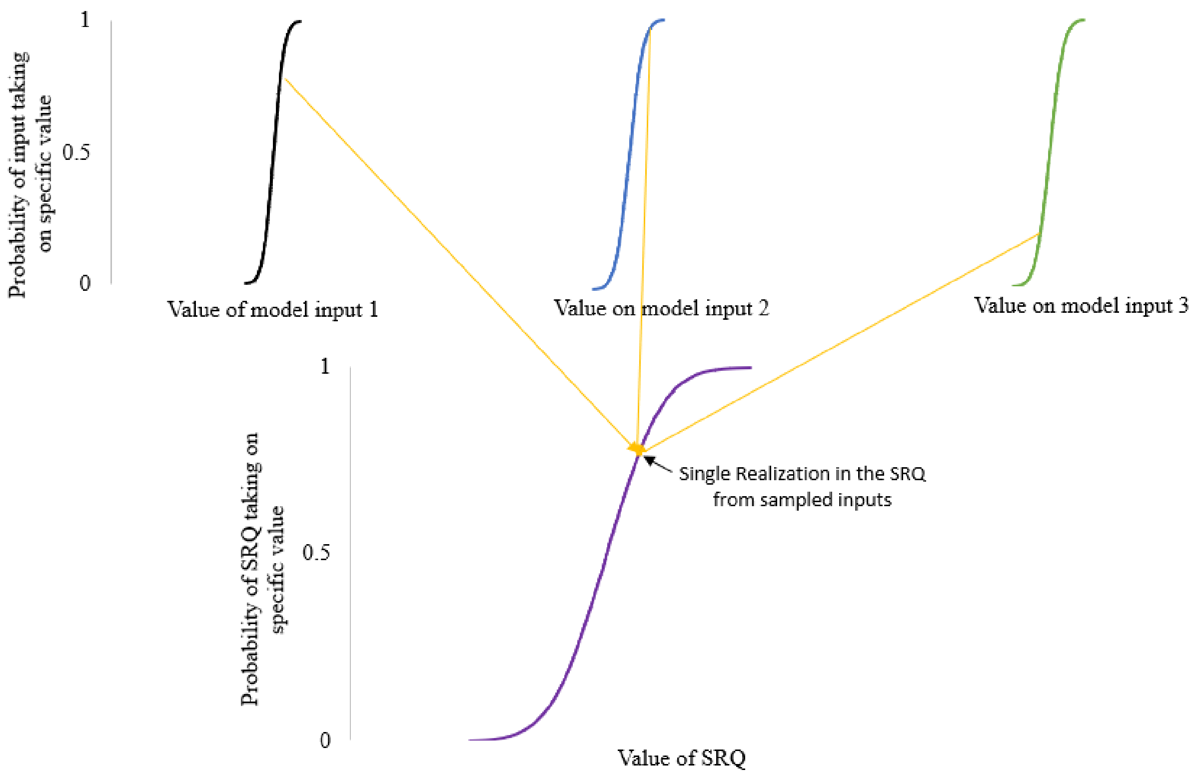

Figure 51. Single realization of a SRQ calculated from a random input sample set. The purple line represents the realization of the variability in the prediction from all N input sample sets.

The sample size used to estimate aleatory uncertainty is 1000. This is higher than needed for convergence, but since probabilities of 0.003 and 0.997 are wanted, this sample size avoids the inconvenience of interpolation to obtain the desired probabilities. For reference, aleatory sample size was more sensitive than epistemic sample size since low probability epistemic iterations are truncated using a probability box (p-box)[6].

In the 2D or second loop, uncertainty in model predictability is quantified. The 1D loop gives information on how much the prediction varies about nominal input values. However, for some inputs (e.g., q''_{rad}), the nominal value is unknown, but estimated to exist over some interval. For enthalpy conductance, it contributes to the erosion and char data distribution "thickness" but where the center of the data is pre-test is uncertainty. This epistemic uncertainty in nominal input values causes the 1D variability to shift. The magnitude and direction of shift is based on epistemic uncertainty of inputs and model form error. There is epistemic uncertainty in both boundary conditions, in surrogate models, and in model from error in ITRAC on the prediction of char depth[37]. The model form error for char is given as an average of 4.2% (overpredicts char depth) with a standard deviation of 6% when the boundary conditions are matched to erosion data. It can be greater in the pretest prediction but is at least this much. The 2D loop can be thought of as a representation of the epistemic probability density function (PDF) on the aleatory CDF. This is shown in Figure 52. Each CDF is a realization of the variability in the prediction and all CDFs are a realization of the credibility in the prediction.

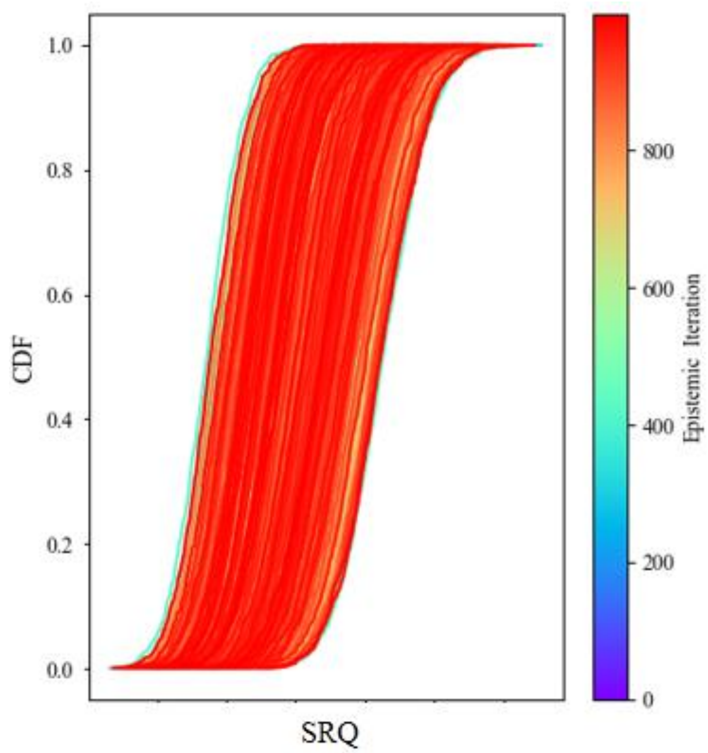

Figure 52. CDFs (variabilities) that are possible over all credible ranges. 1000 epistemic iterations shown.

CDFs at the extremes are representative of the most unlikely scenarios (e.g. lowest probabilities in the epistemic distribution). For example, the far-right CDF in the figure would be the location where g was at its high limit, q''_{rad} was at its high limit, and surrogate model error was positively high. The 99.7% probable location of the far-right CDF would be where all the former epistemic inputs were high, but also where every aleatory input's high limit is stacked up. This is possible, but highly incredible. The most credible CDF is the one right in the middle (50% credible).

To capture a targeted level of credibility, a p-box is used. The p-box truncates the 0-100% epistemic range by limiting CDFs to those that fall within the stated range. A 90% credibility p-box is used here. CDFs in the interval below 5% and above 95% are considered to be outside the range of acceptable credibility. See Figure 53 for an illustration. Depending on the level of real-world risk a prediction is trying to avoid, the p-box can be adjusted up or down.

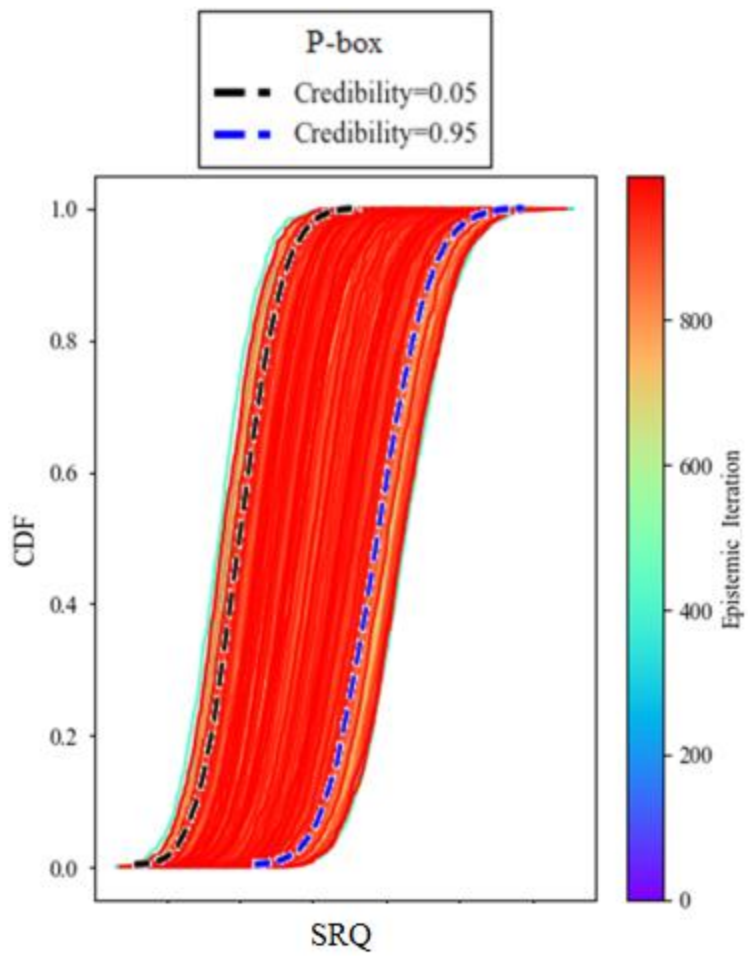

Figure 53. P-box bounding the credible interval of aleatory CDFs.

The width of the p-box represents the predictability of the model and the tails of the 50% credible CDF compared to 50% probability represent the variability in the model. The entirety of the p-box represents where SRQ predictions are likely to reside. In the present application, the left side of the p-box is nonconservative and vice versa. The top of the p-box is more probable than the bottom. The top right corner of the p-box is the most probable and most conservative prediction.

In the nozzle ablation SRQ predictions here, the 99.7% (3σ) probable and 95% credible p-box location is used as the basis for nozzle insulator design thickness. That is to say, "with 95% credibility and 99.7% probability, the SRQ will not be greater than this." For a very high-risk situation (e.g., life, death, financial ruin, political reputation) a decision maker may push the conservative p-box bound. In another scenario a decision maker may be unwilling to accept the additional margin (e.g. nozzle weight too high or additional margin doesn't fit the design space) and instead consider design-risk tradeoff of 95.4% (2σ) probability and 75% confidence.

7.2 UQ PROPAGATION RESULTS

Figure 54 through Figure 66 show the p-box for each station. Each CDF is a representation of the aleatory uncertainty. A CDF with more slope or longer "tails" is a representation of higher aleatory uncertainty. The width of the p-box is representative of the epistemic uncertainty. The solid center line is the 50% credible, 50% probable prediction and is the nominal and most probable prediction. The nominal prediction is not the prediction from ITRAC although they can be the very similar. This is the case for erosion, but for char, this is not the case since model form error exists in the ITRAC prediction. The ITRAC prediction would be shifted to the right from the nominal p-box prediction since there is a tendency for ITRAC to overpredict the char depth.

The scale on the x-axis is held constant to illustrate the reduction in both the nominal depth predictions, but also in the reduction in aleatory and epistemic uncertainties. As the magnitude of the boundary condition is reduced, the amplification of an input's variability on the response of the SRQ is also reduced. The slope becomes less slanted as the heat transfer coefficient is reduced since it is a primary driver in the effect of other aleatory inputs. The width of the p-box shrinks since the $\pm$12.5% epistemic uncertainty is multiplied by a smaller heat transfer coefficient and the contribution from radiation heat flux epistemic uncertainty is diminished.

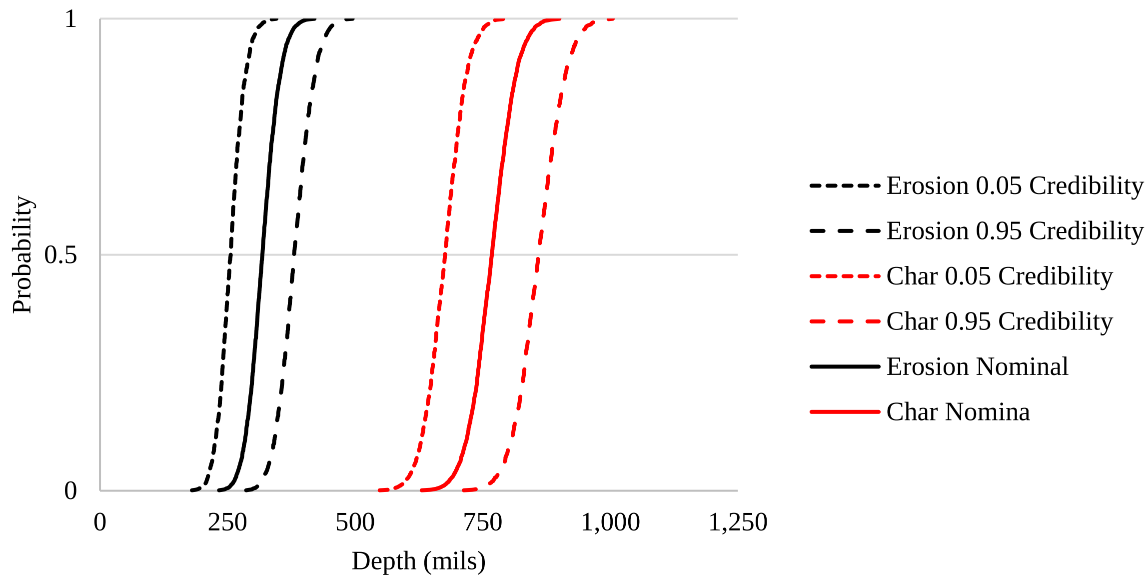

Figure 54. Erosion and Char p-box and Station 1.

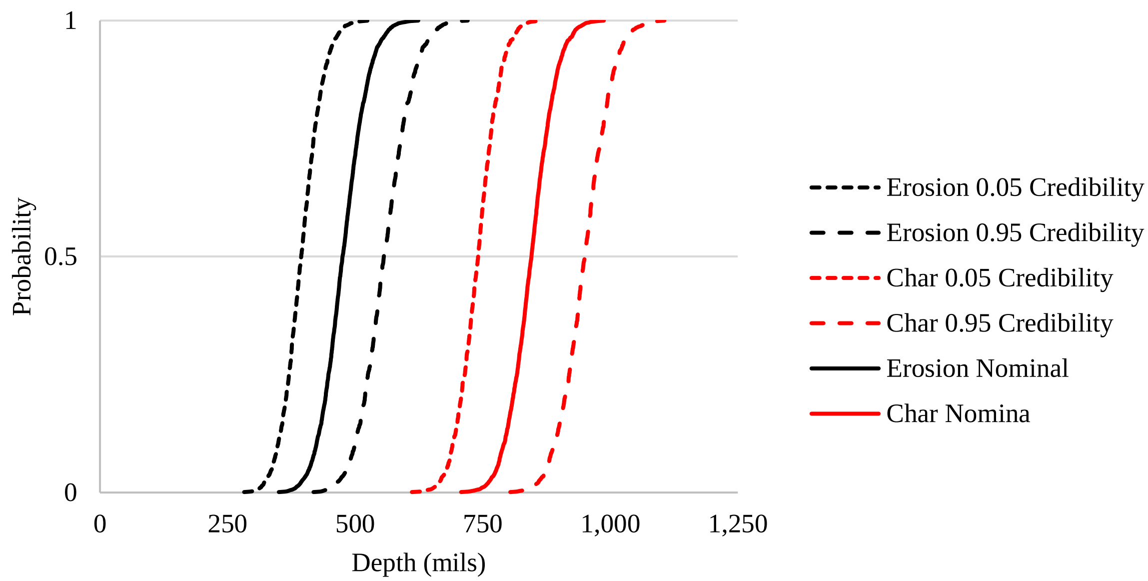

Figure 55. Erosion and Char p-box and Station 3.

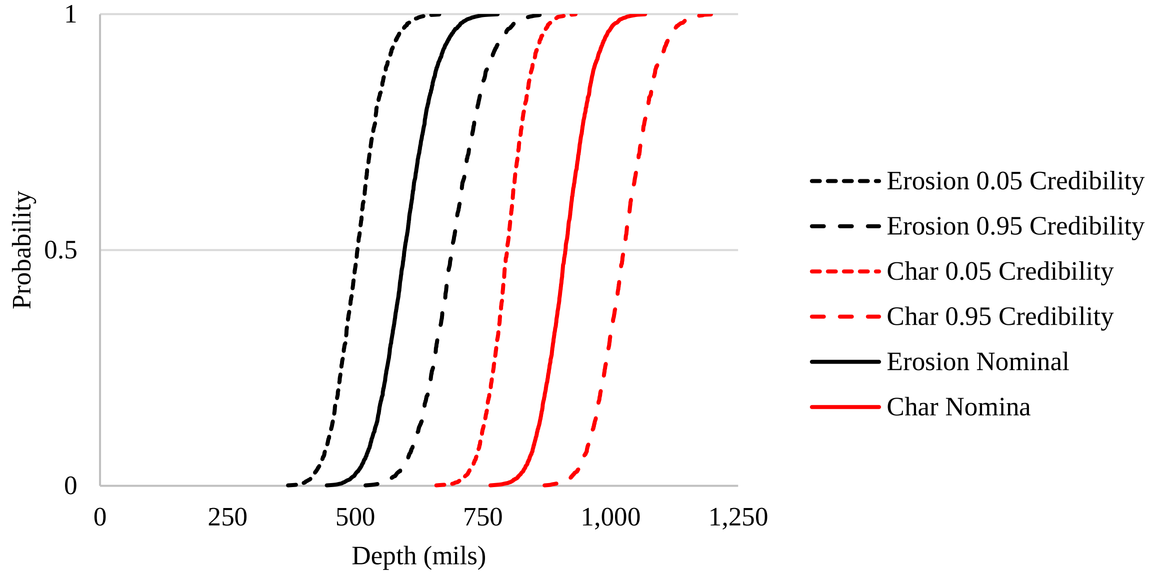

Figure 56. Erosion and Char p-box and Station 6.

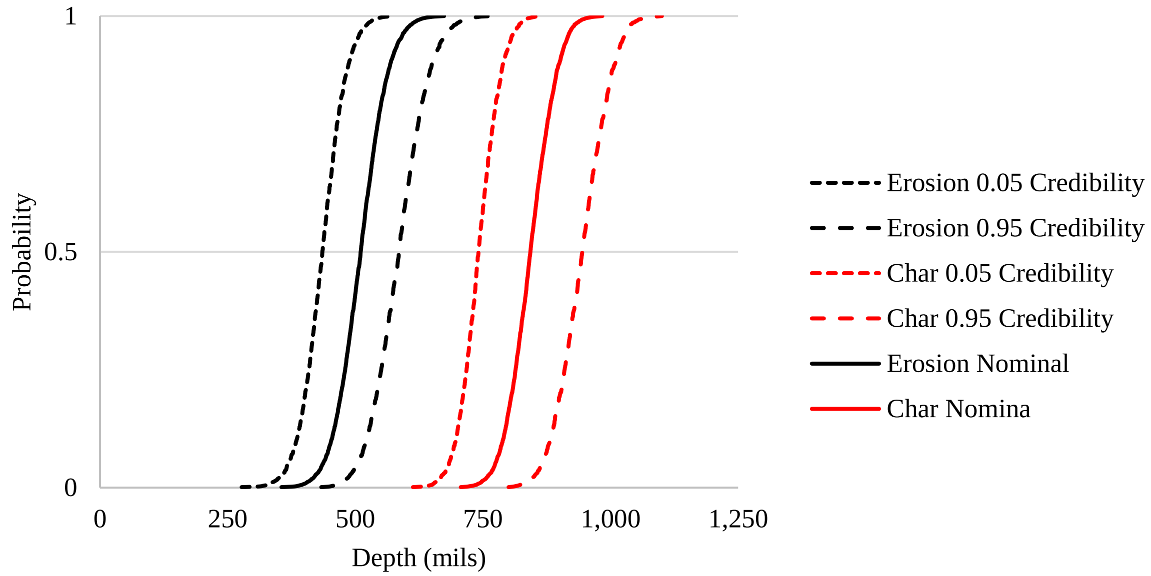

Figure 57. Erosion and Char p-box at Station 8.

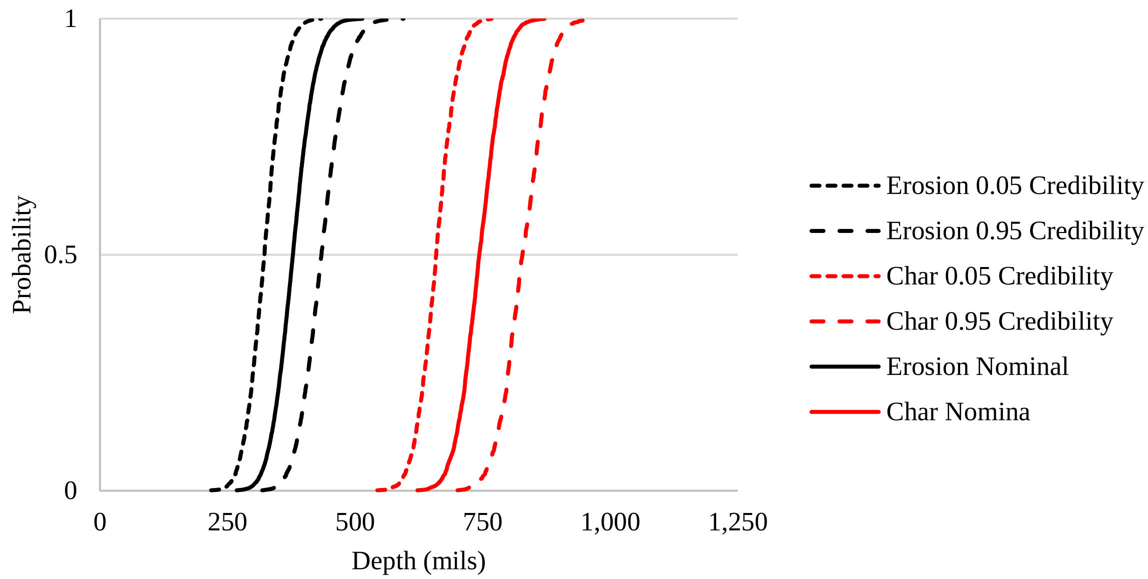

Figure 58.Erosion and Char p-box at Station 10.

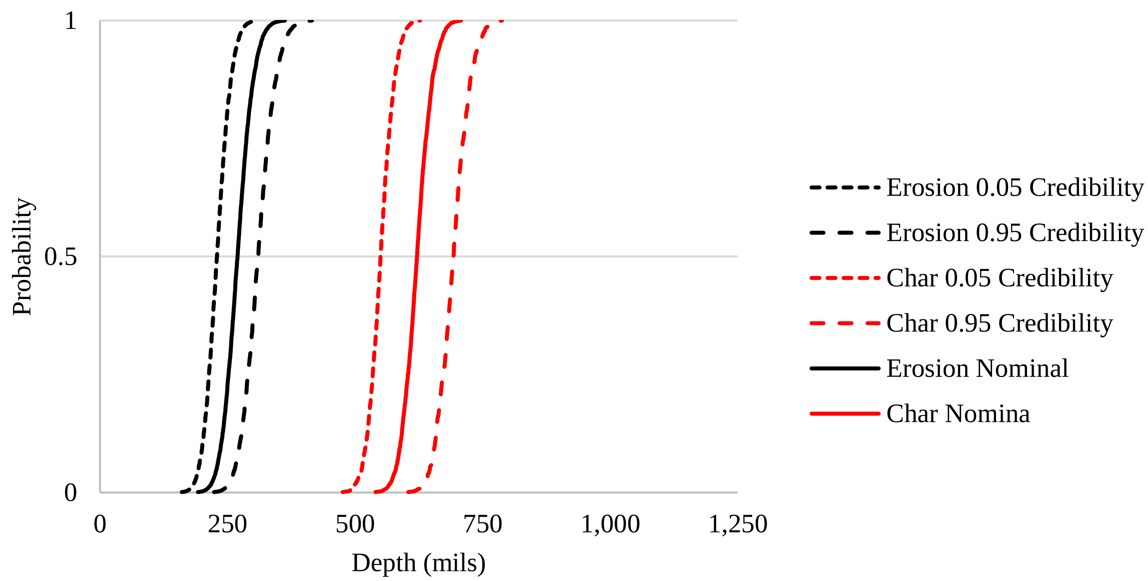

Figure 59.Erosion and Char p-box at Station 17.

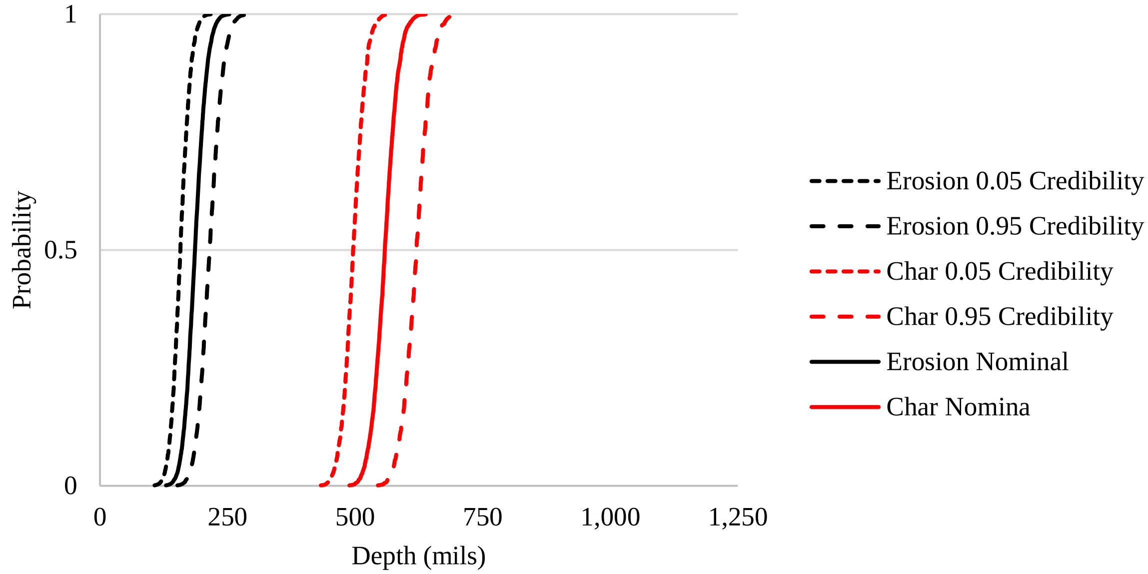

Figure 60.Erosion and Char p-box at Station 19.

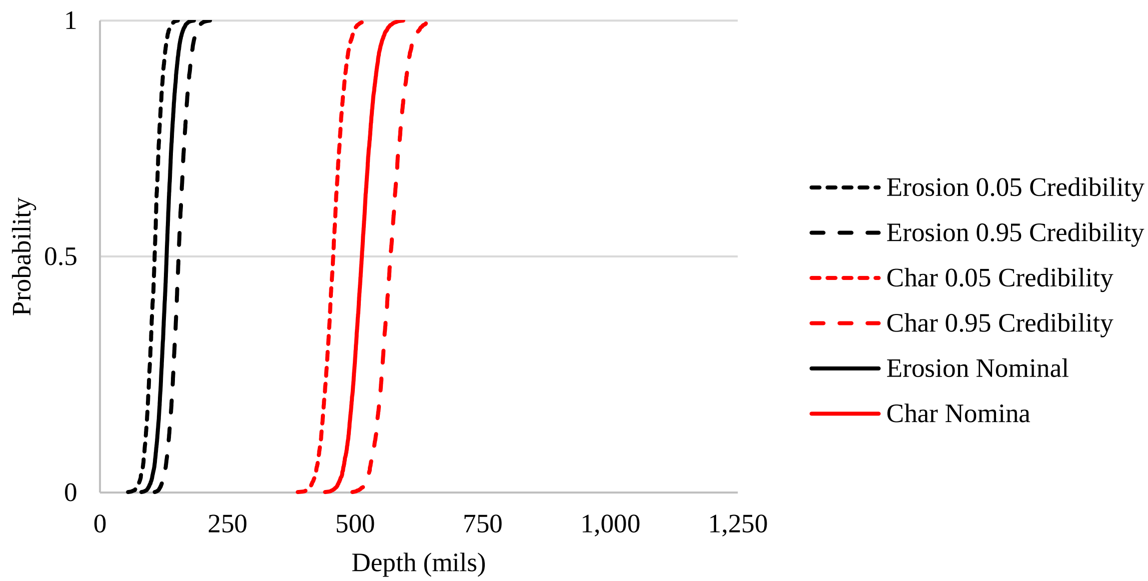

Figure 61.Erosion and Char p-box at Station 20.

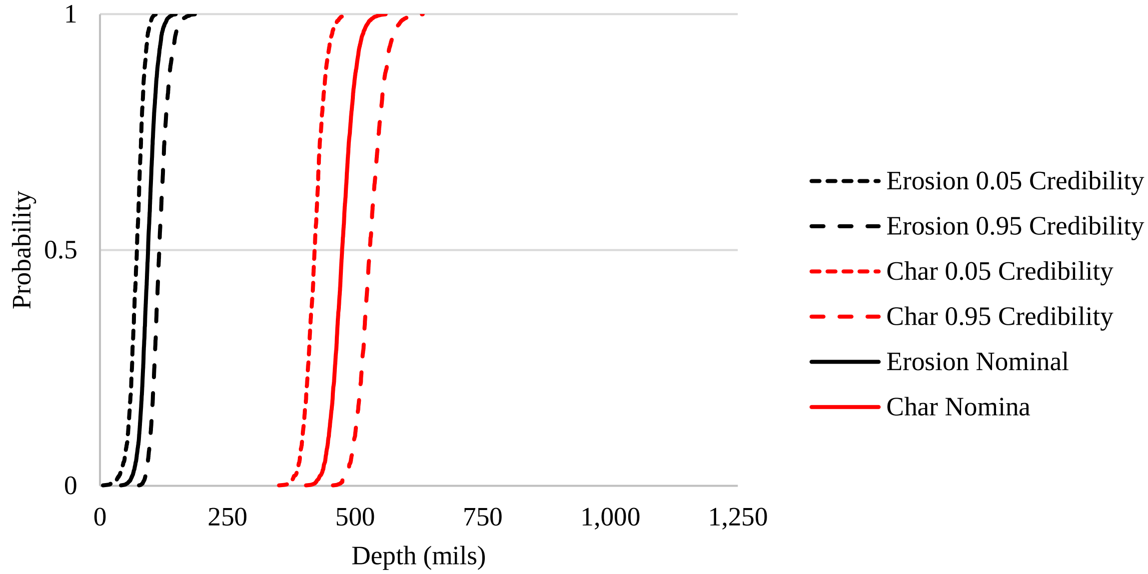

Figure 62.Erosion and Char p-box at Station 21.

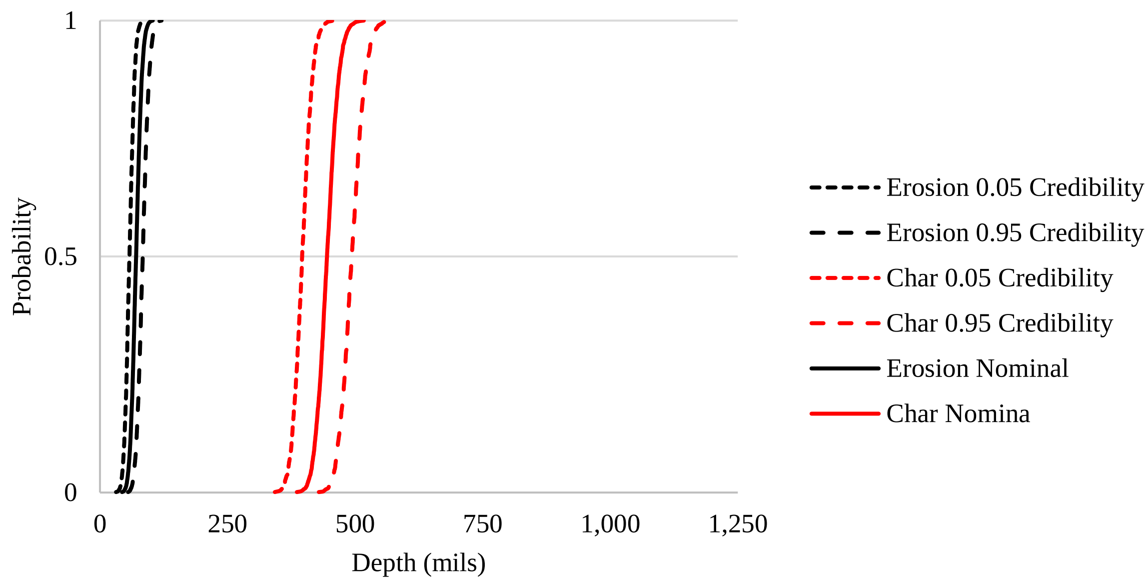

Figure 63.Erosion and Char p-box at Station 22.

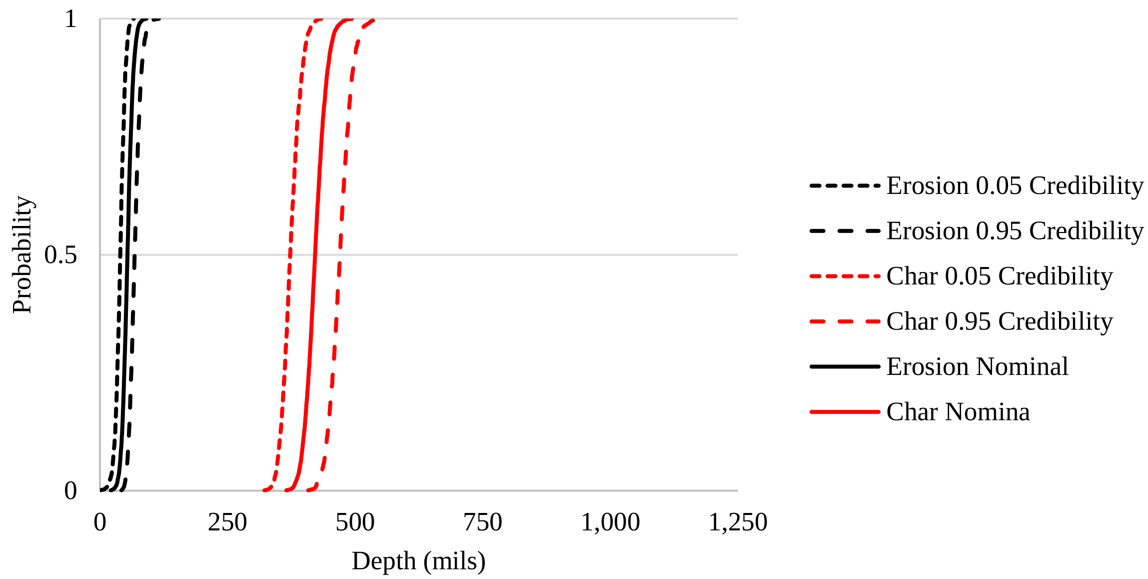

Figure 64. Erosion and Char p-box at Station 23.

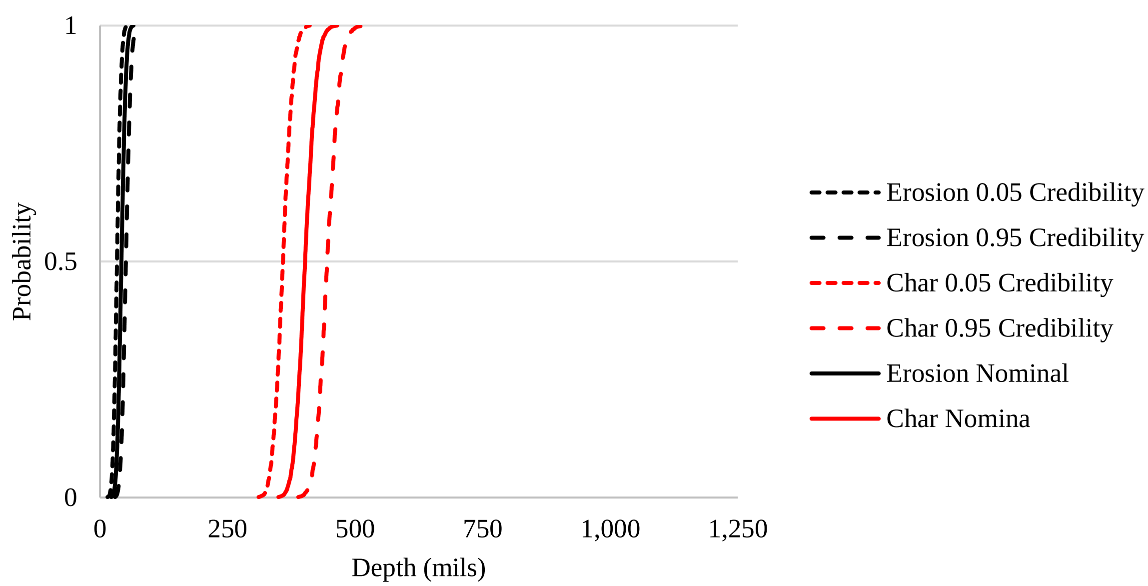

Figure 65. Erosion and Char p-box at Station 24.

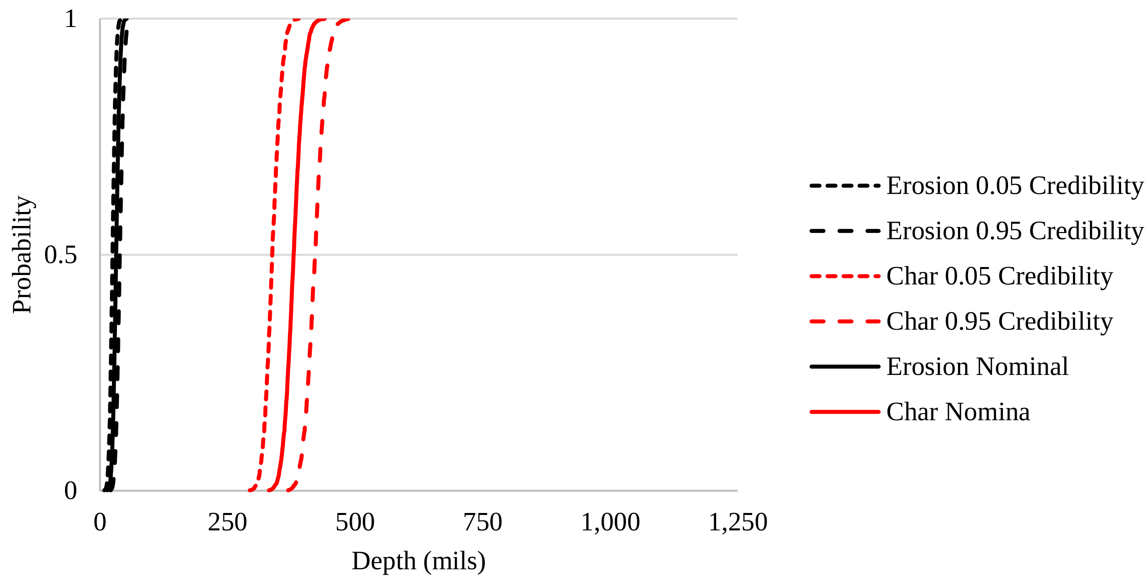

Figure 66. Erosion and Char p-box at Station 25.

7.3 INTERPRETATION OF 2D-UQ PROPAGATION RESULTS.

The uncertainty is derived from station p-boxes using Figure 67 and equations (7.2-7.4). The subscripts A, E, and O attached to the uncertainty, U, are for aleatory, epistemic, and overall uncertainty. The probability at x_1 and x_2 is 99.7%. The probability at x_3, x_4, and x_5 is 50% and the probability at x_6 and x_7 is 0.3%.

Application of equations (7.2 – 7.4) to the CM nozzle is illustrated in Figure 68-Figure 70. Nominal erosion and char are the 50% credible 50% probable values. The uncertainty from equations (7.2-7.4) is subtracted/added to the nominal values. Aleatory uncertainty is slightly greater than epistemic uncertainty. While interesting, this is partly an outcome of the characterization of the uncertainty and choice of distribution used to represent this uncertainty. The results show that there is nearly as much uncertainty in the prediction as there is natural variability SRQs.

In looking at Figure 68, slight discontinuities in erosion aleatory uncertainty in the exit cone are observed. These discontinuities are caused by a sharp SM form error increase in one station vs another where SM form error is low or negligible (see Appendix B for error on PSHM for all stations). Instead of “zigzag” the curves should be continuous in this region. In Figure 70 the discontinuities are more pronounced. This gives some clue that the SM form error is being caused by instability in the PHSM away from fitted sample points. The easiest way to address these discontinuities is by interpolating from stations with low SM form error on each side of a station with high SM form error. This correction method is what is done here. The correction is illustrated in Figure 71. As an alternative, these discontinuities can also be addressed by providing additional fitting points or using the LSM in the exit regions.

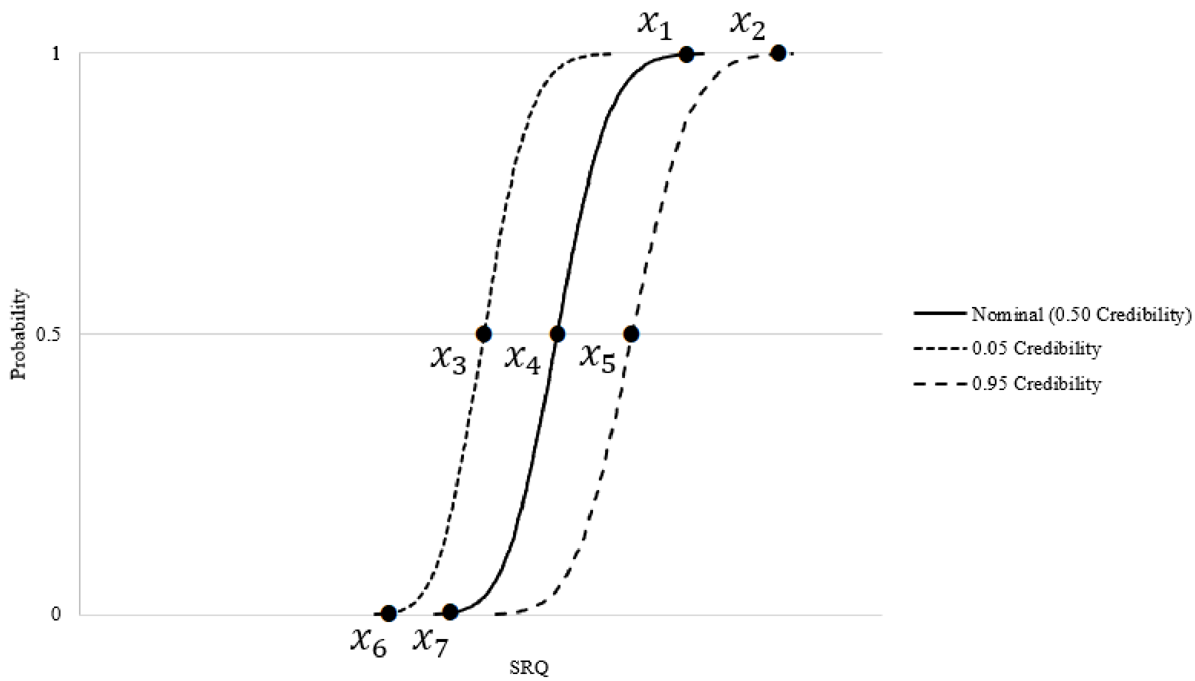

Figure 67. Deriving uncertainty from the p-box.

$$\frac{x_7}{x_4} - 1 \leq U_A \leq \frac{x_1}{x_4} - 1 \tag{7.2}$$

$$\frac{x_3}{x_4} - 1 \leq U_E \leq \frac{x_5}{x_4} - 1 \tag{7.3}$$

$$\frac{x_6}{x_4} - 1 \leq U_O \leq \frac{x_2}{x_4} - 1 \tag{7.4}$$

Figure 72 and Figure 73 show the uncertainty in the motor as a function of location in both a percent difference and a dimensional mils difference. These have been corrected for station 21 and 23 (axial distance of 8 and 4 in. respectively) by interpolating between stations. The uncertainty in erosion is shown to be a strong function of heat transfer coefficient. This is slightly dampened for char depth where it is not as sensitivity to heat transfer coefficient. The ± 28% percent difference for char is nearly constant through the entire axial length of the motor, where for erosion depth, the percentage increases from ±~45% to ±~80% as the erosion depth get small.

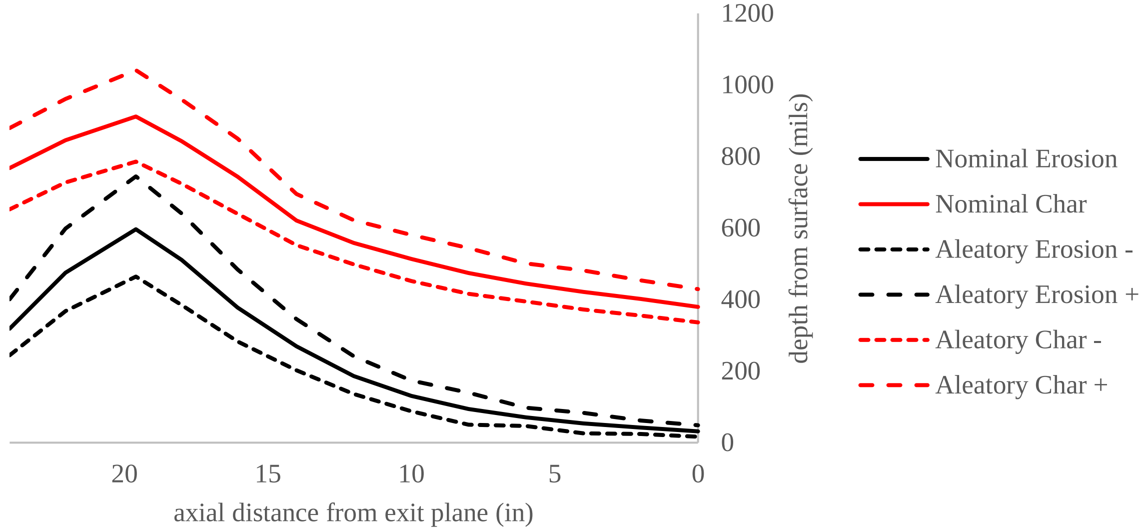

Figure 68. Aleatory uncertainty as a function of nozzle location.

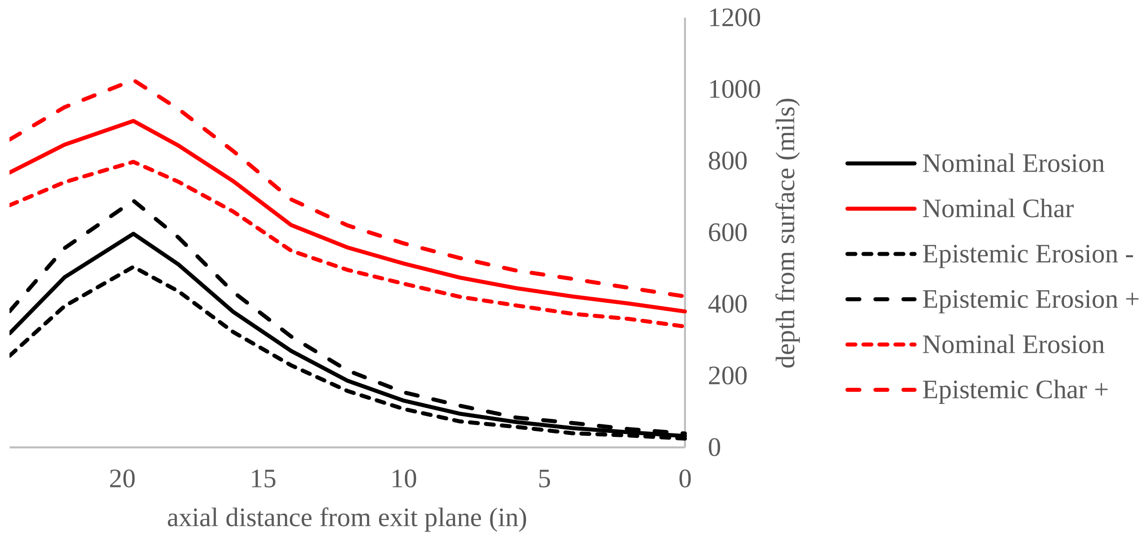

Figure 69. Epistemic uncertainty as a function of nozzle location.

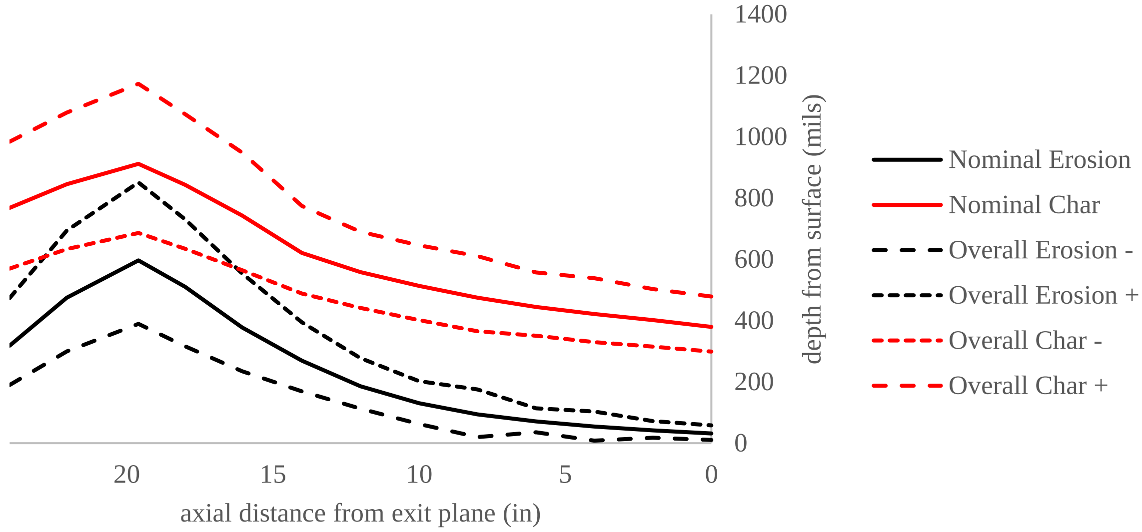

Figure 70. Overall uncertainty as a function of nozzle location.

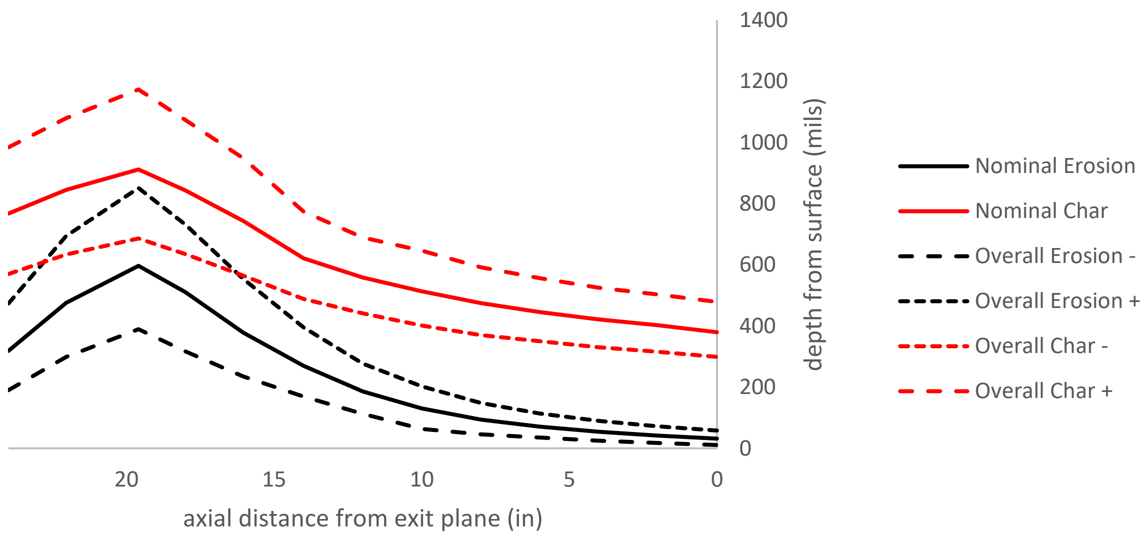

Figure 71. Overall uncertainty as a function of nozzle location (corrected).

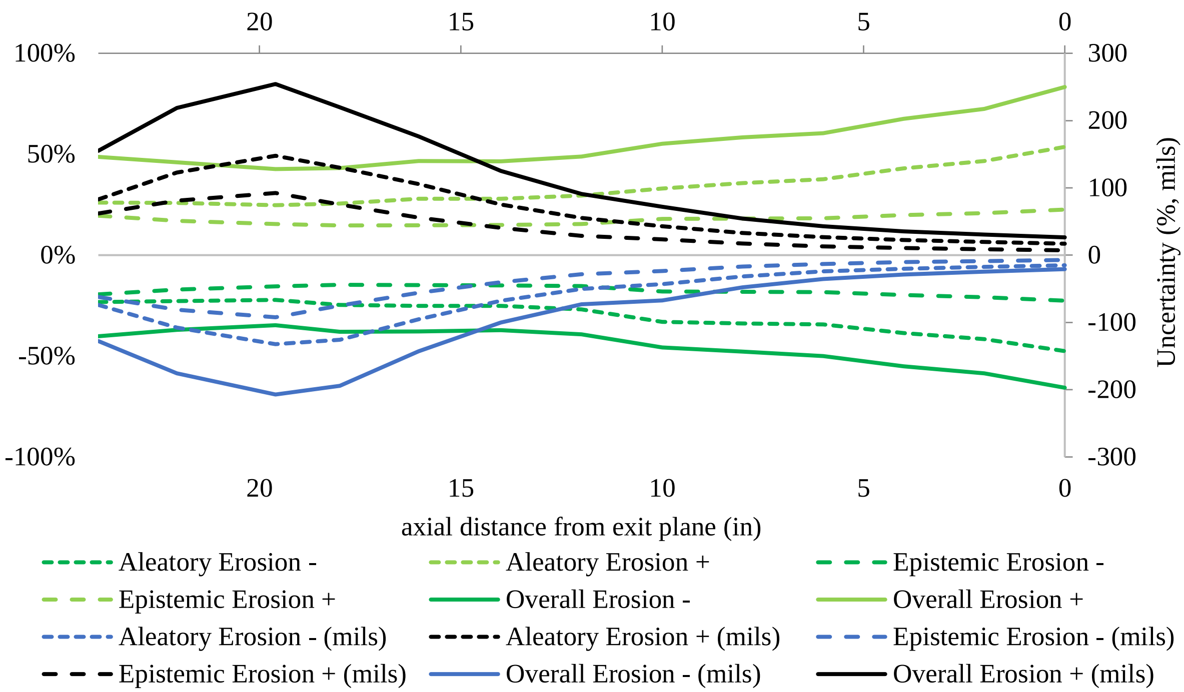

Figure 72. Uncertainty of erosion depth as a function of nozzle location in percent and mils (corrected).

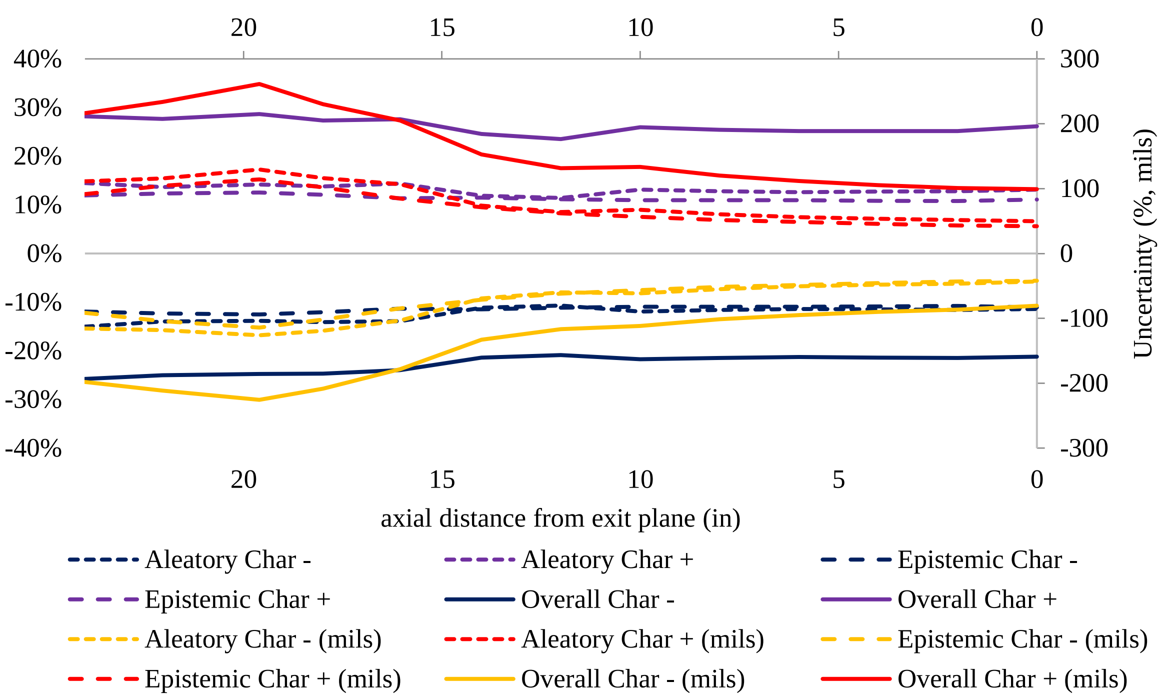

Figure 73. Uncertainty of char depth as a function of nozzle location in percent and mils (corrected).

7.4 COMPARISON WITH CM NOZZLE EROSION AND CHAR POST-FIRE MEASUREMENTS

Figure 74 shows the prediction with overall uncertainty compared to the measured erosion and char depths from the CM nozzle. The nominal erosion prediction is excellent from the entrance through the throat ring, but clearly Bartz's correlation overpredicts in the exit cone even when the 25% reduction is applied. The trend however is excellent compared to the data. Overall uncertainty in the erosion prediction is conservative compared to erosion data. Prediction in char depth is reasonable considering motor conditions post-fire are unknown. Meaning there is no information on how or if this nozzle was quenched. The data when measured could have been indicative of heat soak conditions. The underprediction at the nozzle exit is expected due to strong 2D heat transfer effects (e.g. fin effects, nozzle aft-end heating).

The agreement overall is remarkable considering the assumptions used in characterizing the uncertainty, and the fact that this nozzle is made up of similar, but different materials that were modeled as being the same material. The computational model was 1D throughout and didn't attempt to capture any fin or aft-end heating effects. The heat transfer coefficient was based off a correlation with a single reduction factor applied throughout and the heat transfer variability was based off a non-similar motor that was the same material throughout. No attempt was made to capture impingement effects or erosion effects in the down-step region just aft of the throat.

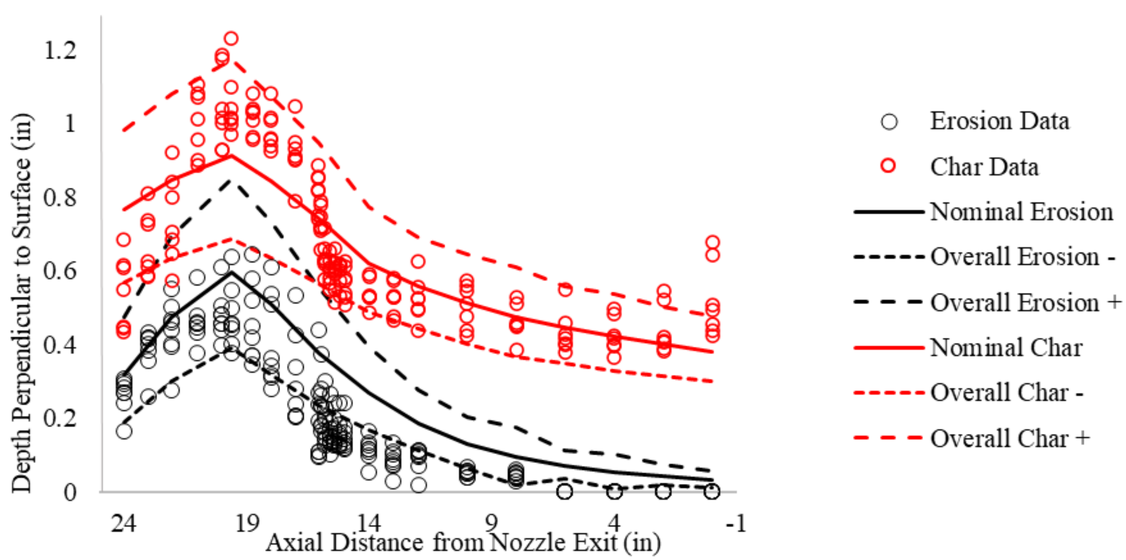

Figure 74. Overall uncertainty compared to measured nozzle erosion and char depths.

Another desirable comparison is how the measured data fits within the aleatory uncertainty and the overall uncertainty. If the nominal prediction was the same as the average measured data, the aleatory variation should bound the data or at least 99.7% (i.e. 3σ) of the data. Since there was epistemic uncertainty in the nominal prediction, there is also a desire to compare the measured data to the overall uncertainty which should bound all data. Figure 75 and Figure 76 show comparison between data and aleatory and overall uncertainties.

About 95% of the measured erosion data fall within the aleatory uncertainty and 99% within the overall uncertainty. Most of the data outside the erosion aleatory uncertainty is in entrance cap and nose ring. The entrance cap and half of the throat ring are different materials than what was modeled. This work did not consider the variability in anything but MX4926. It is also possible that the area just downstream of the throat where a joint exists was subjected to anomalous effects. It is also shows that the "width" of the HIPPO nozzle data that was used to justify aleatory uncertainty in heat transfer coefficient is not as wide as the CM nozzle (see Figure 30 and Figure 31). This is likely the main driver. It could also be that assuming Gamma distributions for densities and heat transfer coefficient was a poor assumption. Certainty characterizing radiation heat flux as being purely epistemic is not helping to capture all data within the aleatory uncertainty bounds.

For the char data, about 85% is within the char aleatory uncertainty and 98% within the overall uncertainty. The data that is outside aleatory uncertainty at the exit is for obvious reasons. In other regions, it could be possibly attributed different materials … different kinetic models. While it was established that variability in kinetics is negligible, an entire change over to different kinetics can drive the azimuthal data spread, especially in an unquenched motor. Like erosion data, using a non-similar motor to correlate aleatory uncertainty in the heat transfer coefficient is driving this along with Gamma distributions on densities and heat transfer coefficient. Characterizing radiation heat transfer differently could also help.

The trend in bounding the data is still very reasonable considering the assumptions and the data availability from the literature.

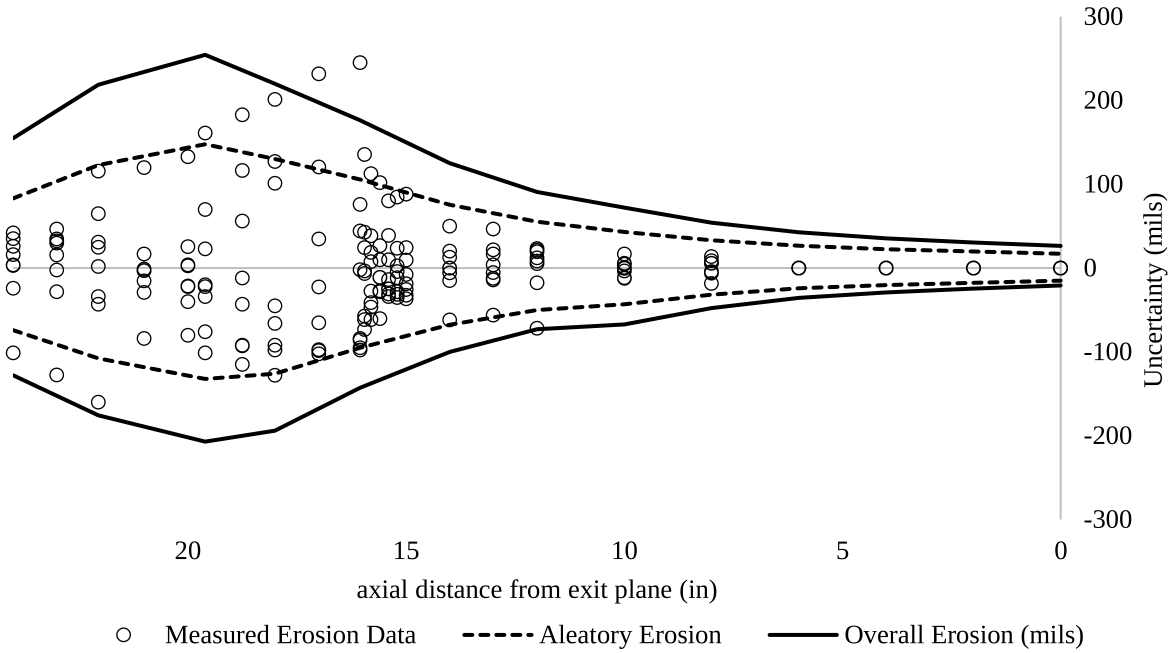

Figure 75. Erosion depth aleatory and overall uncertainty compared to measured erosion data.

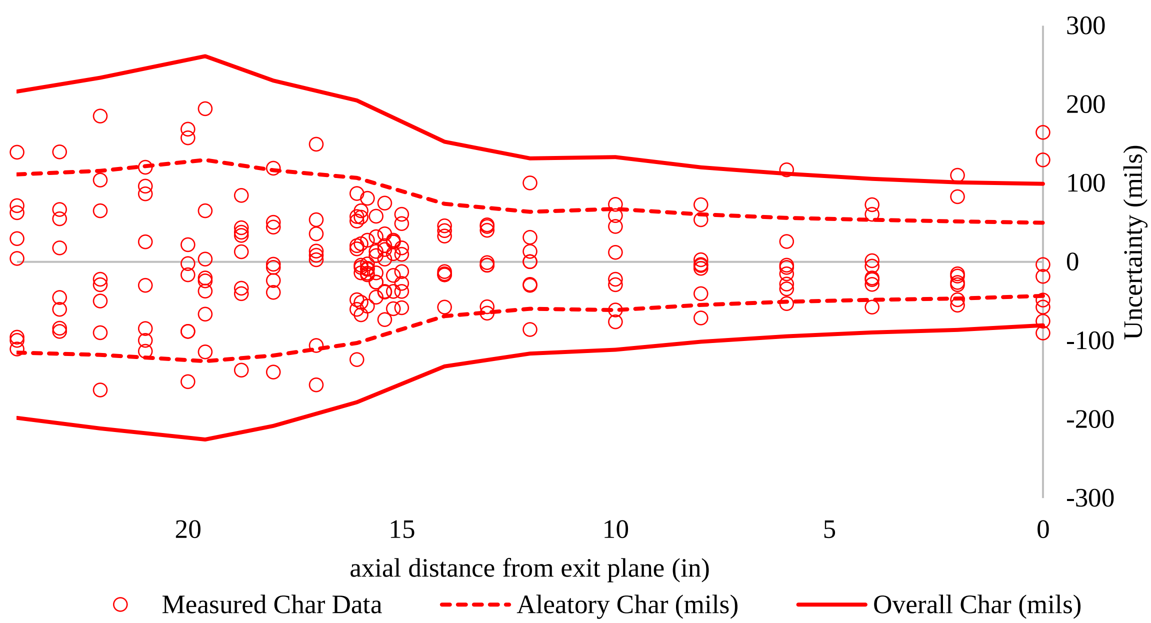

Figure 76. Char depth aleatory and overall uncertainty compared to measured char data.

CHAPTER 8: SAFETY FACTORS, UNCERTAINTY REDUCTION TECHNIQUES, AND FUTURE WORK

The safety factor (SF) method for the CM nozzle given by Arnold et al.[39] is shown in equation (8.1). Comparison is made between this SF and the 2D-UQ methodology. Other safety factor methods can be found in refs. [134-135].

$$\delta_i \geq 2\delta_e + 1.25\delta_c = \delta_{SF} \tag{8.1}$$

Subscripts i, e, c, and SF are initial thickness, erosion depth, char depth from eroded surface, and safety factor. Table 16 compares the SF calculated by Arnold et al.[39] and what was predicted in this work. The results are very similar with the results in this work being slightly more conservative. Arnold et al. say the CCP thickness in the final design was greater than what is in Table 16. This may explain why the thicknesses at station 15 and station 24 that were digitized from Figure 12 are very close to SF depths calculated by Arnold et al.

Figure 77 shows a comparison of the initial CCP material thickness (measured from digitization of Figure 12), material thickness at a 1.0 SF, material thickness required to obtain a 2D-UQ 200°F isotherm depth at the interface between CCP and the steel structure, and the 99.7% probability 95% confident char depth (overall char depth uncertainty). The “X” in the figure is the location of the shear pin tip going through the steel structure and into the CCP. The overall char depth uncertainty prediction indicates the shear pin tip will reach ~1150°R at end-of-burn as a worse case.

Table 16. Comparison between predictions from Arnold et al. and Chemics, ITRAC, Bartz used here.

Station	radius (in)	A/A*	δ_i	δ_e	$\delta_c = \delta_p - \delta_e$	δ_p	δ_{SF}
Arnold et al. (ACE, AGRIEBL, CMA)							
15	4.20	1.44	1.05	0.329	0.376	0.705	1.128
24	8.27	5.58	0.50/---	0.039	0.382	0.421	0.555
Chemics, Bartz, ITRAC							
15	4.20	1.44	1.12	0.330	0.392	0.722	1.150
24	8.27	5.59	0.578/1.128*	0.043	0.376	0.419	0.556

Note: δ_c is not char depth as used throughout this. It is char depth from the eroded surface.
* Depth from CCP surface to Shear pin tip/CCP thickness.

CCP thickness based off the 200°F isotherm is conservatively low enough and provides adequate thermal protection for the adhesives used between the insulator and the steel structure. Also apparent, an initial thickness using a 1.0 SF would not provide the same protection at the bondline in the nozzle exit cone where the insulator is the thinnest. If the heat transfer coefficient was calibrated to match motor data or if it was underpredicted the safety factor case would be even worse, yet still be perceived to be conservative. This is an advantage of the UQ over SF's: UQ shows the whole picture. It gives the decision maker the ability to decide how much risk, if any, could be realized. If this conservative 2D-UQ isotherm depth was used to inform nozzle insulator design thickness, a weight savings of ~30% on average could be realized. Reducing the CCP thickness this much would result in an acceptable shear pin tip temperature which would limit weight savings to ~6% in the exit cone. Alternatives in insulator retention would need to be explored to optimize weight reduction.

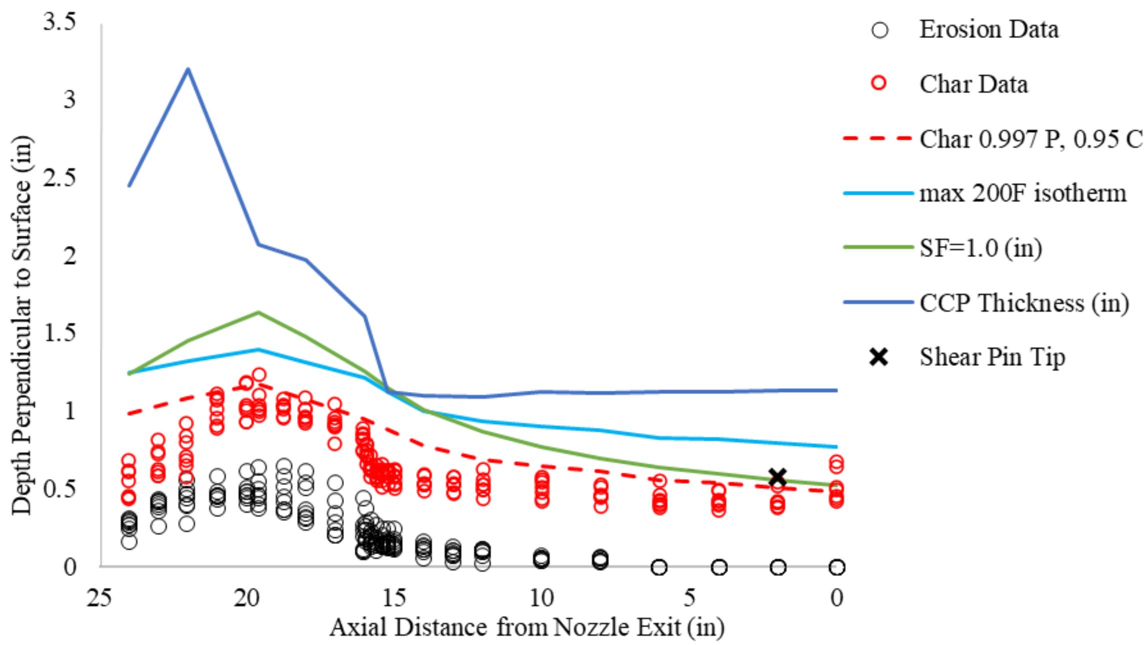

Figure 77. 2D-UQ vs SF=1.0.

An obvious advantage of safety factor methodologies is they remove all the effort to think about and define uncertainties, probabilities, and instead make everything a deterministic "best-estimate" with some conservatism on top. They can be applied efficiently and have served the design community and end customer well for decades. However, the apparent risk reduction in the application of safety factors can be misleading if the prediction is assumed to be nominal with no information on how much variation there is away from nominal. Of course, making nominal predictions with a safety factor in today's regulatory climate is becoming less fashionable. Instead, safety factors are applied to perceived worst-case scenarios resulting in over conservatisms in the design. Strict perceived risk avoidance strategies can lead to a stack up of design safety factors on worse-on-worse case scenarios until the final design is so robust that it's impractical to build or pay for. Or the value of the data that might have been gained is so severely diminished that it is never realized. Additionally, safety factor methods are based on historical data and historical technologies and may not readily transfer to new technologies. Collaboration and integration should be made between the UQ and SF. One proposal would be to develop UQ-informed SF's.

8.1 UNCERTAINTY REDUCTION TECHNIQUES

In this section, three uncertainty reduction techniques are discussed. The first is reduction through real-world testing, the second is via modeling improvements, and the third is in understanding input uncertainty with greater fidelity.

Historically, programs such as NASA's Reusable Solid Rocket Motor[136] had large motor testing campaigns prior to flight and throughout the life of the program. This was necessary both to prove and advance the technology. Additionally, computational tools gave "ballpark" predictions prior to testing and required motor data to anchor predictions.

The value of motor testing is realized by way of comparison to unanchored model predictions, experimental data model anchoring, and like-for-like motor data anchoring. The comparison is shown in Figure 78. The Bartz correlation results shown in Figure 78 is prior to the 25% reduction. The experiment data anchor is the 25% reduced Bartz, and the motor data anchor is calibration of the heat transfer coefficient to the post-test erosion data.

As can be seen, raw predictions greatly overpredict erosion and to a lesser extent char depth. In another motor that has significant mechanical erosion, underprediction is possible. Experimental motors, subscale motors, or motors with similar contours, pressures, burn times can be used to provide some anchoring as seen by the experiment data anchor improvement, but like-for-like motor testing provides the greatest reduction in uncertainty. An additional advantage of testing is it captures phenomena that was not anticipated or included in the model.

Recall in the sensitivity study and during surrogate model development that sensitivity of the inputs were dependent on the heat transfer coefficient. This sensitivity carried forward into the magnitude of aleatory and epistemic uncertainty. An overprediction of the heat transfer coefficient over predicts sensitivity of inputs and over predicts the uncertainty. The opposite is true when the heat transfer is underpredicted. Motor data anchoring allows for reduction or complete removal in epistemic uncertainty in boundary conditions. This is reflected in the station 6 p-boxes shown in Figure 79. The reduction in uncertainty is made by reducing the epistemic uncertainty on g to $\pm$ 5% and eliminating the variation in q''_{rad}. This elimination is made since the nominal boundary condition is no longer uncertain and g still varies to the extremes in the data. A 41% (128 mils) reduction is seen in overall uncertainty for erosion, but not as much is gained in char depth (~10%, 44 mils). This is an estimate of the reduction since actual data matching was not done prior to reducing the epistemic uncertainty on g in the 2D-UQ. If the data was matched prior to reducing epistemic uncertainty, the reduction would be greater. These weight savings are in addition to using the 2D-UQ 200°F isotherm to inform insulator thickness.

A major drawback in using full scale rocket motor testing to calibrate computational models is re-anchoring must be done any time significant changes are made in motor/propellant or nozzle design. The cost to test a single motor is significant in both money and schedule. Any redesign effort from poor pretest predictions is also costly. Even if the model is calibrated to erosion, the model form error on char depth remains uncertain and must be accounted for in insulator design. Char depth model form error can be calibrated out, but it lacks practicality due to uncertainty in heat soak effects.

The second and third uncertainty reduction techniques are aligned with future work. The second method is to continue to develop high fidelity rapid physics-based models with material property characterization and testing to support them. It is assumed that modeling improvements are significant enough to bring the prediction in erosion and char to $\pm$ 10% where char has an average error of 0%. These improvements are also shown in Figure 79. Modeling improvements reduces overall erosion uncertainty by ~15% (60 mils) and overall char uncertainty by ~ 25% (97 mils). This is an estimate. If predicted g was $\pm$ 10% of actual g the reduction would be greater. These weight savings are in addition to using the 2D-UQ 200°F isotherm over a SF methodology. Overall, the char depth uncertainty is more representative of in-depth temperatures. Therefore, modeling improvements using these reduction estimates would save about 15% more weight than motor matching post-test. This additional weight savings is primarily driven by reducing the model form error on the char depth prediction. A combination of modeling improvements and testing is ideal but may not be financially feasible nor timely for future rocket nozzle technology.

Downsides in reducing uncertainty using modeling improvements is the substantial time to mature models and the upfront cost are more than motor testing alone since testing is be needed to support model development and validation. However, better computational models reduce uncertainty for all future motors. They can also be applied to, and inform changes in, design or technology markets more readily than design-build-test strategies.

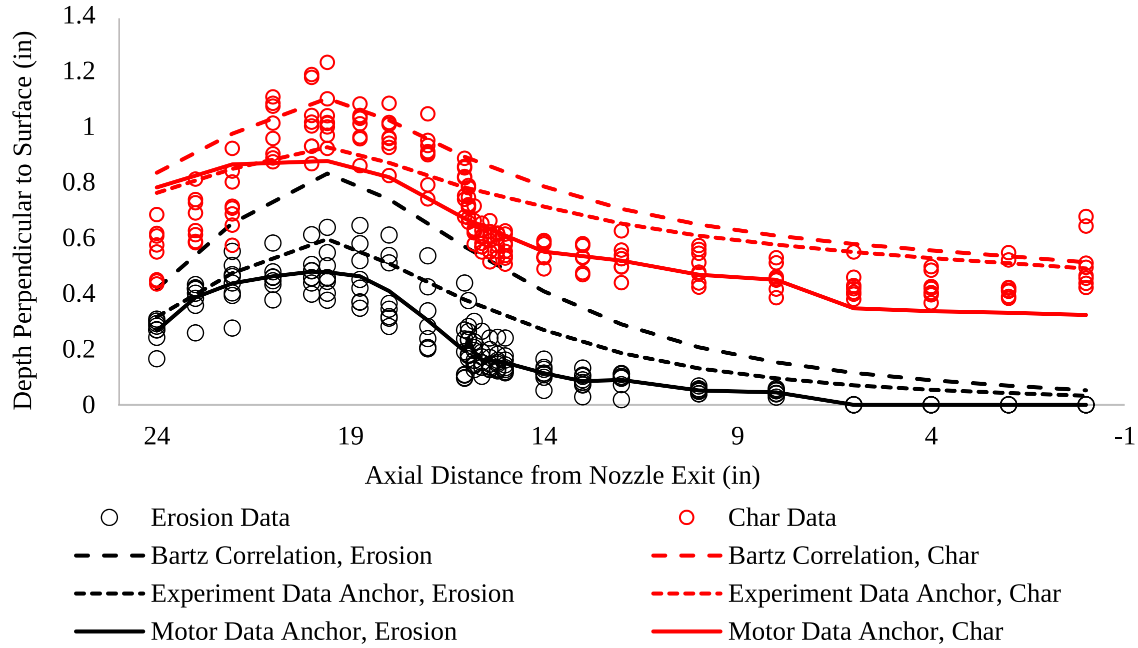

Figure 78. Comparison of raw predictions, experimentally anchored predictions, and motor test anchored predictions compared to motor data.

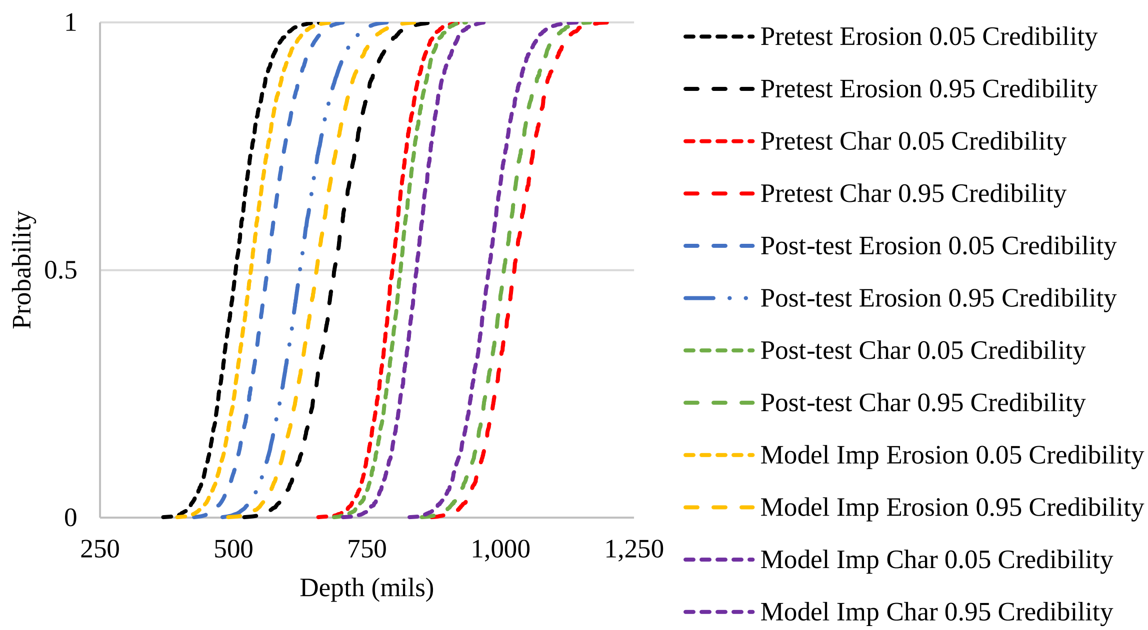

Figure 79. Uncertainty Reduction from post-testing match and modeling improvements.

The last reduction technique is a reduction in the uncertainty of aleatory inputs. But how do we reduce natural variation without some divine intervention? What is meant is that a better understanding of actual aleatory uncertainty values is needed. In this work, assumptional leeway was applied due to sparsity in data. Reduction in aleatory uncertainty will naturally follow the modeling improvement approach. Recognition is also given to opportunities to reduce aleatory variation through improved processing and manufacturing technologies.

8.2 FUTURE WORK

It was mentioned in Chapter 4 that there is an overarching lack of data available in the literature. Because of this, both the aleatory uncertainty in the inputs and the distributions assigned to them have associated assumptions. An area of future work would be do look at the effect of distribution selection and proposing most-likely theoretical distributions.

Modeling improvements are needed in the boundary conditions. The physical phenomena are complex and its astonishing that Bartz's correlation, which is nearly identical to Dittus-Boelter's correlation[95] for fully developed pipe flow, can reasonably predict the conditions in a rocket nozzle. Especially since the flow in a rocket nozzle is not fully developed[26]. Improvement in physics-based rapid transient heat transfer prediction tools is needed. Current CFD methods are computationally slow compared to correlation-based predictions. CFD also relies on accurate prediction of nozzle wall temperatures to accurately predict heat flux. Like Bartz's correlation, CFD relies on augmentation of mechanical erosion models and radiation heat flux models. Mechanical erosion models rely on input estimation by the user or reliance on data anchoring. Until mechanical erosion models are mature and validated, model-form error on char depth is going to continue. Both correlation-based heat transfer coefficients and CFD validation efforts could benefit from testing using nonmetallized propellants (propellants that inherently limit mechanical erosion and have lower emissive properties).

Direct or indirect radiation measurement data inside a SRM rocket nozzle is needed to inform modeling improvements and validate radiation models. Most of the radiation measurement efforts to date are performed on the rocket exhaust plumes. While this is useful, the plume temperatures are a factor lower, and the plume optical thickness is a factor higher, and the form (shape, phase, size) of the alumina particles may be substantially different.

Data is needed in pyrolysis gas enthalpy and heats of pyrolysis/formation. Pyrolysis gas enthalpy nonequilibrium to equilibrium temperature transition data is needed. This could be accomplished by conducting experiments similar to that discussed in ref. [87]. Historically, a single deterministic value for the resin heat of formation has been established and adjustment in the composite heat of formation has been based on resin mass fraction. This method under determines the variability in heat of pyrolysis/formation. Proof that variability in heat of pyrolysis/formation is insignificant is needed before a deterministic value is used.

Although the kinetics were shown to have low impact on erosion and char depth, using low heating values as nominal and extrapolating them to nozzle heating conditions is at least questionable. The kinetic data is obtained at pressures well below that seen in a rocket nozzle, not to mention pyrolysis gas pressure in the pores that could delay further decomposition. While the variation in kinetics may not be a substantial contribution, the model form may contribute to model form error on char depth. Perhaps other reaction mechanisms or combination with equilibrium theory could support this. Additionally, all mass loss in CCP is assumed to originate solely from decomposition of the phenolic resin. This assumption carries over in the elemental composition of the pyrolysis gas which affects reactions in the boundary layer. Excess carbon (e.g. carbon particle filler in the resin) carried away as pyrolysis gasses move through porous char reduces chemical erosion of the charred surface and vice versa. Future work in this area could help quantify this.

Understanding pyrolysis gas flow phenomena and additional mass loss from the carbon cloth and carbon powder filler in the resin may improve model form error on erosion depth and support validation of boundary conditions. This could be informed by doing TGA or high energy ablation on pure cured resin, cured carbon filled resin, and the full cured composite in a series of tests.

Variability in density and specific heat could be used in conjunction with several thermal response tests to establish variability in thermal conductivity. Additionally, thermal response modeling using varying cloth volume fractions could be used to validate and/or improve the thermal conductivity dispersion relationships presented by Clayton[43].

APPENDIX A: ITRAC INPUT FILE AT THE THROAT

```
ITRAC INPUT FILE
9-July-2022
** CM nozzle ST6 (throat)
** A/A* = 1.0
*MOD (Modeling Options)
**
/UNI (Units System)
** SI=0 | English=1 | Metric=2
1
/THE (Temperature Solution)
** none=0 | simple tracking=1 | standard solution=2
2
/PYR (Pyrolysis Solution)
** none=0 | standard=1
1
/PRE (Pressure Solution)
** no advection=0 | simplified advection no pore pressure=1 | simplified advection simplified pore pressure=2 | full advection and pore pressure=3
1
/ERO (Erosion Solution)
** off=0 | thermochemical=1 | mechanical=2 | thermochemical and mechanical=3
1
/BLO (Blowing Factor)
0.4
/STO (Stop Time)
** (s)
50.3
*MAT (Materials)
**
4296 EN-Units
Carbon Cloth Phenolic
**
/DEN Density Table
0.0  91.3
1.0  73.22
**
/HOF Heats of Formation
-363   0.0   -2126   536.0
**
/HOP Heat of Pyrolysis
-293
**
/PKM Pyrolysis Kinetics Multicomponent
0.0825   3.0   2.38E+07 1.40E+04  671.6
0.1125   3.0   5.69E+07 9.76E+08  671.6
**
/SPH Specific Heat Table
0          530      0.21
0          800      0.36
0          1160     0.36
0          1500     0.472
```

```
0         2000    0.484
0         3000    0.493
0         4000    0.498
0         5000    0.5
0         6000    0.5
1         500     0.21
1         1000    0.43
1         1500    0.472
1         2000    0.484
1         3000    0.493
1         4000    0.498
1         5000    0.5
1         6000    0.5
**
/CND Conductivity Table
0         500     2.36E-04        1.39E-04
0         800     2.69E-04        1.58E-04
0         1160    3.11E-04        1.83E-04
0         1500    3.11E-04        1.83E-04
0         6000    3.11E-04        1.83E-04
1         530     3.11E-04        1.83E-04
1         1000    3.15E-04        1.90E-04
1         1500    3.20E-04        1.95E-04
1         2000    4.15E-04        2.35E-04
1         3000    8.95E-04        5.40E-04
1         4000    1.47E-03        1.17E-03
1         5000    2.13E-03        1.88E-03
1         6000    2.84E-03        2.65E-03
**
/RAD Surface Radiation Properties Table
0.0   530.0     0.85 0.85
**
/PGE Pyrolysis Gas Enthalpy
211621.662      536     0
211621.662      1000    438.944
211621.662      1500    911.944
211621.662      2000    1435.944
211621.662      3000    2958.944
211621.662      4000    4934.944
211621.662      5000    6300.944
211621.662      6000    7745.944
**
/DEF (material definitions)
** ITRAC mat no.  |  mat no.  |  db ID  { |  Comments }
1 4926  3
2 10201 0
*DIS (Discretizations)
**
/TIM (Time Step)
** time (s)  |  timestep (s)
0.0      0.01
50.3     0.01
50.4     1.0
1800     1.0
/CUR (Surface Curvature)
** planar=0|cylinder concave=1|cylinder convex=-1|sphere concave=2|sphere convex=-2
```

```
1
/RAD (Radius)
** (ft)
0.2916
/ELE (Element Definitions)
** no of elements  |  matl  |  elem size (ft)  |  angle (deg)  { |  contact resist (ft2-R-s/Btu) }
 2064     1   8.333333E-5           90.0
 325      2   8.333333E-5            0.0
*INI (Initializations)
**
/TEM (Initial Temps)
** temp I  { |  no. of elems }
529.67
/ALP (Initial alpha, extent-of-reaction value, 0 to 1)
** alpha  { |  no. of elems }
0.0
/PRE (Initial Press)
** press (lbf/ft2)  { |  no. of elems }
2116.8
*OUT (Output Control)
**
/INC (Increment Time Step)
** time (s)
0.0
/PYR (Pyrolysis Value, alpha isovalue line)
** extent of reaction
0.02
/CHA (Char Value, alpha isovalue line)
** extent of reaction
0.98
/TEM (107emperature Isotherms)
** temperature I
659.67
1459.67
/ALP (Alpha Isovalues)
** extent of reaction
0.30
/RES (Restart Option)
** none=0  |  restart=1
0
*FTH (Front Thermal)
**
/INC (Incident Radiation)
** time (s)  |  heat flux (Btu/s-ft2)
0.0              491.92
50.3             491.92
50.4             0.000
1800.00          0.000
/VIE (Radiation View Factor)
** time (s)  |  view factor
K.0 1.0
/TCH (Thermochemical)
** time (s)  |  Hr (Btu/lb)  |  h/cp (lb/ft2-s)

0.082207369    1505.342144    0.031642866
0.223720724    1505.342144    0.095661253
```

0.260946387	1505.342144	0.157773352
0.301966029	1505.342144	0.24205323
0.347424555	1505.342144	0.208799712
0.425743232	1505.342144	0.289371215
0.464028164	1505.342144	0.312553169
0.465163046	1505.342144	0.372045559
0.544649162	1505.342144	0.424365847
0.57933017	1505.342144	0.463032097
0.728988367	1505.342144	0.519731518
0.85749171	1505.342144	0.570235425
0.966770138	1505.342144	0.604351345
1.083560825	1505.342144	0.64706584
1.398781285	1505.342144	0.682243759
1.582683649	1505.342144	0.696758019
2.15406431	1505.342144	0.716762071
3.257620869	1505.342144	0.726477191
4.403950043	1505.342144	0.731085111
5.550420306	1505.342144	0.73500634
6.697752876	1505.342144	0.734771888
7.844636738	1505.342144	0.736698041
8.991763475	1505.342144	0.737454406
10.13974541	1505.342144	0.734093336
11.28730584	1505.342144	0.732760781
12.44584803	1505.342144	0.728765021
13.5719388	1505.342144	0.724778227
14.75250892	1505.342144	0.720726222
15.88842934	1505.342144	0.716829
17.01836149	1505.342144	0.708239539
18.17784997	1505.342144	0.699599165
19.30573603	1505.342144	0.692461887
20.47570942	1505.342144	0.683502355
21.58315755	1505.342144	0.674248296
22.77404202	1505.342144	0.664974631
23.96537098	1505.342144	0.653464852
25.04143223	1505.342144	0.644589707
26.22224097	1505.342144	0.633440766
27.36112661	1505.342144	0.623264965
28.52105208	1505.342144	0.612139593
29.70188937	1505.342144	0.600699435
30.81965896	1505.342144	0.591690095
31.66891317	1505.342144	0.582373952
32.70087414	1505.342144	0.572075527
33.85017592	1505.342144	0.561704945
34.99934537	1505.342144	0.551971035
36.13987472	1505.342144	0.541926675
37.29771385	1505.342144	0.532218287
38.44713396	1505.342144	0.521035511
39.59642329	1505.342144	0.510482471
40.74573943	1505.342144	0.499732434
41.89515764	1505.342144	0.488379815
43.03499046	1505.342144	0.477517301
44.19341247	1505.342144	0.468610422
45.45404236	1505.342144	0.455443236
46.28517187	1505.342144	0.437141624
46.875998	1505.342144	0.407180027
47.39174446	1505.342144	0.364054748

```
47.55383647    1505.342144    0.340630892
47.81720531    1505.342144    0.309518037
48.13532856    1505.342144    0.253196218
48.45064364    1505.342144    0.213167253
48.71562598    1505.342144    0.169556004
48.88842095    1505.342144    0.143403106
49.19636562    1505.342144    0.102087952
49.724215      1505.342144    0.04766522
50.29441333    1505.342144    0.039220227
50.4 0.0 0.0
1800 0.0 0.0
*BTH (Back Thermal)
**
*FME (Front Mechanical)
**
*FPR (Front Pressure)
**
/SPE (Pressure BC)
** time (s)  |  press (lbf/ft2)
0.0  50693
*BPR (Back Pressure)
**
*DLL (DLL Options)
**
*STC (Surface Thermochemistry)
**
/DEF (Definitions)
** ITRAC mat no.  |  surf t-chem type  { |  Cm/Ch  |  table no.  |  db ID }
1    1    0.6977  1    3    (Thermochemical) CCP ablating material
/ACE (ACE table database for element potential drivers)
** flag | press (atm)   | B'g   | B'c    | temp   | chem enthalpy   | sens enthalpy  | B'f
1
CM nozzle Thermo at ST6
0    0         Boundary Layer: T=3690.315, P=23.9546
-1 23.9546      0.0          0.0      4000.000  1756.301   917.793      0.0
-1 23.9546      0.0          0.0      3750.000  1601.394   800.351      0.0
-1 23.9546      0.0          0.0      3500.000  1447.657   683.710      0.0
-1 23.9546      0.0          0.0      3250.000  1295.173   567.933      0.0
-1 23.9546      0.0          0.0      3000.000  1144.054   453.108      0.0
-1 23.9546      0.0          0.0      2750.000   994.457   339.351      0.0
-1 23.9546      0.0          0.0      2500.000   846.584   226.822      0.0
-1 23.9546      0.0          0.0      2250.000   700.705   115.729      0.0
-1 23.9546      0.0          0.0      2000.000   557.162     6.342      0.0
-1 23.9546      0.0          0.0      1750.000   416.389  -100.992      0.0
-1 23.9546      0.0          0.0      1500.000   278.917  -205.835      0.0
-1 23.9546      0.0          0.0      1250.000   145.357  -307.652      0.0
-1 23.9546      0.0          0.0      1000.000    16.274  -405.878      0.0
-1 23.9546      0.0          0.0       750.000  -108.106  -500.112      0.0
-1 23.9546      0.0          0.0       500.000  -228.098  -590.347      0.0
 1 23.9546   0.00000    0.54075967      4000.000  3195.705  2451.024      0.0
 1 23.9546   0.00000    0.35593971      3750.000  2329.040  1637.907      0.0
 1 23.9546   0.00000    0.27153035      3500.000  1741.589  1150.878      0.0
 1 23.9546   0.00000    0.22057554      3250.000  1300.709   806.854      0.0
 1 23.9546   0.00000    0.18664281      3000.000   958.686   542.773      0.0
 1 23.9546   0.00000    0.16444977      2750.000   689.541   330.304      0.0
 1 23.9546   0.00000    0.15094600      2500.000   466.820   143.416      0.0
```

1	23.9546	0.00000	0.14346663	2250.000	265.245	-39.309	0.0
1	23.9546	0.00000	0.13962138	2000.000	79.423	-207.544	0.0
1	23.9546	0.00000	0.13725093	1750.000	-81.180	-337.315	0.0
1	23.9546	0.00000	0.13245029	1500.000	-241.253	-457.959	0.0
1	23.9546	0.00000	0.10120526	1250.000	-526.863	-694.473	0.0
1	23.9546	0.00000	0.01871257	1000.000	-1153.894	-1221.649	0.0
1	23.9546	0.05000	0.55737655	4000.000	3321.971	2541.071	0.0
1	23.9546	0.05000	0.35722897	3750.000	2445.686	1715.498	0.0
1	23.9546	0.05000	0.26473294	3500.000	1842.941	1214.064	0.0
1	23.9546	0.05000	0.20862064	3250.000	1386.900	857.421	0.0
1	23.9546	0.05000	0.17130733	3000.000	1031.814	583.465	0.0
1	23.9546	0.05000	0.14706454	2750.000	752.568	364.523	0.0
1	23.9546	0.05000	0.13260947	2500.000	523.160	175.034	0.0
1	23.9546	0.05000	0.12508680	2250.000	317.156	-8.638	0.0
1	23.9546	0.05000	0.12163380	2000.000	125.979	-180.232	0.0
1	23.9546	0.05000	0.11946577	1750.000	-41.990	-315.237	0.0
1	23.9546	0.05000	0.11466622	1500.000	-210.129	-440.625	0.0
1	23.9546	0.05000	0.08287861	1250.000	-507.912	-684.891	0.0
0	23.9546	0.05000	0.00000000	1000.000	-1154.784	-1223.977	0.0
0	23.9546	0.05000	0.00000000	500.000	-1719.549	-1573.401	0.0
1	23.9546	0.10000	0.57387427	4000.000	3438.307	2624.293	0.0
1	23.9546	0.10000	0.35829954	3750.000	2554.563	1788.235	0.0
1	23.9546	0.10000	0.25765860	3500.000	1938.503	1273.907	0.0
1	23.9546	0.10000	0.19635324	3250.000	1468.786	905.646	0.0
1	23.9546	0.10000	0.15563293	3000.000	1101.628	622.382	0.0
1	23.9546	0.10000	0.12929899	2750.000	812.783	397.086	0.0
1	23.9546	0.10000	0.11379825	2500.000	576.735	204.722	0.0
1	23.9546	0.10000	0.10609266	2250.000	366.280	20.003	0.0
1	23.9546	0.10000	0.10294683	2000.000	170.031	-154.636	0.0
1	23.9546	0.10000	0.10099271	1750.000	-4.916	-294.588	0.0
1	23.9546	0.10000	0.09627243	1500.000	-180.783	-424.497	0.0
1	23.9546	0.10000	0.06422396	1250.000	-490.127	-676.011	0.0
0	23.9546	0.10000	0.00000000	1000.000	-1155.405	-1195.736	0.0
0	23.9546	0.10000	0.00000000	750.000	-1530.111	-1470.818	0.0
0	23.9546	0.10000	0.00000000	500.000	-1738.427	-1569.800	0.0
1	23.9546	0.15000	0.59030191	4000.000	3545.772	2701.384	0.0
1	23.9546	0.15000	0.35920829	3750.000	2656.330	1856.495	0.0
1	23.9546	0.15000	0.25037077	3500.000	2028.654	1330.606	0.0
1	23.9546	0.15000	0.18384328	3250.000	1546.579	951.644	0.0
1	23.9546	0.15000	0.13969822	3000.000	1168.261	659.627	0.0
1	23.9546	0.15000	0.11124881	2750.000	870.329	428.155	0.0
1	23.9546	0.15000	0.09464109	2500.000	627.760	232.746	0.0
1	23.9546	0.15000	0.08664794	2250.000	412.870	46.902	0.0
1	23.9546	0.15000	0.08373634	2000.000	211.810	-130.504	0.0
1	23.9546	0.15000	0.08200350	1750.000	30.252	-275.132	0.0
1	23.9546	0.15000	0.07742854	1500.000	-153.023	-409.363	0.0
1	23.9546	0.15000	0.04534089	1250.000	-473.373	-667.702	0.0
0	23.9546	0.15000	0.00000000	1000.000	-1155.809	-1170.045	0.0
0	23.9546	0.15000	0.00000000	750.000	-1539.623	-1460.148	0.0
0	23.9546	0.15000	0.00000000	500.000	-1754.776	-1564.397	0.0
1	23.9546	0.20000	0.60669362	4000.000	3645.292	2772.957	0.0
1	23.9546	0.20000	0.35999624	3750.000	2751.587	1920.628	0.0
1	23.9546	0.20000	0.24291563	3500.000	2113.758	1384.354	0.0
1	23.9546	0.20000	0.17114146	3250.000	1620.493	995.527	0.0
1	23.9546	0.20000	0.12355935	3000.000	1231.854	695.286	0.0
1	23.9546	0.20000	0.09298061	2750.000	925.335	457.854	0.0

1	23.9546	0.20000	0.07522632	2500.000	676.409	259.301	0.0
1	23.9546	0.20000	0.06686700	2250.000	457.126	72.269	0.0
1	23.9546	0.20000	0.06412732	2000.000	251.497	-107.658	0.0
1	23.9546	0.20000	0.06262009	1750.000	63.675	-256.705	0.0
1	23.9546	0.20000	0.05824618	1500.000	-126.704	-395.079	0.0
1	23.9546	0.20000	0.02629518	1250.000	-457.551	-659.875	0.0
0	23.9546	0.20000	0.00000000	1000.000	-1156.039	-1146.442	0.0
0	23.9546	0.20000	0.00000000	750.000	-1548.037	-1449.303	0.0
0	23.9546	0.20000	0.00000000	500.000	-1769.083	-1557.836	0.0
1	23.9546	0.25000	0.62307386	4000.000	3737.675	2839.550	0.0
1	23.9546	0.25000	0.36069409	3750.000	2840.881	1980.958	0.0
1	23.9546	0.25000	0.23532794	3500.000	2194.159	1435.335	0.0
1	23.9546	0.25000	0.15828588	3250.000	1690.744	1037.406	0.0
1	23.9546	0.25000	0.10725794	3000.000	1292.547	729.439	0.0
1	23.9546	0.25000	0.07454248	2750.000	977.923	486.280	0.0
1	23.9546	0.25000	0.05561658	2500.000	722.832	284.536	0.0
1	23.9546	0.25000	0.04683193	2250.000	499.217	96.267	0.0
1	23.9546	0.25000	0.04421095	2000.000	289.238	-85.965	0.0
1	23.9546	0.25000	0.04293120	1750.000	95.480	-239.190	0.0
1	23.9546	0.25000	0.03880548	1500.000	-101.710	-381.537	0.0
1	23.9546	0.25000	0.00713155	1250.000	-442.582	-652.468	0.0
0	23.9546	0.25000	0.00000000	1000.000	-1156.131	-1124.599	0.0
0	23.9546	0.25000	0.00000000	750.000	-1555.557	-1438.526	0.0
0	23.9546	0.25000	0.00000000	500.000	-1781.720	-1550.564	0.0
1	23.9546	0.30000	0.63946058	4000.000	3823.630	2901.638	0.0
1	23.9546	0.30000	0.36132538	3750.000	2924.710	2037.779	0.0
1	23.9546	0.30000	0.22763469	3500.000	2270.184	1483.726	0.0
1	23.9546	0.30000	0.14530595	3250.000	1757.542	1077.385	0.0
1	23.9546	0.30000	0.09082576	3000.000	1350.482	762.163	0.0
1	23.9546	0.30000	0.05597029	2750.000	1028.211	513.515	0.0
1	23.9546	0.30000	0.03585750	2500.000	767.162	308.570	0.0
1	23.9546	0.30000	0.02660309	2250.000	539.291	119.023	0.0
1	23.9546	0.30000	0.02405531	2000.000	325.163	-65.322	0.0
1	23.9546	0.30000	0.02300306	1750.000	125.777	-222.494	0.0
1	23.9546	0.30000	0.01916548	1500.000	-77.945	-368.660	0.0
0	23.9546	0.30000	0.00000000	1250.000	-428.398	-621.127	0.0
0	23.9546	0.30000	0.00000000	1000.000	-1156.113	-1104.266	0.0
0	23.9546	0.30000	0.00000000	750.000	-1562.337	-1427.967	0.0
0	23.9546	0.30000	0.00000000	500.000	-1792.973	-1542.891	0.0
1	23.9546	0.35000	0.65586709	4000.000	3903.781	2959.644	0.0
1	23.9546	0.35000	0.36190862	3750.000	3003.523	2091.363	0.0
1	23.9546	0.35000	0.21985720	3500.000	2342.137	1529.692	0.0
1	23.9546	0.35000	0.13222496	3250.000	1821.089	1115.568	0.0
1	23.9546	0.35000	0.07428763	3000.000	1405.800	793.526	0.0
1	23.9546	0.35000	0.03729144	2750.000	1076.314	539.630	0.0
1	23.9546	0.35000	0.01598312	2500.000	809.523	331.504	0.0
1	23.9546	0.35000	0.00622570	2250.000	577.478	140.644	0.0
1	23.9546	0.35000	0.00371223	2000.000	359.387	-45.643	0.0
1	23.9546	0.35000	0.00288606	1750.000	154.662	-206.547	0.0
0	23.9546	0.35000	0.00000000	1500.000	-55.325	-352.768	0.0
0	23.9546	0.35000	0.00000000	1250.000	-414.944	-591.619	0.0
0	23.9546	0.35000	0.00000000	1000.000	-1156.008	-1085.245	0.0
0	23.9546	0.35000	0.00000000	750.000	-1568.495	-1417.714	0.0
0	23.9546	0.35000	0.00000000	500.000	-1803.065	-1535.032	0.0
1	23.9546	0.40000	0.67230344	4000.000	3978.676	3013.941	0.0
1	23.9546	0.40000	0.36246144	3750.000	3077.764	2141.957	0.0

1	23.9546	0.40000	0.21201274	3500.000	2410.302	1573.390	0.0
1	23.9546	0.40000	0.11906163	3250.000	1881.580	1152.053	0.0
1	23.9546	0.40000	0.05766337	3000.000	1458.639	823.599	0.0
1	23.9546	0.40000	0.01852736	2750.000	1122.341	564.687	0.0
0	23.9546	0.40000	0.00000000	2500.000	850.026	351.362	0.0
0	23.9546	0.40000	0.00000000	2250.000	613.900	182.846	0.0
0	23.9546	0.40000	0.00000000	2000.000	392.014	-3.002	0.0
0	23.9546	0.40000	0.00000000	1750.000	182.222	-182.634	0.0
0	23.9546	0.40000	0.00000000	1500.000	-33.775	-332.609	0.0
0	23.9546	0.40000	0.00000000	1250.000	-402.168	-567.890	0.0
0	23.9546	0.40000	0.00000000	1000.000	-1155.834	-1067.380	0.0
0	23.9546	0.40000	0.00000000	750.000	-1574.124	-1407.817	0.0
0	23.9546	0.40000	0.00000000	500.000	-1812.173	-1527.135	0.0
1	23.9546	0.45000	0.68877719	4000.000	4048.800	3064.860	0.0
1	23.9546	0.45000	0.36298702	3750.000	3147.695	2189.790	0.0
1	23.9546	0.45000	0.20411539	3500.000	2474.942	1614.964	0.0
1	23.9546	0.45000	0.10583126	3250.000	1939.199	1186.934	0.0
1	23.9546	0.45000	0.04096900	3000.000	1509.131	852.444	0.0
0	23.9546	0.45000	0.00000000	2750.000	1166.401	575.947	0.0
0	23.9546	0.45000	0.00000000	2500.000	888.778	409.311	0.0
0	23.9546	0.45000	0.00000000	2250.000	648.666	237.784	0.0
0	23.9546	0.45000	0.00000000	2000.000	423.142	42.643	0.0
0	23.9546	0.45000	0.00000000	1750.000	208.535	-162.422	0.0
0	23.9546	0.45000	0.00000000	1500.000	-13.229	-323.266	0.0
0	23.9546	0.45000	0.00000000	1250.000	-390.024	-548.805	0.0
0	23.9546	0.45000	0.00000000	1000.000	-1155.607	-1050.540	0.0
0	23.9546	0.45000	0.00000000	750.000	-1579.299	-1398.301	0.0
0	23.9546	0.45000	0.00000000	500.000	-1820.441	-1519.302	0.0
1	23.9546	0.50000	0.70529405	4000.000	4114.582	3112.695	0.0
1	23.9546	0.50000	0.36350381	3750.000	3213.757	2235.066	0.0
1	23.9546	0.50000	0.19617680	3500.000	2536.300	1654.553	0.0
1	23.9546	0.50000	0.09254650	3250.000	1994.122	1220.300	0.0
1	23.9546	0.50000	0.02421766	3000.000	1557.404	880.126	0.0
0	23.9546	0.50000	0.00000000	2750.000	1208.595	632.079	0.0
0	23.9546	0.50000	0.00000000	2500.000	925.876	463.147	0.0
0	23.9546	0.50000	0.00000000	2250.000	681.877	289.185	0.0
0	23.9546	0.50000	0.00000000	2000.000	452.860	86.669	0.0
0	23.9546	0.50000	0.00000000	1750.000	233.674	-140.739	0.0
0	23.9546	0.50000	0.00000000	1500.000	6.376	-318.125	0.0
0	23.9546	0.50000	0.00000000	1250.000	-378.470	-533.431	0.0
0	23.9546	0.50000	0.00000000	1000.000	-1155.339	-1034.618	0.0
0	23.9546	0.50000	0.00000000	750.000	-1584.081	-1389.172	0.0
0	23.9546	0.50000	0.00000000	500.000	-1827.983	-1511.603	0.0
1	23.9546	0.55000	0.72185829	4000.000	4176.404	3157.710	0.0
1	23.9546	0.55000	0.36401685	3750.000	3276.218	2277.973	0.0
1	23.9546	0.55000	0.18820671	3500.000	2594.602	1692.282	0.0
1	23.9546	0.55000	0.07921791	3250.000	2046.512	1252.237	0.0
1	23.9546	0.55000	0.00742026	3000.000	1603.581	906.701	0.0
0	23.9546	0.55000	0.00000000	2750.000	1249.020	684.429	0.0
0	23.9546	0.55000	0.00000000	2500.000	961.413	513.395	0.0
0	23.9546	0.55000	0.00000000	2250.000	713.628	337.338	0.0
0	23.9546	0.55000	0.00000000	2000.000	481.250	128.650	0.0
0	23.9546	0.55000	0.00000000	1750.000	257.707	-118.109	0.0
0	23.9546	0.55000	0.00000000	1500.000	25.097	-314.579	0.0
0	23.9546	0.55000	0.00000000	1250.000	-367.469	-521.025	0.0
0	23.9546	0.55000	0.00000000	1000.000	-1155.039	-1019.522	0.0

0	23.9546	0.55000	0.00000000	750.000	-1588.517	-1380.424	0.0
0	23.9546	0.55000	0.00000000	500.000	-1834.894	-1504.085	0.0
1	23.9546	0.60000	0.73847307	4000.000	4234.605	3200.141	0.0
1	23.9546	0.60000	0.36453272	3750.000	3335.351	2318.683	0.0
1	23.9546	0.60000	0.18021326	3500.000	2650.054	1728.269	0.0
1	23.9546	0.60000	0.06585435	3250.000	2096.523	1282.824	0.0
0	23.9546	0.60000	0.00000000	3000.000	1647.778	928.997	0.0
0	23.9546	0.60000	0.00000000	2750.000	1287.771	733.427	0.0
0	23.9546	0.60000	0.00000000	2500.000	995.475	560.437	0.0
0	23.9546	0.60000	0.00000000	2250.000	744.006	382.512	0.0
0	23.9546	0.60000	0.00000000	2000.000	508.393	168.485	0.0
0	23.9546	0.60000	0.00000000	1750.000	280.699	-95.243	0.0
0	23.9546	0.60000	0.00000000	1500.000	42.987	-311.549	0.0
0	23.9546	0.60000	0.00000000	1250.000	-356.984	-510.996	0.0
0	23.9546	0.60000	0.00000000	1000.000	-1154.715	-1005.174	0.0
0	23.9546	0.60000	0.00000000	750.000	-1592.650	-1372.046	0.0
0	23.9546	0.60000	0.00000000	500.000	-1841.253	-1496.775	0.0
1	23.9546	0.65000	0.75514067	4000.000	4289.486	3240.197	0.0
1	23.9546	0.65000	0.36505684	3750.000	3391.405	2357.354	0.0
1	23.9546	0.65000	0.17220336	3500.000	2702.847	1762.624	0.0
1	23.9546	0.65000	0.05246333	3250.000	2144.299	1312.137	0.0
0	23.9546	0.65000	0.00000000	3000.000	1690.105	977.190	0.0
0	23.9546	0.65000	0.00000000	2750.000	1324.936	779.410	0.0
0	23.9546	0.65000	0.00000000	2500.000	1028.143	604.582	0.0
0	23.9546	0.65000	0.00000000	2250.000	773.092	424.953	0.0
0	23.9546	0.65000	0.00000000	2000.000	534.359	206.203	0.0
0	23.9546	0.65000	0.00000000	1750.000	302.707	-72.713	0.0
0	23.9546	0.65000	0.00000000	1500.000	60.095	-308.488	0.0
0	23.9546	0.65000	0.00000000	1250.000	-346.983	-502.876	0.0
0	23.9546	0.65000	0.00000000	1000.000	-1154.374	-991.508	0.0
0	23.9546	0.65000	0.00000000	750.000	-1596.514	-1364.017	0.0
0	23.9546	0.65000	0.00000000	500.000	-1847.126	-1489.693	0.0
1	23.9546	0.70000	0.77186267	4000.000	4341.319	3278.067	0.0
1	23.9546	0.70000	0.36559371	3750.000	3444.606	2394.127	0.0
1	23.9546	0.70000	0.16418283	3500.000	2753.158	1795.448	0.0
1	23.9546	0.70000	0.03905121	3250.000	2189.975	1340.246	0.0
0	23.9546	0.70000	0.00000000	3000.000	1730.664	1022.516	0.0
0	23.9546	0.70000	0.00000000	2750.000	1360.600	822.661	0.0
0	23.9546	0.70000	0.00000000	2500.000	1059.492	646.096	0.0
0	23.9546	0.70000	0.00000000	2250.000	800.961	464.887	0.0
0	23.9546	0.70000	0.00000000	2000.000	559.217	241.890	0.0
0	23.9546	0.70000	0.00000000	1750.000	323.788	-50.925	0.0
0	23.9546	0.70000	0.00000000	1500.000	76.467	-305.035	0.0
0	23.9546	0.70000	0.00000000	1250.000	-337.436	-496.297	0.0
0	23.9546	0.70000	0.00000000	1000.000	-1154.021	-978.467	0.0
0	23.9546	0.70000	0.00000000	750.000	-1600.137	-1356.314	0.0
0	23.9546	0.70000	0.00000000	500.000	-1852.568	-1482.848	0.0
1	23.9546	0.75000	0.78864007	4000.000	4390.347	3313.922	0.0
1	23.9546	0.75000	0.36614704	3750.000	3495.159	2429.135	0.0
1	23.9546	0.75000	0.15615663	3500.000	2801.148	1826.835	0.0
1	23.9546	0.75000	0.02562343	3250.000	2233.675	1367.219	0.0
0	23.9546	0.75000	0.00000000	3000.000	1769.555	1065.234	0.0
0	23.9546	0.75000	0.00000000	2750.000	1394.840	863.423	0.0
0	23.9546	0.75000	0.00000000	2500.000	1089.595	685.207	0.0
0	23.9546	0.75000	0.00000000	2250.000	827.684	502.517	0.0
0	23.9546	0.75000	0.00000000	2000.000	583.031	275.651	0.0

0	23.9546	0.75000	0.00000000	1750.000	343.993	-30.122	0.0
0	23.9546	0.75000	0.00000000	1500.000	92.145	-300.886	0.0
0	23.9546	0.75000	0.00000000	1250.000	-328.315	-490.969	0.0
0	23.9546	0.75000	0.00000000	1000.000	-1153.659	-966.000	0.0
0	23.9546	0.75000	0.00000000	750.000	-1603.544	-1348.910	0.0
0	23.9546	0.75000	0.00000000	500.000	-1857.626	-1476.243	0.0
1	23.9546	0.80000	0.80547344	4000.000	4436.786	3347.915	0.0
1	23.9546	0.80000	0.36671989	3750.000	3543.251	2462.496	0.0
1	23.9546	0.80000	0.14812897	3500.000	2846.967	1856.873	0.0
1	23.9546	0.80000	0.01218465	3250.000	2275.517	1393.118	0.0
0	23.9546	0.80000	0.00000000	3000.000	1806.869	1105.566	0.0
0	23.9546	0.80000	0.00000000	2750.000	1427.734	901.908	0.0
0	23.9546	0.80000	0.00000000	2500.000	1118.518	722.119	0.0
0	23.9546	0.80000	0.00000000	2250.000	853.326	538.029	0.0
0	23.9546	0.80000	0.00000000	2000.000	605.860	307.602	0.0
0	23.9546	0.80000	0.00000000	1750.000	363.372	-10.415	0.0
0	23.9546	0.80000	0.00000000	1500.000	107.170	-295.794	0.0
0	23.9546	0.80000	0.00000000	1250.000	-319.593	-486.660	0.0
0	23.9546	0.80000	0.00000000	1000.000	-1153.293	-954.064	0.0
0	23.9546	0.80000	0.00000000	750.000	-1606.756	-1341.773	0.0
0	23.9546	0.80000	0.00000000	500.000	-1862.341	-1469.878	0.0
1	23.9546	0.85000	0.82236298	4000.000	4480.835	3380.184	0.0
1	23.9546	0.85000	0.36731479	3750.000	3589.053	2494.321	0.0
1	23.9546	0.85000	0.14010344	3500.000	2890.752	1885.642	0.0
0	23.9546	0.85000	0.00000000	3250.000	2315.610	1395.972	0.0
0	23.9546	0.85000	0.00000000	3000.000	1842.693	1143.710	0.0
0	23.9546	0.85000	0.00000000	2750.000	1459.351	938.302	0.0
0	23.9546	0.85000	0.00000000	2500.000	1146.323	757.011	0.0
0	23.9546	0.85000	0.00000000	2250.000	877.948	571.590	0.0
0	23.9546	0.85000	0.00000000	2000.000	627.760	337.856	0.0
0	23.9546	0.85000	0.00000000	1750.000	381.969	8.177	0.0
0	23.9546	0.85000	0.00000000	1500.000	121.577	-289.666	0.0
0	23.9546	0.85000	0.00000000	1250.000	-311.247	-483.183	0.0
0	23.9546	0.85000	0.00000000	1000.000	-1152.925	-942.621	0.0
0	23.9546	0.85000	0.00000000	750.000	-1609.791	-1334.866	0.0
0	23.9546	0.85000	0.00000000	500.000	-1866.747	-1463.750	0.0
1	23.9546	0.90000	0.83930860	4000.000	4522.669	3410.855	0.0
1	23.9546	0.90000	0.36793379	3750.000	3632.721	2524.709	0.0
1	23.9546	0.90000	0.13208311	3500.000	2932.631	1913.217	0.0
0	23.9546	0.90000	0.00000000	3250.000	2354.054	1434.078	0.0
0	23.9546	0.90000	0.00000000	3000.000	1877.106	1179.840	0.0
0	23.9546	0.90000	0.00000000	2750.000	1489.758	972.772	0.0
0	23.9546	0.90000	0.00000000	2500.000	1173.070	790.044	0.0
0	23.9546	0.90000	0.00000000	2250.000	901.607	603.350	0.0
0	23.9546	0.90000	0.00000000	2000.000	648.782	366.526	0.0
0	23.9546	0.90000	0.00000000	1750.000	399.827	25.689	0.0
0	23.9546	0.90000	0.00000000	1500.000	135.403	-282.631	0.0
0	23.9546	0.90000	0.00000000	1250.000	-303.255	-480.389	0.0
0	23.9546	0.90000	0.00000000	1000.000	-1152.557	-931.636	0.0
0	23.9546	0.90000	0.00000000	750.000	-1612.666	-1328.142	0.0
0	23.9546	0.90000	0.00000000	500.000	-1870.875	-1457.852	0.0
1	23.9546	0.95000	0.85630997	4000.000	4562.451	3440.042	0.0
1	23.9546	0.95000	0.36857856	3750.000	3674.396	2553.754	0.0
1	23.9546	0.95000	0.12407057	3500.000	2972.721	1939.669	0.0
0	23.9546	0.95000	0.00000000	3250.000	2390.944	1470.221	0.0
0	23.9546	0.95000	0.00000000	3000.000	1910.186	1214.111	0.0

0	23.9546	0.95000	0.00000000	2750.000	1519.018	1005.466	0.0
0	23.9546	0.95000	0.00000000	2500.000	1198.814	821.362	0.0
0	23.9546	0.95000	0.00000000	2250.000	924.355	633.446	0.0
0	23.9546	0.95000	0.00000000	2000.000	668.975	393.716	0.0
0	23.9546	0.95000	0.00000000	1750.000	416.986	42.186	0.0
0	23.9546	0.95000	0.00000000	1500.000	148.678	-274.963	0.0
0	23.9546	0.95000	0.00000000	1250.000	-295.595	-478.158	0.0
0	23.9546	0.95000	0.00000000	1000.000	-1152.190	-921.079	0.0
0	23.9546	0.95000	0.00000000	750.000	-1615.394	-1321.544	0.0
0	23.9546	0.95000	0.00000000	500.000	-1874.750	-1452.178	0.0
1	23.9546	1.00000	0.87336656	4000.000	4600.325	3467.848	0.0
1	23.9546	1.00000	0.36925043	3750.000	3714.210	2581.539	0.0
1	23.9546	1.00000	0.11606803	3500.000	3011.130	1965.062	0.0
0	23.9546	1.00000	0.00000000	3250.000	2426.368	1504.548	0.0
0	23.9546	1.00000	0.00000000	3000.000	1942.004	1246.663	0.0
0	23.9546	1.00000	0.00000000	2750.000	1547.190	1036.518	0.0
0	23.9546	1.00000	0.00000000	2500.000	1223.607	851.095	0.0
0	23.9546	1.00000	0.00000000	2250.000	946.242	662.002	0.0
0	23.9546	1.00000	0.00000000	2000.000	688.384	419.526	0.0
0	23.9546	1.00000	0.00000000	1750.000	433.484	57.738	0.0
0	23.9546	1.00000	0.00000000	1500.000	161.434	-266.952	0.0
0	23.9546	1.00000	0.00000000	1250.000	-288.248	-476.388	0.0
0	23.9546	1.00000	0.00000000	1000.000	-1151.827	-910.924	0.0
0	23.9546	1.00000	0.00000000	750.000	-1617.987	-1314.997	0.0
0	23.9546	1.00000	0.00000000	500.000	-1878.395	-1446.720	0.0
1	23.9546	1.05000	0.89047772	4000.000	4636.424	3494.368	0.0
1	23.9546	1.05000	0.36995045	3750.000	3752.281	2608.144	0.0
1	23.9546	1.05000	0.10807737	3500.000	3047.959	1989.455	0.0
0	23.9546	1.05000	0.00000000	3250.000	2460.407	1537.193	0.0
0	23.9546	1.05000	0.00000000	3000.000	1972.626	1277.622	0.0
0	23.9546	1.05000	0.00000000	2750.000	1574.329	1066.047	0.0
0	23.9546	1.05000	0.00000000	2500.000	1247.497	879.358	0.0
0	23.9546	1.05000	0.00000000	2250.000	967.313	689.130	0.0
0	23.9546	1.05000	0.00000000	2000.000	707.052	444.049	0.0
0	23.9546	1.05000	0.00000000	1750.000	449.356	72.419	0.0
0	23.9546	1.05000	0.00000000	1500.000	173.699	-258.822	0.0
0	23.9546	1.05000	0.00000000	1250.000	-281.197	-474.997	0.0
0	23.9546	1.05000	0.00000000	1000.000	-1151.468	-901.146	0.0
0	23.9546	1.05000	0.00000000	750.000	-1620.456	-1308.396	0.0
0	23.9546	1.05000	0.00000000	500.000	-1881.831	-1441.471	0.0
1	23.9546	1.10000	0.90764265	4000.000	4670.869	3519.687	0.0
1	23.9546	1.10000	0.37067943	3750.000	3788.719	2633.639	0.0
1	23.9546	1.10000	0.10010017	3500.000	3083.300	2012.905	0.0
0	23.9546	1.10000	0.00000000	3250.000	2493.138	1568.276	0.0
0	23.9546	1.10000	0.00000000	3000.000	2002.114	1307.101	0.0
0	23.9546	1.10000	0.00000000	2750.000	1600.488	1094.163	0.0
0	23.9546	1.10000	0.00000000	2500.000	1270.530	906.256	0.0
0	23.9546	1.10000	0.00000000	2250.000	987.613	714.932	0.0
0	23.9546	1.10000	0.00000000	2000.000	725.018	467.371	0.0
0	23.9546	1.10000	0.00000000	1750.000	464.634	86.299	0.0
0	23.9546	1.10000	0.00000000	1500.000	185.498	-250.726	0.0
0	23.9546	1.10000	0.00000000	1250.000	-274.425	-473.914	0.0
0	23.9546	1.10000	0.00000000	1000.000	-1151.113	-891.724	0.0
0	23.9546	1.10000	0.00000000	750.000	-1622.811	-1301.594	0.0
0	23.9546	1.10000	0.00000000	500.000	-1885.076	-1436.422	0.0
1	23.9546	1.15000	0.92486047	4000.000	4703.770	3543.883	0.0

1	23.9546	1.15000	0.37143797	3750.000	3823.627	2658.093	0.0
1	23.9546	1.15000	0.09213776	3500.000	3117.239	2035.464	0.0
0	23.9546	1.15000	0.00000000	3250.000	2524.632	1597.905	0.0
0	23.9546	1.15000	0.00000000	3000.000	2030.528	1335.204	0.0
0	23.9546	1.15000	0.00000000	2750.000	1625.716	1120.964	0.0
0	23.9546	1.15000	0.00000000	2500.000	1292.748	931.887	0.0
0	23.9546	1.15000	0.00000000	2250.000	1007.180	739.502	0.0
0	23.9546	1.15000	0.00000000	2000.000	742.320	489.572	0.0
0	23.9546	1.15000	0.00000000	1750.000	479.349	99.442	0.0
0	23.9546	1.15000	0.00000000	1500.000	196.858	-242.761	0.0
0	23.9546	1.15000	0.00000000	1250.000	-267.915	-473.080	0.0
0	23.9546	1.15000	0.00000000	1000.000	-1150.765	-882.638	0.0
0	23.9546	1.15000	0.00000000	750.000	-1625.059	-1294.376	0.0
0	23.9546	1.15000	0.00000000	500.000	-1888.145	-1431.564	0.0
1	23.9546	1.20000	0.94213022	4000.000	4735.226	3567.030	0.0
1	23.9546	1.20000	0.37222651	3750.000	3857.095	2681.565	0.0
1	23.9546	1.20000	0.08419124	3500.000	3149.856	2057.179	0.0
0	23.9546	1.20000	0.00000000	3250.000	2554.955	1626.181	0.0
0	23.9546	1.20000	0.00000000	3000.000	2057.922	1362.025	0.0
0	23.9546	1.20000	0.00000000	2750.000	1650.059	1146.538	0.0
0	23.9546	1.20000	0.00000000	2500.000	1314.193	956.337	0.0
0	23.9546	1.20000	0.00000000	2250.000	1026.053	762.923	0.0
0	23.9546	1.20000	0.00000000	2000.000	758.991	510.725	0.0
0	23.9546	1.20000	0.00000000	1750.000	493.530	111.905	0.0
0	23.9546	1.20000	0.00000000	1500.000	207.799	-234.983	0.0
0	23.9546	1.20000	0.00000000	1250.000	-261.655	-472.439	0.0
0	23.9546	1.20000	0.00000000	1000.000	-1150.422	-873.870	0.0
0	23.9546	1.20000	0.00000000	750.000	-1627.209	-1286.452	0.0
0	23.9546	1.20000	0.00000000	500.000	-1891.053	-1426.890	0.0
1	23.9546	1.25000	0.95945090	4000.000	4765.332	3589.193	0.0
1	23.9546	1.25000	0.37304532	3750.000	3889.211	2704.112	0.0
1	23.9546	1.25000	0.07626155	3500.000	3181.225	2078.097	0.0
0	23.9546	1.25000	0.00000000	3250.000	2584.170	1653.193	0.0
0	23.9546	1.25000	0.00000000	3000.000	2084.348	1387.647	0.0
0	23.9546	1.25000	0.00000000	2750.000	1673.560	1170.969	0.0
0	23.9546	1.25000	0.00000000	2500.000	1334.901	979.684	0.0
0	23.9546	1.25000	0.00000000	2250.000	1044.267	785.274	0.0
0	23.9546	1.25000	0.00000000	2000.000	775.064	530.898	0.0
0	23.9546	1.25000	0.00000000	1750.000	507.204	123.741	0.0
0	23.9546	1.25000	0.00000000	1500.000	218.345	-227.424	0.0
0	23.9546	1.25000	0.00000000	1250.000	-255.630	-471.939	0.0
0	23.9546	1.25000	0.00000000	1000.000	-1150.086	-865.404	0.0
0	23.9546	1.25000	0.00000000	750.000	-1629.268	-1277.480	0.0
0	23.9546	1.25000	0.00000000	500.000	-1893.811	-1422.381	0.0
1	23.9546	1.30000	0.97682145	4000.000	4794.170	3610.432	0.0
1	23.9546	1.30000	0.37389455	3750.000	3920.053	2725.788	0.0
1	23.9546	1.30000	0.06834944	3500.000	3211.414	2098.259	0.0
0	23.9546	1.30000	0.00000000	3250.000	2612.333	1679.024	0.0
0	23.9546	1.30000	0.00000000	3000.000	2109.855	1412.150	0.0
0	23.9546	1.30000	0.00000000	2750.000	1696.261	1194.330	0.0
0	23.9546	1.30000	0.00000000	2500.000	1354.909	1002.002	0.0
0	23.9546	1.30000	0.00000000	2250.000	1061.855	806.624	0.0
0	23.9546	1.30000	0.00000000	2000.000	790.571	550.154	0.0
0	23.9546	1.30000	0.00000000	1750.000	520.397	134.998	0.0
0	23.9546	1.30000	0.00000000	1500.000	228.515	-220.102	0.0
0	23.9546	1.30000	0.00000000	1250.000	-249.828	-471.527	0.0

0	23.9546	1.30000	0.00000000	1000.000	-1149.757	-857.226	0.0
0	23.9546	1.30000	0.00000000	750.000	-1631.242	-1267.200	0.0
0	23.9546	1.30000	0.00000000	500.000	-1896.432	-1416.518	0.0
1	23.9546	1.35000	0.99424079	4000.000	4821.820	3630.805	0.0
1	23.9546	1.35000	0.37477424	3750.000	3949.695	2746.641	0.0
1	23.9546	1.35000	0.06045552	3500.000	3240.488	2117.704	0.0
0	23.9546	1.35000	0.00000000	3250.000	2639.500	1703.749	0.0
0	23.9546	1.35000	0.00000000	3000.000	2134.486	1435.605	0.0
0	23.9546	1.35000	0.00000000	2750.000	1718.199	1216.690	0.0
0	23.9546	1.35000	0.00000000	2500.000	1374.249	1023.356	0.0
0	23.9546	1.35000	0.00000000	2250.000	1078.847	827.038	0.0
0	23.9546	1.35000	0.00000000	2000.000	805.538	568.551	0.0
0	23.9546	1.35000	0.00000000	1750.000	533.132	145.718	0.0
0	23.9546	1.35000	0.00000000	1500.000	238.329	-213.023	0.0
0	23.9546	1.35000	0.00000000	1250.000	-244.236	-471.146	0.0
0	23.9546	1.35000	0.00000000	1000.000	-1149.434	-849.322	0.0
0	23.9546	1.35000	0.00000000	750.000	-1633.135	-1255.657	0.0
0	23.9546	1.35000	0.00000000	500.000	-1898.925	-1409.973	0.0
1	23.9546	1.40000	1.01170783	4000.000	4848.351	3650.361	0.0
1	23.9546	1.40000	0.37568434	3750.000	3978.205	2766.715	0.0
1	23.9546	1.40000	0.05258029	3500.000	3268.506	2136.469	0.0
0	23.9546	1.40000	0.00000000	3250.000	2665.720	1727.437	0.0
0	23.9546	1.40000	0.00000000	3000.000	2158.286	1458.077	0.0
0	23.9546	1.40000	0.00000000	2750.000	1739.410	1238.111	0.0
0	23.9546	1.40000	0.00000000	2500.000	1392.954	1043.807	0.0
0	23.9546	1.40000	0.00000000	2250.000	1095.272	846.576	0.0
0	23.9546	1.40000	0.00000000	2000.000	819.994	586.142	0.0
0	23.9546	1.40000	0.00000000	1750.000	545.432	155.940	0.0
0	23.9546	1.40000	0.00000000	1500.000	247.803	-206.188	0.0
0	23.9546	1.40000	0.00000000	1250.000	-238.845	-470.729	0.0
0	23.9546	1.40000	0.00000000	1000.000	-1149.118	-841.679	0.0
0	23.9546	1.40000	0.00000000	750.000	-1634.954	-1243.431	0.0
0	23.9546	1.40000	0.00000000	500.000	-1901.300	-1403.681	0.0
1	23.9546	1.45000	1.02922146	4000.000	4873.831	3669.149	0.0
1	23.9546	1.45000	0.37662470	3750.000	4005.645	2786.054	0.0
1	23.9546	1.45000	0.04472412	3500.000	3295.523	2154.588	0.0
0	23.9546	1.45000	0.00000000	3250.000	2691.040	1750.151	0.0
0	23.9546	1.45000	0.00000000	3000.000	2181.294	1479.626	0.0
0	23.9546	1.45000	0.00000000	2750.000	1759.930	1258.651	0.0
0	23.9546	1.45000	0.00000000	2500.000	1411.052	1063.411	0.0
0	23.9546	1.45000	0.00000000	2250.000	1111.158	865.292	0.0
0	23.9546	1.45000	0.00000000	2000.000	833.962	602.978	0.0
0	23.9546	1.45000	0.00000000	1750.000	557.318	165.699	0.0
0	23.9546	1.45000	0.00000000	1500.000	256.955	-199.592	0.0
0	23.9546	1.45000	0.00000000	1250.000	-233.643	-470.196	0.0
0	23.9546	1.45000	0.00000000	1000.000	-1148.810	-834.285	0.0
0	23.9546	1.45000	0.00000000	750.000	-1636.703	-1232.012	0.0
0	23.9546	1.45000	0.00000000	500.000	-1903.565	-1397.623	0.0
1	23.9546	1.50000	1.04678057	4000.000	4898.320	3687.213	0.0
1	23.9546	1.50000	0.37759514	3750.000	4032.074	2804.696	0.0
1	23.9546	1.50000	0.03688729	3500.000	3321.591	2172.094	0.0
0	23.9546	1.50000	0.00000000	3250.000	2715.507	1771.950	0.0
0	23.9546	1.50000	0.00000000	3000.000	2203.548	1500.307	0.0
0	23.9546	1.50000	0.00000000	2750.000	1779.789	1278.362	0.0
0	23.9546	1.50000	0.00000000	2500.000	1428.573	1082.219	0.0
0	23.9546	1.50000	0.00000000	2250.000	1126.531	883.236	0.0

0	23.9546	1.50000	0.00000000	2000.000	847.467	619.103	0.0
0	23.9546	1.50000	0.00000000	1750.000	568.809	175.025	0.0
0	23.9546	1.50000	0.00000000	1500.000	265.801	-193.230	0.0
0	23.9546	1.50000	0.00000000	1250.000	-228.622	-469.459	0.0
0	23.9546	1.50000	0.00000000	1000.000	-1148.508	-827.130	0.0
0	23.9546	1.50000	0.00000000	750.000	-1638.387	-1222.570	0.0
0	23.9546	1.50000	0.00000000	500.000	-1905.727	-1391.785	0.0
1	23.9546	1.55000	1.06438406	4000.000	4921.875	3704.593	0.0
1	23.9546	1.55000	0.37859539	3750.000	4057.546	2822.678	0.0
1	23.9546	1.55000	0.02907002	3500.000	3346.759	2189.016	0.0
0	23.9546	1.55000	0.00000000	3250.000	2739.160	1792.888	0.0
0	23.9546	1.55000	0.00000000	3000.000	2225.083	1520.172	0.0
0	23.9546	1.55000	0.00000000	2750.000	1799.018	1297.294	0.0
0	23.9546	1.55000	0.00000000	2500.000	1445.541	1100.278	0.0
0	23.9546	1.55000	0.00000000	2250.000	1141.413	900.455	0.0
0	23.9546	1.55000	0.00000000	2000.000	860.531	634.561	0.0
0	23.9546	1.55000	0.00000000	1750.000	579.924	183.949	0.0
0	23.9546	1.55000	0.00000000	1500.000	274.354	-187.095	0.0
0	23.9546	1.55000	0.00000000	1250.000	-223.772	-468.434	0.0
0	23.9546	1.55000	0.00000000	1000.000	-1148.213	-820.204	0.0
0	23.9546	1.55000	0.00000000	750.000	-1640.008	-1214.599	0.0
0	23.9546	1.55000	0.00000000	500.000	-1907.793	-1386.156	0.0
1	23.9546	1.60000	1.08203083	4000.000	4944.547	3721.327	0.0
1	23.9546	1.60000	0.37962516	3750.000	4082.112	2840.034	0.0
1	23.9546	1.60000	0.02127243	3500.000	3371.072	2205.382	0.0
0	23.9546	1.60000	0.00000000	3250.000	2762.039	1813.015	0.0
0	23.9546	1.60000	0.00000000	3000.000	2245.932	1539.268	0.0
0	23.9546	1.60000	0.00000000	2750.000	1817.646	1315.491	0.0
0	23.9546	1.60000	0.00000000	2500.000	1461.983	1117.632	0.0
0	23.9546	1.60000	0.00000000	2250.000	1155.828	916.991	0.0
0	23.9546	1.60000	0.00000000	2000.000	873.173	649.389	0.0
0	23.9546	1.60000	0.00000000	1750.000	590.681	192.495	0.0
0	23.9546	1.60000	0.00000000	1500.000	282.630	-181.177	0.0
0	23.9546	1.60000	0.00000000	1250.000	-219.084	-467.058	0.0
0	23.9546	1.60000	0.00000000	1000.000	-1147.925	-813.498	0.0
0	23.9546	1.60000	0.00000000	750.000	-1641.571	-1207.492	0.0
0	23.9546	1.60000	0.00000000	500.000	-1909.770	-1380.725	0.0
1	23.9546	1.65000	1.09971979	4000.000	4966.385	3737.450	0.0
1	23.9546	1.65000	0.38068410	3750.000	4105.819	2856.795	0.0
1	23.9546	1.65000	0.01349459	3500.000	3394.572	2221.219	0.0
0	23.9546	1.65000	0.00000000	3250.000	2784.180	1832.376	0.0
0	23.9546	1.65000	0.00000000	3000.000	2266.127	1557.637	0.0
0	23.9546	1.65000	0.00000000	2750.000	1835.699	1332.995	0.0
0	23.9546	1.65000	0.00000000	2500.000	1477.921	1134.321	0.0
0	23.9546	1.65000	0.00000000	2250.000	1169.797	932.884	0.0
0	23.9546	1.65000	0.00000000	2000.000	885.415	663.625	0.0
0	23.9546	1.65000	0.00000000	1750.000	601.096	200.688	0.0
0	23.9546	1.65000	0.00000000	1500.000	290.640	-175.469	0.0
0	23.9546	1.65000	0.00000000	1250.000	-214.552	-465.313	0.0
0	23.9546	1.65000	0.00000000	1000.000	-1147.644	-807.002	0.0
0	23.9546	1.65000	0.00000000	750.000	-1643.079	-1200.952	0.0
0	23.9546	1.65000	0.00000000	500.000	-1911.663	-1375.483	0.0
1	23.9546	1.70000	1.11744987	4000.000	4987.435	3752.995	0.0
1	23.9546	1.70000	0.38177182	3750.000	4128.711	2872.992	0.0
1	23.9546	1.70000	0.00573651	3500.000	3417.298	2236.552	0.0
0	23.9546	1.70000	0.00000000	3250.000	2805.618	1851.014	0.0

0	23.9546	1.70000	0.00000000	3000.000	2285.697	1575.321	0.0
0	23.9546	1.70000	0.00000000	2750.000	1853.203	1349.845	0.0
0	23.9546	1.70000	0.00000000	2500.000	1493.377	1150.382	0.0
0	23.9546	1.70000	0.00000000	2250.000	1183.339	948.170	0.0
0	23.9546	1.70000	0.00000000	2000.000	897.274	677.302	0.0
0	23.9546	1.70000	0.00000000	1750.000	611.185	208.550	0.0
0	23.9546	1.70000	0.00000000	1500.000	298.397	-169.962	0.0
0	23.9546	1.70000	0.00000000	1250.000	-210.167	-463.224	0.0
0	23.9546	1.70000	0.00000000	1000.000	-1147.370	-800.708	0.0
0	23.9546	1.70000	0.00000000	750.000	-1644.534	-1194.831	0.0
0	23.9546	1.70000	0.00000000	500.000	-1913.477	-1370.420	0.0
1	23.9546	1.75000	1.13522001	4000.000	5007.737	3767.992	0.0
1	23.9546	1.75000	0.38288794	3750.000	4150.828	2888.651	0.0
0	23.9546	1.75000	0.00000000	3500.000	3439.287	2224.348	0.0
0	23.9546	1.75000	0.00000000	3250.000	2826.386	1868.969	0.0
0	23.9546	1.75000	0.00000000	3000.000	2304.671	1592.357	0.0
0	23.9546	1.75000	0.00000000	2750.000	1870.182	1366.076	0.0
0	23.9546	1.75000	0.00000000	2500.000	1508.373	1165.851	0.0
0	23.9546	1.75000	0.00000000	2250.000	1196.475	962.883	0.0
0	23.9546	1.75000	0.00000000	2000.000	908.768	690.452	0.0
0	23.9546	1.75000	0.00000000	1750.000	620.962	216.100	0.0
0	23.9546	1.75000	0.00000000	1500.000	305.912	-164.646	0.0
0	23.9546	1.75000	0.00000000	1250.000	-205.923	-460.848	0.0
0	23.9546	1.75000	0.00000000	1000.000	-1147.102	-794.610	0.0
0	23.9546	1.75000	0.00000000	750.000	-1645.940	-1189.044	0.0
0	23.9546	1.75000	0.00000000	500.000	-1915.218	-1365.527	0.0
1	23.9546	1.80000	1.15302918	4000.000	5027.331	3782.469	0.0
1	23.9546	1.80000	0.38403202	3750.000	4172.209	2903.799	0.0
0	23.9546	1.80000	0.00000000	3500.000	3460.575	2242.795	0.0
0	23.9546	1.80000	0.00000000	3250.000	2846.513	1886.277	0.0
0	23.9546	1.80000	0.00000000	3000.000	2323.074	1608.779	0.0
0	23.9546	1.80000	0.00000000	2750.000	1886.658	1381.722	0.0
0	23.9546	1.80000	0.00000000	2500.000	1522.927	1180.758	0.0
0	23.9546	1.80000	0.00000000	2250.000	1209.221	977.055	0.0
0	23.9546	1.80000	0.00000000	2000.000	919.912	703.103	0.0
0	23.9546	1.80000	0.00000000	1750.000	630.442	223.357	0.0
0	23.9546	1.80000	0.00000000	1500.000	313.197	-159.513	0.0
0	23.9546	1.80000	0.00000000	1250.000	-201.812	-458.253	0.0
0	23.9546	1.80000	0.00000000	1000.000	-1146.840	-788.699	0.0
0	23.9546	1.80000	0.00000000	750.000	-1647.300	-1183.539	0.0
0	23.9546	1.80000	0.00000000	500.000	-1916.889	-1360.798	0.0
1	23.9546	1.85000	1.17087636	4000.000	5046.253	3796.453	0.0
1	23.9546	1.85000	0.38520362	3750.000	4192.890	2918.460	0.0
0	23.9546	1.85000	0.00000000	3500.000	3481.194	2260.588	0.0
0	23.9546	1.85000	0.00000000	3250.000	2866.029	1902.972	0.0
0	23.9546	1.85000	0.00000000	3000.000	2340.931	1624.620	0.0
0	23.9546	1.85000	0.00000000	2750.000	1902.653	1396.813	0.0
0	23.9546	1.85000	0.00000000	2500.000	1537.059	1195.134	0.0
0	23.9546	1.85000	0.00000000	2250.000	1221.594	990.713	0.0
0	23.9546	1.85000	0.00000000	2000.000	930.723	715.282	0.0
0	23.9546	1.85000	0.00000000	1750.000	639.636	230.337	0.0
0	23.9546	1.85000	0.00000000	1500.000	320.261	-154.556	0.0
0	23.9546	1.85000	0.00000000	1250.000	-197.830	-455.505	0.0
0	23.9546	1.85000	0.00000000	1000.000	-1146.585	-782.969	0.0
0	23.9546	1.85000	0.00000000	750.000	-1648.615	-1178.281	0.0
0	23.9546	1.85000	0.00000000	500.000	-1918.494	-1356.223	0.0

1	23.9546	1.90000	1.18876056	4000.000	5064.537	3809.968	0.0
1	23.9546	1.90000	0.38640229	3750.000	4212.905	2932.658	0.0
0	23.9546	1.90000	0.00000000	3500.000	3501.175	2277.760	0.0
0	23.9546	1.90000	0.00000000	3250.000	2884.960	1919.086	0.0
0	23.9546	1.90000	0.00000000	3000.000	2358.266	1639.911	0.0
0	23.9546	1.90000	0.00000000	2750.000	1918.187	1411.379	0.0
0	23.9546	1.90000	0.00000000	2500.000	1550.787	1209.006	0.0
0	23.9546	1.90000	0.00000000	2250.000	1233.610	1003.887	0.0
0	23.9546	1.90000	0.00000000	2000.000	941.214	727.016	0.0
0	23.9546	1.90000	0.00000000	1750.000	648.558	237.057	0.0
0	23.9546	1.90000	0.00000000	1500.000	327.114	-149.766	0.0
0	23.9546	1.90000	0.00000000	1250.000	-193.970	-452.658	0.0
0	23.9546	1.90000	0.00000000	1000.000	-1146.336	-777.414	0.0
0	23.9546	1.90000	0.00000000	750.000	-1649.888	-1173.243	0.0
0	23.9546	1.90000	0.00000000	500.000	-1920.038	-1351.795	0.0
1	23.9546	1.95000	1.20668081	4000.000	5082.214	3823.038	0.0
1	23.9546	1.95000	0.38762756	3750.000	4232.285	2946.412	0.0
0	23.9546	1.95000	0.00000000	3500.000	3520.547	2294.344	0.0
0	23.9546	1.95000	0.00000000	3250.000	2903.332	1934.649	0.0
0	23.9546	1.95000	0.00000000	3000.000	2375.101	1654.678	0.0
0	23.9546	1.95000	0.00000000	2750.000	1933.280	1425.445	0.0
0	23.9546	1.95000	0.00000000	2500.000	1564.127	1222.401	0.0
0	23.9546	1.95000	0.00000000	2250.000	1245.284	1016.600	0.0
0	23.9546	1.95000	0.00000000	2000.000	951.400	738.326	0.0
0	23.9546	1.95000	0.00000000	1750.000	657.219	243.531	0.0
0	23.9546	1.95000	0.00000000	1500.000	333.766	-145.135	0.0
0	23.9546	1.95000	0.00000000	1250.000	-190.226	-449.756	0.0
0	23.9546	1.95000	0.00000000	1000.000	-1146.093	-772.027	0.0
0	23.9546	1.95000	0.00000000	750.000	-1651.121	-1168.406	0.0
0	23.9546	1.95000	0.00000000	500.000	-1921.524	-1347.509	0.0
1	23.9546	2.00000	1.22463615	4000.000	5099.314	3835.683	0.0
1	23.9546	2.00000	0.38887896	3750.000	4251.059	2959.745	0.0
0	23.9546	2.00000	0.00000000	3500.000	3539.336	2310.368	0.0
0	23.9546	2.00000	0.00000000	3250.000	2921.169	1949.689	0.0
0	23.9546	2.00000	0.00000000	3000.000	2391.456	1668.949	0.0
0	23.9546	2.00000	0.00000000	2750.000	1947.949	1439.038	0.0
0	23.9546	2.00000	0.00000000	2500.000	1577.094	1235.342	0.0
0	23.9546	2.00000	0.00000000	2250.000	1256.630	1028.876	0.0
0	23.9546	2.00000	0.00000000	2000.000	961.294	749.235	0.0
0	23.9546	2.00000	0.00000000	1750.000	665.630	249.771	0.0
0	23.9546	2.00000	0.00000000	1500.000	340.225	-140.656	0.0
0	23.9546	2.00000	0.00000000	1250.000	-186.594	-446.830	0.0
0	23.9546	2.00000	0.00000000	1000.000	-1145.856	-766.803	0.0
0	23.9546	2.00000	0.00000000	750.000	-1652.315	-1163.753	0.0
0	23.9546	2.00000	0.00000000	500.000	-1922.955	-1343.357	0.0
1	23.9546	2.05000	1.24262567	4000.000	5115.865	3847.925	0.0
1	23.9546	2.05000	0.39015600	3750.000	4269.255	2972.674	0.0
0	23.9546	2.05000	0.00000000	3500.000	3557.569	2325.861	0.0
0	23.9546	2.05000	0.00000000	3250.000	2938.493	1964.230	0.0
0	23.9546	2.05000	0.00000000	3000.000	2407.352	1682.747	0.0
0	23.9546	2.05000	0.00000000	2750.000	1962.211	1452.180	0.0
0	23.9546	2.05000	0.00000000	2500.000	1589.705	1247.853	0.0
0	23.9546	2.05000	0.00000000	2250.000	1267.662	1040.738	0.0
0	23.9546	2.05000	0.00000000	2000.000	970.907	759.764	0.0
0	23.9546	2.05000	0.00000000	1750.000	673.802	255.791	0.0
0	23.9546	2.05000	0.00000000	1500.000	346.498	-136.323	0.0

0	23.9546	2.05000	0.00000000	1250.000	-183.069	-443.905	0.0
0	23.9546	2.05000	0.00000000	1000.000	-1145.624	-761.736	0.0
0	23.9546	2.05000	0.00000000	750.000	-1653.473	-1159.271	0.0
0	23.9546	2.05000	0.00000000	500.000	-1924.334	-1339.334	0.0
1	23.9546	2.10000	1.26064846	4000.000	5131.893	3859.781	0.0
1	23.9546	2.10000	0.39145821	3750.000	4286.900	2985.218	0.0
0	23.9546	2.10000	0.00000000	3500.000	3575.269	2340.848	0.0
0	23.9546	2.10000	0.00000000	3250.000	2955.327	1978.298	0.0
0	23.9546	2.10000	0.00000000	3000.000	2422.807	1696.096	0.0
0	23.9546	2.10000	0.00000000	2750.000	1976.083	1464.894	0.0
0	23.9546	2.10000	0.00000000	2500.000	1601.972	1259.953	0.0
0	23.9546	2.10000	0.00000000	2250.000	1278.393	1052.206	0.0
0	23.9546	2.10000	0.00000000	2000.000	980.252	769.931	0.0
0	23.9546	2.10000	0.00000000	1750.000	681.744	261.602	0.0
0	23.9546	2.10000	0.00000000	1500.000	352.595	-132.128	0.0
0	23.9546	2.10000	0.00000000	1250.000	-179.646	-440.998	0.0
0	23.9546	2.10000	0.00000000	1000.000	-1145.398	-756.822	0.0
0	23.9546	2.10000	0.00000000	750.000	-1654.597	-1154.947	0.0
0	23.9546	2.10000	0.00000000	500.000	-1925.663	-1335.434	0.0
1	23.9546	2.15000	1.27870365	4000.000	5147.421	3871.270	0.0
1	23.9546	2.15000	0.39278511	3750.000	4304.018	2997.393	0.0
0	23.9546	2.15000	0.00000000	3500.000	3592.460	2355.353	0.0
0	23.9546	2.15000	0.00000000	3250.000	2971.690	1991.915	0.0
0	23.9546	2.15000	0.00000000	3000.000	2437.840	1709.018	0.0
0	23.9546	2.15000	0.00000000	2750.000	1989.581	1477.199	0.0
0	23.9546	2.15000	0.00000000	2500.000	1613.911	1271.663	0.0
0	23.9546	2.15000	0.00000000	2250.000	1288.833	1063.299	0.0
0	23.9546	2.15000	0.00000000	2000.000	989.338	779.754	0.0
0	23.9546	2.15000	0.00000000	1750.000	689.466	267.215	0.0
0	23.9546	2.15000	0.00000000	1500.000	358.521	-128.066	0.0
0	23.9546	2.15000	0.00000000	1250.000	-176.320	-438.122	0.0
0	23.9546	2.15000	0.00000000	1000.000	-1145.178	-752.056	0.0
0	23.9546	2.15000	0.00000000	750.000	-1655.688	-1150.772	0.0
0	23.9546	2.15000	0.00000000	500.000	-1926.946	-1331.650	0.0
1	23.9546	2.20000	1.29679038	4000.000	5162.474	3882.408	0.0
1	23.9546	2.20000	0.39413620	3750.000	4320.631	3009.216	0.0
0	23.9546	2.20000	0.00000000	3500.000	3609.162	2369.400	0.0
0	23.9546	2.20000	0.00000000	3250.000	2987.602	2005.102	0.0
0	23.9546	2.20000	0.00000000	3000.000	2452.466	1721.531	0.0
0	23.9546	2.20000	0.00000000	2750.000	2002.718	1489.116	0.0
0	23.9546	2.20000	0.00000000	2500.000	1625.532	1283.002	0.0
0	23.9546	2.20000	0.00000000	2250.000	1298.996	1074.035	0.0
0	23.9546	2.20000	0.00000000	2000.000	998.178	789.251	0.0
0	23.9546	2.20000	0.00000000	1750.000	696.976	272.640	0.0
0	23.9546	2.20000	0.00000000	1500.000	364.284	-124.130	0.0
0	23.9546	2.20000	0.00000000	1250.000	-173.089	-435.285	0.0
0	23.9546	2.20000	0.00000000	1000.000	-1144.962	-747.434	0.0
0	23.9546	2.20000	0.00000000	750.000	-1656.747	-1146.738	0.0
0	23.9546	2.20000	0.00000000	500.000	-1928.185	-1327.980	0.0
1	23.9546	2.25000	1.31490781	4000.000	5177.072	3893.212	0.0
1	23.9546	2.25000	0.39551103	3750.000	4336.763	3020.700	0.0
0	23.9546	2.25000	0.00000000	3500.000	3625.397	2383.009	0.0
0	23.9546	2.25000	0.00000000	3250.000	3003.081	2017.880	0.0
0	23.9546	2.25000	0.00000000	3000.000	2466.702	1733.656	0.0
0	23.9546	2.25000	0.00000000	2750.000	2015.510	1500.662	0.0
0	23.9546	2.25000	0.00000000	2500.000	1636.850	1293.986	0.0

0	23.9546	2.25000	0.00000000	2250.000	1308.891	1084.432	0.0
0	23.9546	2.25000	0.00000000	2000.000	1006.780	798.437	0.0
0	23.9546	2.25000	0.00000000	1750.000	704.284	277.886	0.0
0	23.9546	2.25000	0.00000000	1500.000	369.890	-120.316	0.0
0	23.9546	2.25000	0.00000000	1250.000	-169.947	-432.495	0.0
0	23.9546	2.25000	0.00000000	1000.000	-1144.752	-742.952	0.0
0	23.9546	2.25000	0.00000000	750.000	-1657.775	-1142.835	0.0
0	23.9546	2.25000	0.00000000	500.000	-1929.381	-1324.417	0.0
1	23.9546	2.30000	1.33305516	4000.000	5191.236	3903.696	0.0
1	23.9546	2.30000	0.39690910	3750.000	4352.434	3031.861	0.0
0	23.9546	2.30000	0.00000000	3500.000	3641.183	2396.201	0.0
0	23.9546	2.30000	0.00000000	3250.000	3018.145	2030.266	0.0
0	23.9546	2.30000	0.00000000	3000.000	2480.564	1745.410	0.0
0	23.9546	2.30000	0.00000000	2750.000	2027.969	1511.854	0.0
0	23.9546	2.30000	0.00000000	2500.000	1647.875	1304.632	0.0
0	23.9546	2.30000	0.00000000	2250.000	1318.529	1094.503	0.0
0	23.9546	2.30000	0.00000000	2000.000	1015.154	807.326	0.0
0	23.9546	2.30000	0.00000000	1750.000	711.396	282.961	0.0
0	23.9546	2.30000	0.00000000	1500.000	375.347	-116.617	0.0
0	23.9546	2.30000	0.00000000	1250.000	-166.891	-429.756	0.0
0	23.9546	2.30000	0.00000000	1000.000	-1144.546	-738.607	0.0
0	23.9546	2.30000	0.00000000	750.000	-1658.775	-1139.057	0.0
0	23.9546	2.30000	0.00000000	500.000	-1930.538	-1320.956	0.0
1	23.9546	2.35000	1.35123162	4000.000	5204.984	3913.873	0.0
1	23.9546	2.35000	0.39832995	3750.000	4367.662	3042.712	0.0
0	23.9546	2.35000	0.00000000	3500.000	3656.539	2408.995	0.0
0	23.9546	2.35000	0.00000000	3250.000	3032.809	2042.279	0.0
0	23.9546	2.35000	0.00000000	3000.000	2494.065	1756.809	0.0
0	23.9546	2.35000	0.00000000	2750.000	2040.108	1522.709	0.0
0	23.9546	2.35000	0.00000000	2500.000	1658.617	1314.956	0.0
0	23.9546	2.35000	0.00000000	2250.000	1327.919	1104.266	0.0
0	23.9546	2.35000	0.00000000	2000.000	1023.309	815.932	0.0
0	23.9546	2.35000	0.00000000	1750.000	718.321	287.874	0.0
0	23.9546	2.35000	0.00000000	1500.000	380.658	-113.029	0.0
0	23.9546	2.35000	0.00000000	1250.000	-163.918	-427.070	0.0
0	23.9546	2.35000	0.00000000	1000.000	-1144.346	-734.396	0.0
0	23.9546	2.35000	0.00000000	750.000	-1659.747	-1135.398	0.0
0	23.9546	2.35000	0.00000000	500.000	-1931.657	-1317.595	0.0
1	23.9546	2.40000	1.36943644	4000.000	5218.335	3923.758	0.0
1	23.9546	2.40000	0.39977311	3750.000	4382.466	3053.265	0.0
0	23.9546	2.40000	0.00000000	3500.000	3671.482	2421.407	0.0
0	23.9546	2.40000	0.00000000	3250.000	3047.088	2053.935	0.0
0	23.9546	2.40000	0.00000000	3000.000	2507.219	1767.870	0.0
0	23.9546	2.40000	0.00000000	2750.000	2051.939	1533.240	0.0
0	23.9546	2.40000	0.00000000	2500.000	1669.089	1324.971	0.0
0	23.9546	2.40000	0.00000000	2250.000	1337.072	1113.733	0.0
0	23.9546	2.40000	0.00000000	2000.000	1031.252	824.269	0.0
0	23.9546	2.40000	0.00000000	1750.000	725.066	292.633	0.0
0	23.9546	2.40000	0.00000000	1500.000	385.831	-109.547	0.0
0	23.9546	2.40000	0.00000000	1250.000	-161.025	-424.439	0.0
0	23.9546	2.40000	0.00000000	1000.000	-1144.150	-730.316	0.0
0	23.9546	2.40000	0.00000000	750.000	-1660.693	-1131.851	0.0
0	23.9546	2.40000	0.00000000	500.000	-1932.739	-1314.328	0.0
1	23.9546	2.45000	1.38766888	4000.000	5231.305	3933.361	0.0
1	23.9546	2.45000	0.40123812	3750.000	4396.864	3063.533	0.0
0	23.9546	2.45000	0.00000000	3500.000	3686.028	2433.455	0.0

0	23.9546	2.45000	0.00000000	3250.000	3060.999	2065.249	0.0
0	23.9546	2.45000	0.00000000	3000.000	2520.039	1778.607	0.0
0	23.9546	2.45000	0.00000000	2750.000	2063.473	1543.462	0.0
0	23.9546	2.45000	0.00000000	2500.000	1679.299	1334.691	0.0
0	23.9546	2.45000	0.00000000	2250.000	1345.995	1122.918	0.0
0	23.9546	2.45000	0.00000000	2000.000	1038.993	832.349	0.0
0	23.9546	2.45000	0.00000000	1750.000	731.638	297.244	0.0
0	23.9546	2.45000	0.00000000	1500.000	390.870	-106.167	0.0
0	23.9546	2.45000	0.00000000	1250.000	-158.207	-421.864	0.0
0	23.9546	2.45000	0.00000000	1000.000	-1143.958	-726.366	0.0
0	23.9546	2.45000	0.00000000	750.000	-1661.613	-1128.411	0.0
0	23.9546	2.45000	0.00000000	500.000	-1933.787	-1311.152	0.0
1	23.9546	2.50000	1.40592822	4000.000	5243.911	3942.696	0.0
1	23.9546	2.50000	0.40272453	3750.000	4410.873	3073.526	0.0
0	23.9546	2.50000	0.00000000	3500.000	3700.193	2445.155	0.0
0	23.9546	2.50000	0.00000000	3250.000	3074.555	2076.237	0.0
0	23.9546	2.50000	0.00000000	3000.000	2532.538	1789.034	0.0
0	23.9546	2.50000	0.00000000	2750.000	2074.721	1553.390	0.0
0	23.9546	2.50000	0.00000000	2500.000	1689.258	1344.129	0.0
0	23.9546	2.50000	0.00000000	2250.000	1354.697	1131.834	0.0
0	23.9546	2.50000	0.00000000	2000.000	1046.539	840.182	0.0
0	23.9546	2.50000	0.00000000	1750.000	738.042	301.715	0.0
0	23.9546	2.50000	0.00000000	1500.000	395.781	-102.884	0.0
0	23.9546	2.50000	0.00000000	1250.000	-155.464	-419.345	0.0
0	23.9546	2.50000	0.00000000	1000.000	-1143.771	-722.544	0.0
0	23.9546	2.50000	0.00000000	750.000	-1662.509	-1125.072	0.0
0	23.9546	2.50000	0.00000000	500.000	-1934.802	-1308.063	0.0
1	23.9546	2.55000	1.42421377	4000.000	5256.167	3951.774	0.0
1	23.9546	2.55000	0.40423189	3750.000	4424.507	3083.256	0.0
0	23.9546	2.55000	0.00000000	3500.000	3713.992	2456.521	0.0
0	23.9546	2.55000	0.00000000	3250.000	3087.769	2086.912	0.0
0	23.9546	2.55000	0.00000000	3000.000	2544.728	1799.164	0.0
0	23.9546	2.55000	0.00000000	2750.000	2085.693	1563.034	0.0
0	23.9546	2.55000	0.00000000	2500.000	1698.974	1353.297	0.0
0	23.9546	2.55000	0.00000000	2250.000	1363.187	1140.491	0.0
0	23.9546	2.55000	0.00000000	2000.000	1053.897	847.781	0.0
0	23.9546	2.55000	0.00000000	1750.000	744.286	306.052	0.0
0	23.9546	2.55000	0.00000000	1500.000	400.567	-99.694	0.0
0	23.9546	2.55000	0.00000000	1250.000	-152.790	-416.883	0.0
0	23.9546	2.55000	0.00000000	1000.000	-1143.588	-718.852	0.0
0	23.9546	2.55000	0.00000000	750.000	-1663.381	-1121.831	0.0
0	23.9546	2.55000	0.00000000	500.000	-1935.785	-1305.058	0.0
1	23.9546	2.60000	1.44252485	4000.000	5268.089	3960.604	0.0
1	23.9546	2.60000	0.40575975	3750.000	4437.781	3092.733	0.0
0	23.9546	2.60000	0.00000000	3500.000	3727.438	2467.568	0.0
0	23.9546	2.60000	0.00000000	3250.000	3100.653	2097.287	0.0
0	23.9546	2.60000	0.00000000	3000.000	2556.619	1809.010	0.0
0	23.9546	2.60000	0.00000000	2750.000	2096.400	1572.407	0.0
0	23.9546	2.60000	0.00000000	2500.000	1708.456	1362.207	0.0
0	23.9546	2.60000	0.00000000	2250.000	1371.472	1148.901	0.0
0	23.9546	2.60000	0.00000000	2000.000	1061.074	855.155	0.0
0	23.9546	2.60000	0.00000000	1750.000	750.375	310.260	0.0
0	23.9546	2.60000	0.00000000	1500.000	405.235	-96.593	0.0
0	23.9546	2.60000	0.00000000	1250.000	-150.185	-414.476	0.0
0	23.9546	2.60000	0.00000000	1000.000	-1143.409	-715.288	0.0
0	23.9546	2.60000	0.00000000	750.000	-1664.231	-1118.683	0.0

0	23.9546	2.60000	0.00000000	500.000	-1936.739	-1302.133	0.0
1	23.9546	2.65000	1.46086080	4000.000	5279.689	3969.196	0.0
1	23.9546	2.65000	0.40730769	3750.000	4450.710	3101.966	0.0
0	23.9546	2.65000	0.00000000	3500.000	3740.544	2478.308	0.0
0	23.9546	2.65000	0.00000000	3250.000	3113.221	2107.375	0.0
0	23.9546	2.65000	0.00000000	3000.000	2568.223	1818.583	0.0
0	23.9546	2.65000	0.00000000	2750.000	2106.851	1581.520	0.0
0	23.9546	2.65000	0.00000000	2500.000	1717.712	1370.869	0.0
0	23.9546	2.65000	0.00000000	2250.000	1379.558	1157.074	0.0
0	23.9546	2.65000	0.00000000	2000.000	1068.076	862.314	0.0
0	23.9546	2.65000	0.00000000	1750.000	756.314	314.345	0.0
0	23.9546	2.65000	0.00000000	1500.000	409.788	-93.578	0.0
0	23.9546	2.65000	0.00000000	1250.000	-147.645	-412.124	0.0
0	23.9546	2.65000	0.00000000	1000.000	-1143.234	-711.855	0.0
0	23.9546	2.65000	0.00000000	750.000	-1665.059	-1115.623	0.0
0	23.9546	2.65000	0.00000000	500.000	-1937.664	-1299.286	0.0
1	23.9546	2.70000	1.47922099	4000.000	5290.980	3977.561	0.0
1	23.9546	2.70000	0.40887528	3750.000	4463.306	3110.965	0.0
0	23.9546	2.70000	0.00000000	3500.000	3753.324	2488.754	0.0
0	23.9546	2.70000	0.00000000	3250.000	3125.483	2117.187	0.0
0	23.9546	2.70000	0.00000000	3000.000	2579.549	1827.895	0.0
0	23.9546	2.70000	0.00000000	2750.000	2117.054	1590.384	0.0
0	23.9546	2.70000	0.00000000	2500.000	1726.750	1379.293	0.0
0	23.9546	2.70000	0.00000000	2250.000	1387.454	1165.020	0.0
0	23.9546	2.70000	0.00000000	2000.000	1074.910	869.266	0.0
0	23.9546	2.70000	0.00000000	1750.000	762.110	318.313	0.0
0	23.9546	2.70000	0.00000000	1500.000	414.230	-90.646	0.0
0	23.9546	2.70000	0.00000000	1250.000	-145.168	-409.826	0.0
0	23.9546	2.70000	0.00000000	1000.000	-1143.063	-708.554	0.0
0	23.9546	2.70000	0.00000000	750.000	-1665.867	-1112.648	0.0
0	23.9546	2.70000	0.00000000	500.000	-1938.561	-1296.513	0.0
1	23.9546	2.75000	1.49760480	4000.000	5301.975	3985.707	0.0
1	23.9546	2.75000	0.41046211	3750.000	4475.583	3119.738	0.0
0	23.9546	2.75000	0.00000000	3500.000	3765.789	2498.918	0.0
0	23.9546	2.75000	0.00000000	3250.000	3137.450	2126.735	0.0
0	23.9546	2.75000	0.00000000	3000.000	2590.608	1836.956	0.0
0	23.9546	2.75000	0.00000000	2750.000	2127.019	1599.009	0.0
0	23.9546	2.75000	0.00000000	2500.000	1735.577	1387.489	0.0
0	23.9546	2.75000	0.00000000	2250.000	1395.165	1172.749	0.0
0	23.9546	2.75000	0.00000000	2000.000	1081.582	876.022	0.0
0	23.9546	2.75000	0.00000000	1750.000	767.767	322.168	0.0
0	23.9546	2.75000	0.00000000	1500.000	418.565	-87.792	0.0
0	23.9546	2.75000	0.00000000	1250.000	-142.751	-407.581	0.0
0	23.9546	2.75000	0.00000000	1000.000	-1142.896	-705.385	0.0
0	23.9546	2.75000	0.00000000	750.000	-1666.654	-1109.754	0.0
0	23.9546	2.75000	0.00000000	500.000	-1939.433	-1293.811	0.0
1	23.9546	2.80000	1.51601164	4000.000	5312.685	3993.642	0.0
1	23.9546	2.80000	0.41206776	3750.000	4487.552	3128.294	0.0
0	23.9546	2.80000	0.00000000	3500.000	3777.951	2508.811	0.0
0	23.9546	2.80000	0.00000000	3250.000	3149.133	2136.029	0.0
0	23.9546	2.80000	0.00000000	3000.000	2601.408	1845.776	0.0
0	23.9546	2.80000	0.00000000	2750.000	2136.753	1607.405	0.0
0	23.9546	2.80000	0.00000000	2500.000	1744.201	1395.466	0.0
0	23.9546	2.80000	0.00000000	2250.000	1402.698	1180.269	0.0
0	23.9546	2.80000	0.00000000	2000.000	1088.097	882.588	0.0
0	23.9546	2.80000	0.00000000	1750.000	773.290	325.915	0.0

0	23.9546	2.80000	0.00000000	1500.000	422.797	-85.015	0.0
0	23.9546	2.80000	0.00000000	1250.000	-140.393	-405.388	0.0
0	23.9546	2.80000	0.00000000	1000.000	-1142.732	-702.350	0.0
0	23.9546	2.80000	0.00000000	750.000	-1667.422	-1106.939	0.0
0	23.9546	2.80000	0.00000000	500.000	-1940.279	-1291.178	0.0
1	23.9546	2.85000	1.53444092	4000.000	5323.120	4001.374	0.0
1	23.9546	2.85000	0.41369183	3750.000	4499.225	3136.641	0.0
0	23.9546	2.85000	0.00000000	3500.000	3789.821	2518.444	0.0
0	23.9546	2.85000	0.00000000	3250.000	3160.542	2145.079	0.0
0	23.9546	2.85000	0.00000000	3000.000	2611.959	1854.364	0.0
0	23.9546	2.85000	0.00000000	2750.000	2146.264	1615.579	0.0
0	23.9546	2.85000	0.00000000	2500.000	1752.629	1403.232	0.0
0	23.9546	2.85000	0.00000000	2250.000	1410.060	1187.588	0.0
0	23.9546	2.85000	0.00000000	2000.000	1094.460	888.972	0.0
0	23.9546	2.85000	0.00000000	1750.000	778.684	329.559	0.0
0	23.9546	2.85000	0.00000000	1500.000	426.930	-82.310	0.0
0	23.9546	2.85000	0.00000000	1250.000	-138.091	-403.245	0.0
0	23.9546	2.85000	0.00000000	1000.000	-1142.572	-699.444	0.0
0	23.9546	2.85000	0.00000000	750.000	-1668.172	-1104.197	0.0
0	23.9546	2.85000	0.00000000	500.000	-1941.102	-1288.611	0.0
1	23.9546	2.90000	1.55289208	4000.000	5333.292	4008.912	0.0
1	23.9546	2.90000	0.41533394	3750.000	4510.612	3144.786	0.0
0	23.9546	2.90000	0.00000000	3500.000	3801.408	2527.827	0.0
0	23.9546	2.90000	0.00000000	3250.000	3171.686	2153.894	0.0
0	23.9546	2.90000	0.00000000	3000.000	2622.268	1862.730	0.0
0	23.9546	2.90000	0.00000000	2750.000	2155.560	1623.542	0.0
0	23.9546	2.90000	0.00000000	2500.000	1760.867	1410.797	0.0
0	23.9546	2.90000	0.00000000	2250.000	1417.255	1194.715	0.0
0	23.9546	2.90000	0.00000000	2000.000	1100.678	895.182	0.0
0	23.9546	2.90000	0.00000000	1750.000	783.953	333.104	0.0
0	23.9546	2.90000	0.00000000	1500.000	430.967	-79.676	0.0
0	23.9546	2.90000	0.00000000	1250.000	-135.844	-401.151	0.0
0	23.9546	2.90000	0.00000000	1000.000	-1142.416	-696.664	0.0
0	23.9546	2.90000	0.00000000	750.000	-1668.904	-1101.528	0.0
0	23.9546	2.90000	0.00000000	500.000	-1941.901	-1286.108	0.0
1	23.9546	2.95000	1.57136457	4000.000	5343.209	4016.261	0.0
1	23.9546	2.95000	0.41699369	3750.000	4521.724	3152.736	0.0
0	23.9546	2.95000	0.00000000	3500.000	3812.724	2536.969	0.0
0	23.9546	2.95000	0.00000000	3250.000	3182.574	2162.483	0.0
0	23.9546	2.95000	0.00000000	3000.000	2632.345	1870.881	0.0
0	23.9546	2.95000	0.00000000	2750.000	2164.648	1631.300	0.0
0	23.9546	2.95000	0.00000000	2500.000	1768.921	1418.167	0.0
0	23.9546	2.95000	0.00000000	2250.000	1424.289	1201.657	0.0
0	23.9546	2.95000	0.00000000	2000.000	1106.755	901.225	0.0
0	23.9546	2.95000	0.00000000	1750.000	789.102	336.553	0.0
0	23.9546	2.95000	0.00000000	1500.000	434.911	-77.109	0.0
0	23.9546	2.95000	0.00000000	1250.000	-133.649	-399.105	0.0
0	23.9546	2.95000	0.00000000	1000.000	-1142.262	-694.003	0.0
0	23.9546	2.95000	0.00000000	750.000	-1669.619	-1098.927	0.0
0	23.9546	2.95000	0.00000000	500.000	-1942.678	-1283.666	0.0
1	23.9546	3.00000	1.58985787	4000.000	5352.883	4023.430	0.0
1	23.9546	3.00000	0.41867072	3750.000	4532.571	3160.498	0.0
0	23.9546	3.00000	0.00000000	3500.000	3823.777	2545.880	0.0
0	23.9546	3.00000	0.00000000	3250.000	3193.215	2170.856	0.0
0	23.9546	3.00000	0.00000000	3000.000	2642.197	1878.827	0.0
0	23.9546	3.00000	0.00000000	2750.000	2173.535	1638.863	0.0

0	23.9546	3.00000	0.00000000	2500.000	1776.798	1425.350	0.0
0	23.9546	3.00000	0.00000000	2250.000	1431.168	1208.421	0.0
0	23.9546	3.00000	0.00000000	2000.000	1112.695	907.108	0.0
0	23.9546	3.00000	0.00000000	1750.000	794.134	339.911	0.0
0	23.9546	3.00000	0.00000000	1500.000	438.766	-74.607	0.0
0	23.9546	3.00000	0.00000000	1250.000	-131.505	-397.106	0.0
0	23.9546	3.00000	0.00000000	1000.000	-1142.112	-691.452	0.0
0	23.9546	3.00000	0.00000000	750.000	-1670.317	-1096.392	0.0
0	23.9546	3.00000	0.00000000	500.000	-1943.434	-1281.284	0.0
1	23.9546	3.05000	1.60837146	4000.000	5362.320	4030.425	0.0
1	23.9546	3.05000	0.42036465	3750.000	4543.161	3168.080	0.0
0	23.9546	3.05000	0.00000000	3500.000	3834.576	2554.568	0.0
0	23.9546	3.05000	0.00000000	3250.000	3203.617	2179.019	0.0
0	23.9546	3.05000	0.00000000	3000.000	2651.830	1886.574	0.0
0	23.9546	3.05000	0.00000000	2750.000	2182.227	1646.236	0.0
0	23.9546	3.05000	0.00000000	2500.000	1784.503	1432.353	0.0
0	23.9546	3.05000	0.00000000	2250.000	1437.897	1215.013	0.0
0	23.9546	3.05000	0.00000000	2000.000	1118.504	912.835	0.0
0	23.9546	3.05000	0.00000000	1750.000	799.053	343.181	0.0
0	23.9546	3.05000	0.00000000	1500.000	442.534	-72.168	0.0
0	23.9546	3.05000	0.00000000	1250.000	-129.409	-395.152	0.0
0	23.9546	3.05000	0.00000000	1000.000	-1141.966	-689.003	0.0
0	23.9546	3.05000	0.00000000	750.000	-1670.999	-1093.921	0.0
0	23.9546	3.05000	0.00000000	500.000	-1944.170	-1278.959	0.0
1	23.9546	3.10000	1.62690485	4000.000	5371.531	4037.252	0.0
1	23.9546	3.10000	0.42207512	3750.000	4553.505	3175.486	0.0
0	23.9546	3.10000	0.00000000	3500.000	3845.130	2563.041	0.0
0	23.9546	3.10000	0.00000000	3250.000	3213.788	2186.981	0.0
0	23.9546	3.10000	0.00000000	3000.000	2661.254	1894.130	0.0
0	23.9546	3.10000	0.00000000	2750.000	2190.731	1653.427	0.0
0	23.9546	3.10000	0.00000000	2500.000	1792.041	1439.182	0.0
0	23.9546	3.10000	0.00000000	2250.000	1444.480	1221.441	0.0
0	23.9546	3.10000	0.00000000	2000.000	1124.185	918.414	0.0
0	23.9546	3.10000	0.00000000	1750.000	803.863	346.367	0.0
0	23.9546	3.10000	0.00000000	1500.000	446.218	-69.789	0.0
0	23.9546	3.10000	0.00000000	1250.000	-127.361	-393.243	0.0
0	23.9546	3.10000	0.00000000	1000.000	-1141.822	-686.647	0.0
0	23.9546	3.10000	0.00000000	750.000	-1671.665	-1091.511	0.0
0	23.9546	3.10000	0.00000000	500.000	-1944.886	-1276.689	0.0
1	23.9546	3.15000	1.64545754	4000.000	5380.522	4043.917	0.0
1	23.9546	3.15000	0.42380179	3750.000	4563.610	3182.723	0.0
0	23.9546	3.15000	0.00000000	3500.000	3855.447	2571.308	0.0
0	23.9546	3.15000	0.00000000	3250.000	3223.736	2194.749	0.0
0	23.9546	3.15000	0.00000000	3000.000	2670.473	1901.503	0.0
0	23.9546	3.15000	0.00000000	2750.000	2199.052	1660.443	0.0
0	23.9546	3.15000	0.00000000	2500.000	1799.419	1445.845	0.0
0	23.9546	3.15000	0.00000000	2250.000	1450.922	1227.710	0.0
0	23.9546	3.15000	0.00000000	2000.000	1129.742	923.851	0.0
0	23.9546	3.15000	0.00000000	1750.000	808.568	349.471	0.0
0	23.9546	3.15000	0.00000000	1500.000	449.822	-67.469	0.0
0	23.9546	3.15000	0.00000000	1250.000	-125.359	-391.375	0.0
0	23.9546	3.15000	0.00000000	1000.000	-1141.681	-684.376	0.0
0	23.9546	3.15000	0.00000000	750.000	-1672.317	-1089.160	0.0
0	23.9546	3.15000	0.00000000	500.000	-1945.583	-1274.473	0.0
1	23.9546	3.20000	1.66402908	4000.000	5389.302	4050.425	0.0
1	23.9546	3.20000	0.42554432	3750.000	4573.485	3189.797	0.0

0	23.9546	3.20000	0.00000000	3500.000	3865.536	2579.375	0.0
0	23.9546	3.20000	0.00000000	3250.000	3233.468	2202.330	0.0
0	23.9546	3.20000	0.00000000	3000.000	2679.495	1908.697	0.0
0	23.9546	3.20000	0.00000000	2750.000	2207.197	1667.290	0.0
0	23.9546	3.20000	0.00000000	2500.000	1806.640	1452.347	0.0
0	23.9546	3.20000	0.00000000	2250.000	1457.228	1233.826	0.0
0	23.9546	3.20000	0.00000000	2000.000	1135.181	929.149	0.0
0	23.9546	3.20000	0.00000000	1750.000	813.171	352.497	0.0
0	23.9546	3.20000	0.00000000	1500.000	453.347	-65.204	0.0
0	23.9546	3.20000	0.00000000	1250.000	-123.401	-389.550	0.0
0	23.9546	3.20000	0.00000000	1000.000	-1141.543	-682.184	0.0
0	23.9546	3.20000	0.00000000	750.000	-1672.954	-1086.866	0.0
0	23.9546	3.20000	0.00000000	500.000	-1946.263	-1272.307	0.0
1	23.9546	3.25000	1.68261900	4000.000	5397.878	4056.783	0.0
1	23.9546	3.25000	0.42730236	3750.000	4583.137	3196.713	0.0
0	23.9546	3.25000	0.00000000	3500.000	3875.403	2587.250	0.0
0	23.9546	3.25000	0.00000000	3250.000	3242.991	2209.731	0.0
0	23.9546	3.25000	0.00000000	3000.000	2688.325	1915.721	0.0
0	23.9546	3.25000	0.00000000	2750.000	2215.170	1673.974	0.0
0	23.9546	3.25000	0.00000000	2500.000	1813.710	1458.693	0.0
0	23.9546	3.25000	0.00000000	2250.000	1463.402	1239.794	0.0
0	23.9546	3.25000	0.00000000	2000.000	1140.503	934.315	0.0
0	23.9546	3.25000	0.00000000	1750.000	817.675	355.447	0.0
0	23.9546	3.25000	0.00000000	1500.000	456.796	-62.993	0.0
0	23.9546	3.25000	0.00000000	1250.000	-121.485	-387.765	0.0
0	23.9546	3.25000	0.00000000	1000.000	-1141.408	-680.064	0.0
0	23.9546	3.25000	0.00000000	750.000	-1673.577	-1084.627	0.0
0	23.9546	3.25000	0.00000000	500.000	-1946.925	-1270.192	0.0
1	23.9546	3.30000	1.70122687	4000.000	5406.257	4062.995	0.0
1	23.9546	3.30000	0.42907558	3750.000	4592.574	3203.477	0.0
0	23.9546	3.30000	0.00000000	3500.000	3885.055	2594.940	0.0
0	23.9546	3.30000	0.00000000	3250.000	3252.311	2216.958	0.0
0	23.9546	3.30000	0.00000000	3000.000	2696.971	1922.579	0.0
0	23.9546	3.30000	0.00000000	2750.000	2222.977	1680.501	0.0
0	23.9546	3.30000	0.00000000	2500.000	1820.634	1464.890	0.0
0	23.9546	3.30000	0.00000000	2250.000	1469.447	1245.620	0.0
0	23.9546	3.30000	0.00000000	2000.000	1145.714	939.353	0.0
0	23.9546	3.30000	0.00000000	1750.000	822.083	358.325	0.0
0	23.9546	3.30000	0.00000000	1500.000	460.172	-60.835	0.0
0	23.9546	3.30000	0.00000000	1250.000	-119.611	-386.019	0.0
0	23.9546	3.30000	0.00000000	1000.000	-1141.275	-678.010	0.0
0	23.9546	3.30000	0.00000000	750.000	-1674.187	-1082.440	0.0
0	23.9546	3.30000	0.00000000	500.000	-1947.570	-1268.124	0.0
1	23.9546	3.35000	1.71985226	4000.000	5414.446	4069.066	0.0
1	23.9546	3.35000	0.43086368	3750.000	4601.802	3210.092	0.0
0	23.9546	3.35000	0.00000000	3500.000	3894.501	2602.450	0.0
0	23.9546	3.35000	0.00000000	3250.000	3261.435	2224.016	0.0
0	23.9546	3.35000	0.00000000	3000.000	2705.437	1929.279	0.0
0	23.9546	3.35000	0.00000000	2750.000	2230.624	1686.875	0.0
0	23.9546	3.35000	0.00000000	2500.000	1827.415	1470.942	0.0
0	23.9546	3.35000	0.00000000	2250.000	1475.369	1251.309	0.0
0	23.9546	3.35000	0.00000000	2000.000	1150.816	944.268	0.0
0	23.9546	3.35000	0.00000000	1750.000	826.399	361.132	0.0
0	23.9546	3.35000	0.00000000	1500.000	463.476	-58.727	0.0
0	23.9546	3.35000	0.00000000	1250.000	-117.777	-384.310	0.0
0	23.9546	3.35000	0.00000000	1000.000	-1141.145	-676.017	0.0

0	23.9546	3.35000	0.00000000	750.000	-1674.783	-1080.304	0.0
0	23.9546	3.35000	0.00000000	500.000	-1948.199	-1266.103	0.0
1	23.9546	3.40000	1.73849475	4000.000	5422.451	4075.001	0.0
1	23.9546	3.40000	0.43266633	3750.000	4610.830	3216.565	0.0
0	23.9546	3.40000	0.00000000	3500.000	3903.745	2609.788	0.0
0	23.9546	3.40000	0.00000000	3250.000	3270.368	2230.913	0.0
0	23.9546	3.40000	0.00000000	3000.000	2713.729	1935.824	0.0
0	23.9546	3.40000	0.00000000	2750.000	2238.115	1693.103	0.0
0	23.9546	3.40000	0.00000000	2500.000	1834.059	1476.854	0.0
0	23.9546	3.40000	0.00000000	2250.000	1481.170	1256.866	0.0
0	23.9546	3.40000	0.00000000	2000.000	1155.813	949.065	0.0
0	23.9546	3.40000	0.00000000	1750.000	830.624	363.872	0.0
0	23.9546	3.40000	0.00000000	1500.000	466.712	-56.668	0.0
0	23.9546	3.40000	0.00000000	1250.000	-115.982	-382.639	0.0
0	23.9546	3.40000	0.00000000	1000.000	-1141.018	-674.083	0.0
0	23.9546	3.40000	0.00000000	750.000	-1675.368	-1078.218	0.0
0	23.9546	3.40000	0.00000000	500.000	-1948.813	-1264.127	0.0
1	23.9546	3.45000	1.75715394	4000.000	5430.278	4080.804	0.0
1	23.9546	3.45000	0.43448324	3750.000	4619.663	3222.899	0.0
0	23.9546	3.45000	0.00000000	3500.000	3912.795	2616.959	0.0
0	23.9546	3.45000	0.00000000	3250.000	3279.118	2237.653	0.0
0	23.9546	3.45000	0.00000000	3000.000	2721.852	1942.220	0.0
0	23.9546	3.45000	0.00000000	2750.000	2245.454	1699.190	0.0
0	23.9546	3.45000	0.00000000	2500.000	1840.569	1482.632	0.0
0	23.9546	3.45000	0.00000000	2250.000	1486.854	1262.295	0.0
0	23.9546	3.45000	0.00000000	2000.000	1160.708	953.747	0.0
0	23.9546	3.45000	0.00000000	1750.000	834.763	366.548	0.0
0	23.9546	3.45000	0.00000000	1500.000	469.881	-54.655	0.0
0	23.9546	3.45000	0.00000000	1250.000	-114.224	-381.004	0.0
0	23.9546	3.45000	0.00000000	1000.000	-1140.893	-672.202	0.0
0	23.9546	3.45000	0.00000000	750.000	-1675.939	-1076.178	0.0
0	23.9546	3.45000	0.00000000	500.000	-1949.411	-1262.194	0.0
1	23.9546	3.50000	1.77582943	4000.000	5437.933	4086.480	0.0
1	23.9546	3.50000	0.43631410	3750.000	4628.307	3229.100	0.0
0	23.9546	3.50000	0.00000000	3500.000	3921.656	2623.968	0.0
0	23.9546	3.50000	0.00000000	3250.000	3287.689	2244.241	0.0
0	23.9546	3.50000	0.00000000	3000.000	2729.812	1948.473	0.0
0	23.9546	3.50000	0.00000000	2750.000	2252.647	1705.140	0.0
0	23.9546	3.50000	0.00000000	2500.000	1846.950	1488.279	0.0
0	23.9546	3.50000	0.00000000	2250.000	1492.424	1267.600	0.0
0	23.9546	3.50000	0.00000000	2000.000	1165.504	958.318	0.0
0	23.9546	3.50000	0.00000000	1750.000	838.818	369.160	0.0
0	23.9546	3.50000	0.00000000	1500.000	472.985	-52.688	0.0
0	23.9546	3.50000	0.00000000	1250.000	-112.503	-379.403	0.0
0	23.9546	3.50000	0.00000000	1000.000	-1140.771	-670.372	0.0
0	23.9546	3.50000	0.00000000	750.000	-1676.499	-1074.185	0.0
0	23.9546	3.50000	0.00000000	500.000	-1949.996	-1260.303	0.0
1	23.9546	3.55000	1.79452086	4000.000	5445.422	4092.033	0.0
1	23.9546	3.55000	0.43815862	3750.000	4636.768	3235.170	0.0
0	23.9546	3.55000	0.00000000	3500.000	3930.335	2630.821	0.0
0	23.9546	3.55000	0.00000000	3250.000	3296.087	2250.683	0.0
0	23.9546	3.55000	0.00000000	3000.000	2737.613	1954.587	0.0
0	23.9546	3.55000	0.00000000	2750.000	2259.698	1710.957	0.0
0	23.9546	3.55000	0.00000000	2500.000	1853.204	1493.801	0.0
0	23.9546	3.55000	0.00000000	2250.000	1497.885	1272.786	0.0
0	23.9546	3.55000	0.00000000	2000.000	1170.204	962.783	0.0

0	23.9546	3.55000	0.00000000	1750.000	842.790	371.711	0.0
0	23.9546	3.55000	0.00000000	1500.000	476.026	-50.765	0.0
0	23.9546	3.55000	0.00000000	1250.000	-110.817	-377.836	0.0
0	23.9546	3.55000	0.00000000	1000.000	-1140.651	-668.590	0.0
0	23.9546	3.55000	0.00000000	750.000	-1677.048	-1072.236	0.0
0	23.9546	3.55000	0.00000000	500.000	-1950.566	-1258.452	0.0
1	23.9546	3.60000	1.81322784	4000.000	5452.750	4097.467	0.0
1	23.9546	3.60000	0.44001653	3750.000	4645.053	3241.115	0.0
0	23.9546	3.60000	0.00000000	3500.000	3938.837	2637.524	0.0
0	23.9546	3.60000	0.00000000	3250.000	3304.317	2256.983	0.0
0	23.9546	3.60000	0.00000000	3000.000	2745.259	1960.566	0.0
0	23.9546	3.60000	0.00000000	2750.000	2266.610	1716.646	0.0
0	23.9546	3.60000	0.00000000	2500.000	1859.337	1499.201	0.0
0	23.9546	3.60000	0.00000000	2250.000	1503.239	1277.857	0.0
0	23.9546	3.60000	0.00000000	2000.000	1174.812	967.145	0.0
0	23.9546	3.60000	0.00000000	1750.000	846.683	374.204	0.0
0	23.9546	3.60000	0.00000000	1500.000	479.006	-48.884	0.0
0	23.9546	3.60000	0.00000000	1250.000	-109.165	-376.301	0.0
0	23.9546	3.60000	0.00000000	1000.000	-1140.533	-666.854	0.0
0	23.9546	3.60000	0.00000000	750.000	-1677.585	-1070.329	0.0
0	23.9546	3.60000	0.00000000	500.000	-1951.123	-1256.641	0.0
1	23.9546	3.65000	1.83195003	4000.000	5459.922	4102.785	0.0
1	23.9546	3.65000	0.44188754	3750.000	4653.166	3246.938	0.0
0	23.9546	3.65000	0.00000000	3500.000	3947.167	2644.080	0.0
0	23.9546	3.65000	0.00000000	3250.000	3312.383	2263.146	0.0
0	23.9546	3.65000	0.00000000	3000.000	2752.757	1966.416	0.0
0	23.9546	3.65000	0.00000000	2750.000	2273.388	1722.212	0.0
0	23.9546	3.65000	0.00000000	2500.000	1865.350	1504.483	0.0
0	23.9546	3.65000	0.00000000	2250.000	1508.489	1282.816	0.0
0	23.9546	3.65000	0.00000000	2000.000	1179.329	971.407	0.0
0	23.9546	3.65000	0.00000000	1750.000	850.499	376.640	0.0
0	23.9546	3.65000	0.00000000	1500.000	481.928	-47.045	0.0
0	23.9546	3.65000	0.00000000	1250.000	-107.546	-374.798	0.0
0	23.9546	3.65000	0.00000000	1000.000	-1140.418	-665.160	0.0
0	23.9546	3.65000	0.00000000	750.000	-1678.112	-1068.465	0.0
0	23.9546	3.65000	0.00000000	500.000	-1951.667	-1254.869	0.0
1	23.9546	3.70000	1.85068707	4000.000	5466.944	4107.992	0.0
1	23.9546	3.70000	0.44377138	3750.000	4661.113	3252.642	0.0
0	23.9546	3.70000	0.00000000	3500.000	3955.331	2650.495	0.0
0	23.9546	3.70000	0.00000000	3250.000	3320.292	2269.176	0.0
0	23.9546	3.70000	0.00000000	3000.000	2760.109	1972.139	0.0
0	23.9546	3.70000	0.00000000	2750.000	2280.035	1727.658	0.0
0	23.9546	3.70000	0.00000000	2500.000	1871.249	1509.651	0.0
0	23.9546	3.70000	0.00000000	2250.000	1513.639	1287.667	0.0
0	23.9546	3.70000	0.00000000	2000.000	1183.758	975.573	0.0
0	23.9546	3.70000	0.00000000	1750.000	854.241	379.022	0.0
0	23.9546	3.70000	0.00000000	1500.000	484.791	-45.245	0.0
0	23.9546	3.70000	0.00000000	1250.000	-105.960	-373.327	0.0
0	23.9546	3.70000	0.00000000	1000.000	-1140.304	-663.508	0.0
0	23.9546	3.70000	0.00000000	750.000	-1678.628	-1066.640	0.0
0	23.9546	3.70000	0.00000000	500.000	-1952.199	-1253.133	0.0
1	23.9546	3.75000	1.86943862	4000.000	5473.819	4113.090	0.0
1	23.9546	3.75000	0.44566780	3750.000	4668.899	3258.232	0.0
0	23.9546	3.75000	0.00000000	3500.000	3963.333	2656.774	0.0
0	23.9546	3.75000	0.00000000	3250.000	3328.047	2275.079	0.0
0	23.9546	3.75000	0.00000000	3000.000	2767.320	1977.741	0.0

0	23.9546	3.75000	0.00000000	2750.000	2286.556	1732.987	0.0
0	23.9546	3.75000	0.00000000	2500.000	1877.035	1514.709	0.0
0	23.9546	3.75000	0.00000000	2250.000	1518.690	1292.414	0.0
0	23.9546	3.75000	0.00000000	2000.000	1188.102	979.646	0.0
0	23.9546	3.75000	0.00000000	1750.000	857.909	381.350	0.0
0	23.9546	3.75000	0.00000000	1500.000	487.600	-43.484	0.0
0	23.9546	3.75000	0.00000000	1250.000	-104.404	-371.885	0.0
0	23.9546	3.75000	0.00000000	1000.000	-1140.193	-661.895	0.0
0	23.9546	3.75000	0.00000000	750.000	-1679.134	-1064.854	0.0
0	23.9546	3.75000	0.00000000	500.000	-1952.718	-1251.433	0.0
1	23.9546	3.80000	1.88820436	4000.000	5480.552	4118.083	0.0
1	23.9546	3.80000	0.44757653	3750.000	4676.529	3263.711	0.0
0	23.9546	3.80000	0.00000000	3500.000	3971.178	2662.920	0.0
0	23.9546	3.80000	0.00000000	3250.000	3335.652	2280.856	0.0
0	23.9546	3.80000	0.00000000	3000.000	2774.394	1983.225	0.0
0	23.9546	3.80000	0.00000000	2750.000	2292.954	1738.205	0.0
0	23.9546	3.80000	0.00000000	2500.000	1882.712	1519.659	0.0
0	23.9546	3.80000	0.00000000	2250.000	1523.647	1297.060	0.0
0	23.9546	3.80000	0.00000000	2000.000	1192.363	983.629	0.0
0	23.9546	3.80000	0.00000000	1750.000	861.507	383.627	0.0
0	23.9546	3.80000	0.00000000	1500.000	490.354	-41.759	0.0
0	23.9546	3.80000	0.00000000	1250.000	-102.879	-370.472	0.0
0	23.9546	3.80000	0.00000000	1000.000	-1140.084	-660.320	0.0
0	23.9546	3.80000	0.00000000	750.000	-1679.630	-1063.105	0.0
0	23.9546	3.80000	0.00000000	500.000	-1953.226	-1249.768	0.0
1	23.9546	3.85000	1.90698398	4000.000	5487.148	4122.975	0.0
1	23.9546	3.85000	0.44949733	3750.000	4684.007	3269.081	0.0
0	23.9546	3.85000	0.00000000	3500.000	3978.871	2668.937	0.0
0	23.9546	3.85000	0.00000000	3250.000	3343.113	2286.514	0.0
0	23.9546	3.85000	0.00000000	3000.000	2781.334	1988.594	0.0
0	23.9546	3.85000	0.00000000	2750.000	2299.232	1743.313	0.0
0	23.9546	3.85000	0.00000000	2500.000	1888.284	1524.507	0.0
0	23.9546	3.85000	0.00000000	2250.000	1528.511	1301.608	0.0
0	23.9546	3.85000	0.00000000	2000.000	1196.544	987.525	0.0
0	23.9546	3.85000	0.00000000	1750.000	865.037	385.855	0.0
0	23.9546	3.85000	0.00000000	1500.000	493.055	-40.072	0.0
0	23.9546	3.85000	0.00000000	1250.000	-101.384	-369.087	0.0
0	23.9546	3.85000	0.00000000	1000.000	-1139.977	-658.781	0.0
0	23.9546	3.85000	0.00000000	750.000	-1680.117	-1061.393	0.0
0	23.9546	3.85000	0.00000000	500.000	-1953.723	-1248.136	0.0
1	23.9546	3.90000	1.92577715	4000.000	5493.611	4127.768	0.0
1	23.9546	3.90000	0.45142994	3750.000	4691.338	3274.347	0.0
0	23.9546	3.90000	0.00000000	3500.000	3986.416	2674.831	0.0
0	23.9546	3.90000	0.00000000	3250.000	3350.433	2292.054	0.0
0	23.9546	3.90000	0.00000000	3000.000	2788.145	1993.853	0.0
0	23.9546	3.90000	0.00000000	2750.000	2305.394	1748.316	0.0
0	23.9546	3.90000	0.00000000	2500.000	1893.752	1529.254	0.0
0	23.9546	3.90000	0.00000000	2250.000	1533.285	1306.061	0.0
0	23.9546	3.90000	0.00000000	2000.000	1200.647	991.336	0.0
0	23.9546	3.90000	0.00000000	1750.000	868.499	388.035	0.0
0	23.9546	3.90000	0.00000000	1500.000	495.705	-38.419	0.0
0	23.9546	3.90000	0.00000000	1250.000	-99.917	-367.730	0.0
0	23.9546	3.90000	0.00000000	1000.000	-1139.872	-657.276	0.0
0	23.9546	3.90000	0.00000000	750.000	-1680.594	-1059.716	0.0
0	23.9546	3.90000	0.00000000	500.000	-1954.208	-1246.537	0.0
1	23.9546	3.95000	1.94458358	4000.000	5499.945	4132.465	0.0

1	23.9546	3.95000	0.45337414	3750.000	4698.526	3279.511	0.0
0	23.9546	3.95000	0.00000000	3500.000	3993.817	2680.603	0.0
0	23.9546	3.95000	0.00000000	3250.000	3357.616	2297.482	0.0
0	23.9546	3.95000	0.00000000	3000.000	2794.830	1999.004	0.0
0	23.9546	3.95000	0.00000000	2750.000	2311.442	1753.217	0.0
0	23.9546	3.95000	0.00000000	2500.000	1899.121	1533.904	0.0
0	23.9546	3.95000	0.00000000	2250.000	1537.971	1310.422	0.0
0	23.9546	3.95000	0.00000000	2000.000	1204.674	995.066	0.0
0	23.9546	3.95000	0.00000000	1750.000	871.897	390.168	0.0
0	23.9546	3.95000	0.00000000	1500.000	498.306	-36.800	0.0
0	23.9546	3.95000	0.00000000	1250.000	-98.478	-366.400	0.0
0	23.9546	3.95000	0.00000000	1000.000	-1139.769	-655.804	0.0
0	23.9546	3.95000	0.00000000	750.000	-1681.063	-1058.074	0.0
0	23.9546	3.95000	0.00000000	500.000	-1954.683	-1244.970	0.0
1	23.9546	4.00000	1.96340297	4000.000	5506.153	4137.069	0.0
1	23.9546	4.00000	0.45532968	3750.000	4705.575	3284.576	0.0
0	23.9546	4.00000	0.00000000	3500.000	4001.079	2686.259	0.0
0	23.9546	4.00000	0.00000000	3250.000	3364.665	2302.799	0.0
0	23.9546	4.00000	0.00000000	3000.000	2801.393	2004.051	0.0
0	23.9546	4.00000	0.00000000	2750.000	2317.381	1758.019	0.0
0	23.9546	4.00000	0.00000000	2500.000	1904.391	1538.459	0.0
0	23.9546	4.00000	0.00000000	2250.000	1542.573	1314.694	0.0
0	23.9546	4.00000	0.00000000	2000.000	1208.626	998.717	0.0
0	23.9546	4.00000	0.00000000	1750.000	875.232	392.256	0.0
0	23.9546	4.00000	0.00000000	1500.000	500.858	-35.213	0.0
0	23.9546	4.00000	0.00000000	1250.000	-97.065	-365.095	0.0
0	23.9546	4.00000	0.00000000	1000.000	-1139.667	-654.365	0.0
0	23.9546	4.00000	0.00000000	750.000	-1681.522	-1056.464	0.0
0	23.9546	4.00000	0.00000000	500.000	-1955.148	-1243.434	0.0
1	23.9546	4.05000	1.98223505	4000.000	5512.239	4141.583	0.0
1	23.9546	4.05000	0.45729635	3750.000	4712.490	3289.544	0.0
0	23.9546	4.05000	0.00000000	3500.000	4008.205	2691.801	0.0
0	23.9546	4.05000	0.00000000	3250.000	3371.585	2308.010	0.0
0	23.9546	4.05000	0.00000000	3000.000	2807.837	2008.997	0.0
0	23.9546	4.05000	0.00000000	2750.000	2323.212	1762.724	0.0
0	23.9546	4.05000	0.00000000	2500.000	1909.567	1542.923	0.0
0	23.9546	4.05000	0.00000000	2250.000	1547.091	1318.879	0.0
0	23.9546	4.05000	0.00000000	2000.000	1212.507	1002.291	0.0
0	23.9546	4.05000	0.00000000	1750.000	878.506	394.300	0.0
0	23.9546	4.05000	0.00000000	1500.000	503.363	-33.659	0.0
0	23.9546	4.05000	0.00000000	1250.000	-95.679	-363.816	0.0
0	23.9546	4.05000	0.00000000	1000.000	-1139.568	-652.956	0.0
0	23.9546	4.05000	0.00000000	750.000	-1681.974	-1054.887	0.0
0	23.9546	4.05000	0.00000000	500.000	-1955.603	-1241.927	0.0
1	23.9546	4.10000	2.00107954	4000.000	5518.208	4146.009	0.0
1	23.9546	4.10000	0.45927392	3750.000	4719.274	3294.420	0.0
0	23.9546	4.10000	0.00000000	3500.000	4015.198	2697.234	0.0
0	23.9546	4.10000	0.00000000	3250.000	3378.379	2313.118	0.0
0	23.9546	4.10000	0.00000000	3000.000	2814.164	2013.846	0.0
0	23.9546	4.10000	0.00000000	2750.000	2328.939	1767.336	0.0
0	23.9546	4.10000	0.00000000	2500.000	1914.651	1547.299	0.0
0	23.9546	4.10000	0.00000000	2250.000	1551.529	1322.981	0.0
0	23.9546	4.10000	0.00000000	2000.000	1216.318	1005.791	0.0
0	23.9546	4.10000	0.00000000	1750.000	881.720	396.302	0.0
0	23.9546	4.10000	0.00000000	1500.000	505.823	-32.136	0.0
0	23.9546	4.10000	0.00000000	1250.000	-94.319	-362.561	0.0

0	23.9546	4.10000	0.00000000	1000.000	-1139.470	-651.577	0.0
0	23.9546	4.10000	0.00000000	750.000	-1682.416	-1053.341	0.0
0	23.9546	4.10000	0.00000000	500.000	-1956.049	-1240.450	0.0
1	23.9546	4.15000	2.01993616	4000.000	5524.061	4150.351	0.0
1	23.9546	4.15000	0.46126217	3750.000	4725.930	3299.204	0.0
0	23.9546	4.15000	0.00000000	3500.000	4022.064	2702.559	0.0
0	23.9546	4.15000	0.00000000	3250.000	3385.051	2318.126	0.0
0	23.9546	4.15000	0.00000000	3000.000	2820.379	2018.598	0.0
0	23.9546	4.15000	0.00000000	2750.000	2334.564	1771.858	0.0
0	23.9546	4.15000	0.00000000	2500.000	1919.645	1551.588	0.0
0	23.9546	4.15000	0.00000000	2250.000	1555.888	1327.002	0.0
0	23.9546	4.15000	0.00000000	2000.000	1220.061	1009.219	0.0
0	23.9546	4.15000	0.00000000	1750.000	884.876	398.264	0.0
0	23.9546	4.15000	0.00000000	1500.000	508.238	-30.643	0.0
0	23.9546	4.15000	0.00000000	1250.000	-92.983	-361.330	0.0
0	23.9546	4.15000	0.00000000	1000.000	-1139.374	-650.226	0.0
0	23.9546	4.15000	0.00000000	750.000	-1682.851	-1051.825	0.0
0	23.9546	4.15000	0.00000000	500.000	-1956.485	-1239.000	0.0
1	23.9546	4.20000	2.03880466	4000.000	5529.803	4154.609	0.0
1	23.9546	4.20000	0.46326089	3750.000	4732.463	3303.901	0.0
0	23.9546	4.20000	0.00000000	3500.000	4028.804	2707.781	0.0
0	23.9546	4.20000	0.00000000	3250.000	3391.603	2323.036	0.0
0	23.9546	4.20000	0.00000000	3000.000	2826.484	2023.259	0.0
0	23.9546	4.20000	0.00000000	2750.000	2340.090	1776.291	0.0
0	23.9546	4.20000	0.00000000	2500.000	1924.551	1555.794	0.0
0	23.9546	4.20000	0.00000000	2250.000	1560.171	1330.943	0.0
0	23.9546	4.20000	0.00000000	2000.000	1223.738	1012.577	0.0
0	23.9546	4.20000	0.00000000	1750.000	887.976	400.185	0.0
0	23.9546	4.20000	0.00000000	1500.000	510.610	-29.179	0.0
0	23.9546	4.20000	0.00000000	1250.000	-91.672	-360.122	0.0
0	23.9546	4.20000	0.00000000	1000.000	-1139.279	-648.903	0.0
0	23.9546	4.20000	0.00000000	750.000	-1683.278	-1050.338	0.0
0	23.9546	4.20000	0.00000000	500.000	-1956.912	-1237.579	0.0
1	23.9546	4.25000	2.05768478	4000.000	5535.437	4158.788	0.0
1	23.9546	4.25000	0.46526988	3750.000	4738.875	3308.511	0.0
0	23.9546	4.25000	0.00000000	3500.000	4035.423	2712.902	0.0
0	23.9546	4.25000	0.00000000	3250.000	3398.040	2327.851	0.0
0	23.9546	4.25000	0.00000000	3000.000	2832.481	2027.830	0.0
0	23.9546	4.25000	0.00000000	2750.000	2345.521	1780.640	0.0
0	23.9546	4.25000	0.00000000	2500.000	1929.372	1559.918	0.0
0	23.9546	4.25000	0.00000000	2250.000	1564.380	1334.808	0.0
0	23.9546	4.25000	0.00000000	2000.000	1227.350	1015.867	0.0
0	23.9546	4.25000	0.00000000	1750.000	891.020	402.068	0.0
0	23.9546	4.25000	0.00000000	1500.000	512.940	-27.743	0.0
0	23.9546	4.25000	0.00000000	1250.000	-90.383	-358.936	0.0
0	23.9546	4.25000	0.00000000	1000.000	-1139.186	-647.607	0.0
0	23.9546	4.25000	0.00000000	750.000	-1683.698	-1048.880	0.0
0	23.9546	4.25000	0.00000000	500.000	-1957.331	-1236.183	0.0
1	23.9546	4.30000	2.07657628	4000.000	5540.966	4162.888	0.0
1	23.9546	4.30000	0.46728893	3750.000	4745.171	3313.038	0.0
0	23.9546	4.30000	0.00000000	3500.000	4041.924	2717.925	0.0
0	23.9546	4.30000	0.00000000	3250.000	3404.363	2332.575	0.0
0	23.9546	4.30000	0.00000000	3000.000	2838.375	2032.313	0.0
0	23.9546	4.30000	0.00000000	2750.000	2350.857	1784.905	0.0
0	23.9546	4.30000	0.00000000	2500.000	1934.110	1563.964	0.0
0	23.9546	4.30000	0.00000000	2250.000	1568.516	1338.598	0.0

0	23.9546	4.30000	0.00000000	2000.000	1230.900	1019.092	0.0
0	23.9546	4.30000	0.00000000	1750.000	894.012	403.913	0.0
0	23.9546	4.30000	0.00000000	1500.000	515.229	-26.335	0.0
0	23.9546	4.30000	0.00000000	1250.000	-89.118	-357.773	0.0
0	23.9546	4.30000	0.00000000	1000.000	-1139.095	-646.337	0.0
0	23.9546	4.30000	0.00000000	750.000	-1684.110	-1047.450	0.0
0	23.9546	4.30000	0.00000000	500.000	-1957.741	-1234.814	0.0
1	23.9546	4.35000	2.09547891	4000.000	5546.392	4166.912	0.0
1	23.9546	4.35000	0.46931785	3750.000	4751.352	3317.483	0.0
0	23.9546	4.35000	0.00000000	3500.000	4048.310	2722.853	0.0
0	23.9546	4.35000	0.00000000	3250.000	3410.576	2337.209	0.0
0	23.9546	4.35000	0.00000000	3000.000	2844.167	2036.712	0.0
0	23.9546	4.35000	0.00000000	2750.000	2356.102	1789.089	0.0
0	23.9546	4.35000	0.00000000	2500.000	1938.767	1567.932	0.0
0	23.9546	4.35000	0.00000000	2250.000	1572.581	1342.316	0.0
0	23.9546	4.35000	0.00000000	2000.000	1234.388	1022.253	0.0
0	23.9546	4.35000	0.00000000	1750.000	896.951	405.722	0.0
0	23.9546	4.35000	0.00000000	1500.000	517.478	-24.954	0.0
0	23.9546	4.35000	0.00000000	1250.000	-87.875	-356.630	0.0
0	23.9546	4.35000	0.00000000	1000.000	-1139.005	-645.091	0.0
0	23.9546	4.35000	0.00000000	750.000	-1684.515	-1046.047	0.0
0	23.9546	4.35000	0.00000000	500.000	-1958.143	-1233.470	0.0
1	23.9546	4.40000	2.11439244	4000.000	5551.718	4170.863	0.0
1	23.9546	4.40000	0.47135645	3750.000	4757.423	3321.849	0.0
0	23.9546	4.40000	0.00000000	3500.000	4054.584	2727.689	0.0
0	23.9546	4.40000	0.00000000	3250.000	3416.681	2341.757	0.0
0	23.9546	4.40000	0.00000000	3000.000	2849.860	2041.029	0.0
0	23.9546	4.40000	0.00000000	2750.000	2361.258	1793.195	0.0
0	23.9546	4.40000	0.00000000	2500.000	1943.345	1571.827	0.0
0	23.9546	4.40000	0.00000000	2250.000	1576.577	1345.964	0.0
0	23.9546	4.40000	0.00000000	2000.000	1237.816	1025.352	0.0
0	23.9546	4.40000	0.00000000	1750.000	899.839	407.496	0.0
0	23.9546	4.40000	0.00000000	1500.000	519.688	-23.598	0.0
0	23.9546	4.40000	0.00000000	1250.000	-86.654	-355.509	0.0
0	23.9546	4.40000	0.00000000	1000.000	-1138.917	-643.870	0.0
0	23.9546	4.40000	0.00000000	750.000	-1684.913	-1044.670	0.0
0	23.9546	4.40000	0.00000000	500.000	-1958.537	-1232.151	0.0
1	23.9546	4.45000	2.13331665	4000.000	5556.948	4174.742	0.0
1	23.9546	4.45000	0.47340455	3750.000	4763.386	3326.139	0.0
0	23.9546	4.45000	0.00000000	3500.000	4060.748	2732.435	0.0
0	23.9546	4.45000	0.00000000	3250.000	3422.683	2346.220	0.0
0	23.9546	4.45000	0.00000000	3000.000	2855.456	2045.265	0.0
0	23.9546	4.45000	0.00000000	2750.000	2366.327	1797.225	0.0
0	23.9546	4.45000	0.00000000	2500.000	1947.846	1575.649	0.0
0	23.9546	4.45000	0.00000000	2250.000	1580.507	1349.544	0.0
0	23.9546	4.45000	0.00000000	2000.000	1241.187	1028.391	0.0
0	23.9546	4.45000	0.00000000	1750.000	902.678	409.235	0.0
0	23.9546	4.45000	0.00000000	1500.000	521.860	-22.268	0.0
0	23.9546	4.45000	0.00000000	1250.000	-85.454	-354.408	0.0
0	23.9546	4.45000	0.00000000	1000.000	-1138.830	-642.673	0.0
0	23.9546	4.45000	0.00000000	750.000	-1685.304	-1043.318	0.0
0	23.9546	4.45000	0.00000000	500.000	-1958.923	-1230.855	0.0
1	23.9546	4.50000	2.15225131	4000.000	5562.083	4178.551	0.0
1	23.9546	4.50000	0.47546195	3750.000	4769.244	3330.353	0.0
0	23.9546	4.50000	0.00000000	3500.000	4066.806	2737.094	0.0
0	23.9546	4.50000	0.00000000	3250.000	3428.582	2350.601	0.0

0	23.9546	4.50000	0.00000000	3000.000	2860.959	2049.424	0.0
0	23.9546	4.50000	0.00000000	2750.000	2371.311	1801.181	0.0
0	23.9546	4.50000	0.00000000	2500.000	1952.272	1579.401	0.0
0	23.9546	4.50000	0.00000000	2250.000	1584.370	1353.057	0.0
0	23.9546	4.50000	0.00000000	2000.000	1244.500	1031.371	0.0
0	23.9546	4.50000	0.00000000	1750.000	905.468	410.941	0.0
0	23.9546	4.50000	0.00000000	1500.000	523.995	-20.962	0.0
0	23.9546	4.50000	0.00000000	1250.000	-84.274	-353.326	0.0
0	23.9546	4.50000	0.00000000	1000.000	-1138.745	-641.498	0.0
0	23.9546	4.50000	0.00000000	750.000	-1685.688	-1041.991	0.0
0	23.9546	4.50000	0.00000000	500.000	-1959.302	-1229.582	0.0
1	23.9546	4.55000	2.17119620	4000.000	5567.127	4182.292	0.0
1	23.9546	4.55000	0.47752848	3750.000	4775.000	3334.494	0.0
0	23.9546	4.55000	0.00000000	3500.000	4072.761	2741.667	0.0
0	23.9546	4.55000	0.00000000	3250.000	3434.382	2354.902	0.0
0	23.9546	4.55000	0.00000000	3000.000	2866.370	2053.507	0.0
0	23.9546	4.55000	0.00000000	2750.000	2376.212	1805.065	0.0
0	23.9546	4.55000	0.00000000	2500.000	1956.625	1583.084	0.0
0	23.9546	4.55000	0.00000000	2250.000	1588.170	1356.506	0.0
0	23.9546	4.55000	0.00000000	2000.000	1247.759	1034.295	0.0
0	23.9546	4.55000	0.00000000	1750.000	908.212	412.614	0.0
0	23.9546	4.55000	0.00000000	1500.000	526.094	-19.681	0.0
0	23.9546	4.55000	0.00000000	1250.000	-83.114	-352.264	0.0
0	23.9546	4.55000	0.00000000	1000.000	-1138.661	-640.345	0.0
0	23.9546	4.55000	0.00000000	750.000	-1686.066	-1040.689	0.0
0	23.9546	4.55000	0.00000000	500.000	-1959.673	-1228.333	0.0
1	23.9546	4.60000	2.19015112	4000.000	5572.082	4185.967	0.0
1	23.9546	4.60000	0.47960397	3750.000	4780.656	3338.564	0.0
0	23.9546	4.60000	0.00000000	3500.000	4078.615	2746.158	0.0
0	23.9546	4.60000	0.00000000	3250.000	3440.085	2359.126	0.0
0	23.9546	4.60000	0.00000000	3000.000	2871.691	2057.516	0.0
0	23.9546	4.60000	0.00000000	2750.000	2381.033	1808.878	0.0
0	23.9546	4.60000	0.00000000	2500.000	1960.907	1586.700	0.0
0	23.9546	4.60000	0.00000000	2250.000	1591.908	1359.892	0.0
0	23.9546	4.60000	0.00000000	2000.000	1250.963	1037.163	0.0
0	23.9546	4.60000	0.00000000	1750.000	910.909	414.256	0.0
0	23.9546	4.60000	0.00000000	1500.000	528.158	-18.422	0.0
0	23.9546	4.60000	0.00000000	1250.000	-81.974	-351.220	0.0
0	23.9546	4.60000	0.00000000	1000.000	-1138.579	-639.214	0.0
0	23.9546	4.60000	0.00000000	750.000	-1686.437	-1039.409	0.0
0	23.9546	4.60000	0.00000000	500.000	-1960.038	-1227.105	0.0
1	23.9546	4.65000	2.20911587	4000.000	5576.949	4189.577	0.0
1	23.9546	4.65000	0.48168825	3750.000	4786.215	3342.564	0.0
0	23.9546	4.65000	0.00000000	3500.000	4084.370	2750.568	0.0
0	23.9546	4.65000	0.00000000	3250.000	3445.694	2363.274	0.0
0	23.9546	4.65000	0.00000000	3000.000	2876.926	2061.453	0.0
0	23.9546	4.65000	0.00000000	2750.000	2385.776	1812.624	0.0
0	23.9546	4.65000	0.00000000	2500.000	1965.118	1590.252	0.0
0	23.9546	4.65000	0.00000000	2250.000	1595.584	1363.217	0.0
0	23.9546	4.65000	0.00000000	2000.000	1254.115	1039.978	0.0
0	23.9546	4.65000	0.00000000	1750.000	913.562	415.868	0.0
0	23.9546	4.65000	0.00000000	1500.000	530.188	-17.187	0.0
0	23.9546	4.65000	0.00000000	1250.000	-80.853	-350.195	0.0
0	23.9546	4.65000	0.00000000	1000.000	-1138.498	-638.103	0.0
0	23.9546	4.65000	0.00000000	750.000	-1686.803	-1038.153	0.0
0	23.9546	4.65000	0.00000000	500.000	-1960.395	-1225.898	0.0

1	23.9546	4.70000	2.22809024	4000.000	5581.732	4193.124	0.0
1	23.9546	4.70000	0.48378115	3750.000	4791.680	3346.497	0.0
0	23.9546	4.70000	0.00000000	3500.000	4090.029	2754.900	0.0
0	23.9546	4.70000	0.00000000	3250.000	3451.211	2367.348	0.0
0	23.9546	4.70000	0.00000000	3000.000	2882.075	2065.321	0.0
0	23.9546	4.70000	0.00000000	2750.000	2390.442	1816.303	0.0
0	23.9546	4.70000	0.00000000	2500.000	1969.262	1593.741	0.0
0	23.9546	4.70000	0.00000000	2250.000	1599.202	1366.482	0.0
0	23.9546	4.70000	0.00000000	2000.000	1257.216	1042.741	0.0
0	23.9546	4.70000	0.00000000	1750.000	916.172	417.450	0.0
0	23.9546	4.70000	0.00000000	1500.000	532.184	-15.973	0.0
0	23.9546	4.70000	0.00000000	1250.000	-79.751	-349.187	0.0
0	23.9546	4.70000	0.00000000	1000.000	-1138.418	-637.013	0.0
0	23.9546	4.70000	0.00000000	750.000	-1687.162	-1036.919	0.0
0	23.9546	4.70000	0.00000000	500.000	-1960.746	-1224.713	0.0
1	23.9546	4.75000	2.24707404	4000.000	5586.433	4196.611	0.0
1	23.9546	4.75000	0.48588251	3750.000	4797.052	3350.364	0.0
0	23.9546	4.75000	0.00000000	3500.000	4095.595	2759.156	0.0
0	23.9546	4.75000	0.00000000	3250.000	3456.638	2371.351	0.0
0	23.9546	4.75000	0.00000000	3000.000	2887.141	2069.121	0.0
0	23.9546	4.75000	0.00000000	2750.000	2395.033	1819.917	0.0
0	23.9546	4.75000	0.00000000	2500.000	1973.340	1597.168	0.0
0	23.9546	4.75000	0.00000000	2250.000	1602.761	1369.689	0.0
0	23.9546	4.75000	0.00000000	2000.000	1260.267	1045.452	0.0
0	23.9546	4.75000	0.00000000	1750.000	918.739	419.002	0.0
0	23.9546	4.75000	0.00000000	1500.000	534.148	-14.781	0.0
0	23.9546	4.75000	0.00000000	1250.000	-78.666	-348.196	0.0
0	23.9546	4.75000	0.00000000	1000.000	-1138.339	-635.942	0.0
0	23.9546	4.75000	0.00000000	750.000	-1687.516	-1035.706	0.0
0	23.9546	4.75000	0.00000000	500.000	-1961.091	-1223.547	0.0
1	23.9546	4.80000	2.26606708	4000.000	5591.053	4200.038	0.0
1	23.9546	4.80000	0.48799217	3750.000	4802.335	3354.166	0.0
0	23.9546	4.80000	0.00000000	3500.000	4101.069	2763.338	0.0
0	23.9546	4.80000	0.00000000	3250.000	3461.977	2375.284	0.0
0	23.9546	4.80000	0.00000000	3000.000	2892.126	2072.854	0.0
0	23.9546	4.80000	0.00000000	2750.000	2399.550	1823.468	0.0
0	23.9546	4.80000	0.00000000	2500.000	1977.353	1600.535	0.0
0	23.9546	4.80000	0.00000000	2250.000	1606.264	1372.840	0.0
0	23.9546	4.80000	0.00000000	2000.000	1263.269	1048.115	0.0
0	23.9546	4.80000	0.00000000	1750.000	921.264	420.527	0.0
0	23.9546	4.80000	0.00000000	1500.000	536.080	-13.609	0.0
0	23.9546	4.80000	0.00000000	1250.000	-77.600	-347.223	0.0
0	23.9546	4.80000	0.00000000	1000.000	-1138.262	-634.891	0.0
0	23.9546	4.80000	0.00000000	750.000	-1687.864	-1034.514	0.0
0	23.9546	4.80000	0.00000000	500.000	-1961.429	-1222.402	0.0
1	23.9546	4.85000	2.28506917	4000.000	5595.595	4203.406	0.0
1	23.9546	4.85000	0.49010998	3750.000	4807.530	3357.906	0.0
0	23.9546	4.85000	0.00000000	3500.000	4106.454	2767.447	0.0
0	23.9546	4.85000	0.00000000	3250.000	3467.230	2379.149	0.0
0	23.9546	4.85000	0.00000000	3000.000	2897.032	2076.523	0.0
0	23.9546	4.85000	0.00000000	2750.000	2403.997	1826.958	0.0
0	23.9546	4.85000	0.00000000	2500.000	1981.302	1603.844	0.0
0	23.9546	4.85000	0.00000000	2250.000	1609.711	1375.937	0.0
0	23.9546	4.85000	0.00000000	2000.000	1266.223	1050.729	0.0
0	23.9546	4.85000	0.00000000	1750.000	923.749	422.024	0.0
0	23.9546	4.85000	0.00000000	1500.000	537.981	-12.458	0.0

0	23.9546	4.85000	0.00000000	1250.000	-76.550	-346.265	0.0
0	23.9546	4.85000	0.00000000	1000.000	-1138.186	-633.858	0.0
0	23.9546	4.85000	0.00000000	750.000	-1688.206	-1033.343	0.0
0	23.9546	4.85000	0.00000000	500.000	-1961.761	-1221.276	0.0
1	23.9546	4.90000	2.30408015	4000.000	5600.060	4206.718	0.0
1	23.9546	4.90000	0.49223579	3750.000	4812.639	3361.584	0.0
0	23.9546	4.90000	0.00000000	3500.000	4111.752	2771.485	0.0
0	23.9546	4.90000	0.00000000	3250.000	3472.400	2382.947	0.0
0	23.9546	4.90000	0.00000000	3000.000	2901.860	2080.129	0.0
0	23.9546	4.90000	0.00000000	2750.000	2408.374	1830.388	0.0
0	23.9546	4.90000	0.00000000	2500.000	1985.190	1607.096	0.0
0	23.9546	4.90000	0.00000000	2250.000	1613.105	1378.979	0.0
0	23.9546	4.90000	0.00000000	2000.000	1269.130	1053.297	0.0
0	23.9546	4.90000	0.00000000	1750.000	926.194	423.494	0.0
0	23.9546	4.90000	0.00000000	1500.000	539.852	-11.327	0.0
0	23.9546	4.90000	0.00000000	1250.000	-75.517	-345.324	0.0
0	23.9546	4.90000	0.00000000	1000.000	-1138.111	-632.843	0.0
0	23.9546	4.90000	0.00000000	750.000	-1688.543	-1032.192	0.0
0	23.9546	4.90000	0.00000000	500.000	-1962.087	-1220.169	0.0
1	23.9546	4.95000	2.32309983	4000.000	5604.451	4209.975	0.0
1	23.9546	4.95000	0.49436945	3750.000	4817.665	3365.203	0.0
0	23.9546	4.95000	0.00000000	3500.000	4116.966	2775.455	0.0
0	23.9546	4.95000	0.00000000	3250.000	3477.489	2386.682	0.0
0	23.9546	4.95000	0.00000000	3000.000	2906.614	2083.674	0.0
0	23.9546	4.95000	0.00000000	2750.000	2412.682	1833.760	0.0
0	23.9546	4.95000	0.00000000	2500.000	1989.017	1610.293	0.0
0	23.9546	4.95000	0.00000000	2250.000	1616.446	1381.970	0.0
0	23.9546	4.95000	0.00000000	2000.000	1271.993	1055.819	0.0
0	23.9546	4.95000	0.00000000	1750.000	928.601	424.938	0.0
0	23.9546	4.95000	0.00000000	1500.000	541.693	-10.215	0.0
0	23.9546	4.95000	0.00000000	1250.000	-74.501	-344.399	0.0
0	23.9546	4.95000	0.00000000	1000.000	-1138.037	-631.846	0.0
0	23.9546	4.95000	0.00000000	750.000	-1688.875	-1031.060	0.0
0	23.9546	4.95000	0.00000000	500.000	-1962.407	-1219.080	0.0
1	23.9546	5.00000	2.34212804	4000.000	5608.769	4213.178	0.0
1	23.9546	5.00000	0.49651082	3750.000	4822.610	3368.764	0.0
0	23.9546	5.00000	0.00000000	3500.000	4122.097	2779.358	0.0
0	23.9546	5.00000	0.00000000	3250.000	3482.498	2390.353	0.0
0	23.9546	5.00000	0.00000000	3000.000	2911.293	2087.159	0.0
0	23.9546	5.00000	0.00000000	2750.000	2416.924	1837.074	0.0
0	23.9546	5.00000	0.00000000	2500.000	1992.786	1613.436	0.0
0	23.9546	5.00000	0.00000000	2250.000	1619.736	1384.910	0.0
0	23.9546	5.00000	0.00000000	2000.000	1274.810	1058.297	0.0
0	23.9546	5.00000	0.00000000	1750.000	930.970	426.357	0.0
0	23.9546	5.00000	0.00000000	1500.000	543.505	-9.122	0.0
0	23.9546	5.00000	0.00000000	1250.000	-73.501	-343.488	0.0
0	23.9546	5.00000	0.00000000	1000.000	-1137.964	-630.866	0.0
0	23.9546	5.00000	0.00000000	750.000	-1689.201	-1029.948	0.0

*

END

APPENDIX B: PHSM VS ITRAC AT EACH STATION

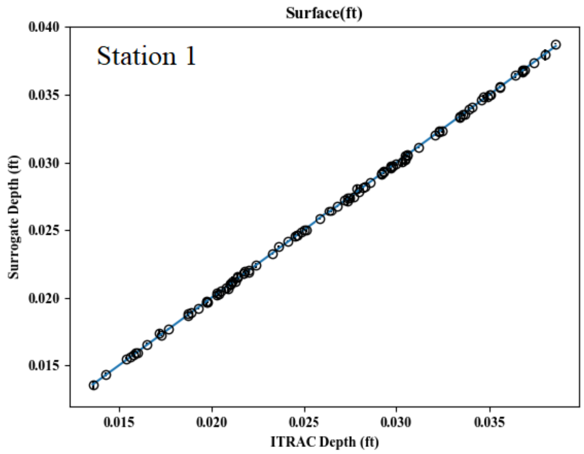

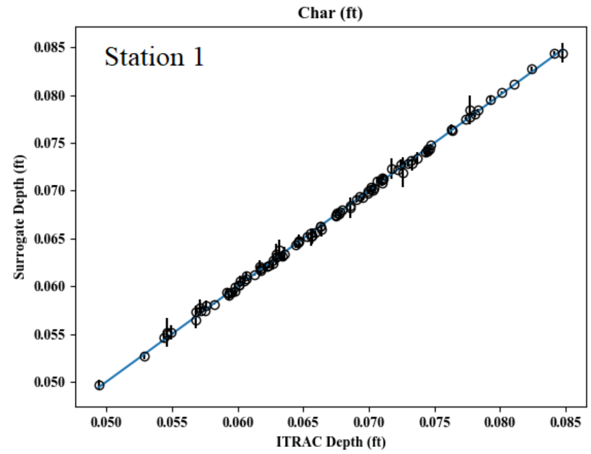

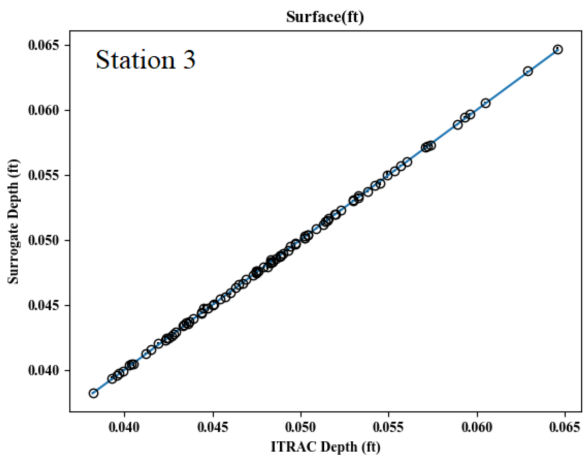

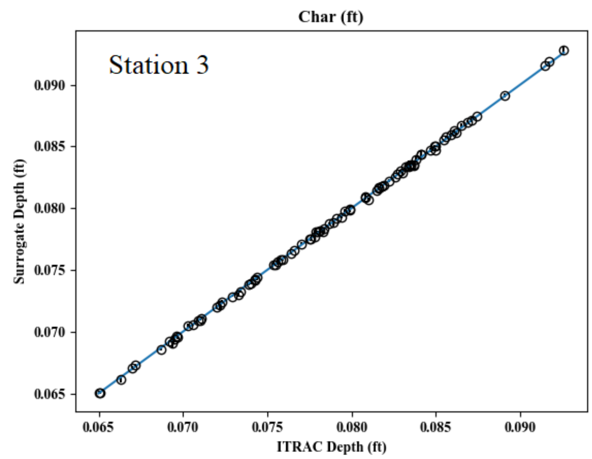

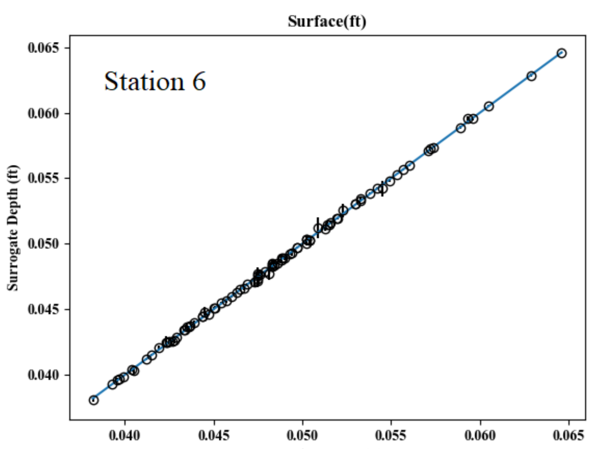

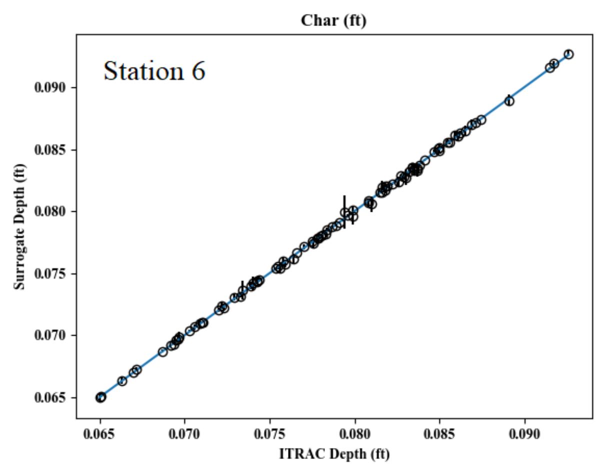

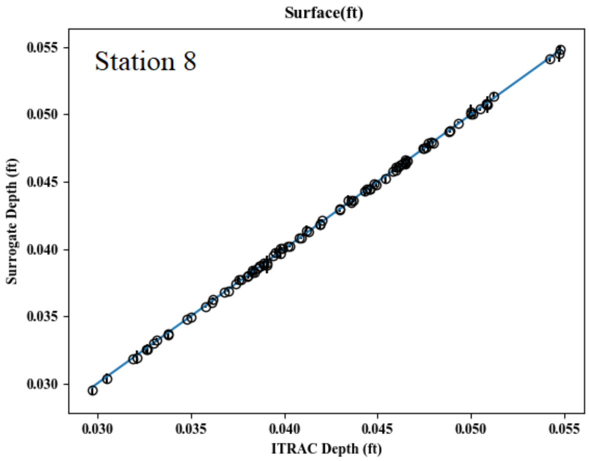
Surface(ft)
Station 8
Surrogate Depth (ft)
0.055
0.050
0.045
0.040
0.035
0.030
0.030 0.035 0.040 0.045 0.050 0.055
ITRAC Depth (ft)

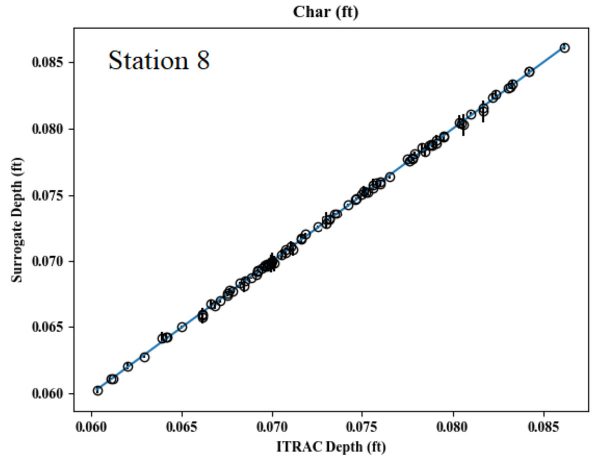
Char (ft)
Station 8
Surrogate Depth (ft)
0.085
0.080
0.075
0.070
0.065
0.060
0.060 0.065 0.070 0.075 0.080 0.085
ITRAC Depth (ft)

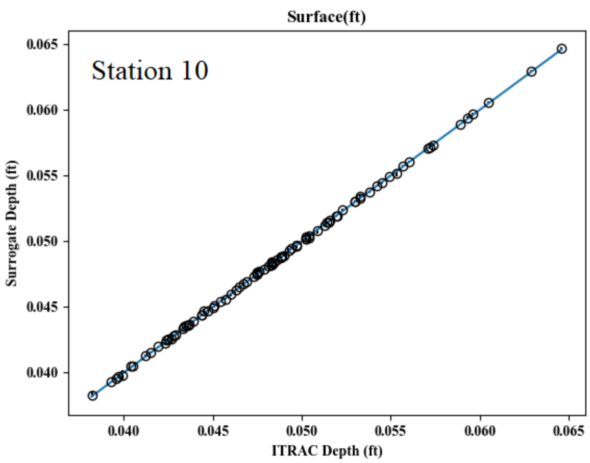
Surface(ft)
Station 10
Surrogate Depth (ft)
0.065
0.060
0.055
0.050
0.045
0.040
0.040 0.045 0.050 0.055 0.060 0.065
ITRAC Depth (ft)

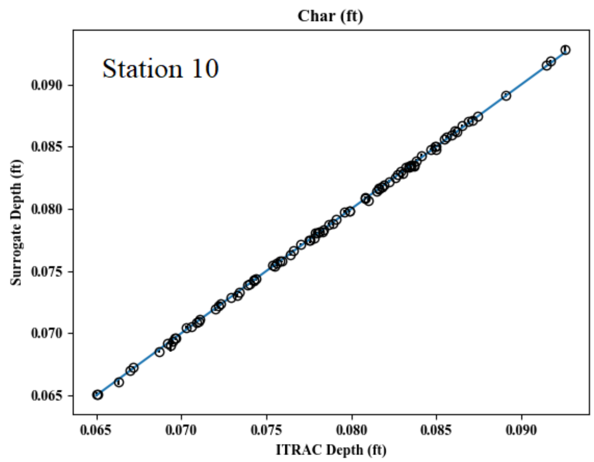
Char (ft)
Station 10
Surrogate Depth (ft)
0.090
0.085
0.080
0.075
0.070
0.065
0.065 0.070 0.075 0.080 0.085 0.090
ITRAC Depth (ft)

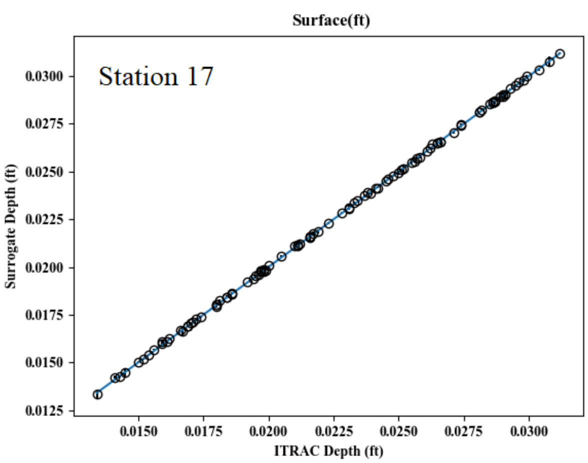
Surface(ft)
Station 17
Surrogate Depth (ft)
0.0300
0.0275
0.0250
0.0225
0.0200
0.0175
0.0150
0.0125
0.0150 0.0175 0.0200 0.0225 0.0250 0.0275 0.0300
ITRAC Depth (ft)

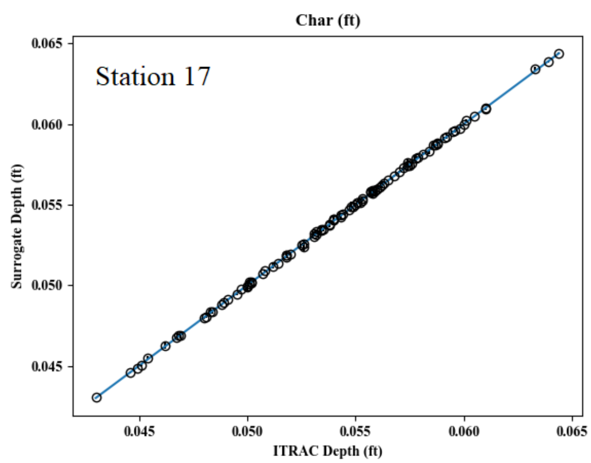
Char (ft)
Station 17
Surrogate Depth (ft)
0.065
0.060
0.055
0.050
0.045
0.045 0.050 0.055 0.060 0.065
ITRAC Depth (ft)

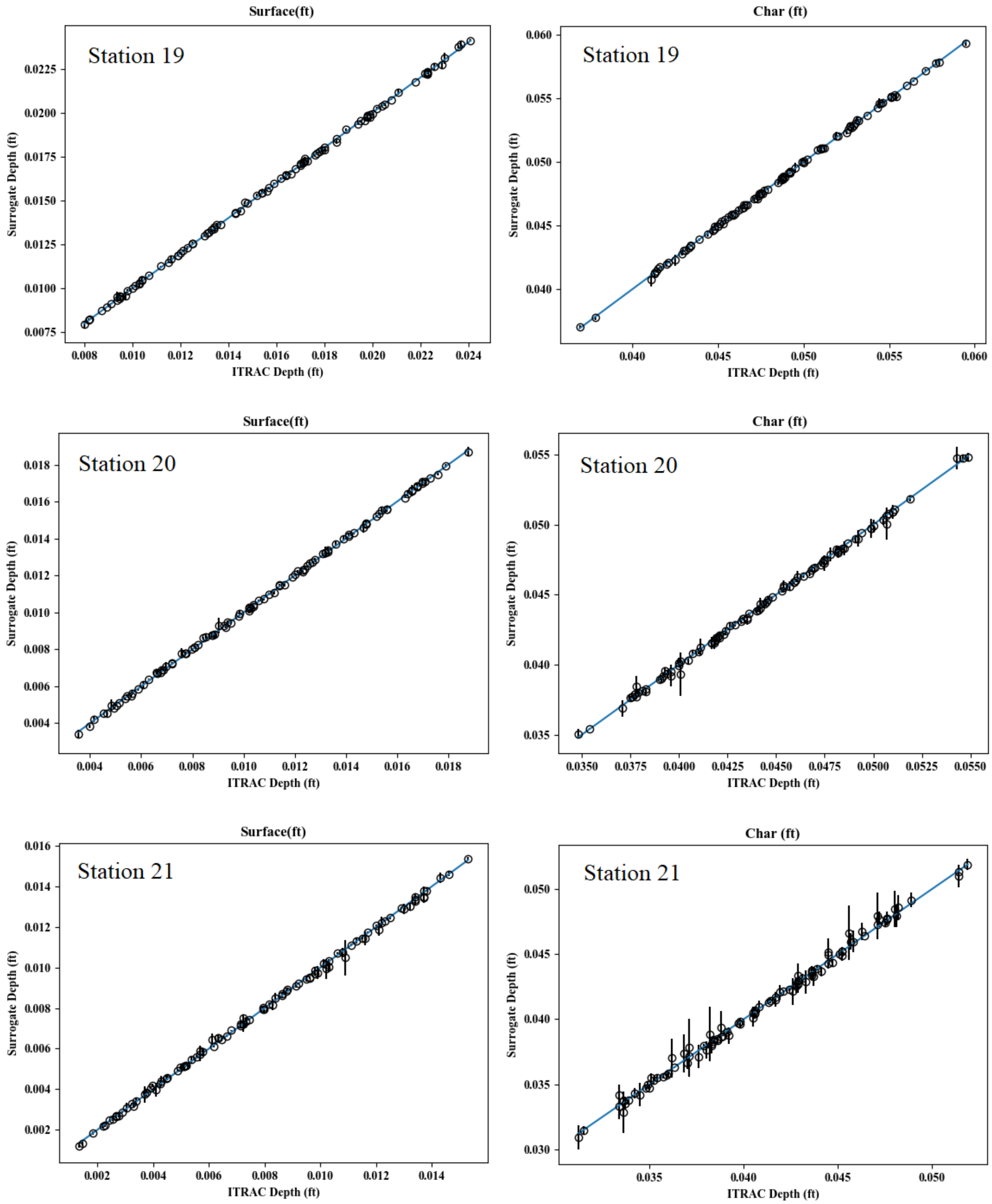
Surface(ft)
Station 19
Surrogate Depth (ft)
ITRAC Depth (ft)
Char (ft)
Station 19
Surrogate Depth (ft)
ITRAC Depth (ft)
Surface(ft)
Station 20
Surrogate Depth (ft)
ITRAC Depth (ft)
Char (ft)
Station 20
Surrogate Depth (ft)
ITRAC Depth (ft)
Surface(ft)
Station 21
Surrogate Depth (ft)
ITRAC Depth (ft)
Char (ft)
Station 21
Surrogate Depth (ft)
ITRAC Depth (ft)

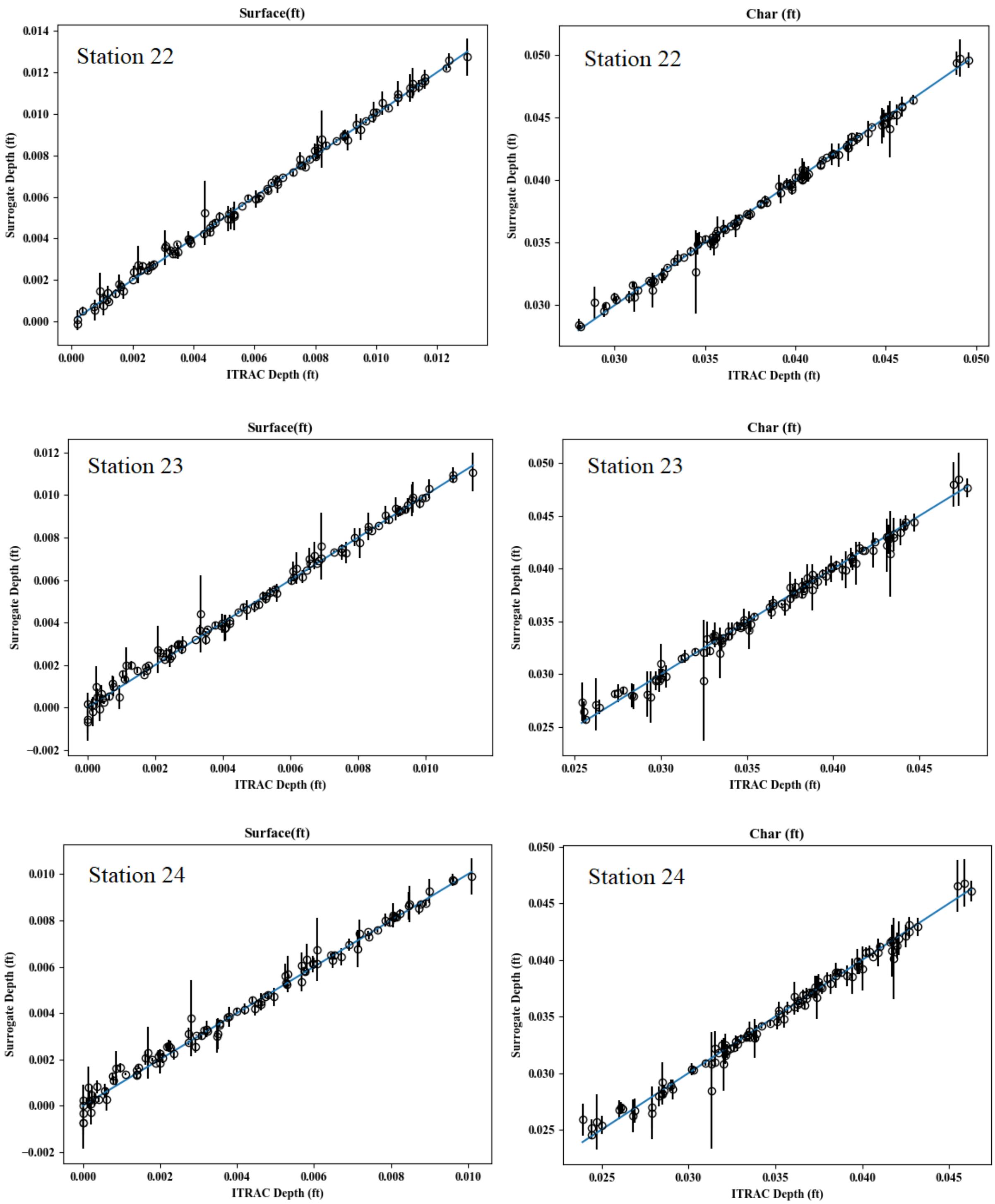
Surface(ft)
Station 22
Surrogate Depth (ft)
ITRAC Depth (ft)
Char (ft)
Station 22
Surrogate Depth (ft)
ITRAC Depth (ft)
Surface(ft)
Station 23
Surrogate Depth (ft)
ITRAC Depth (ft)
Char (ft)
Station 23
Surrogate Depth (ft)
ITRAC Depth (ft)
Surface(ft)
Station 24
Surrogate Depth (ft)
ITRAC Depth (ft)
Char (ft)
Station 24
Surrogate Depth (ft)
ITRAC Depth (ft)

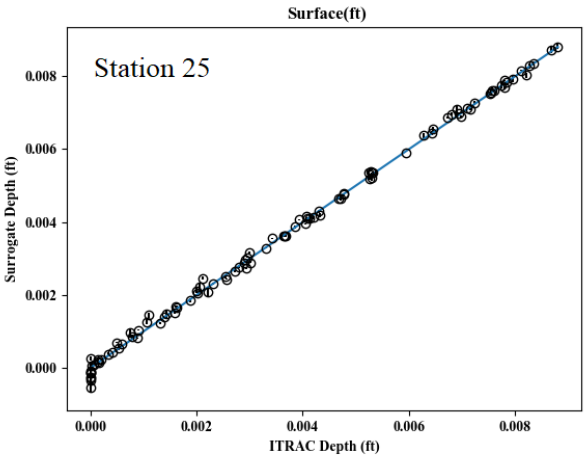
Surface(ft)
Station 25
Surrogate Depth (ft)
ITRAC Depth (ft)
0.000
0.002
0.004
0.006
0.008

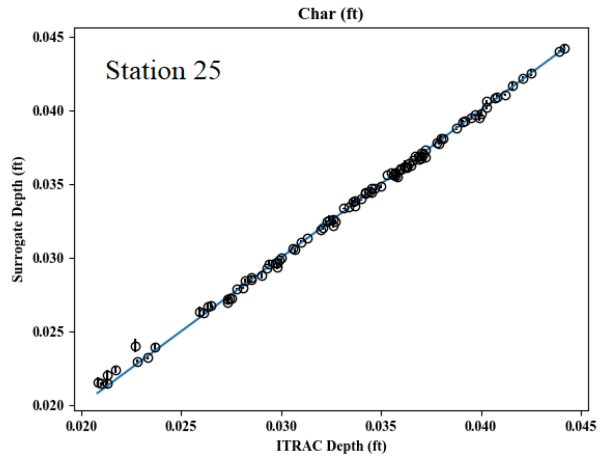
Char (ft)
Station 25
Surrogate Depth (ft)
ITRAC Depth (ft)
0.020
0.025
0.030
0.035
0.040
0.045

REFERENCES

[1] S. Clark, “Spaceflight Now,” 20 09 2022. [Online]. Available: https://spaceflightnow.com/2022/07/06/worlds-rockets-on-pace-for-record-year-of-launch-activity/#:~:text=Last%20year%2C%20the%20world%27s%20launch,was%20129%2C%20set%20in%201984..

[2] B. E. Goldberg, K. Everhart, R. Stevens, N. Babbitt III, P. Clemens, and L. Stout, “System Engineering Toolbox for Design-Oriented Engineers,” NASA Reference Publication 1358, Marshall Space Flight Center, 1994.

[3] L. G. Crespo, S. P. Kenny, and D. P. Giesy, “The NASA Langley Multidisciplinary Uncertainty Quantification Challenge,” AIAA 2014-1347, NASA Multidisciplinary UQ Challenge I, AIAA, 2014.

[4] L. G. Crespo, S. P. Kenny, and D. P. Giesy, “The NASA Langley Challenge on Optimization Under Uncertainty,” 30th European Safety and Reliability Conference and the 15th Probabilistic Safety Assessment and Management Conference, ESREL2020, Research Publishing, 2020.

[5] N. N. Mansour, J. L. Pittman and L. E. Olson, “Fundamental Aeronautics Hypersonics Project: Overview,” in *39th AIAA Thermophysics Conference*, Miami, 2007.

[6] M. E. Ewing, B. C. Liechty and D. L. Black, “A General Methodology for Uncertainty Quantification in Engineering Analyses Using a Credible Probability Box,” *Journal of Verification, Validation and Uncertainty Quantification*, 2018.

[7] M. Rivier, J. Lachaud and P. M. Congedo, “Ablative Thermal Protection System Under Uncertainties: Effect of Pyrolysis Gas Composition,” HAL Open Science, Talence Cedex, 2019.

[8] S. R. Copeland, M. Mahzari, I. Cozmuta and J. J. Alonso, “A Statistics-Based Material Property Analysis to Support Ablation Simulation UQ Efforts,” in *53rd AIAA/ASME/ASCE/AHS/ASC Structures, Structural Dynamics and Materials Conference*, Honolulu, 2012.

[9] D. Bose, M. Wrigth and T. Gokcen, “Uncertainty and Sensitivity Analysis of Thermochemical Modeling for Titan Atmospheric Entry,” in *37th AIAA Thermophysics Conference*, Portland, 2004.

[10] D. Bose, M. J. Wright and G. E. Palmer, “Uncertainty Analysis of Laminar Aeroheating Predictions for Mars Entries,” *Journal of Thermophysics and Heat Transfer,* pp. 652-662, 2006.

[11] Y. K. Chen, T. Squire, B. Laub and M. Wright, “Monte Carlo Analysis for Spacecraft Thermal Protection System Design,” in *9th AIAA/ASME Joint Thermophysics and Heat Transfer Conference,* San Fransisco, 2006.

[12] W. Xie, Y. Yang, M. Songhe, T. Peng, J. Yuan, F. Scarpa, C. Xu and H. Jin, “Probabilistic Reliability Analysis of Carbon/Carbon Composite Nozzle Cones with Uncertain Paramters,” *Journal of Spacecraft and Rockets,* pp. Vol. 56, No. 6, 2019.

[13] I. Sobol, “Global Sensitivity Indices for Nonlinear Mathematical Models and their Monte Carlo Estimates,” *Mathematics and Computers in Simulation,* pp. 271-280, 2001.

[14] J. M. Lyon, “Introduction to Rocket Propulsion, RD-PR-91-17,” U.S. Army Missile Command, Redstone Arsenal, 1991.

[15] W. C. Andrepont and R. M. Felix, “The History of Large Solid Rocket Motor Development in the United States,” in *30th AIAA/ASME/SAEYASEE Joint Propulsion Conference*, Indianapolis, 1994.

[16] Evans, P. R., “Composite Motor Case Design,” in *Desing Methods in Solid Rocket Motors,* AGARD Lecture Series No. 150, pp. 4A1-4A11, Specialised Printing Services Limited, Loughton, 1988.

[17] G. P. Sutton, Rocket Propulsion Elements, 7th Edition, New York: John Wiley & Sons, Inc, 2001.

[18] Northrop Grumman , “Northrop Grumman News Room,” 2015 July 2015. [Online]. Available: https://news.northropgrumman.com/news/features/solid-rocket-motors-reliable-safe-simple. [Accessed 26 Sept 2022].

[19] R. A. Ellis, “Solid Rocket Motor Nozzles, NASA SP-8115,” Natioal Aeronautics and Space Administration, Cleveland, 1975.

[20] S. D. Williams, “Thermal Protection Materials,” NASA-RP-1289, Houston, 1992.

[21] N. A. Kimmel, “Alternate Nozzle Ablative Materials Program,” JPL Publication 84-58, Pasadena, 1984.

[22] R. Acharya and K. K. Kuo, “Effect of Pressure and Propellant Composition on Graphite Rocket Nozzle Erosion Rate”, *Propulsion and Power*, Vol. 23, No. 6, pp. 1242-1254, 2007.

[23] S. T. Keswani, E. Andiroglu, J. D. Campbell, and K. K. Kuo, “Recession Behavior of Graphitic Nozzles in Simulated Rocket Motors,” *Spacecraft*, Vol. 22, No. 4, pp. 396-397, 1985.

[24] NASA, “Application of Ablative Composites to Nozzles for Reusable Solid Rocket Motors,” 20 Sept 2022. [Online]. Available: https://llis.nasa.gov/lesson/672.

[25] W. L. Oberkampf and C. J. Roy, Verification and Validation in Scientific Computing, Cambridge: Cambridge University Press, 2010.

[26] D. R. Bartz, “A Simple Equation for Rapid Estimation of Rocket Nozzle Convective Heat Transfer Coefficients,” *Jet Propulsion*, pp. 49-51, 1957.

[27] A. Murphy and K. Kwong, “Nozzle Control Bulletin, Aerotherm RP TM-75-86,” Acurex Aerotherm Corporation, 1975.

[28] J. R. Mathis and L. R. C., “Development of Low Cost Ablative Nozzles for Solid Propellant Rocket Motors, Vol II,” Thiokol Chemical Corporation, Brigham City, 1970.

[29] R. M. Kendall, E. P. Bartlett, R. A. Rindal and C. B. Moyer, “An Analysis of the Coupled Chemically Reacting Boundary Layer and Charring Ablator, Part I, Summary Report, NASA CR-1060,” NASA, 1968.

[30] C. B. Moyer and R. A. Rindal, “An Analysis of the Coupled Chemically Reacting Boundary Layer and Charring Ablator, Part II, Finite Difference Solution for the In-Depth Response of Charring Materials Considering Surface Chemical and Energy Balance, NASA CR-1061,” 1968.

[31] E. P. Bartlett and R. M. Kendall, “An Analysis of the Coupled Chemically Reacting Boundary Layer and Charring Ablator, Part III, Nonsimilar Solution of the Multicomponent Laminar Boundary Layer by an Integral Matrix Method,” NASA-1062, 1968.

[32] E. P. Bartlett, R. M. Kendall and P. A. Rindall, “An Analysis of the Coupled Chemically Reacting Boundary Layer and Charring Ablator, Part IV, A Unified Approximation for Mixture Transport Properties for Multicomponent Boundary-Layer Applications,” NASA CR-1063, 1968.

[33] R. M. Kendal, “An Analysis of the Coupled Chemically Reacting Boundary Layer and Charring Ablator, Part V, A General Approach to the Thermochemical Solution of Mixed Equilibrium-Nonequilibrium, Homogenous or Heterogenous Systems,” NASA CR-1064, 1968.

[34] C. A. Powers and R. M. Kendall, “User’s Manual, Aerotherm Chemical Equilibrium (ACE) Computer Program,” Aerotherm Corporation, Mountain View, 1969.

[35] M. E. Ewing and T. S. Laker, “Numerical Modeling of Ablation Heat Transfer,” *Journal of Thermodynamics and Heat Transfer,* pp. Vol. 27 No.4 615-632 , 2013.

[36] M. E. Ewing and D. A. Isaac, “Mathematical Modeling of Multiphase Chemical Equilibrium,” *Journal of Thermophysics and Heat Transfer*, pp. Vol. 29 No. 3 551-562, 2015.

[37] M. E. Ewing, D. A. Isaac, H. H. Dewey, C. W. Smith and Z. D. Harman, “Multidimensional Modeling in Ablation Heat Transfer,” *Journal of Thermophysics and Heat Transfer,* Pending.

[38] B. F. Blackwell and M. A. Howard, "An Element Potential Based Chemical Equilibrium Solver for Gas/Surface Thermochemistry," in *50th AIAA Aerospace Sciences Meeting including the New Horizons Forum and Aerospace Exposition*, Nashville, 2012.

[39] J. Arnold, J. Dodson and B. Laub, "Subscale Solid Motor Nozzle Tests – Phase IV and Nozzle Materials Screening and Thermal Characterization – Phase V," NASA CR-161254, Mountain View, 1979.

[40] J. W. Schaefer and T. J. Dahm, "Final Report, Studies of Nozzle Ablative Material Performance for Large Solid Boosters," NASA CR-72080, Palo Alto, 1966.

[41] Aerotherm, "Aerotherm Real Gas Energy Integral Boundary Layer Program (ARGEIBL)," Aerotherm UM-75-69, 1975.

[42] Chase, C. A., Wischmann, E. E., "IUS Validation Phase Motor Testing," in *AIAA/SAE 14th Joint Propulsion Conference*, Las Vegas, 1978.

[43] W. A. Clayton, "Thermal Conductivity of Ablative Chars," AFML-TR-69-313, WP Air Force Base, 1969.

[44] NASA, "Statistical Characterization of Carbon Phenolic Prepreg Materials," NASA NAS8-36298, 1988.

[45] J. Lachaud, J. B. Scoggins, M. T. E., M. G. Meyer and N. N. Mansour, "A generic local thermal equilibrium model for porous reactive materials submitted to high temperatures," *International Journal of Heat and Mass Transfer*, pp. 1406-1417, 2016.

[46] D. C. Montgomery and G. C. Runger, "Applied Statistics and Probability for Engineers," 4th Edition, John Wiley and Sons, Danvers, 2007.

[47] M. G. Morgan and M. Henrion, Uncertainty, A Guide to Dealing with Uncertainty in Quantitative Risk and Policy Analysis, Cambridge: Cambridge University Press, 1990.

[48] W. A. Clayton, P. B. Kennedy, R. J. Evans, J. E. Cotton, A. C. Francisco, T. J. Fabish, E. A. Eldridge and J. F. Lagedrost, “Thermal Properties of Ablative Chars,” AFML, 1967.

[49] M. L. Minges, “Thermophysical Characteristics of High-Performance Ablative Composities,” in *Ablative Plastics*, New York, Marcel Dekker Inc., 1971, pp. 287-312.

[50] F. Schultz, “Investigation of the Effect of Material Properties on Composite Material Behavior,” NASA CR-71295, Cleveland, 1966.

[51] B. William, “Final Report, Standardization of Carbon-Phenolic Materials and Processes, Volume II,” Mississippi State University, Mississippi, 1988.

[52] G. F. L. Ehlers, “Thermogravimetric Analsysi of Polymers,” ASD TR 61-622, 1962.

[53] W. W. Wendlandt, Thermal Analysis, 3rd Edition, New York: John Wiley & Sons, 1986.

[54] J. H. Flynn and L. A. Wall, “General Treatment of the Themogravimetry of Polymers,” *Journal of Research of the National Bureau of Standards – A Physics and Chemistry*, pp. 487-523, 1966.

[55] W. B. Hall, “Final Report, Standardization of the Carbon-Phenolic Materials and Proccesses, Volume II,” Mississippi State University, Mississippi, 1988.

[56] D. L. Schmidt, “Ablative Polymers in Aerospace Technology,” in *Ablative Plastics*, New York, Mercel Dekker, 1971, pp. 1-39.

[57] R. Y. Wen, L. F. Sonnabend and R. Eddy, “The Synthesis and Characterization of Some Potential Ablative Polymers,” in *Ablative Plastics*, New York, Mercel Dekker, 1971, pp. 145-157.

[58] M. L. Williams, “The Chemistry and Mechanics of Combustion with Applications to Rocket Engine Systems,” Unversity of Utah, UTEC DO 68-055, Salt Lake City, 1968.

[59] H. E. Goldstein, “Kinetics of Nylon and Phenolic Pyrolysis,” Lockheed Missiles & Space Company, Sunnyvale, 1965.

[60] R. W. Farmer, “Thermogravimetry of Phenol-Formaldehyde Polcondensates,” AFML-TR-65-246, WP Air Force Base, 1967.

[61] H. L. Friedman, “The Kinetics of Thermal Degradation of Charring Plastics,” General Electric Space Sciences Laboratory, 1961.

[62] W. Yuan, Y. Wang, Z. Luo, F. Chen, H. Li and T. Zhoa, “Improved Peformances of SiBCN Powders Modified Phenolic Resin-Carbon Fiber Composites,” *MDPI Processes,* 2021.

[63] G. F. Sykes and J. B. Nelson, “Thermoanalysis of Ablation Materials,” in *American Institute of Chemical Engineers Meeting*, Houston, 1967.

[64] J. B. Nelson, “Determination of Kinetics Parameters of Six Ablation Polymers by Thermogravimetric Analysis,” NASA TN D-3919, Washington D.C., 1967.

[65] C. Chang and J. R. Tackett, “Characterization of phenolic resins with thermogravimetry-mass spectrometry,” *Thermochimica Acta,* pp. 181-190, 1991.

[66] E. H. Stokes, “Kinetics of Pyrolysis Mass Loss from Cured Phenolic Resin,” *Journal of Thermophysics and Heat Transfer,* pp. Vol. 9 No. 2 352-358, 1995.

[67] K. Schellhase, J. H. Koo, J. J. Buffy, H. Wu and E. Liu, “Development of New Thermal Protection Systems Based on Silica/Polysiloxane Composites: Properties Characterization II,” in *SAMPE Conference Proceedings,* Seattle, 2017.

[68] K. J. Schellhase, J. H. Koo, H. Wu and J. J. Buffy, “Experimental Characterization of Material Properties of Novel/Polysiloxane Ablative,” *Journal of Spacecraft and Rockets,* 2018.

[69] J. D. Nam and J. C. Seferis, “Volatile Evolution in Thermoset Composites from Processing to Degradation,” *Science and Engineering of Composite Materials,* pp. 211-225, 1993.

[70] H. W. Lochte, E. L. Strauss and R. T. Conley, “The Themo-oxidative Degration of Phenol Formaldeyhyde Polcondensates. Thermogravimetric and Elemental Composition Studies of Char Formation,” *Journal of Applied Polymer Sciences,* pp. 2799-2810, 1965.

[71] M. Ladacki, J. V. Hamilton and S. N. Choz, “Heat of Pyrolysis of Resin in Silica Phenolic Ablator,” *AIAA Journal,* pp. 1798-1802, 1966.

[72] P. S. Chen and W. C. Stevens, “Novel Molecular Sources for Dispersing Boron in Carbon-Carbon Composites,” Air Force Office of Scientific Research, Bolling AFB, 1991.

[73] I. O. Salyer, H. S. Wilson and A. L. Wurstner, “Analysis of Thermal Degradation of Glass Reinforced Phenolic and Epoxy Laminates,” Air Force Systems Command ASD-TDR-62-939, WP Air Force Base, 1963.

[74] T. Boghozian, M. Stackpoole and G. Gonzales, *Characterization of New TPS Resins,* Moffett Field, CA: NASA.

[75] B. S. Marks and L. Rubin, “Ablative Resins for Hyperthermal Environments,” in *Ablative Plastics,* New York, Marcel Dekker, 1971, pp. 229-245.

[76] G. A. Binegar, J. A. Noblet, R. D. Zaldivar, P. M. Sheaffer and G. S. Rellick, “Effects of Heat Treatment on Microstructure and Flexural Properties of Unidirectional Carbon-Carbon Composites,” Air Force Systems Comman SSD-TR-89-87, El Segundo, 1989.

[77] K. A. Trick, T. E. Saliba and S. S. Sandhu, “A Kinetic Model of the Pyrolysis of Phenolic Resin in a Carbon/Phenolic Composite,” *Carbon,* pp. 393-401, 1997.

[78] R. C. Laramee and C. R. Canada, “High Temperature Testing and Application of Carbonaceous Materials for Solid Propellant Rocket Motor Nozzles,” in *AIAA/SAE 14th Joint Propulsion Conference,* Las Vegas, 1978.

[79] C. D. Pears, W. T. Engelke and J. D. Thornburg, “The Thermal and Mechanical Properties of Five Ablative Reinforced Plastics from Room Temperature to 750F,” AFML-TR-65-133, 1965.

[80] W. T. Engelke, C. M. J. Pyron and C. D. Pears, “Thermal and Mechanical Properties of a NonDegraded and Thermally Degraded Phenolic Carbon Composite,” NASA CR-896, Washington, D.C., 1967.

[81] D. Z. Dang, *Thermal and Structural Response Modeling of a Woven Thermal Protection System,* Ann Arbor: University of Michigan, 2021.

[82] M. Miller-Oana, P. Neff, M. Valdez, A. Powell, M. Packard and L. S. Walker, "Oxidation Behavior of Aerospace Materials in High Enthalpy Flows Using an Oxyacetylen Torch Facility," *Journal of the American Ceramic Society,* 2015.

[83] ASTM E285-08, "Standard Test Method for Oxyacetylene Ablation Testing of Thermal Insulation Materials," ASTM, 2020.

[84] M. R. Haddock, G. M. Wendel and R. V. Cook, "NARC Rayon Replacement Program for the RSRM Nozzle, Phase IV Qualification and Implementaiton Status," *AIAA*, 2005.

[85] E. M. Liston, in *Albative Plastics,* New York, Marcel Dekker, 1971, p. 379.

[86] R. A. Rindal, K. J. Clark, C. B. Moyer and D. T. Flood, "Experimental and Theoretical Analysis of Ablative Material Response in a Liquid-Propellant Rocket Engine," NASA CR-72301, Cleveland, 1967.

[87] W. D. Brewer, C. W. Stroud and R. K. Clark, "Effect of the Chemical State of Pyrolysis Gases," NASA TN D-4975, Washington, D.C., 1968.

[88] T. Ozawa, "A New Method of Analyzing Thermogravimetric Data," *Electrotechnical Laboratory,* pp. 1881-1886, 1965.

[89] C. D. Doyle, "Evaluation of Experimental Polymers," WADD Technical Report 60-283, WP Air Force Base, 1960.

[90] A. Kmita, W. Knauer, M. Holtzer, K. Hodor, G. Piwowarski, A. Rocniak, and K. Gorecki, "The Decomposition Process and Kinetics Analysis of Commericial Based on Phenol-Formaldehyde, Using in Metal Casting" *Applied Thermal Engineering*, vol. 156, pp. 263-275, 2019.

[91] S. Vyazovkin, A. K. Burnham, L. Favergeon, N. Koga, E. Moukhina, L. A. Perez-Maqueda and N. Sbirrazzuoli, “ICTAC Kinetics Committee Recommendations for Analysis of Multi-step Kinetics,” *Thermochimica Acta*, 2020.

[92] ASTM International, “E1131 – 08, Standard Test Method for Composition Analysis by Thermogravimetry,” ASTM International, West Conshohocken, 2014.

[93] G. R. Wilson, “Hemispherical Spectral Emittance of Ablations Chars, Carbon, and Zirconia (to 3700 K),” NASA SP-55, Langley, 1964.

[94] L. Biasetto, M. Manzolaro and A. Andrighetto, “Emissivity Measurements of Opaque Gray Bodies up to 2000C by a Dual-Frequency Pyrometer,” *The European Physical Journal A*, pp. 167-171, 2008.

[95] F. P. Incropera and D. P. Dewitt, Fundamentals of Heat and Mass Transfer, 7th Edtion, Hoboken: John Wiley & Sons, 2011.

[96] J. E. Janssen and R. N. Schmidt, “The Measurement of Total Surface Area,” NASA SP-55, San Fransisco, 1964.

[97] R. B. Merrill, “The Effects of Micrometeoroids on the Emittance of Solids,” NASA SP-55, San Fransisco, 1964.

[98] B. K. Heath and F. Aydogan, “Radiation Heat Transfer in the Fuel of Nuclear Rocket,” *Journal of Thermal Engineering*, pp. 786-793, 2015.

[99] W. M. Kays, Convective Heat and Mass Transfer, New York: McGraw-Hill, 1966.

[100] M. Wool and J. W. Schaefer, “Sensitivity Analysis of PG Recession Predictability to Response Measurements,” Aerotherm TM-70-6, 1970.

[101] Y. A. Cengel and A. J. Ghajar, Heat and Mass Transfer Fundamentals & Applications, 4th Edition, New York: McGraw-Hill, 2011.

[102] P. G. Cross, “Radiative Heat Transfer in Solid Rocket Nozzles,” *Journal of Spacecraft and Rockets,* pp. 247-260, 2020.

[103] Stephens, Wendall A., “High Chamber Pressure Blast Tube and Nozzle Material Evaluation. Volume 1,” AFRPL-TR-73-60, Edwards, 1974.

[104] Baran, W. J., “Development of a Miniature Solid Propellant Rocket Motor for use in Plume Simulation Studies,” Calspan Report No. AA-4018-W-10, Hunstville, 1974.

[105] T. V. O’Hara, J. B. Henry, W. A. Stephen, “84-IN. Propellant Catridges and Grains,” Vol. III – Appendix, Report No. AFRPL-TR-77-92, Sunnyvale, 1977.

[106] S. J. Morizumi and H. J. Carpenter, “Thermal Radiation from the Exhaust Plume of An Aluminized Composite Propellant Rocket,” TRW Space Technology Laboratories, Norton Air Force Base, 1964.

[107] G. F. Knoll, Radiation Detection and Measurement, 3rd Edition, Hoboken: John Wiley & Sons, 2000.

[108] R. W. Hermsen, “Aluminum Oxide Particle Size for Solid Rocket Motor Performance Prediction,” in *AIAA 19th Aerospace Sciences Meeting*, St. Louis , 1981.

[109] A. Gany and L. H. Caveny, “Agglomeration and Ignition Mechanism of Aluminum Particles in Solid Propellants,” *Symposium on Combustion,* vol. 17, no. 1, pp. 1453-1461, 1979.

[110] J. Harrison and M. Q. Brewster, “Simple Model of Thermal Emission from Burning Aluminum in Solid Propellants,” *Journal of Thermophysics and Heat Transfer,* vol. 23, no. 3, pp. 630-634, 2009.

[111] R. A. Reed, “Review of Aluminum Oxide Rocket Exhaust Particles,” in *AIAA 28th Thermophysics Conference*, Orlando, 1993.

[112] P. F. Parais, “Non-Contanct Thermophysical Property Measurements of Liquid and Undercooled Alumina,” *Japanese Journal of Applied Pysics,* pp. 1496-1500, 2004.

[113] T. Kondo, H. Muta, K. Kurosaki, F. Kargi and A. Yamaji, “Density and viscosity of liquid ZrO2 measured by aerodynamic levitation technique,” *Heliyon*, 2019.

[114] A. D. Kirshenbaum and J. A. Cahill, “The Density of Aluminum Oxide,” *Journal of Inorganic Nuclear Chemistry*, pp. 283-287, 1960.

[115] S. M. Arnold, P. L. Murthy, B. A. Bednarcyk, J. W. Lawson, J. D. Monk and C. W. J. Bauschlicher, "Multiscale Modeling of Carbon-Phenolic Composite Thermal Protection Materials: Atomistic to Effective Properties," NASA/TM-2016-219124, Cleveland, 2016.

[116] P. G. Cross, "Reduced Reaction Mechanism fo Rocket Nozzle Ablation Simulations," in *AIAA Aviation Forum*, Denver, 2017.

[117] M. R. Wool, D. L. Baker and M. A. J., "Material Performance of Carbon Phenolic Ablators and Pyrolytic Graphite Coatings in Nozzles Subjected to Multiplie Pulse Duty Cycles," AFRPL-TR-71-130, Edwards Air Force Base, 1971.

[118] C. M. Pittman and W. D. Brewer, "Analytical Determination of the Effect of Thermal Property Variations on the Performance of a Charring Ablator," NASA TN D-3486, Washington, D.C., 1966.

[119] L. Hillberg, "Influence of Material Properties on Re-Entry Vehicle Heat Shield Design," in *AIAA/ASME 8th Structures, Structural Dynamics and Materials Conference*, 1967.

[120] P. Kolodziej, "Strategies and Approaches to TPS Design," in *Critical Technologies for Hypersonic Vehicle Development*, Belgium, 2004.

[121] B. Heath, B. Liechty and M. Ewing, "Ablation Heat Transfer Surrogate Modeling Methods and Assessment," in *12th Ablation Workshop*, Lexington, 2022.

[122] R. H. Myers, Response Surface Methodoloy, Newton: Allyn & Bacon, 1971.

[123] A. I. J. Forrester, A. Sobester and A. J. Keane, Engineering Design via Surrogate Modeling: A Practical Guide, New York: John Wiley & Sons, 2008.

[124] S. Guo, "An introduction to Surrogate modeling, Part I: Fundamentals," 10 Sept 2022. [Online]. Available: https://towardsdatascience.com/an-introduction-to-surrogate-modeling-part-i-fundamentals-84697ce4d241.

[125] N. V. Queipo, R. T. Haftka, W. Shyy, R. V. Tushar Goel and K. P. Tucker, *Surrogate-based Analysis and Optimization*, NASA NAG8-1791, 2005.

[126] C. E. Rasmussen and C. K. L. Williams, Gaussian Procces for Machine Learning, Cambridge: The MIT Press, 2006.

[127] J. Sacks, W. J. Welch, T. J. Mitchell and H. P. Wynn, "Deisng and Analysis of Computer Experiments," *Statistical Science*, pp. 409-435, 1989.

[128] B. Rosenbaum, *Efficient Global Surrogate Models for Response and Expensive Simulations*, Trier, 2013.

[129] J. K. Vaurio, "Response Surface Techniques Developed for Probabilistic Analysis of Accident Consequences," in *National Topical Meeting on Probabilistic Analysis of Nuclear Reactor Safety*, Los Angeles, 1978.

[130] W. R. Madych and S. A. Nelson, "Polyharmonic Cardinal Splines," *Journal of Approximation Theory*, pp. 141-156, 1990.

[131] A. H. S. Ang and W. H. Tang, Probability Concepts in Engineering: Emphasis on Applications to Civil and Environmental Engineering, New York: Wiley, 2007.

[132] M. D. McKay, R. J. Beckman and W. J. Conover, "A Comparison of Three Methods for Selecting Values of Input Variables in the Analysis of Output from a Computer Code," *Technometrics*, vol. 21, no. 2, pp. 239-245, 1979.

[133] R. L. Iman, J. M. Davenport and D. K. Zeigler, "Latin Hypercube Sampling (Program User's Guide)," Sandia National Laboratoria, Albuquerque, 1980.

[134] D. J. Rasky, P. Kolodziej, M. E. Newfield, B. Laub and Y. K. Chen, "Assessing Factors of Safety, Margins of Safety, and Reliability of Thermal Protection Systems," in *36th AIAA Thermophysics Conference*, Orlando, 2003.

[135] A. Mazzaracchio, "Determination of the Margin of Safety in Thermal Protection System Sizing Process," *International Journal of Mechanical Engineering and Technology,* vol. 9, no. 1, pp. 112-117, 2018.

[136] D. R. Moore and W. J. Phelps, *Reusable Solid Rocket Motor - Accomplishments, Lessons, and a Culture of Success,* Huntsville: AIAA, 2011.